CASL-U-2017-1408-000

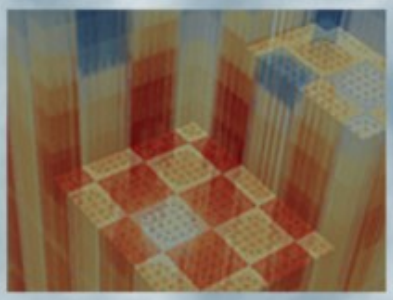

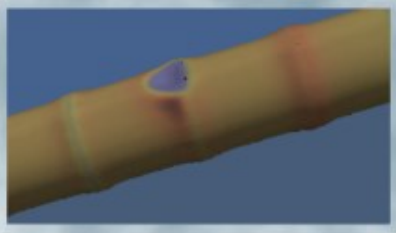

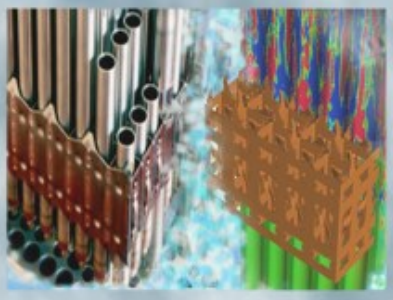

Demonstration of Coupled Tiamat Quarter Core Calculations on Watts Bar Unit 1, Cycle 1

Shane Stimpson
Kevin Clarno
Jeffrey Powers
Benjamin Collins
Oak Ridge National Laboratory

Roger Pawlowski
Alex Toth
Sandia National Laboratories

Russell Gardner
Stephen Novascone
Stephanie Pitts
Jason Hales
Giovanni Pastore
Idaho National Laboratory

August 18, 2017

REVISION LOG

Revision	Date	Affected Pages	Revision Description
0	08/18/2017	All	Original Report

Document pages that are:

Export Controlled: None

IP/Proprietary/NDA Controlled: None

Sensitive Controlled: None

Unlimited: All

Approved for Public Release: YES

Requested Distribution:

To: Kevin Clarno, PHI Lead

Copy: Thomas Downar, PHI Deputy

Jeff Banta, CASL Program Manager

EXECUTIVE SUMMARY

This report corresponds to milestone L2:PHI.P15.03, which is intended to demonstrate the Tiamat coupling on quarter core problems for Watts Bar Unit 1, Cycle 1. Two modes of operation are available in Tiamat: (1) Tiamat-Inline, which performs a one-way coupling between MPACT/CTF and Bison, and (2) Tiamat-Coupled, which solves all three codes at each outer iteration, passing power and temperature distributions as appropriate.

Based on the previous milestone, which focused on single assembly demonstrations in which the initial status of the quarter core results was shown, a number of improvements were made to (1) shorten the time spent writing HDF5 files, (2) improve the logic used to determine when to run subgroup self-shielding, (3) improve the time adaptive time stepping, and (4) allow for rotational symmetry.

Additional improvements have been made to the 1.5D Bison input to provide better consistency when compared to a 2D-RZ. Comparisons are made on a simple single rod regression test so that much better agreement is observed in terms of gap closure. However, ~20 K temperature differences are still observed, with roughly a 2–4× speedup. While this is a relatively small run time improvement, it has been crucial to demonstrating on larger problems, and it has proved to be more stable than 2D-RZ cases. MOOSE/Bison stability is paramount in Tiamat cases. If any single rod fails at any point, the entire calculation fails. The calculations presented here use MOOSE/Bison source versions from May 2017 as newer source demonstrates convergence issues, but excellent robustness is observed with the older source.

Simulations of Watts Bar Unit 1, Cycle 1 were conducted on the Panacea cluster for both Tiamat-Inline and Tiamat-Coupled. The Tiamat-Coupled case was executed on 1,984 cores (900 MPACT/CTF and 1,040 Bison). This yields 12–13 Bison rods per process and an overall runtime of roughly 67 hours (~133,000 core-hours). The Tiamat-Inline case took roughly 36 hours to complete on 1,504 cores (~54,000 core-hours). For comparison, a similar case of just MPACT/CTF recently took around 36,000 core-hours. Therefore, for Tiamat-Inline, one would anticipate using roughly 1.5× the resources of MPACT/CTF alone, and for Tiamat-Coupled, roughly 3–4× the resources would be used.

A detailed comparison of the differences between Tiamat-Inline and Tiamat-Coupled is presented herein. Some differences are expected, as the Inline results use a 2D-RZ–generated temperature table. However, these comparisons provide important insights into the effects that are potentially being missed by the current temperature table approach. Typically, a difference of less than 2 ppm boron concentration is observed and ~1% maximum pin power difference, with a typical RMS difference of roughly 0.15%. This suggests that temperature tables perform fairly well, and the history effects neglected by them are likely small.

While this report showcases efforts taken to develop and demonstrate the Tiamat capability on a target problem in support of the PCI challenge problem, there is still fertile ground for future extensions. In particular, work can be performed to consolidate and overlap some of the processes used between MPACT and Bison, assuming that memory considerations are reasonable. This would reduce the number of core-hours used in coupled calculations significantly. Future work can also focus on improving the fidelity of the solve by passing radial power information from MPACT, potentially in the form of shape functions, allowing Bison to use a more informed representation of the radial power distribution with depletion when compared to the internal model it currently uses. Considering multicycle and transient applications will likely be of near term interest as the capability continues to mature.

CONTENTS

FIGURES

ACRONYMS

2D/1D	two-dimensional/one-dimensional method
BOC	beginning of cycle
BOL	beginning of life
CASL	Consortium for Advanced Simulation of Light Water Reactors
CMFD	coarse mesh finite difference
CTF	Cobra-TF
EFPD	effective full power day
EOC	end of cycle
fima	fissions per initial metal atom
GWd	gigawatt-days
HFP	hot full power
HZP	hot zero power
IFBA	integral fuel burnable absorber
INF	CASL Infrastructure focus area
INL	Idaho National Laboratory
K	kelvin
LHR	linear heat rate
LOCA	loss of coolant accident
LWR	light water reactor
NEM	nodal expansion method
MOC	middle of cycle (or method of characteristics)
MPa	megapascal
MT	metric ton
ORNL	Oak Ridge National Laboratory
PCI	pellet clad interaction
PCMI	pellet clad mechanical interaction
VERA	Virtual Environment for Reactor Analysis
WBN1	Watts Bar Nuclear Unit 1

1. INTRODUCTION

1.1 Motivation

For several years now, the core simulator capabilities provided by coupled MPACT and CTF calculations have been stable and mature. Incorporating additional physics to these simulations is extremely important to the challenge problems presented by the Consortium for Advanced Simulation of Light Water Reactors (CASL). For example, coupling MAMBA to simulate the CRUD formation and resulting CRUD-induced power shift have been a focus of recent efforts [1]. This has generated significant interest from industry partners and potential collaborators. Similarly, coupling Bison to provide fuel performance simulations has been a very important driver for the pellet-clad interaction (PCI) milestones. A few different approaches have been developed for this coupling.

- The first and most basic approach is a simple file-based one-way coupling between MPACT/CTF and Bison in which MPACT/CTF coupled simulations are run to completion, and the output from those simulations is then used to build a separate Bison input for each rod in the core. While this capability has provided a lot of results for larger scale problems and has been used as a screening tool for PCI analysis, there is no feedback from the Bison rods to the MPACT/CTF simulations.
- The next two approaches are available through Tiamat, which is a driver package that handles the coupling between MPACT, CTF, and Bison.
    - The first is referred to as *Tiamat-Inline*, which provides the same one-way coupling as the file-based approach, but all of the power and temperature data from MPACT/CTF are passed internally to Bison. T
    - The second is *Tiamat-Coupled*, which couples all three codes, solving each outer iteration. With this approach, MPACT is solved first, then Bison and CTF both execute concurrently using the power information from MPACT. Bison also uses the clad outer surface temperature as a boundary condition, but it is using a lagged value from CTF from the previous outer iteration.

These approaches have resulted in significant progress on the PCI challenge problem. Ideally, using Tiamat will become more common for typical production-level analysis problems as performance improvements are made in the future.

In the remainder of this section, the Virtual Environment for Reactor Analysis (VERA) components are described for clarity, along with milestone objectives. This is followed by a description of the single assembly and the current status of the quarter core demonstrations.

1.2 VERA Description

VERA is a simulation environment being developed by CASL comprised of codes that are collectively used for nuclear reactor modeling and simulation. The primary deterministic neutron transport solver is MPACT, and CTF is the subchannel thermal hydraulics solver. Much of the work in this report relates to the Bison fuel performance code. Figure 1.2.1 shows the components of VERA.

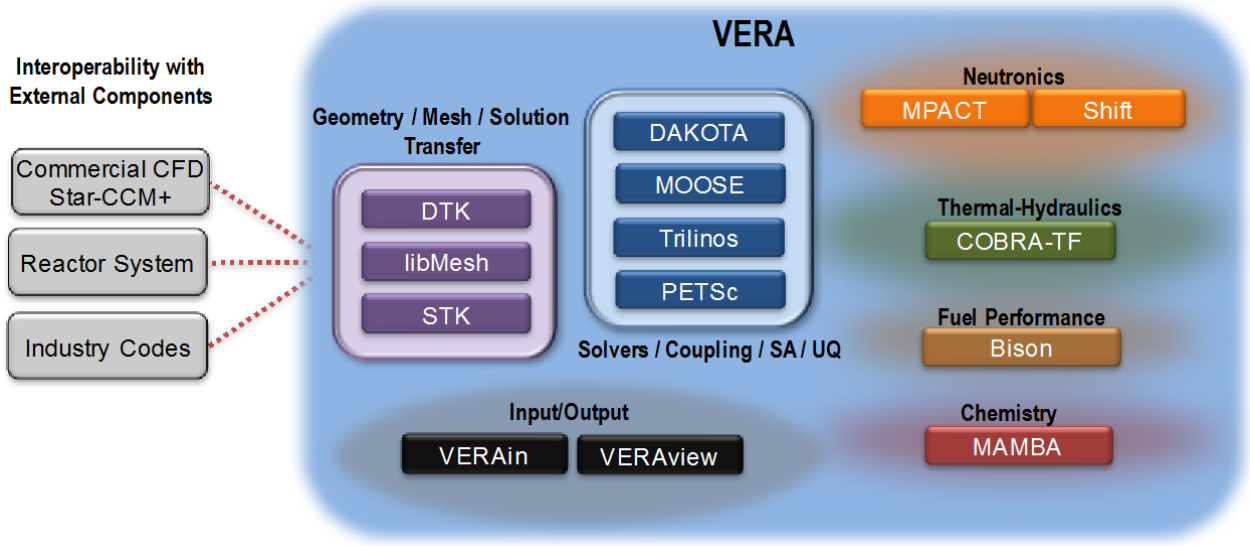

Figure 1.2.1. VERA Components.

MPACT

The MPACT neutron transport solver being developed collaboratively by Oak Ridge National Laboratory (ORNL) and the University of Michigan (UM) provides pin-resolved flux and power distributions [2]. To solve three-dimensional (3D) problems, it employs the 2D/1D method, which decomposes the problem into a 1D axial stack of 2D radial planes [3,4]. Typically, 2D Method of Characteristics (2D MOC) is used to solve each radial plane, and 1D nodal methods are used to solve axially along each rod. While there are a variety of axial solvers available, the nodal expansion method (NEM)-P_3 solver is the default, wrapping a one-node NEM kernel [5]. These 2D and 1D solvers are coupled together through transverse leakage terms to ensure neutron conservation, and they are accelerated using 3D coarse mesh finite difference (CMFD).

CTF

CTF is a subchannel TH code being developed by ORNL and North Carolina State University (NCSU) specifically for light water reactor (LWR) analysis [6]. It simulates two-phase flow with a three-field representation—liquid, droplet, and vapor—assuming that the liquid and droplet fields are in dynamic equilibrium, leaving two energy conservation equations. CTF provides significantly higher resolution and physics detail than the internal thermal hydraulics solver (Simplified TH) in MPACT, resulting in longer execution times.

Bison

The Bison fuel performance code is being developed by Idaho National Laboratory (INL) to provide single-rod fuel performance modeling capability so users can assess best-estimate values of design criteria and the impact of plant operation and fuel rod design on thermo-mechanical behavior such as pellet-cladding interaction (PCI) failures in pressurized water reactors (PWRs) [7,8] Because PCI is controlled by a complex relationship of multiple physics, modeling PCI requires an integral fuel performance code to simulate the fundamental processes of these behaviors. Bison is built on INL's Multiphysics Object Oriented Simulation Environment (MOOSE) package [9,10] which uses the finite element method for geometric representation and a Jacobian Free Newton-Krylov (JFNK) scheme to solve systems of partial differential equations [10]. For this work, Bison uses a 2D azimuthally symmetric (RZ) smeared-pellet thermomechanical fuel pin model with boundary and heat source data from VERA to generate the time-dependent power shape/history and moderator temperature inputs needed for Bison.

Tiamat
Tiamat is the driver package between MPACT, CTF, and Bison, handling the necessary data communication through DTK and the general execution of the coupled simulation [11,12]. There are currently two modes of operation: (1) Tiamat-Inline, which provides a one-way data transfer between MPACT/CTF and Bison where temperatures from Bison are not sent back to MPACT/CTF, and (2) Tiamat-Coupled, in which all three codes execute every outer iteration, which is effectively a residual calculation consisting of a single neutronics, thermal hydraulics, and fuel performance update. In coupled mode, MPACT sends power distribution data to CTF and Bison, CTF provides the clad outer surface data to Bison and the coolant data to MPACT, and Bison provides the fuel temperature back to MPACT.

1.3 Overview o,f Tiamat Modes of Operation

Recent efforts have developed a new Tiamat calculation scheme in which the MPACT/CTF coupling is the same, but now Tiamat solves each Bison pin concurrently with CTF. For each user-defined time step, MPACT computes the axial power distribution within each rod at the end time and passes it to both CTF and Bison and then passes the latest solution for the clad surface temperature from CTF to Bison. Tiamat instructs a MOOSE MultiApp to (1) restore every rod to the last backup, (2) independently adaptively time step each rod to the next user-defined state, and (3) then pass the fuel temperature back to MPACT. When the new fully coupled capability is used with 2D Bison, the power from MPACT would axially redistribute within the fuel rod so the clad surface heat flux from Bison would provide a thermal source for CTF. Because the 1.5D Bison only transfers heat radially, there is no need to lag the power distribution from a given iteration.

It is also important to note that by running Bison and CTF at the same time, the cladding's outer surface temperature boundary condition used by Bison that comes from CTF is actually lagged by an outer iteration. At convergence there is no issue, but outer surface temperature also does not change substantially, so it likely has very little impact on the overall convergence. In fact, when comparing the number of iterations to a normal MPACT/CTF calculation, the Tiamat coupled calculation seems to consistently take fewer outer iterations. With the boundary condition lagged, it is effectively relaxing its impact, which could be leading to more optimal convergence. Figure 1.2.2 shows a flowchart of new, fully coupled Tiamat calculation scheme. MPACT and CTF share processors because of the internal coupling there, but the Bison calculations are performed on a different set of processors entirely.

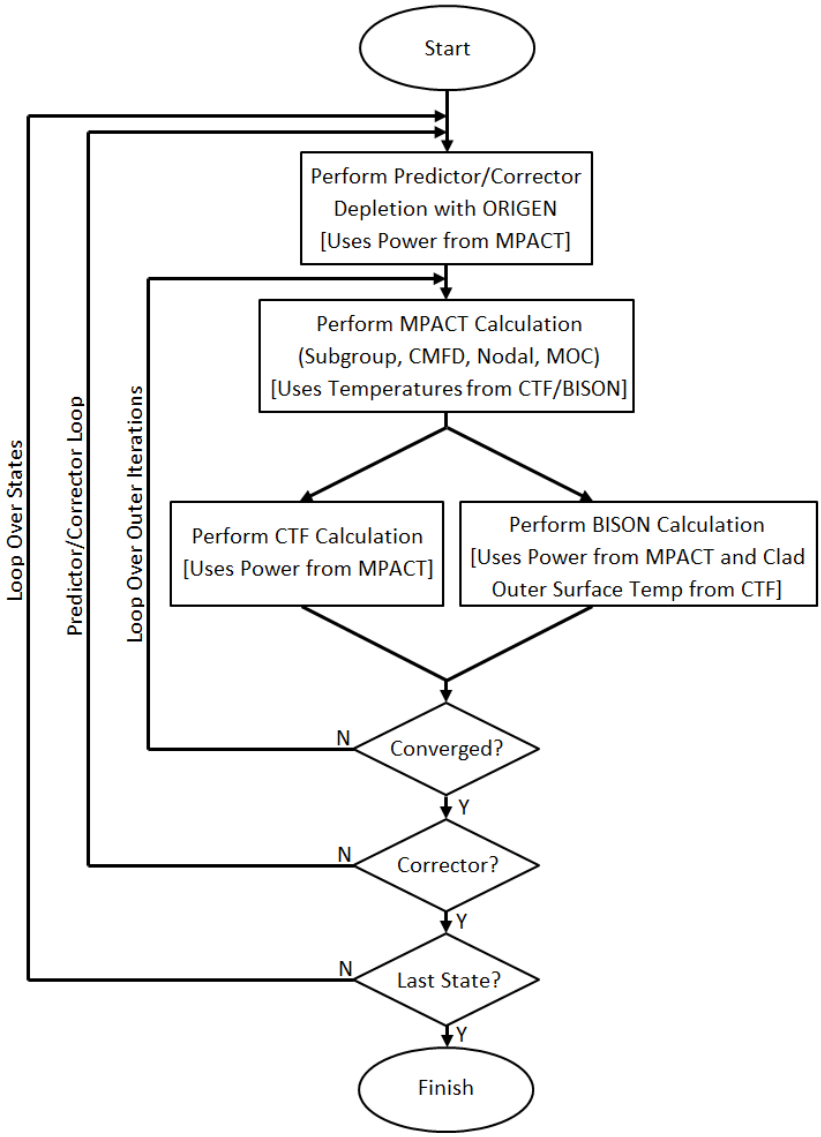

Figure 1.2.2. Flowchart of the Tiamat Fully Coupled Calculation.

Figure 1.2.3 shows a comparable flowchart for the Tiamat-Inline calculation in which MPACT and CTF are fully converged together, and then the processors dedicated to Bison solves will run the Bison cases while the MPACT/CTF processors continue with the next state. Therefore, the Bison processors lag behind the MPACT/CTF processors by a statepoint. The MPACT/CTF calculation will not proceed past one iteration ahead if the Bison calculation takes longer. This does not typically occur, although select statepoints may take longer than others, particularly during power ramps.

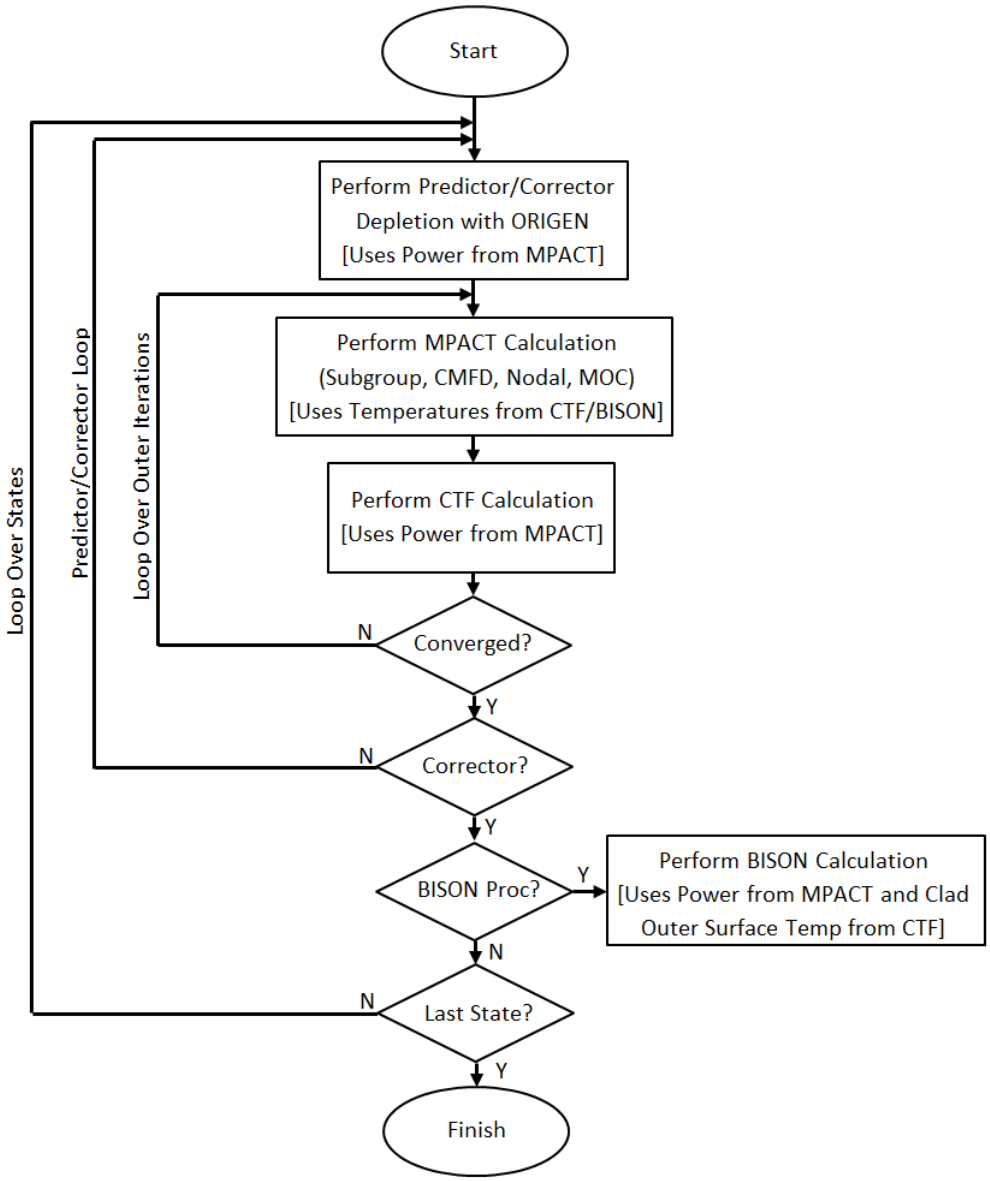

Figure 1.2.3. Flowchart of the Tiamat Inline Calculation.

1.4 Milestone Objectives

The primary goal of this milestone is to demonstrate Tiamat coupled calculations on a quarter core problem. The focus of this demonstration is on Watts Bar Unit 1, Cycle 1. This milestone also builds on the single assembly demonstration in which the initial quarter core demonstration was presented. This demonstration highlighted some areas for improvement, especially with respect to various performance aspects in Tiamat. These areas have been the focus of development in the past two months and are much improved. Another goal was to flush out any remaining issues with the 1.5D Bison capability provided by INL. As a result of working with the Bison team, most of the larger disagreements between 1.5D and 2D-RZ accuracy have been resolved, and the current status of those comparisons is presented. Overall, the goals of this milestone have been met, demonstrating the capability and providing some insights into what will be necessary for this tool to be considered a production-level capability.

2. RECENT IMPROVEMENTS TO TIAMAT

Tiamat development began several years ago, while coupling between MPACT and CTF was still relatively new, and VERA-CS did not yet include depletion. The initial MPACT-CTF coupled capability used the DTK transfer tools to pass power (fully converged in MPACT) to CTF and the temperature and densities (fully converged in CTF) to MPACT. The initial coupled Tiamat capability was built using the same DTK interfaces with additional transfers for Bison: the power from MPACT to Bison, the fuel temperature (fully converged in Bison) to MPACT, the clad surface heat flux (fully converged in Bison) to CTF, and the clad surface temperature (fully converged in CTF) to Bison. Because Bison is always run as a time-dependent execution, this required that Tiamat ensure coordinated time-stepping of every Bison pin in the problem. Because each pin could be at a different state and could require a smaller time step for accuracy, the overall computational burden of coordinating time-stepping of thousands of Bison pins was staggering. This constrained progress and created a very awkward algorithm for a single ramp to full power, and it would be difficult to extend to depletion calculations.

Eventually, a new MPACT/CTF coupling was formulated using internal data passing, which allowed MPACT to embed the thermal-hydraulics and fuel temperature solver within each neutron transport outer iteration instead of fully converging MPACT between CTF updates. This approach has proven to be much more computationally efficient and has been the default for some time. The Tiamat-Inline capability was developed to take advantage of this efficient coupling and robust algorithm by simply transferring, in memory, the Bison source-term and boundary conditions from MPACT and CTF, respectively. This allowed each Bison pin to adaptively time step between each of the user-defined depletion steps communicated from MPACT. With the freedom to converge independently, the computational cost of Bison and management constraints of Tiamat-Inline were dramatically reduced from the original Tiamat. However, the robustness requirements for Bison are extremely high when used within an integrated solver executing thousands of fuel performance calculations at once with unpredictable source-term and boundary condition variation: every pin must converge every time, or the entire Tiamat-Inline solver would crash. Therefore, older versions of MOOSE and Bison were used (May 2017). Newer versions of the source were met with substantial convergence issues. However, using an older source allowed all calculations to run smoothly.

While several key developments were covered in the single assembly demonstration milestone [13] which are also included here for completeness, several more recent improvements have been made based on feedback from that report, including: (1) improvement of the subgroup logic to limit running self-shielding calculations when unnecessary, (2) reduction of the time spent writing HDF5 files from Tiamat, and (3) incorporation of rotational symmetry into the data transfers in the Coupler routines in MPACT.

2.1 MOOSE Backup/Restore Capability

The new fully coupled mode requires Bison to be repeatedly solved over the same time interval during the course of a coupled solve, with new power and clad surface temperatures being provided at each coupled iteration. However, the way that Tiamat uses Bison with timestep subcycling—allowing the individual Bison apps to choose their own manner of stepping through time to reach the target time provided by MPACT—the state of each app is automatically updated after each solve. This means that any subsequent calls to advance the Bison model evaluator to the same time would have no effect, as the apps have already been solved to that target time. Hence, the fully coupled mode of Tiamat requires the ability to rewind the Bison apps to their states at the beginning of the coupled solve in order to re-solve the time interval. Fortunately, the ability to do this was recently introduced into the MOOSE multiapp framework. This feature works through two interface functions: one which serializes and saves off the current stateful data in all the apps, and another

which restores the apps to the previously saved state. In fully coupled Tiamat, this feature is used by saving the multiapp state at the beginning of a coupled solve, and restoring to the saved state prior to any subsequent attempts to resolve that time interval with new power and clad conditions.

There are still a few outstanding issues related to this capability. Most notably, unexpected behavior is observed when attempting to save off and restore to the initial state. When attempting this, restored Bison solves begin subcycling with the minimum allowable timestep, which is 1.0e-14 by default. This issue seems to be related to some restartable data being incorrectly initialized or restored in the MOOSE timestepper. This issue has been reported to the MOOSE team and is being addressed. This is currently dealt with in Tiamat by simply performing the first state solve in uncoupled mode. As the first state typically solves to HZP, this should have little impact on overall accuracy, as the feedback between Bison and MPACT/CTF should be fairly minimal under these conditions.

2.2 Burnup Improvements

In addition to the coupling approach changes, modifications were made to the burnup interface to improve the accuracy in Tiamat. The Bison team implemented a new vector postprocessor that effectively evaluates the auxiliary variable manipulated by Tiamat, parsing it as a function, allowing it to be fed into the burnup block. However, Tiamat directly manipulates an axial fission rate auxiliary variable, so an additional function was necessary to convert the axial fission rate into an axial power before being used by the burnup block. Figure 2.2.1 shows these blocks from a sample input. At the bottom, one can see the vector postprocessor (vec_post) that uses a line value sample function to evaluate the casl_fission_rate (from Tiamat) at many points axially. The fission_rate_auxvar_value_function in the Functions block is used to turn the vector postprocessor results into a function field. However, as this is still the fission rate data, the fission_rate_convert_to_LHR function is used to convert it to linear heat rate (W/m). This conversion process takes place inside the burnup block as fission_rate_convert_to_LHR is passed into the rod_ave_lin_pow field and fission_rate_auxvar_value_function through the axial_power_profile field. These two fields are then multiplied internally to produce the local linear heat rate value at each point axially, and the burnup block is still handling the intrapellet distribution internally.

```
# ================================================== #
# Time- and Space-Dependent Source and BCs
# ================================================== #
[Functions]
...
  [./fission_rate_convert_to_LHR]
    type = PiecewiseLinear
    x = '-100 0 5000'
    y = '1.68662971E-15 1.68662971E-15 1.68662971E-15'
    scale_factor = 1
  [../]
  [./fission_rate_auxvar_value_function]
    type = VectorPostprocessorFunction
    component = 1
    argument_column = y
    value_column = casl_fission_rate
    vectorpostprocessor_name = vec_post
  [../]
  [./q]
    type = CompositeFunction
    functions = 'fission_rate_convert_to_LHR fission_rate_auxvar_value_function'
  [../]
[]

# ================================================== #
# Burnup Equation Set
# ================================================== #
[Burnup]
  [./burnup]
    block = 3
    rod_ave_lin_pow = fission_rate_convert_to_LHR
    axial_power_profile = fission_rate_auxvar_value_function
    num_radial = 80
    num_axial = 100
    fuel_inner_radius = 0.0
    fuel_outer_radius =
    fuel_volume_ratio = 1.0
    i_enrich = '3.100e-02 9.690e-01 0.0000e+00 0.0000e+00 0.0000e+00 0.0000e+00'
    RPF = RPF
  [../]
[]
...
[VectorPostprocessors]
  [./vec_post]
    type = LineValueSampler
    variable = casl_fission_rate
    start_point = '0 0 0'
    end_point = '0 3.6575 0'
    num_points = 50
    sort_by = y
    execute_on = linear
  [../]
[]
```

Figure 2.2.1. Input File Excerpt Showing the Necessary Changes.

Figure 2.2.2 provides an example of the burnups that can be extracted from the Tiamat with these changes, showing both axial and radial dependence, as expected.

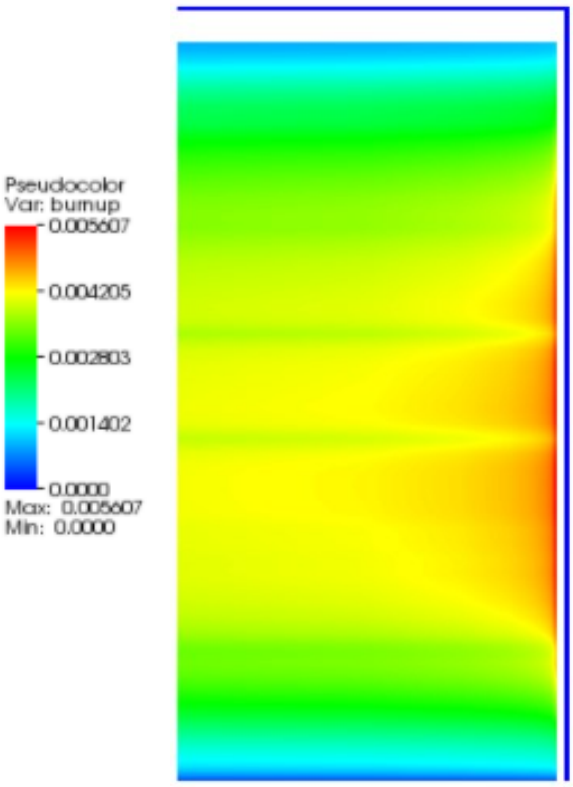

Figure 2.2.2. Improved Burnup (fima) Example with Both Axial and Radial Dependence.

As part of his comparison work, Jeffrey Powers (ORNL) observed some discrepancies in the burnup between standalone Bison and Tiamat cases. This is still being investigated, but the modifications shown in this section have drastically improved the burnup distributions predicted by Tiamat.

2.3 Subgroup Self-Shielding Logic

In the single assembly milestone report [13], it was observed that the subgroup self-shielding calculation was effectively being performed at nearly every outer iteration. The self-shielding calculation is typically only performed for the first few outer iterations following a predictor or corrector step. This defect was related to the fact that both CTF and Bison were solving for the fuel temperature, and the proper change in fuel temperature was not being properly communicated in MPACT. This was resolved by having Tiamat inform MPACT of the change in fuel temperature. If the temperature is converged well enough (less than 5 Kelvin at all points), then the self-shielding calculation is bypassed. The resolution of this defect translates to tangible performance improvements, as the self-shielding calculation is a non-trivial amount of work.

2.4 HDF5 Writing Efficiency

The same report [13] describes how the time Tiamat spent writing to the HDF5 file was about one hour per statepoint. With a total of 32 statepoints in the demonstration case, resolving this could have a substantial impact on the overall walltime. Previously, Tiamat was creating a dataset for each Bison pin, writing it to the file, and closing the dataset. Instead, a row-based scheme was implemented so that all pins in a row owned by the same Bison proc are written together. As will be seen in the results, this has reduced the overhead from ~60 minutess to ~5 minutes, which is considered to be sufficiently fast.

2.5 More Aggressive Adaptive Timestepping

Previously, the time stepping in Bison was allowed to gradually build up, starting at 100 seconds. However, when the second state is encountered, which spans several days, it can take a substantial amount of runtime to complete the calculation. Instead, Tiamat informs Bison to start solving the state in one time step. If a smaller timestep is needed, Bison will cut back as necessary. This seems to reduce the runtime in the early states considerably.

2.6 Rotational Symmetry

For quarter core problems, rotational symmetry along the west and north faces is the current default in VERA. Previously, limitations in the MPACT Coupler routines prohibited the use of rotational symmetry, so Tiamat cases were forced to use mirror symmetry. While this is acceptable for many cases, including the one presented in the results here, anything past Cycle 1 for Watts Bar Unit 1 requires rotational symmetry. The fix for this was relatively simple and involved minor changes to the tags used in the MPI data passing calls.

2.7 Restart Capability

As the calculation proceeds, the user can instruct VERA to write restart files. In MPACT/CTF calculations, this typically means that just MPACT will write a restart file. However, with Tiamat, the Bison calculations can be informed to write similar data after any statepoint in the calculation. Then the calculation can be restarted from any point with those files written. In the quarter core results shown later, 4 restart points were specified, so Bison data are stored for all of those points. Currently, the data for each restart is fairly large at roughly 130 GB. By comparison, the Exodus files, which contain the finite element data for all rods at all statepoints, are a little over 100 GB in total. Therefore, there may be some room for improvement by trimming those files down.

3. STATUS OF 1.5D BISON PERFORMANCE AND ACCURACY

3.1 Background

Historically, VERA's usage of Bison has focused on 2D-RZ simulations, but these have been found be both slower and less robust than desired for coupled cases such as those provided by Tiamat. In February 2017, the Bison team delivered an initial 1.5D capability which effectively solves the fuel rod using an axial stack of 1D-radial problems. All of the 1D-radial problems are coupled together through the gas pressure, and an axial pressure applied to the fuel/clad, axial conduction is ignored. Energy conservation and stress divergence are solved along each plane using finite elements in 1D with thermal and mechanical contact. Axial effects are accounted for by summing displacements in each slice using a generalized plane strain formulation. Figure 3.1.1 shows an illustration describing the 1.5D capability [14].

The goal of the 1.5D capability is to resolve computational performance issues of speed and robustness that were observed with the 2D-RZ models. The Bison team also released a report documenting the verification and validation efforts of the 1.5D model, comparing it to 2D-RZ calculations [15].

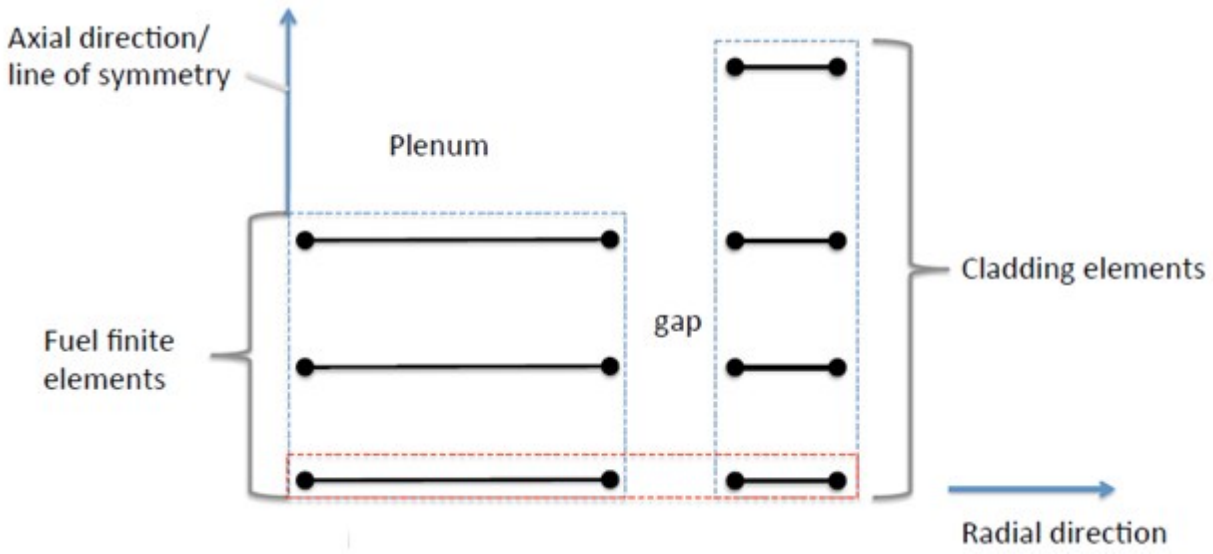

Figure 3.1.1. 1.5D Capability Illustration [14].

3.2 Testing

To test this capability, one of the regressions tests was chosen. It is a simple, single rod problem that starts at nominal power and observes two 10% power increases at ~1 and ~4.5 GWd/MT. Both a 2D-RZ and a 1.5D version were executed on 12 processors. The 2D-RZ case took 302 seconds, and the 1.5D case took 130 seconds, so only about a 2.3× speedup was realized. Both cases used 6 radial mesh in the fuel and 3 in the clad, but the 2D case used 100 axial quadratic finite elements, and the 1.5D case used 49 axial planes in the fuel. Even though this was only a relatively small speedup, this 2–4× improvement has been crucial to obtaining a reasonable walltime for larger cases such as the quarter core demonstration.The figures below show the current status of the solution differences between 2D and 1.5D. Figure 3.2.1 shows the output power reported by Bison, which should basically be an echo of the input power (or very close with minor errors due to finite element integration). Both 1.5D and 2D cases sufficiently conserve the input power in this case.

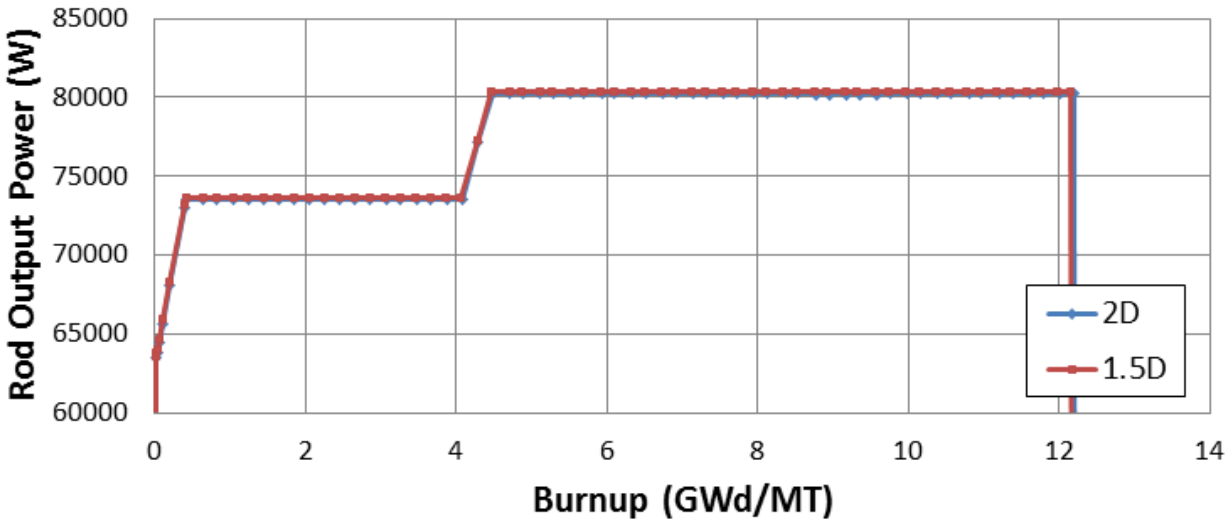

Figure 3.2.1. Rod Output Power [W] Comparison Between 1.5D and 2D-RZ Standalone Bison Cases.

Figure 3.2.2 shows the fuel-clad gap thickness. As expected, the gap quickly decreases near BOC as the rod expands from CZP to HFP, and it gradually continues to decrease with burnup. In the single assembly demonstration report [13], large discrepancies were observed as the 1.5D case achieved contact much quicker than the 2D case. Fortunately, issues in the input specification were identified and resolved with help from Stephanie Pitts (INL) of the Bison team, and much better agreement is observed with respect to gap closure.

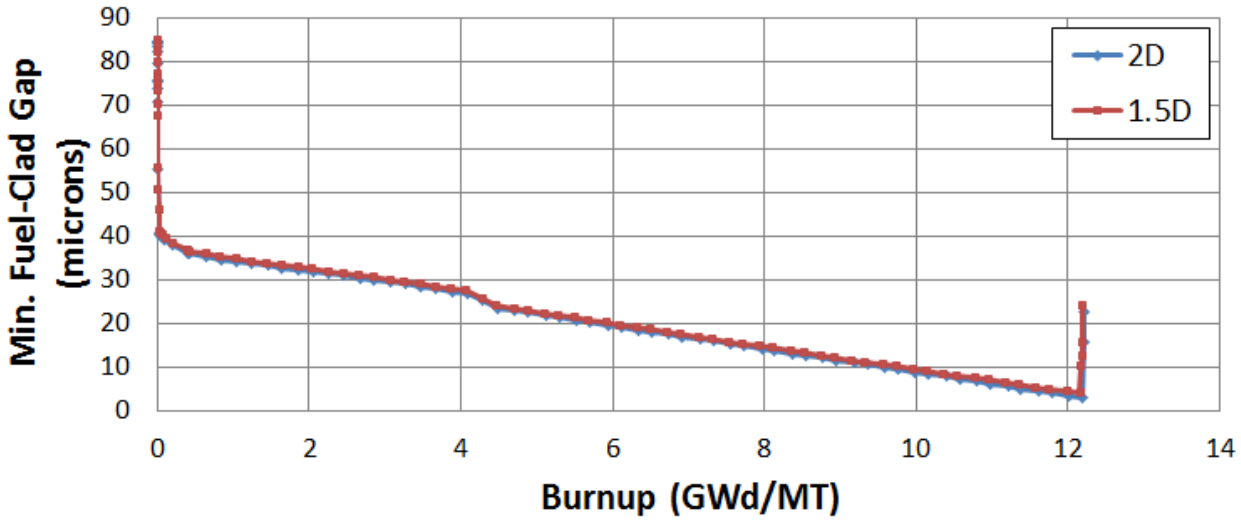

Figure 3.2.2. Minimum Fuel-Clad Gap Thickness [microns] Comparison between 1.5D and 2D-RZ Standalone Bison Cases.

Figures 3.2.3 and 3.2.4 show the average and maximum centerline fuel temperatures. In the previous report, ~50 K differences were seen, but with the new input modifications, differences of roughly 20 K are observed.

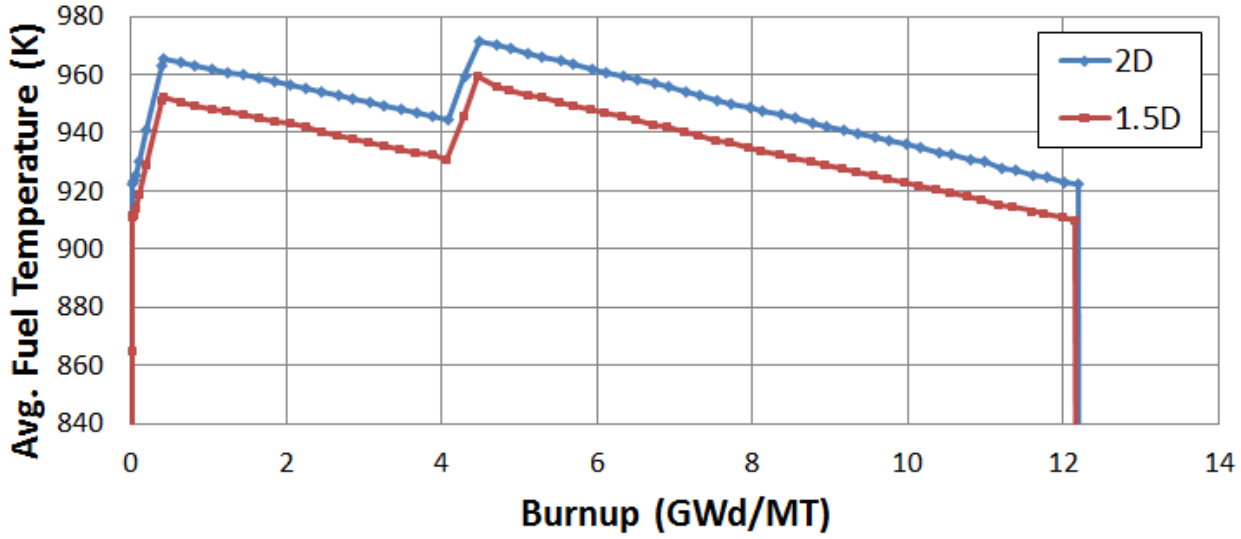

Figure 3.2.3. Average Fuel Temperature (K) Comparison between 1.5D and 2D-RZ Standalone Bison Cases.

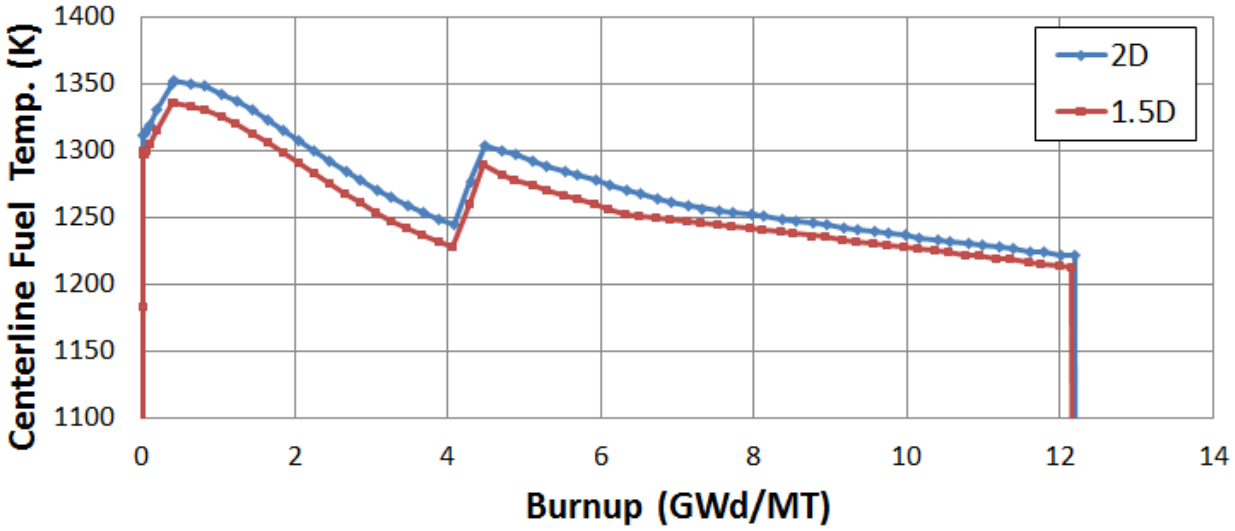

Figure 3.2.4. Maximum Centerline Fuel Temperature (K) Comparison between 1.5D and 2D-RZ Standalone Bison Cases.

4. QUARTER CORE DEMONSTRATION

4.1 Watts Bar Unit 1, Cycle 1 Description

The Watts Bar Nuclear Plant is a Westinghouse four-loop PWR operated by the Tennessee Valley Authority (TVA) and has been online since 1996. It began with a 3,411 MWth power rating, but it had a 1.4% power uprate in 2001. It is currently operating in its fifteenth cycle, logging over 6,000 effective full power days (EFPDs) of operation [20].

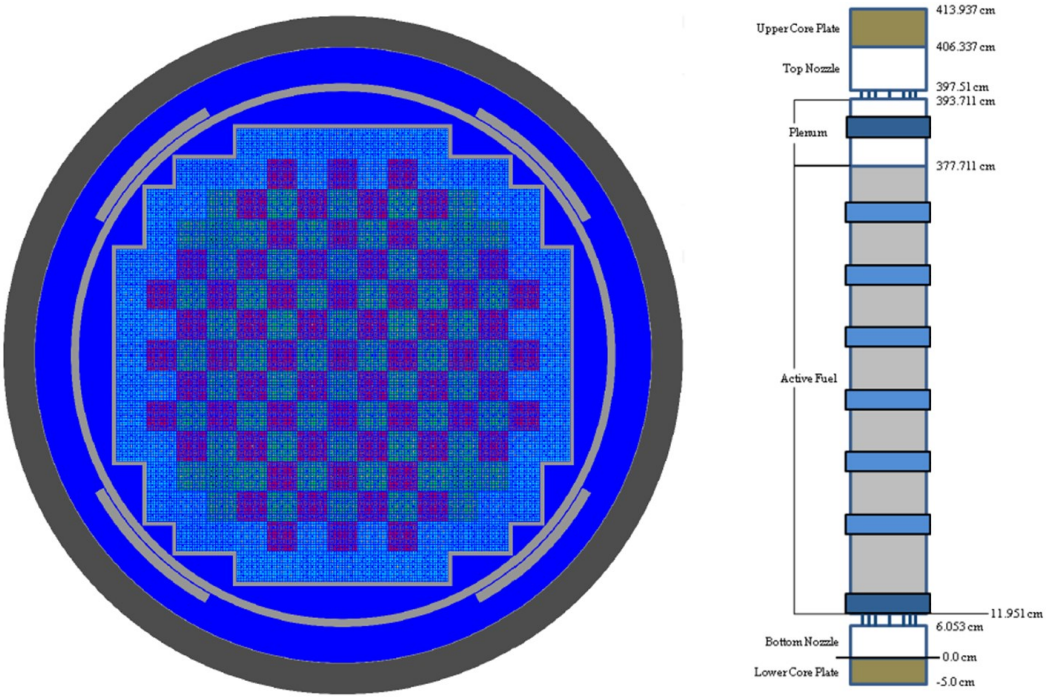

Figure 4.1.1. Watts Bar Unit 1 – Core Geometry.

The left component of Figure 4.1.1 shows a 2D slice of the WBN1 Cycle 1 full core layout. VERA currently does not model the core barrel, pads, or vessel, which are shown in the diagram. The unit has 193 Westinghouse 17 × 17 fuel assemblies which are 12 feet tall with 264 fuel rods and 25 guide/instrumentation tubes. On the right side of Fig. 4.1.1 is a typical axial layout of a fuel assembly used in the nonproprietary model. It includes upper/lower core plate, nozzles, and gaps, with two Inconel and six Zircaloy spacer grids. Figure 4.1.2 shows the core layout in Cycle 1; each assembly is color-coded based on enrichment, and select assemblies include the number of Pyrex rods in the assembly.

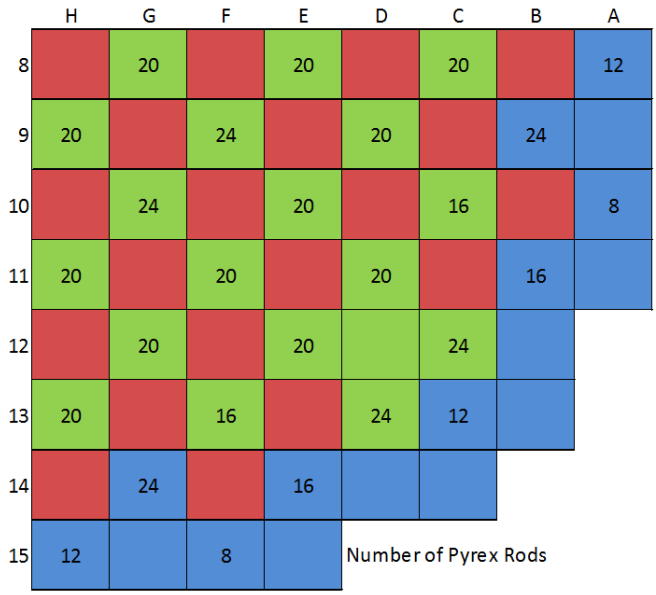

Figure 4.1.2. Watts Bar Unit 1 – Cycle 1 Core Layout [16].

Figure 4.1.3 shows the idealized power history for Cycle 1 that was used in the VERA simulation. Cycle 1 has a more gradual ramp to power than is seen in subsequent cycles. Shortly after 14 gigawatt-days per metric ton (GWd/MT) in Cycle 1, VERA imposes a step change to 86.9% power. This change can pose a problem for Tiamat, so a small burnup increment of 0.05 GWd/MT was added to each point in the step change as an approximation. At all other statepoints, Bison uses a linear interpolation of the power.

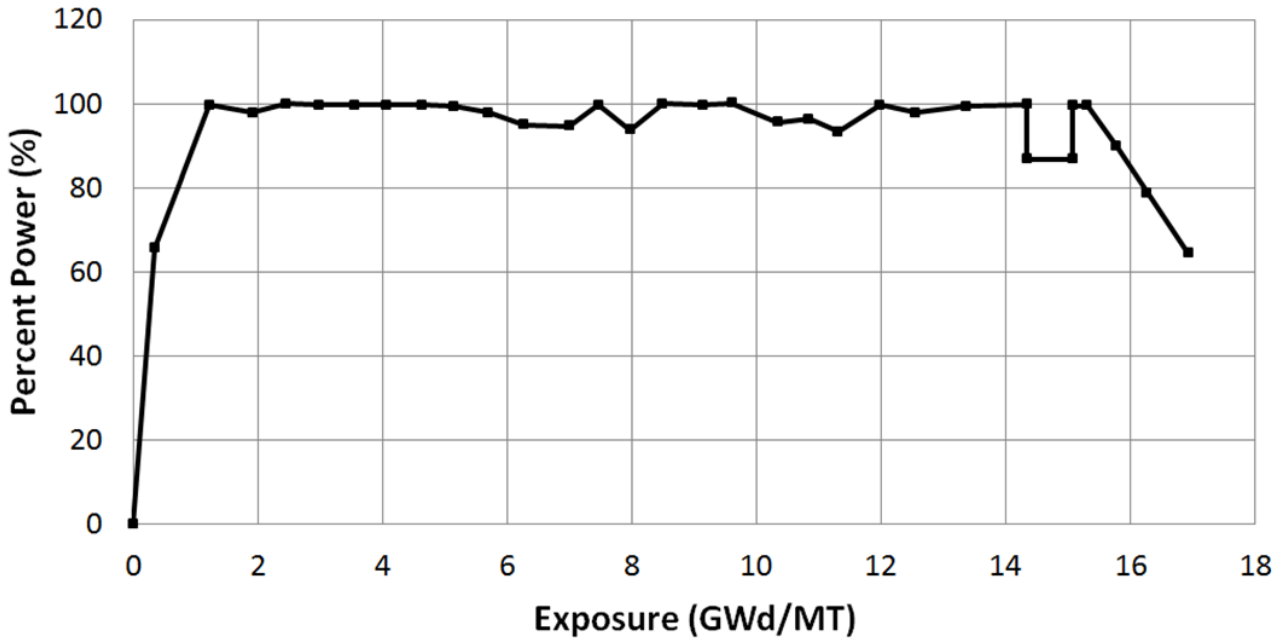

Figure 4.1.3. Watts Bar Unit 1 – Cycle 1 VERA Power History [18].

4.2 Results

The quarter core cases demonstrated here were executed on the Panacea cluster. The Tiamat-Coupled case was executed on 1,984 cores (900 MPACT/CTF and 1040 Bison). This yields 12–13 Bison rods per process and an overall runtime of roughly 67 hours (~133,000 core-hours). The Tiamat-Inline case took roughly 36 hours on 1,504 cores (~54,000 core-hours). For comparison, a similar case of just MPACT/CTF recently took around 36,000 core-hours. Therefore, for Tiamat-Inline, roughly 1.5× the resources of MPACT/CTF alone would be required, and for Tiamat-Coupled roughly 3–4× would be needed.

The remainder of this section focuses on the fully coupled results, particularly the performance. Figure 4.2.1 shows the timing per statepoint, where much of the fluctuation comes from the time spent solving in Bison. This holds true expect for the last three statepoints, which also require more outer iterations than usual. Therefore, all three codes used more time than usual, but the states with the highest Bison runtime are the two states included in the ramp to HFP and the states involving the changes in power between 14 and 15 GWd/MT.

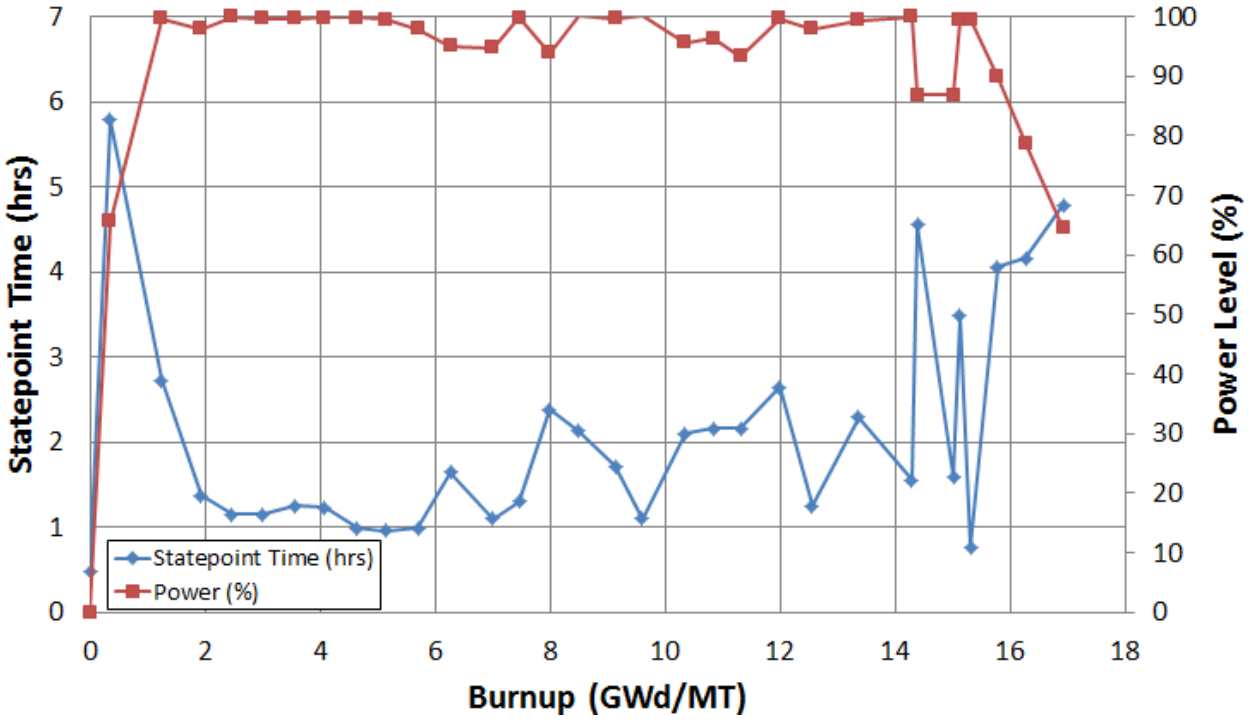

Figure 4.2.1. Watts Bar Unit 1 – Cycle 1, Fully Coupled Tiamat Timing Per Statepoint.

Figure 4.2.2 shows a similar plot, except the statepoint run time is compared to the absolute change in core power. As expected, the runtime tends to increase along with the changes in power.

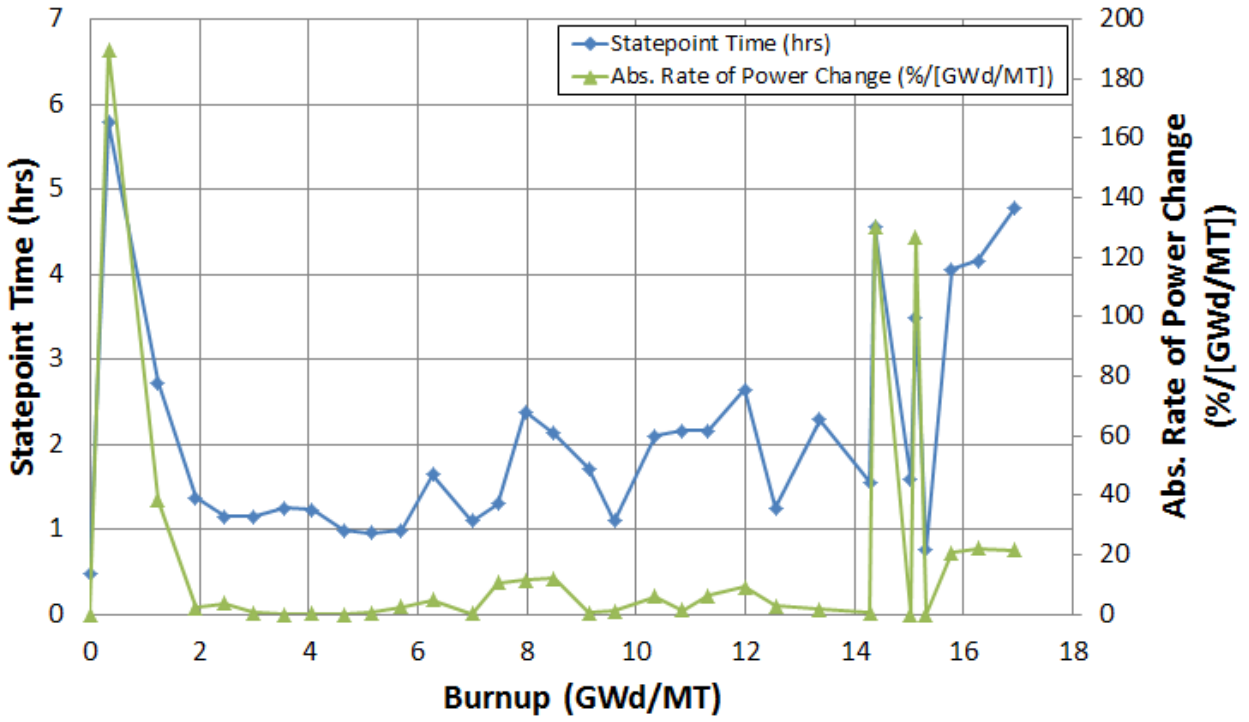

Figure 4.2.2. Watts Bar Unit 1 – Cycle 1, Fully Coupled Tiamat Timing per Outer Statepoint re the Change in Core Power.

Figure 4.2.3 shows the timing per outer iteration for the fully coupled case for all states. The timing components are divided into two categories: (1) MPACT+ORIGEN and (2) CTF+Bison. This was done because of how the timing data are reported to the log file. Since CTF and Bison are run concurrently, it is difficult to distinguish the runtime of each from the log file, but Bison is likely a using most of the time based on comparisons to outer iterations in MPACT/CTF calculations.

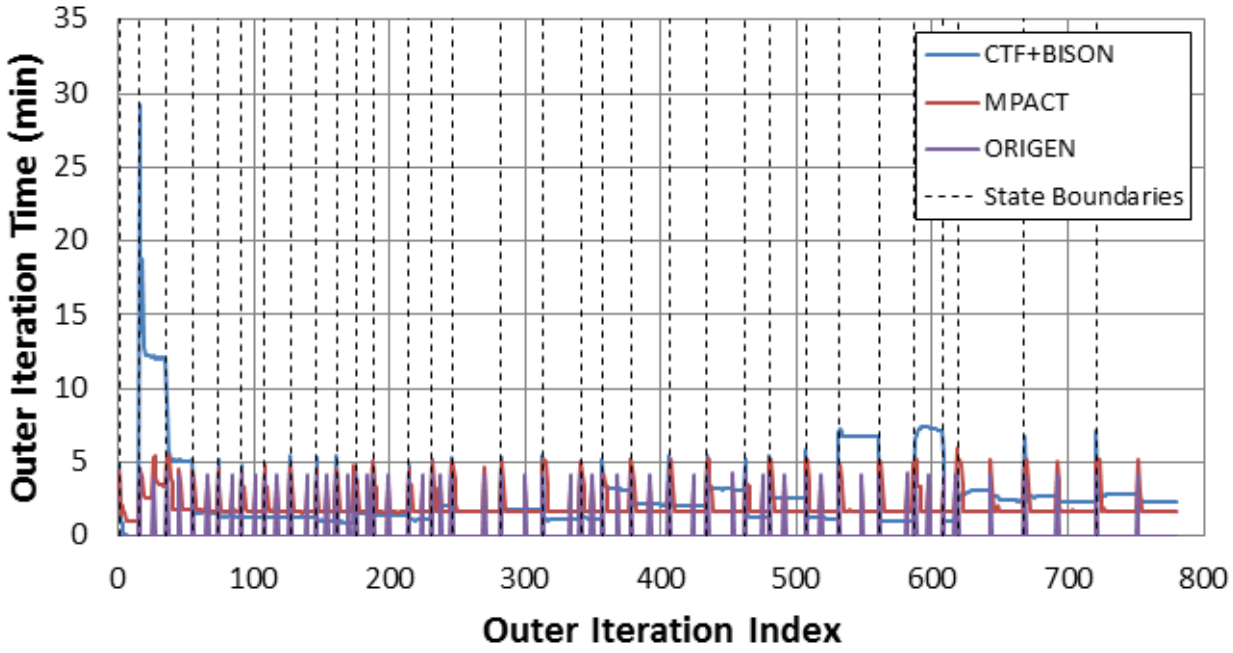

Figure 4.2.3. Watts Bar Unit 1 – Cycle 1, Fully Coupled Tiamat Timing per Outer Iteration.

Figure 4.2.4 shows the timing results with CTF and Bison only. It can be seen that in the second state, which is ramping to 65.7% power, Bison is taking roughly 12 minutes per outer iteration, which is much higher than the 1–2 minutes needed for most statepoints. It spikes later in the cycle during the change in power to and from 86.9% power, with Bison taking 7–8 minutes per outer iteration.

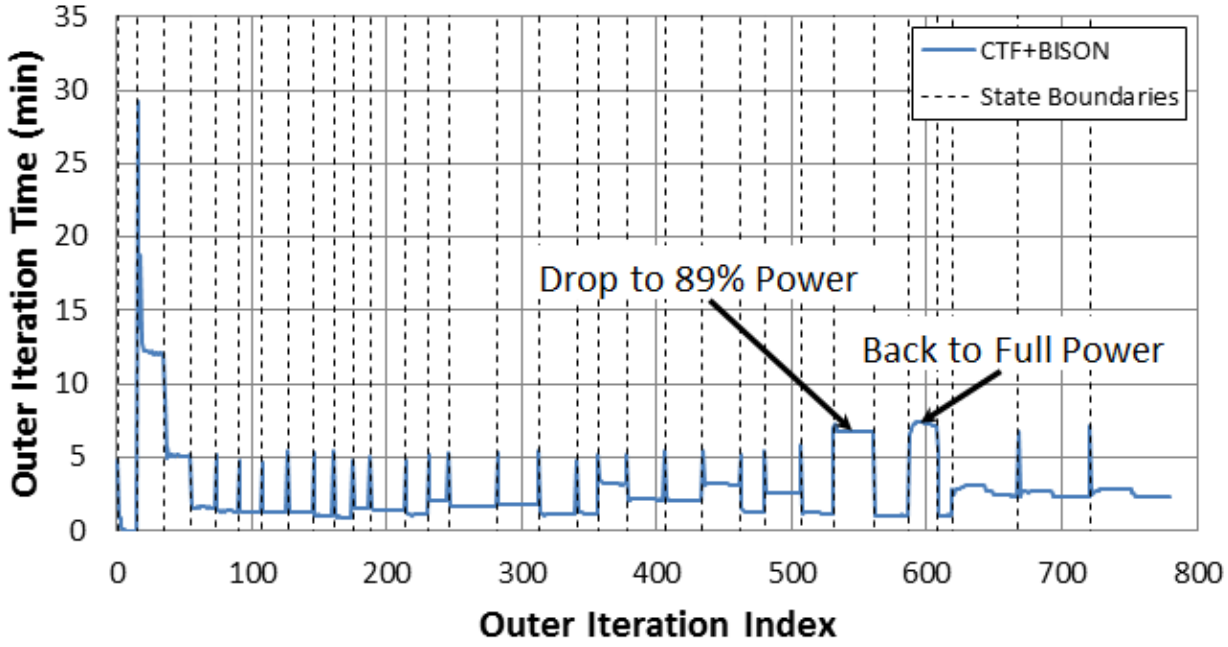

Figure 4.2.4. Watts Bar Unit 1 – Cycle 1, Fully Coupled Tiamat Timing per Outer Iteration (Only CTF/Bison).

A better visual of what occurs early in the calculation is provided in Figure 4.2.5, which shows the same timing data, but for only the first 4 statepoints. From this figure, it is much easier to see some of the noteworthy characteristics. For example, the predictor and corrector steps, which are the only contribution of ORIGEN to the runtime, can easily be identified from the spike in MPACT+ORIGEN data. Additionally, Bison run time increases dramatically during the second state, which is the 65.7% power statepoint in the ramp to HFP. Because of this increase, State 2 took a total of 6 hours to complete compared to the rough average of 1–2 hours for the rest of the statepoints. The Bison runtime is still elevated during the third state, which is nearly full power, but eventually the Bison time per outer iteration becomes comparable to the MPACT runtime for the rest of the calculation. However, that is with the exception of the first outer iteration in each statepoint, which is where the HDF5 data are collected from Bison and written to the file.

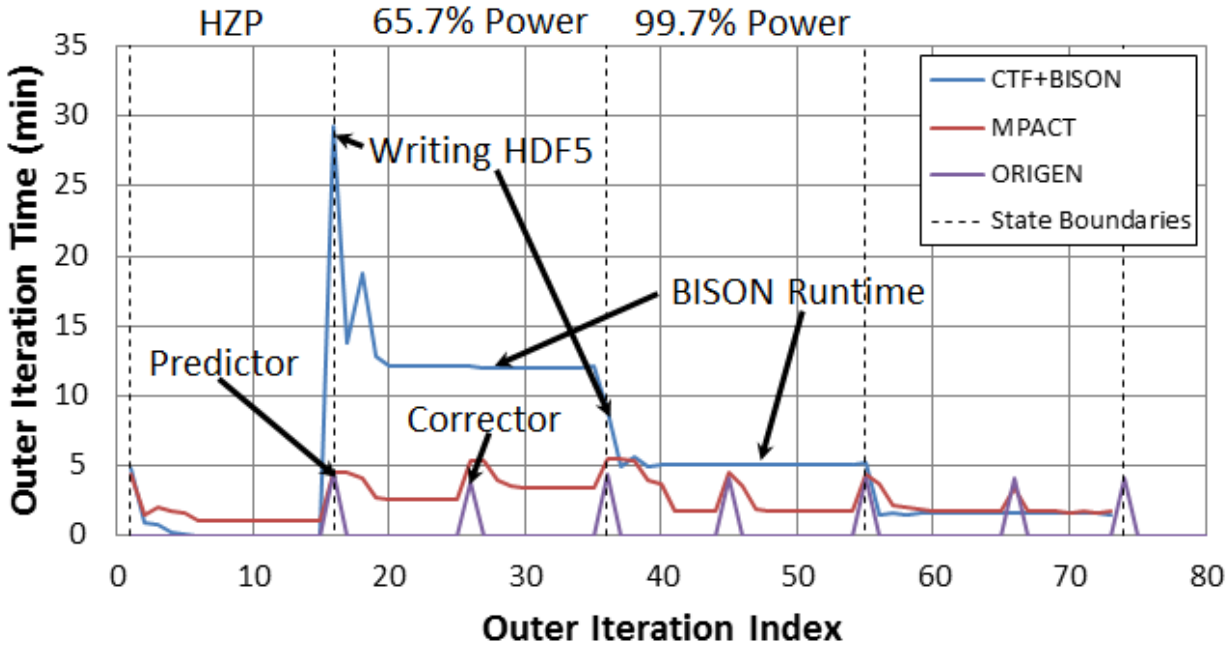

Figure 4.2.5. Watts Bar Unit 1 – Cycle 1, Fully Coupled Tiamat Timing per Outer Iteration (First 4 Statepoints).

Figures 4.2.6–4.2.9 showcase the quarter core Tiamat-Coupled results for (1) average fuel temperature, (2) fuel-clad gap, (3) maximum clad hoop stress, and (4) burnup. All figures show the results for near BOC (left) and near EOC (right) with the radial distributions at ~200 cm axially (about mid-core) shown on the top and the axial profiles near the north boundary shown on the bottom. The full set of results for all statepoints is shown in Appendix A.

In Figure 4.2.6, the fuel temperature is seen to peak near the beginning of the cycle at the first hot full power statepoint. At this point, the fuel has essentially only experienced thermal expansion with basically negligible depletion/irradiation effects (densification, swelling, creep, etc.). For this reason, the fuel temperatures are highest because the fuel-clad gap is still large (as can be seen in Figure 4.2.7). As the cycle progresses, it can be seen that the fuel-clad gap closes for most of the rods by EOC, and the fuel temperature distribution flattens out considerably. Much of this is also attributable to the flattening of the power distribution, as the higher enriched assemblies and Pyrex burnable absorbed rods have depleted and the peaking is reduced.

For much of the cycle, the clad hoop stress values (Figure 4.2.8) are negative they are driven by the difference between the rod's internal pressure (~1–2 MPa) and the coolant pressure (~15 MPa). With a higher external pressure, a compressive force is applied to the cladding. About two thirds of the way through the cycle, fuel-clad contact begins to occur, and the hoop stress values begin to increase and become tensile as the fuel applies force to the clad. The peak hoop stress value of ~27 MPa is very similar to results obtained with a standalone one-way coupling using 2D-RZ rods at roughly 30 MPa.

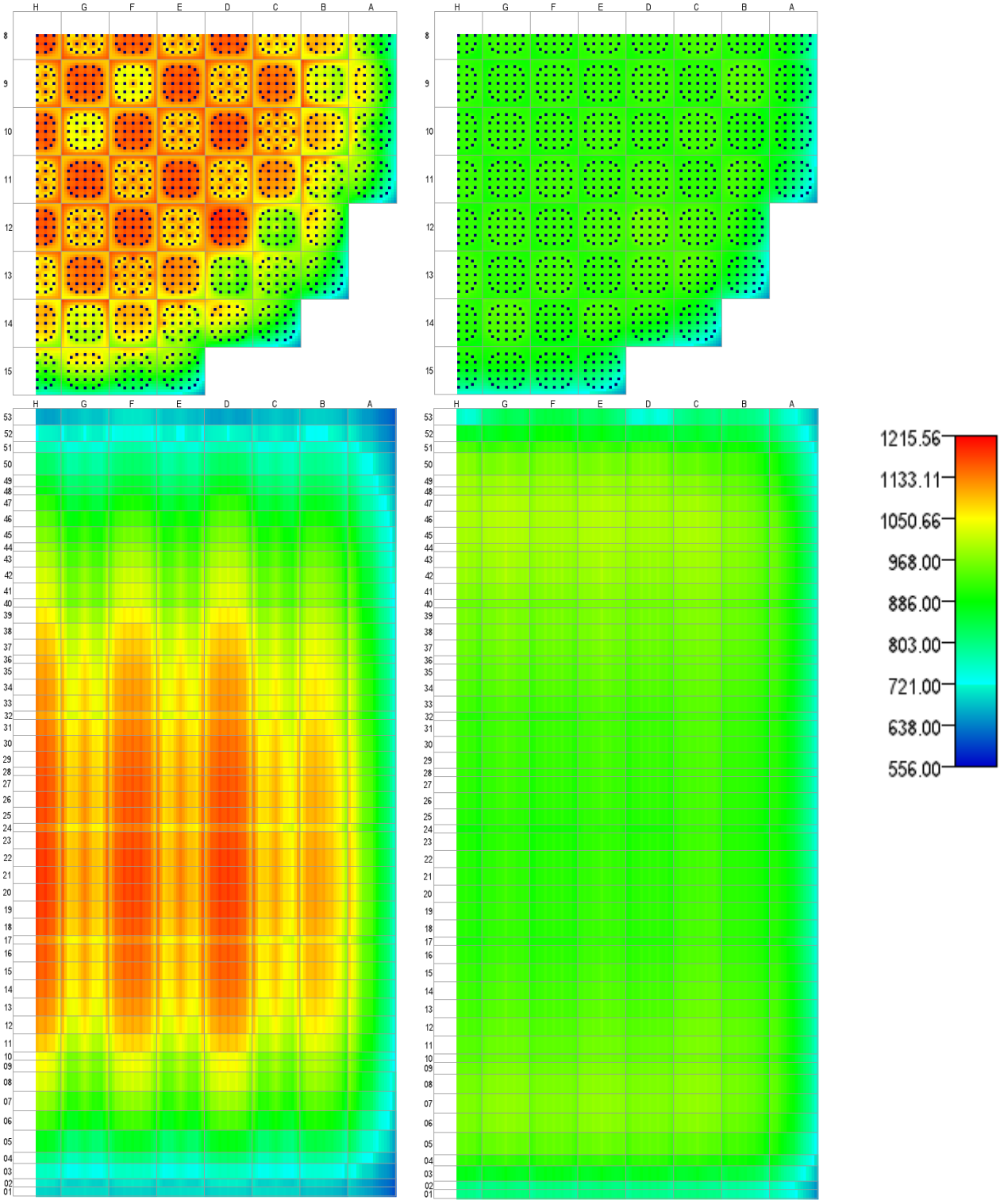

Figure 4.2.6. Watts Bar Unit 1 – Cycle 1, Average Fuel Temperature (K) Distributions.

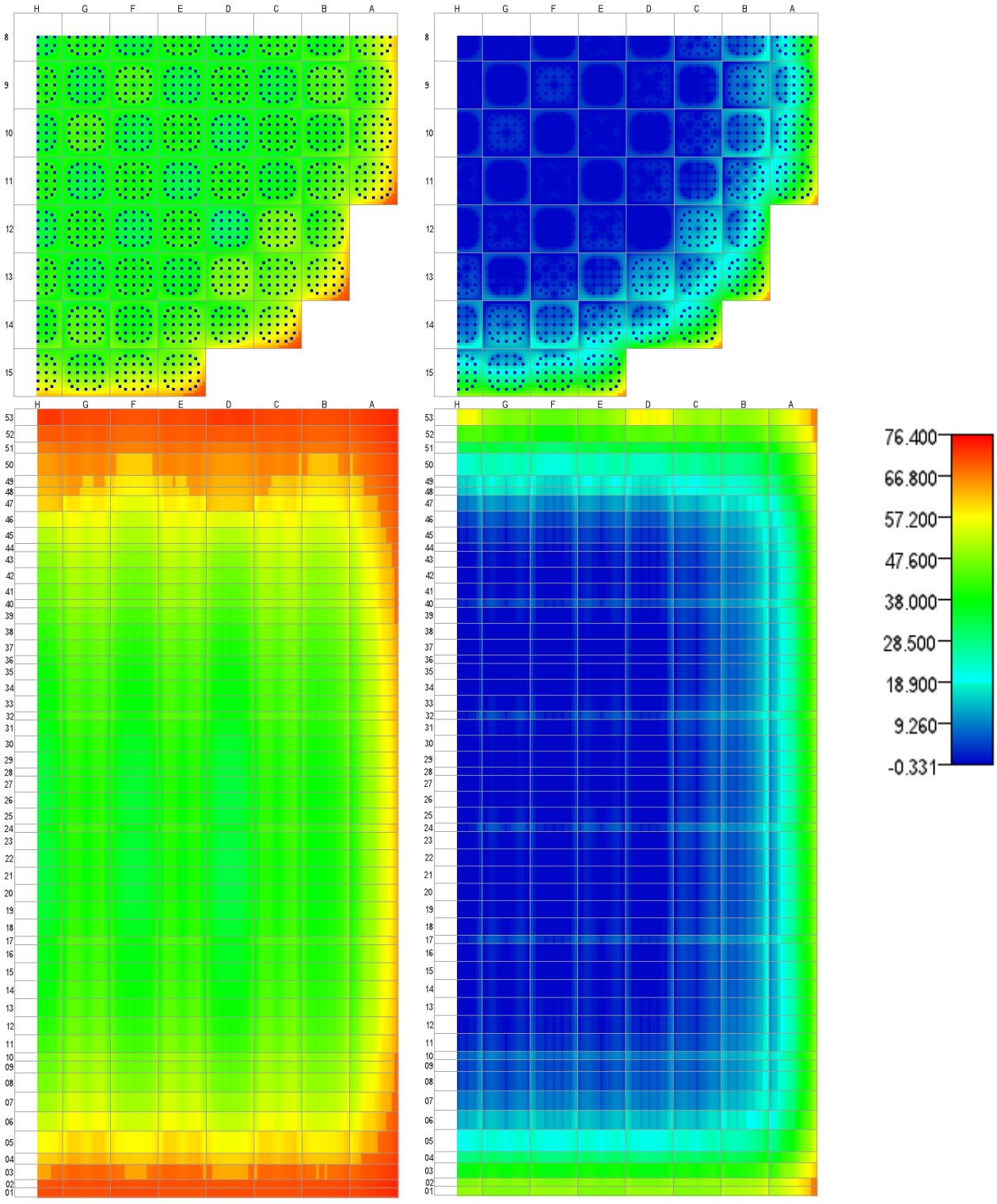

Figure 4.2.7. Watts Bar Unit 1 – Cycle 1, Fuel-Clad Gap (microns) Distributions.

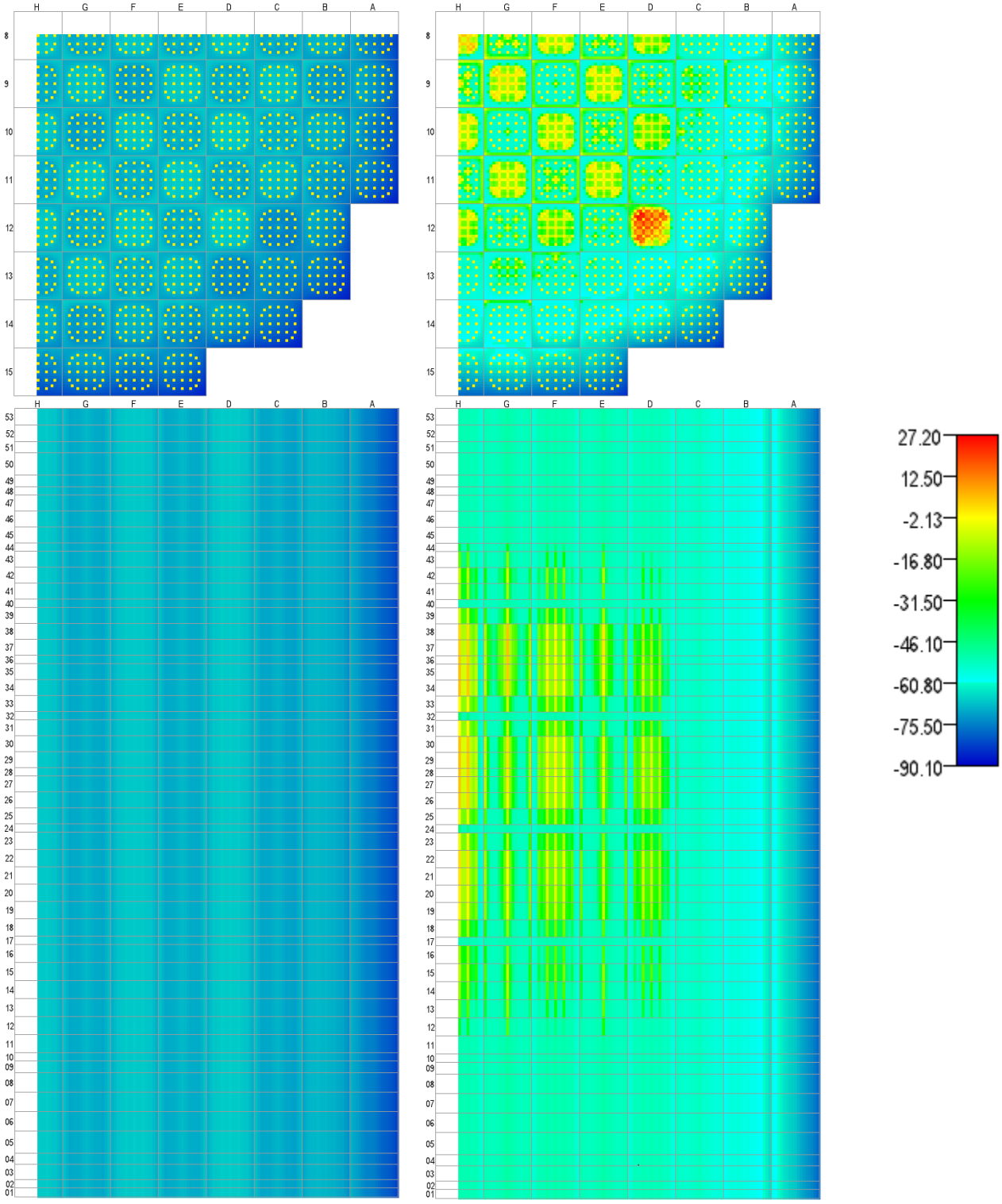

Figure 4.2.8. Watts Bar Unit 1 – Cycle 1, Maximum Clad Hoop Stress (MPa) Distributions.

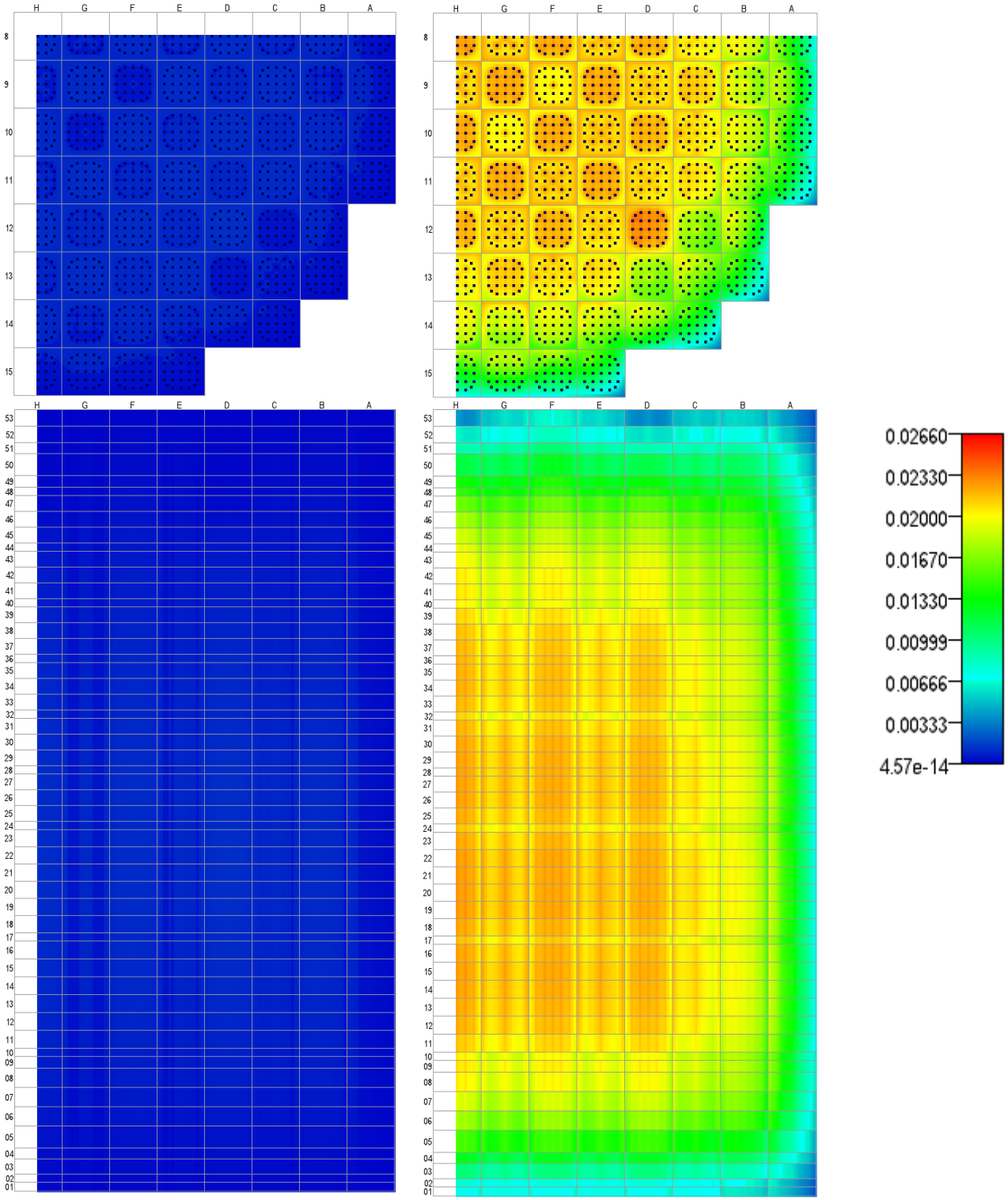

BOC **EOC**

Figure 4.2.9. Watts Bar Unit 1 – Cycle 1, Burnup [fima] Distributions.

4.3 Aggregate Component Timing Discussion

Because of how the Coupled calculation is performed where both CTF and BISON are run concurrently, we do not current have the timer information separating CTF from BISON. However, aggregate timing information is reported at the end of the Tiamat simulation, which allows for greater insight into the run time of various components. Despite 15 hours lost during the simulation due to a file system outage, aggregate timing estimates of various components are available per Figure 4.3.1.

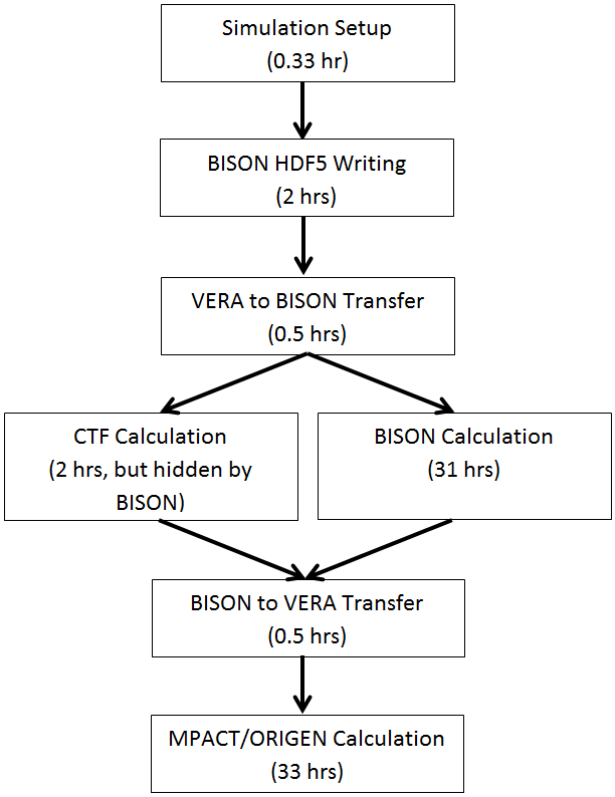

Figure 4.3.1. Estimated Timing Breakdown of Tiamat Components

From this we see that roughly 49% of the approximately 67 hour walltime is spent performing MPACT and ORIGEN calculations, 46% is spent running BISON, 3% gathering data and writing to the HDF5 file, approximately 1.5% performing transfers between VERA and BISON, and 0.5% performing initialization. It is worth noting that nearly 2 hrs is spent performing the CTF calculations, but most (if not all) of this is hidden by the BISON runtime.

Table 4.3.1 shows a timing comparison between the two modes of operation in Tiamat (Coupled and Inline) and MPACT/CTF calculations without BISON. For clarity, whereas Tiamat Coupled solves MPACT, CTF, and BISON every outer iteration and feeds BISON fuel temperature back to MPACT/CTF, Tiamat Inline performs a one –way coupling between MPACT/CTF and BISON, feeding no information back from BISON. With this approach, much of the BISON run time can be hidden to limit the impact on walltime as BISON calculations lag a statepoint and run concurrently with MPACT/CTF. In each of the three cases, MPACT uses 900 cores, of which 193 are active during the CTF solve and 707 are idle. For the cases with Bison, Inline uses an additional 604 cores for Bison, and Coupled uses an additional 1,084 cores for a total of 1,504 and 1,984, respectively.

Table 4.3.1. Timing Breakdown Comparison between Coupled, Inline, and MPACT/CTF

Calculation Step	Time (hrs)			Comments
	Coupled	Inline	MPACT/CTF	
Simulation Setup	0.33	0.33	0.33	
BISON HDF5 Writing	2.00	1.00	---	Reduced in Inline because lower number of BISON cores
VERA to BISON Transfer	0.50	0.02	---	Reduced in Inline as it is only called once per statepoint
CTF Calculation	*2.00*	2.00	2.00	Same, but not masked in Inline by BISON runtime
BISON Calculation	31.00*	*2.70*†	---	Once per statepoint in Inline; mostly masked by MPACT/CTF time
BISON to VERA Transfer	0.50	---	---	Not called in Inline
MPACT/ORIGEN Calculation	33.00	33.00	33.00	

Italics indicate that most or all of the time has no impact on overall walltime as it is hidden by other components

* Coupled was executed with 1,084 cores for BISON over a total of 780 outer iterations

† Inline was executed 604 cores for BISON with a total of 32 BISON calculations (once per statepoint)

4.4 Reactivity and Power Comparisons to Tiamat-Inline

One possible important comparison from the Tiamat-Coupled and Tiamat-Inline cases is to assess the effect of using temperature tables on the reactivity and power distribution in MPACT. For example, MPACT/CTF cases and Tiamat-Inline both use a 2D-RZ Bison-generated temperature table, whereas Tiamat-Coupled updates the fuel temperatures in MPACT directly from the Bison calculations being performed. This can impact the reactivity and power distributions throughout the core. It is understood that there are some differences between 2D-RZ, which is used in the temperature table, and 1.5D, which is used in Tiamat-Coupled, so some differences are expected. However, the temperature table is generated using several uniform LHR cases, and the history effects of the time-dependent behavior is difficult to discern, particularly as the power distribution changes with depletion.

Figure 4.4.1 shows the critical boron concentration as a function of burnup for three different cases: (1) MPACT/CTF with the current default temperature table, (2) Tiamat-Inline with a temperature table more consistent with the current Bison templates used in Tiamat, and (3) Tiamat-Coupled results with fuel temperature feedback from Tiamat. The current default temperature table used in MPACT/CTF has lower fuel temperatures than the most recent table. Several adjustments have been made to default values in the Bison templates that have led to higher temperatures, but the newest table (as used in Tiamat-Inline) has not been made default yet. As such, reactivity differences between MPACT/CTF and Tiamat (~15–20 ppm) are expected. Comparing inline to coupled Tiamat, which has more consistent temperature table and template values, good agreement is observed in reactivity, with a 1–2 ppm difference throughout most of the cycle.

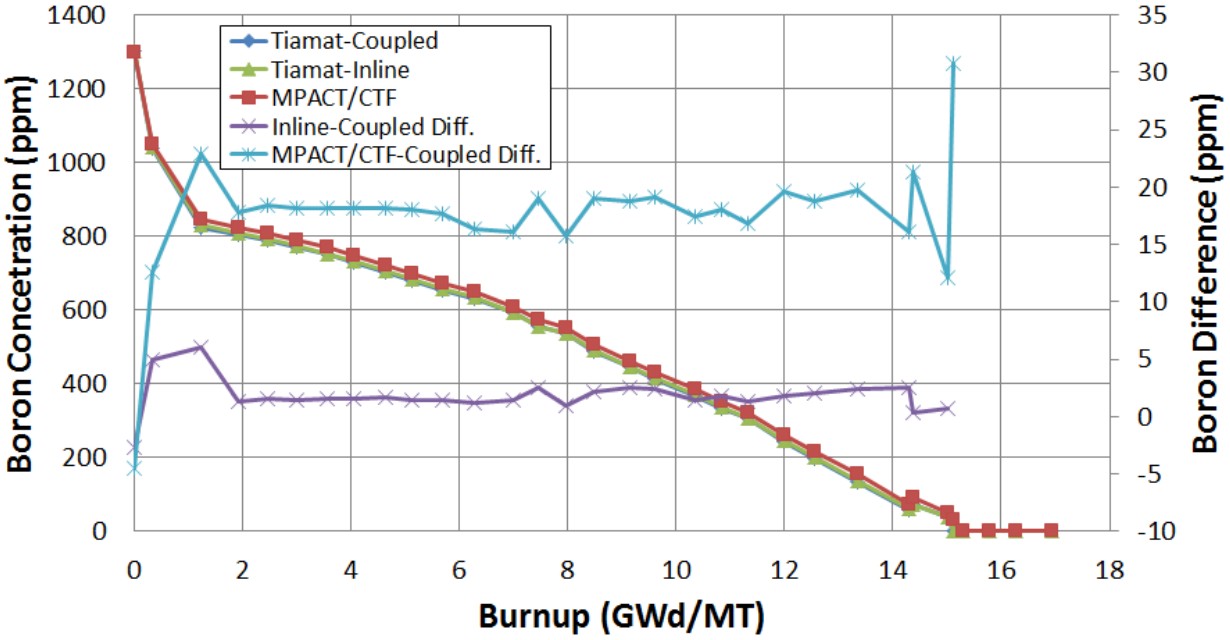

Figure 4.4.1. MPACT/CTF, Inline, and Coupled Boron Letdown Curves.

Table 4.4.1 shows the root mean square (RMS) and maximum (MAX) differences between the power distributions reported from Tiamat-Inline and Tiamat-Coupled. A maximum difference of roughly 1% is observed at the first HFP statepoint at 1.230 GWd/MT with a typical maximum around 0.3–0.4% for most states and a typical RMS near 0.15%.

Table 4.4.1. Difference in Inline and Coupled Normalized Power Distributions

State	Burnup (GWd/MT)	RMS (%)	MAX (%)
1	0.000	0.018	0.061
2	0.346	0.218	0.543
3	1.230	0.445	1.053
4	1.919	0.172	0.592
5	2.457	0.182	0.428
6	2.994	0.152	0.377
7	3.562	0.131	0.331
8	4.065	0.146	0.370
9	4.642	0.128	0.338
10	5.139	0.238	0.583
11	5.700	0.140	0.348
12	6.273	0.161	0.420
13	7.000	0.173	0.428
14	7.463	0.163	0.379
15	7.978	0.195	0.474
16	8.493	0.174	0.423
17	9.140	0.109	0.391
18	9.602	0.153	0.364
19	10.344	0.122	0.308
20	10.842	0.125	0.321
21	11.314	0.140	0.361
22	11.988	0.279	0.659
23	12.552	0.058	0.174
24	13.360	0.133	0.357
25	14.285	0.063	0.218
26	14.385	0.136	0.410
27	15.018	0.114	0.288
28	15.118	0.317	0.689
29	15.308	0.066	0.207
30	15.774	0.073	0.203
31	16.270	0.150	0.399
32	16.932	0.416	0.969

Figure 4.4.2 shows a similar radial and axial profile as in Figures 4.2.6–4.2.9, except for the pin power differences between Tiamat-Inline and Tiamat-Coupled (Inline minus Coupled). The range of pin power differences is typically between -1.0% and 1.0%.

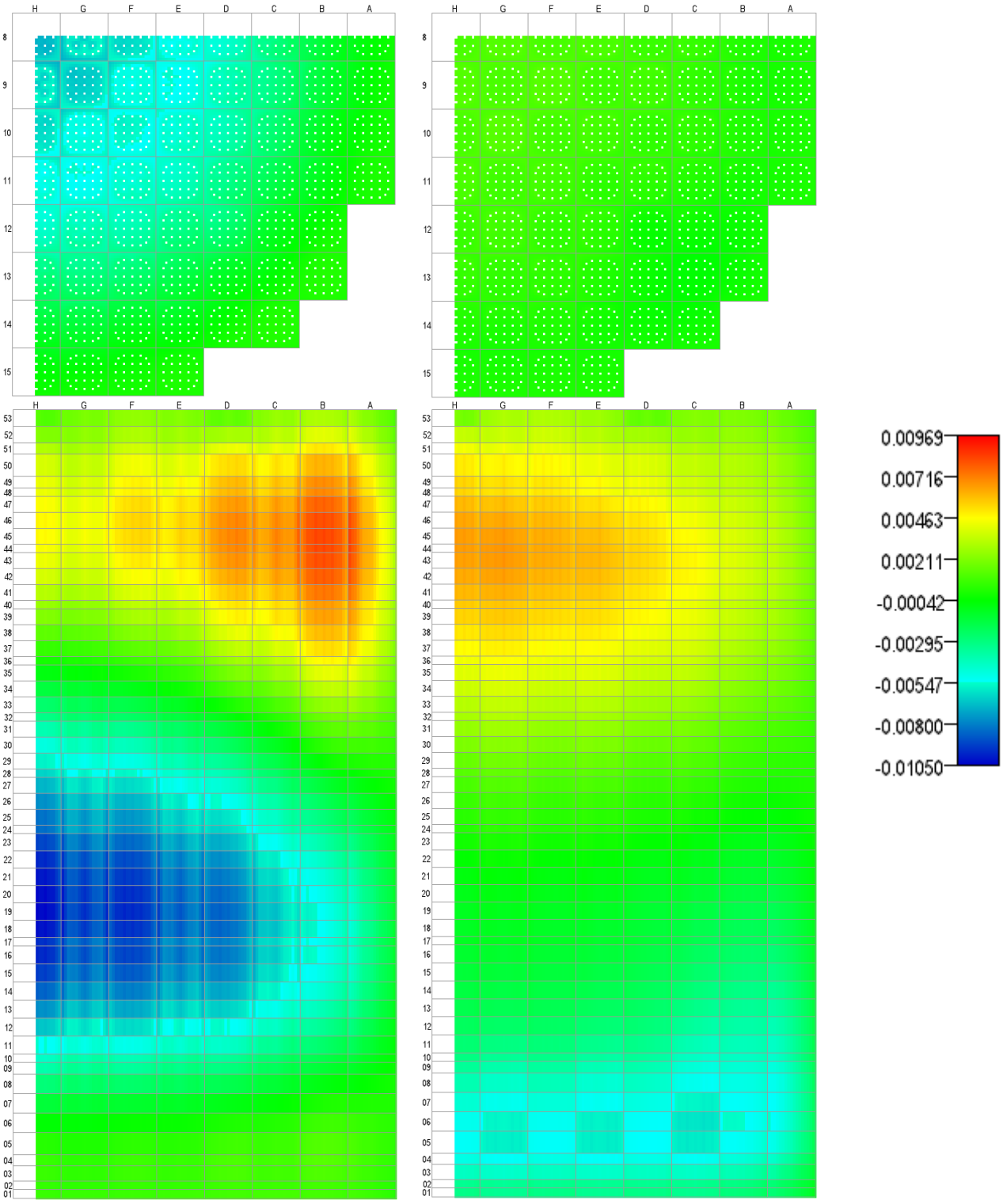

Figure 4.3.2. Watts Bar Unit 1 – Cycle 1, Normalized Pin Power Differences between Tiamat-Inline and Tiamat-Coupled.

These results show that the reactivity effect (< 2 ppm) is small, though the power distribution impact is more noticeable at roughly 1% maximum difference. Some differences are expected because of known differences between the 2D-RZ and 1.5D approaches, but in general, the impact seems small.

The fact that the reactivity effect is fairly constant throughout the cycle suggests that the history effects neglected by the temperature tables are likely small.

5. CONCLUSIONS AND FUTURE WORK

This report presents the latest efforts in developing and demonstrating a coupled Tiamat capability, highlighting the results gathered from quarter core calculations of Watts Bar Unit 1, Cycle 1. Comparisons are also presented between the coupled and inline Tiamat modes of operation. In total, the coupled calculation required ~133,000 core-hours (67 hours on 1,984 cores). For comparison, the inline case took ~54,000 core-hours (36 hours on 1,504 cores) and MPACT/CTF alone took ~36,000 core-hours. Much of the additional time spent performing the couple calculation is spent in Bison, so future efforts to improve the runtime of the 1.5D capability will likely be very effective in reducing the overall run time of the entire calculation. Many of the results looked very similar to those obtained from the standalone capability, which used the 2D-RZ models. Specifically, coupled Tiamat predicts a peak hoop stress of 27.2 MPa, which can be directly compared to the ~30 MPa estimated in standalone. In general, the fuel temperatures are higher than in the current default temperature table used in MPACT/CTF, but this is expected due to some default parameter changes that have occurred since that table was generated.

While this milestone has been successful in demonstrating the capability, there is room for future extensions and improvements. In particular, MPACT currently passes a radially averaged power profile over each axial slice, and Bison approximates the intrapellet radial power profile using an internal model. Passing the radial power distribution from MPACT, potentially in the form of a radial shape function, would improve the consistency between MPACT and Bison. Additionally, recent analyses were performed to assess the impact of passing the clad fast flux from MPACT into Bison [21] instead of using a fast flux factor, which is the default. Similar changes should be made in Tiamat to allow for a more explicit representation of the clad fast flux distribution, which can impact clad creep and growth.

Another improvement would be to overlap the MPACT and Bison cores. At present, separate cores are used for MPACT and Bison, but in the coupled algorithm, it was seen that MPACT and Bison are never run concurrently, so the calculations for these could be performed on the same processors. One concern with this is memory, as MPACT typically requires 2.0–2.5 GB per process for 3D quarter core problems when run on ~1000 cores. Each Bison rod requires ~100MB of memory, and 14–18 rods would need to be shared by each processor. On machines with 4 GB per core, this could be a tight fit, but it has a large payoff in guaranteeing a more efficient use of each processor.

Future work should also focus on extending the application space of Tiamat to include both multicycle cases, leveraging the existing restart capability, and also transient cases in support of other challenge problems, such as with LOCA. In transient cases, it is more likely that having a coupled methodology between MPACT, CTF, and Bison will have the largest impact on accuracy and fidelity.

6. ACKNOWLEDGMENTS

The authors also wish to acknowledge the Tennessee Valley Authority and the Westinghouse Electric Company for their data contributions to build the VERA simulation models. Many thanks are also due to Michael Galloway, Mark Baird, and Jeffrey Banta for their help in getting the simulations completed on the Panacea cluster, and also to Stuart Slattery for his time in sorting out performance issues related to how Tiamat was interfacing with DTK.

This work was supported by the Consortium for Advanced Simulation of Light Water Reactors (www.casl.gov), an energy innovation hub (http://www.energy.gov/hubs) for modeling and simulation of nuclear reactors under US Department of Energy (DOE) Contract No. DE-AC05-00OR22725.

Many of the figures shown here were generated using the VERAView software package [22].

7. REFERENCES

1. B. Collins et al., "Simulation of CRUD Induced Power Shift Using the VERA Core Simulator and MAMBA," *Proc. of PHYSOR 2016*, Sun Valley, Idaho, USA (May 1–5, 2015).
2. *MPACT TEAM, MPACT Theory Manual*, Version 2.0.0, Technical Report CASL-U-2015-0078-000, Oak Ridge National Laboratory and University of Michigan (2015).
3. B. Collins et al., "Stability and Accuracy of 3D Neutron Transport Simulations Using the 2D/1D Method in MPACT," *Journal of Computational Physics*, **326**, 612 (2016).
4. B. Collins et al., "Assessment of 2D/1D Capability in MPACT," *Proc. PHYSOR 2014*, Kyoto, Japan, September 28–October 3 (2014).
5. S. G. Stimpson, B. S. Collins, and T. J. Downar, "Axial Transport Solvers for the 2D/1D Scheme in MPACT," *Proc. PHYSOR 2014*, Kyoto, Japan, September 28–October 3 (2014).
6. M. N. Avramova, *CTF: A Thermal Hydraulic Sub-Channel Code for LWR Transient Analyses, User's Manual*. Technical Report, Pennsylvania State University, Department of Nuclear Engineering (2009).
7. R. O. Montgomery et al., "Peregrine: Advanced modeling of pellet-cladding interaction (pci) failure in lwrs," in: *Proc. TopFuel 2012 Reactor Fuel Performance Conference*. Manchester, United Kingdom (2012).
8. R. O. Montgomery et al., "Advanced pellet-cladding interaction modeling using the US DOE CASL fuel performance code: Peregrine," in: *Transactions of the American Nuclear Society Anual Meeting*. Reno, Nevada (2014).
9. D. Gaston et al., "Moose: A parallel computational framework for coupled systems of nonlinear equations," *Nuclear Engineering Design,* 239: pp. 1768–1778 (2009).
10. R. Williamson et al., "Multidimensional multiphysics simulation of nuclear fuel behavior," *Journal of Nuclear Materials*, 423: pp. 149–163 (2012).
11. R. P. Pawlowski et al., "Design of a high fidelity core simulator for analysis of pellet clad interaction," *Proc. M&C 2015*, Nashville, TN, USA (2015).
12. K. T. Clarno et al., "High fidelity modeling of pellet-clad interaction using the CASL virtual environment for reactor applications," *Proc. M&C 2015*. Nashville, TN, USA (2015).
13. S. Stimpson et al., *Demonstration of Coupled Tiamat Single Assembly Calculations*, CASL-U-2017-1357-000, Oak Ridge National Laboratory (June 16, 2017).
14. J. D. Hales et al., *1.5D Bison Simulation Capability*, CASL-U-2017-1260-000 (2017).
15. S. A. Pitts et al., *Verify and Validate 1.5D Capability, L3:FMC.FUEL.P15.05*, CASL-U-2017-1380-000 (2017).
16. A. T. Godfrey, *VERA Core Physics Benchmark Progression Problem Specifications*, CASL-U-2012-0131-004 (2014).
17. S. Stimpson, K. Clarno, J. Powers, and R. Pawlowski, *Standalone Bison Fuel Performance Results for Watts Bar Unit 1, Cycles 1-3*, CASL-I-2015-1010-001, Oak Ridge National Laboratory (March 7, 2016).
18. S. G. Stimpson, J. J. Powers, K. T. Clarno, R. P. Pawlowski, and R. N. Bratton, "Assessment of Pellet-Clad Interaction Indicators in Watts Bar Unit 1, Cycles 1-3 Using VERA," *Proc. PHYSOR 2016*, Sun Valley, Idaho, USA (May 1-5, 2016).

19. S. G. Stimpson, J. J. Powers, K. T. Clarno, R. P. Pawlowski, "Assessment of Pellet-Clad Interaction with VERA: WBN1, Cycles 6-7," in *Proc. Top Fuel 2016*, Boise, Idaho, USA (September 11–16, 2016).
20. A. Godfrey et al., *VERA Benchmarking Results for Watts Bar Nuclear Plant Unit 1 Cycles 1-12*. Technical Report CASL-U-2015-0206-000, Oak Ridge National Laboratory. Available online http://www.casl.gov/docs/CASL-U-2015-0206-000.pdf (2015).
21. S. Stimpson et al., "Effect of Clad Fast Neutron Flux Distribution on Quarter-Core Fuel Performance Calculations with BISON," *Proc. WRFPM 2017*, Jeju, Korea (September 10–14, 2017).
22. A. Godfrey and R. Lee, *VERAView User's Guide*, Technical Report CASL-U-2016-1058-000, Oak Ridge National Laboratory, (2016).

APPENDIX A – TIAMAT COUPLED EXPANDED RESULTS

A.1. Radially Averaged Fuel Temperature

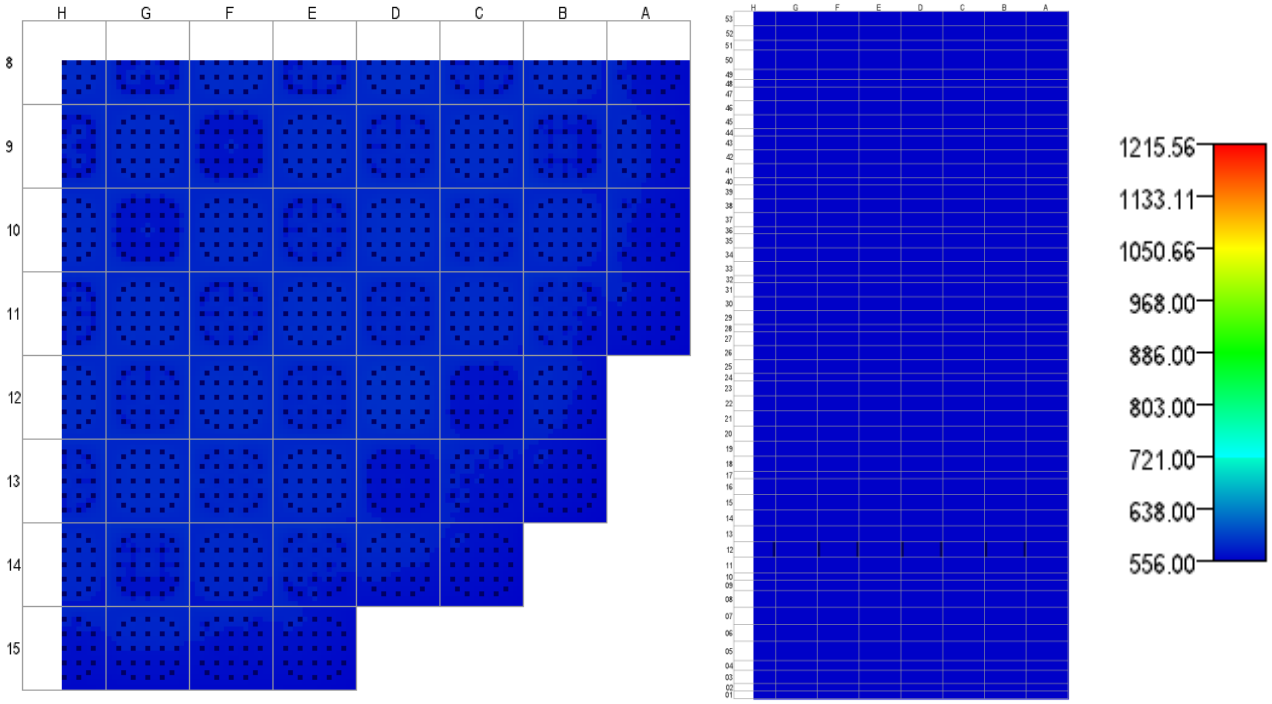

Figure A.1.1. Radially Averaged Fuel Temperature (K), State 1, 0.000 GWd/MT.

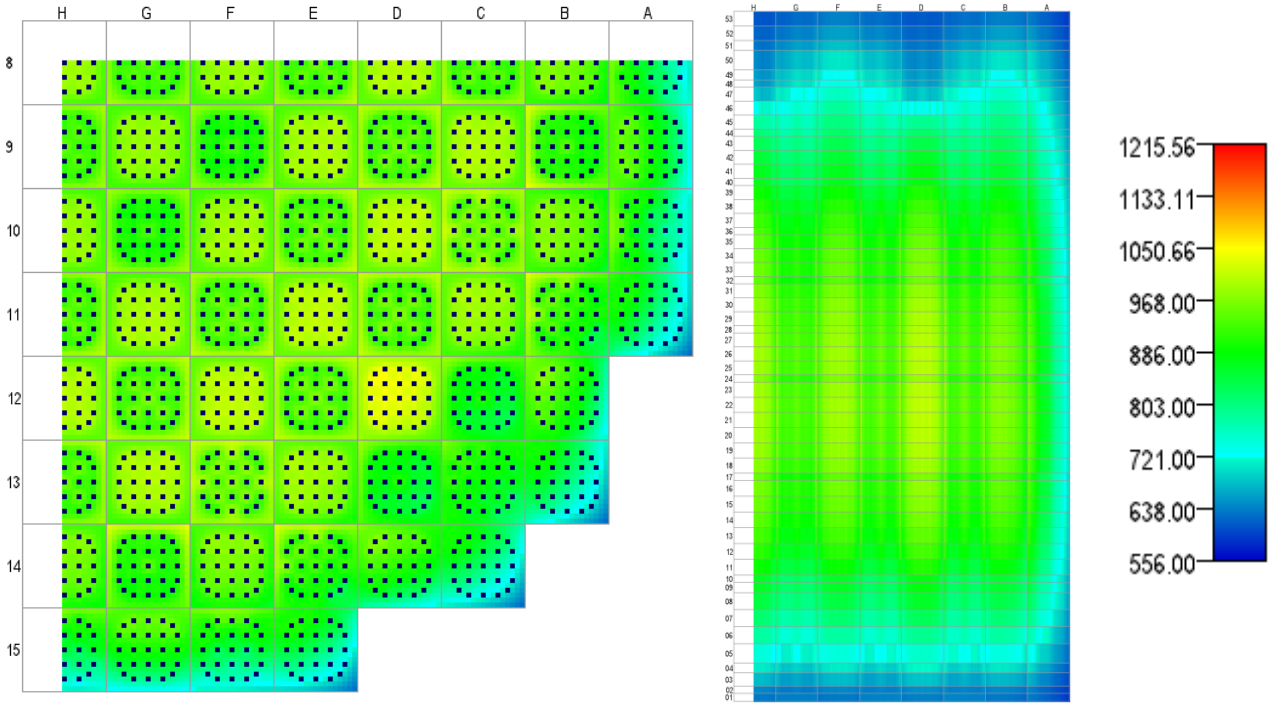

Figure A.1.2. Radially Averaged Fuel Temperature (K), State 2, 0.346 GWd/MT.

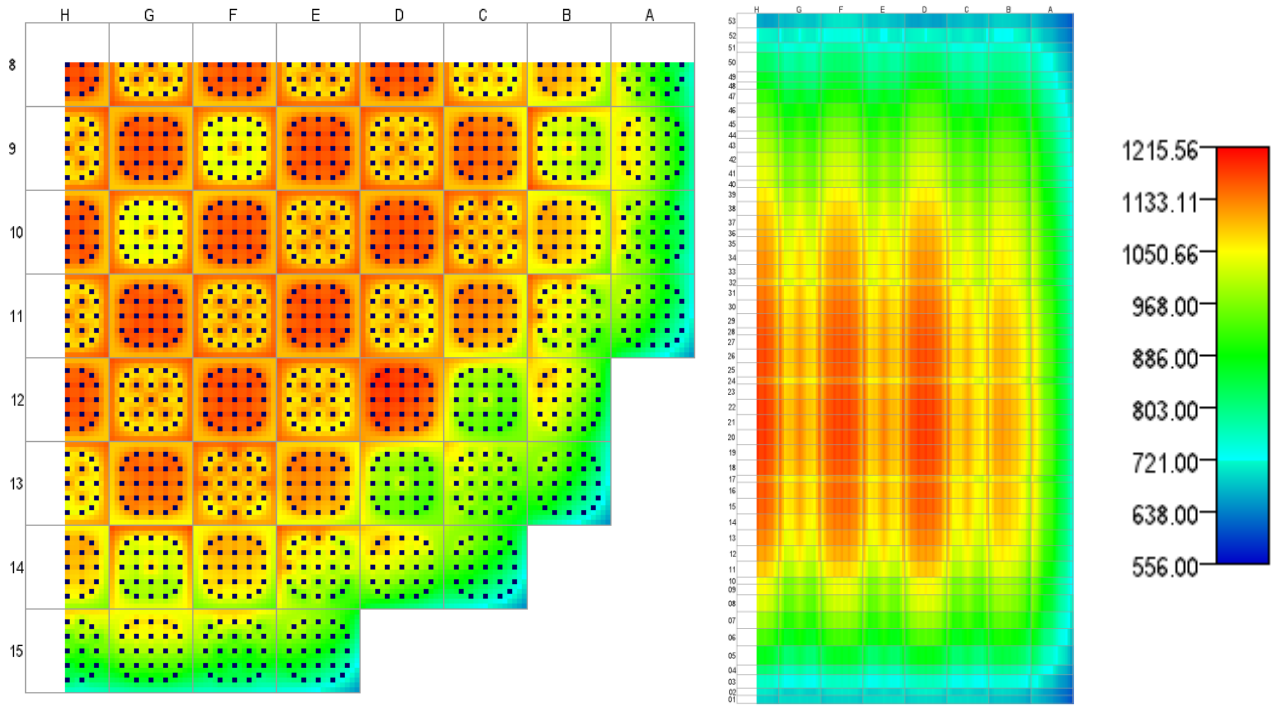

Figure A.1.3. Radially Averaged Fuel Temperature (K), State 3, 1.230 GWd/MT.

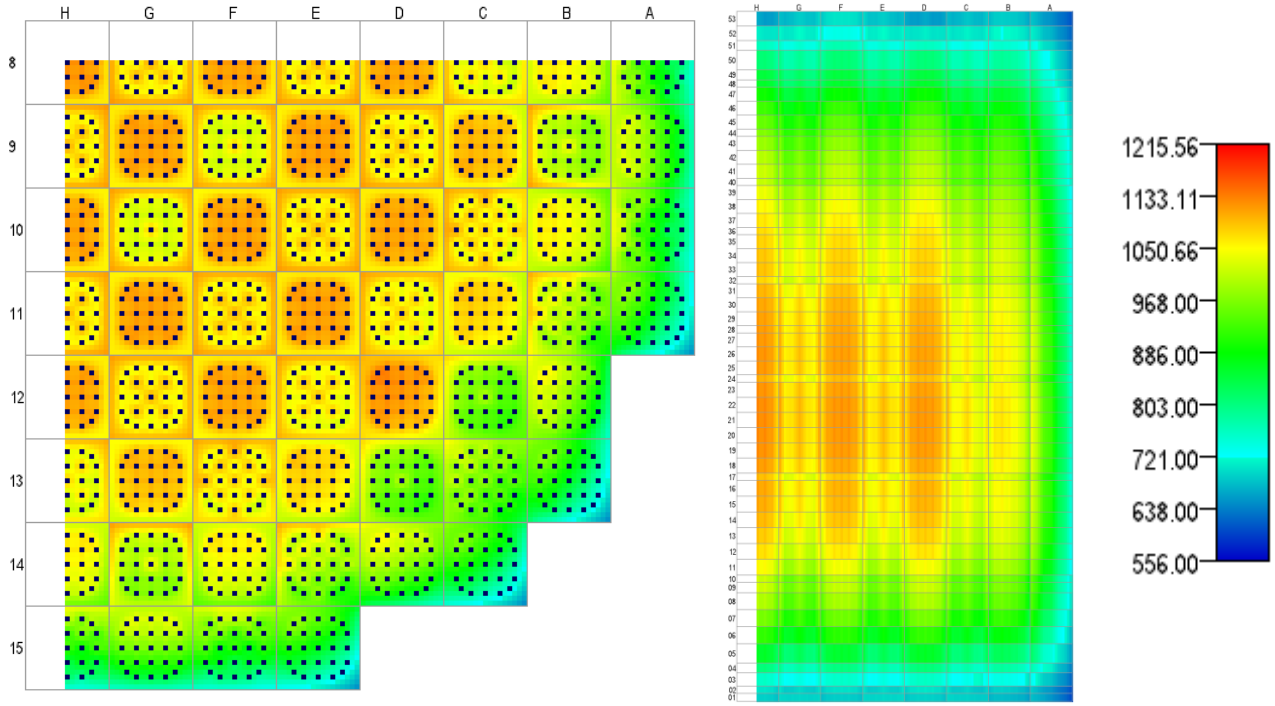

Figure A.1.4. Radially Averaged Fuel Temperature (K), State 4, 1.919 GWd/MT.

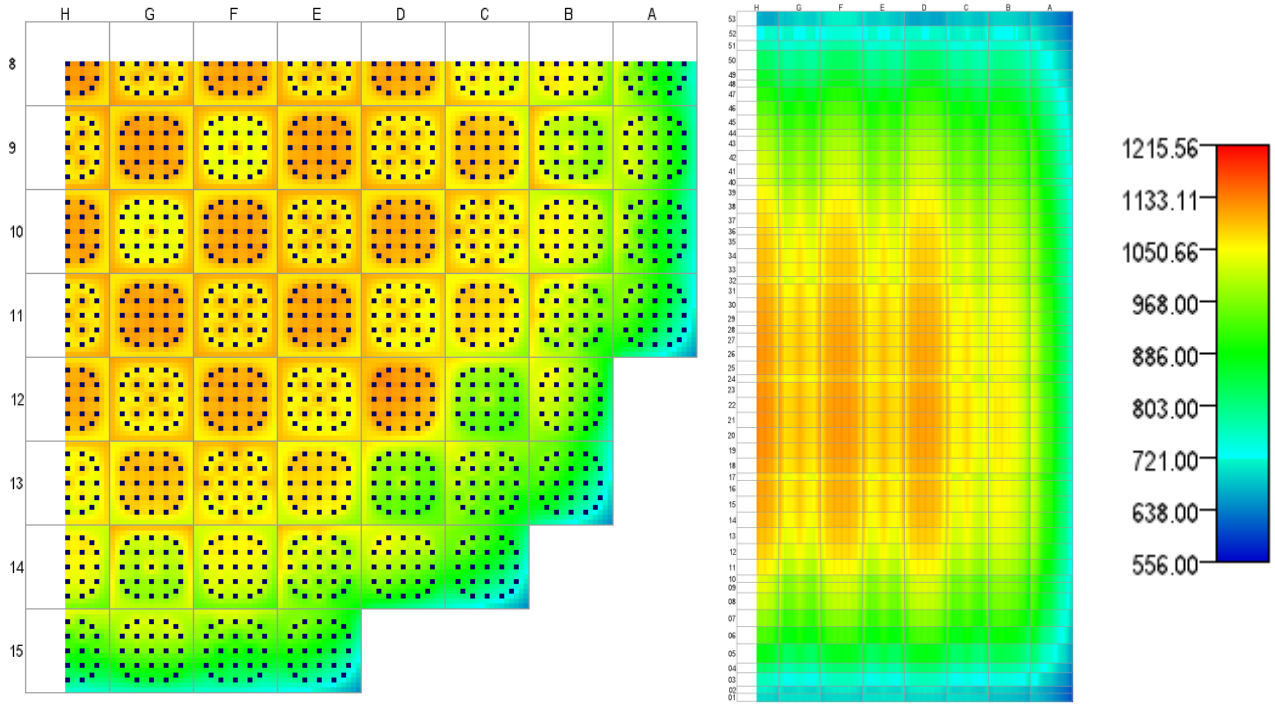

Figure A.1.5. Radially Averaged Fuel Temperature (K), State 5, 2.457 GWd/MT.

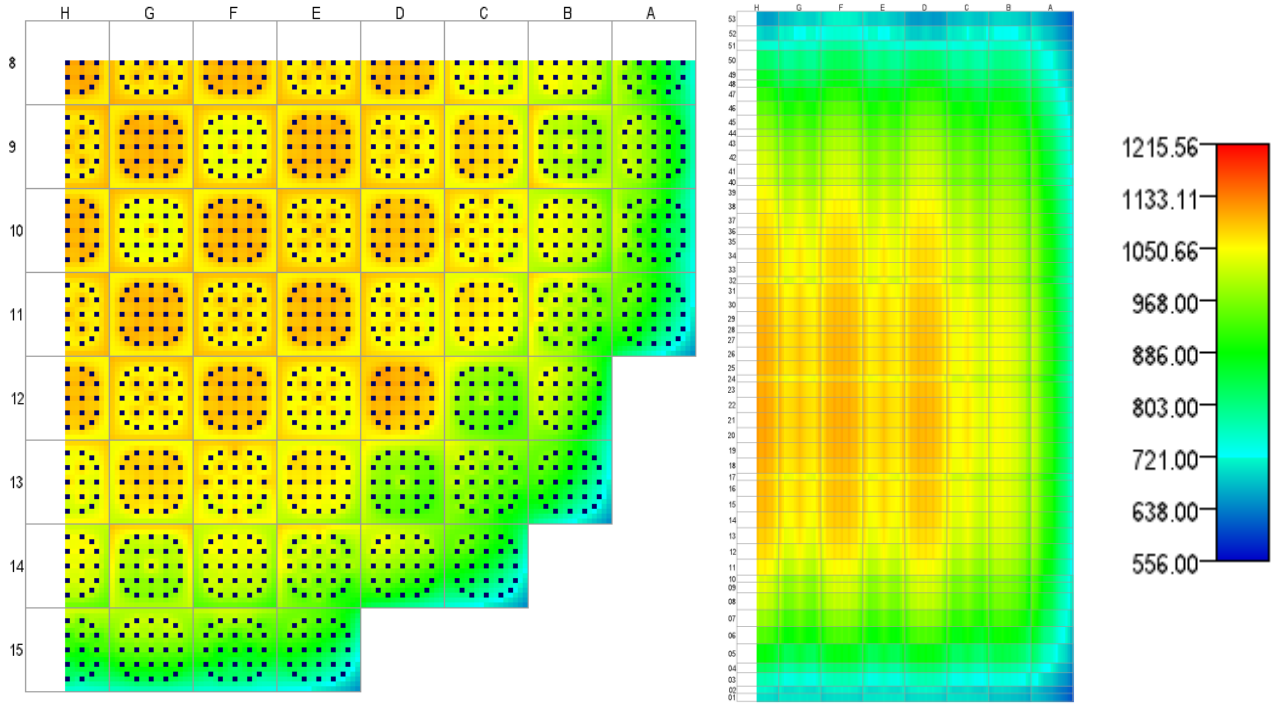

Figure A.1.6. Radially Averaged Fuel Temperature (K), State 6, 2.994 GWd/MT.

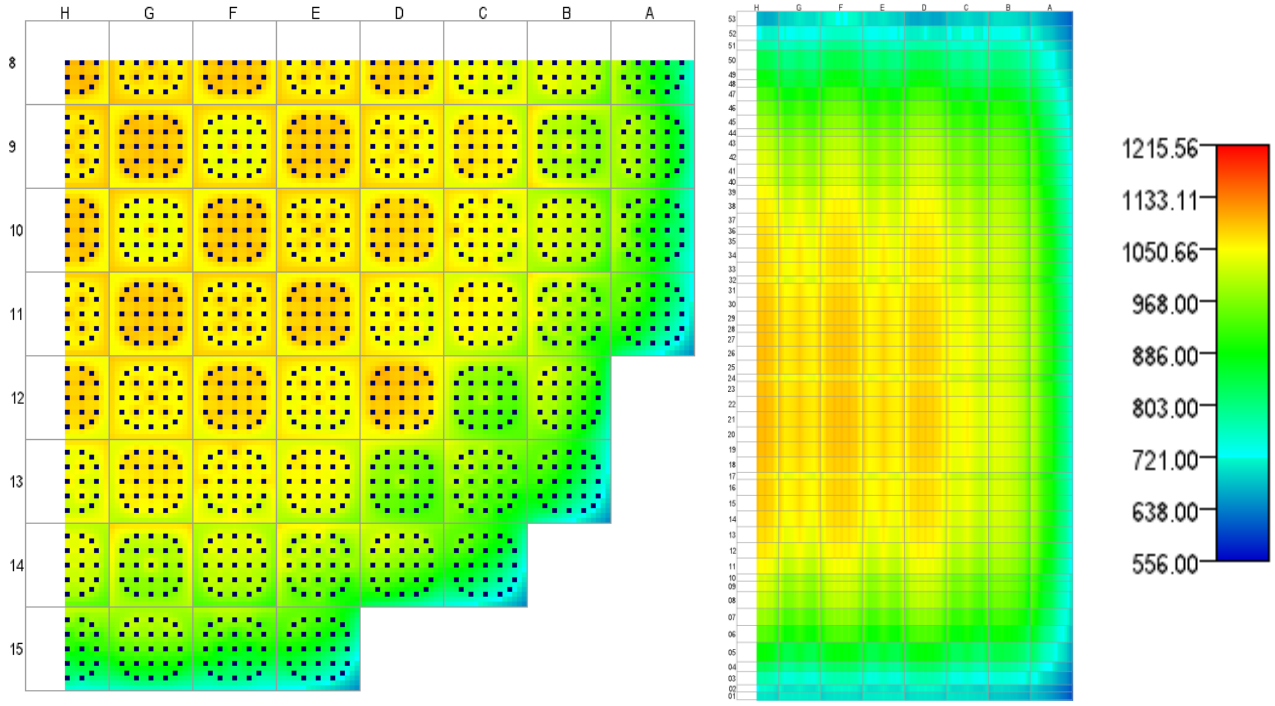

Figure A.1.7. Radially Averaged Fuel Temperature (K), State 7, 3.562 GWd/MT

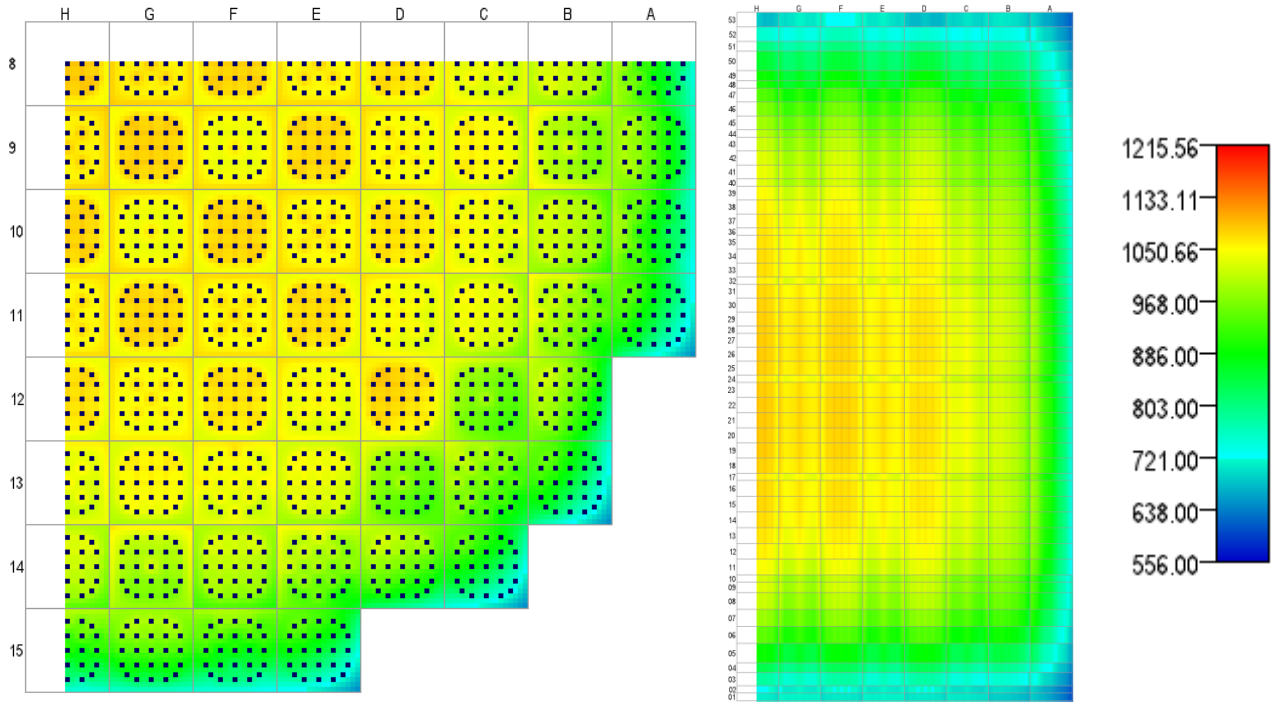

Figure A.1.8. Radially Averaged Fuel Temperature (K) , State 8, 4.065 GWd/MT.

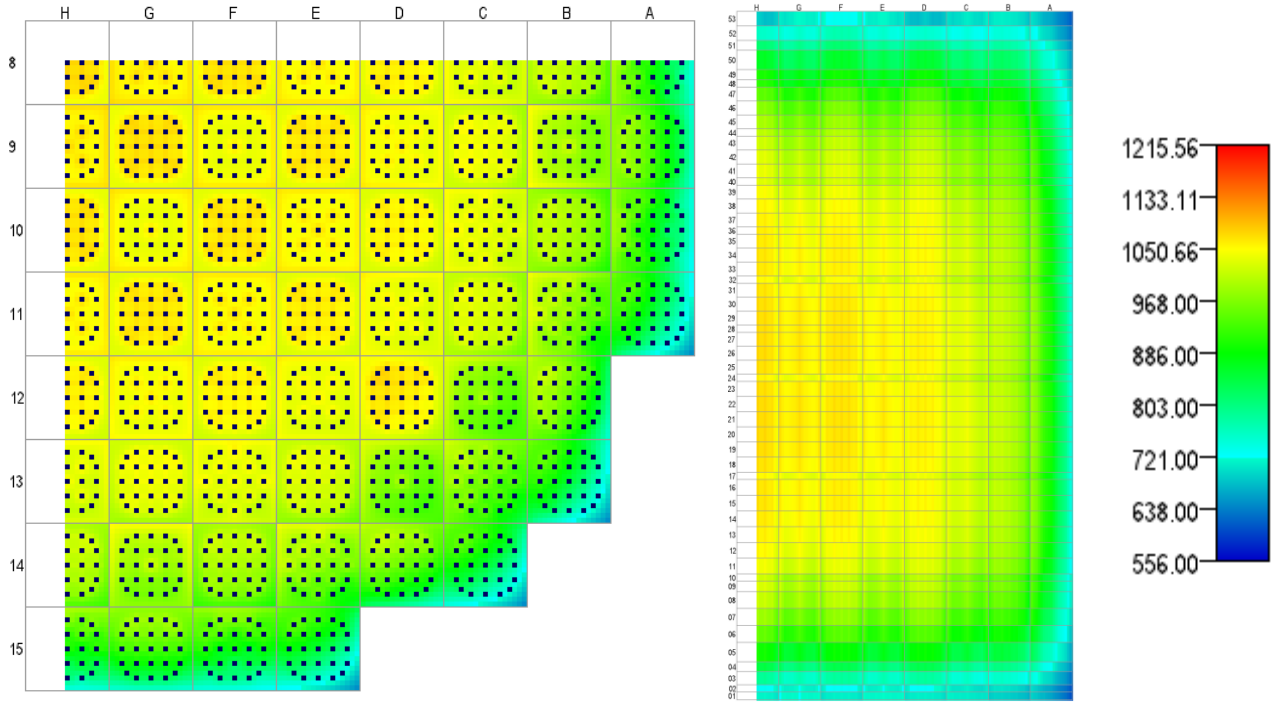

Figure A.1.9. Radially Averaged Fuel Temperature (K), State 9, 4.642 GWd/MT

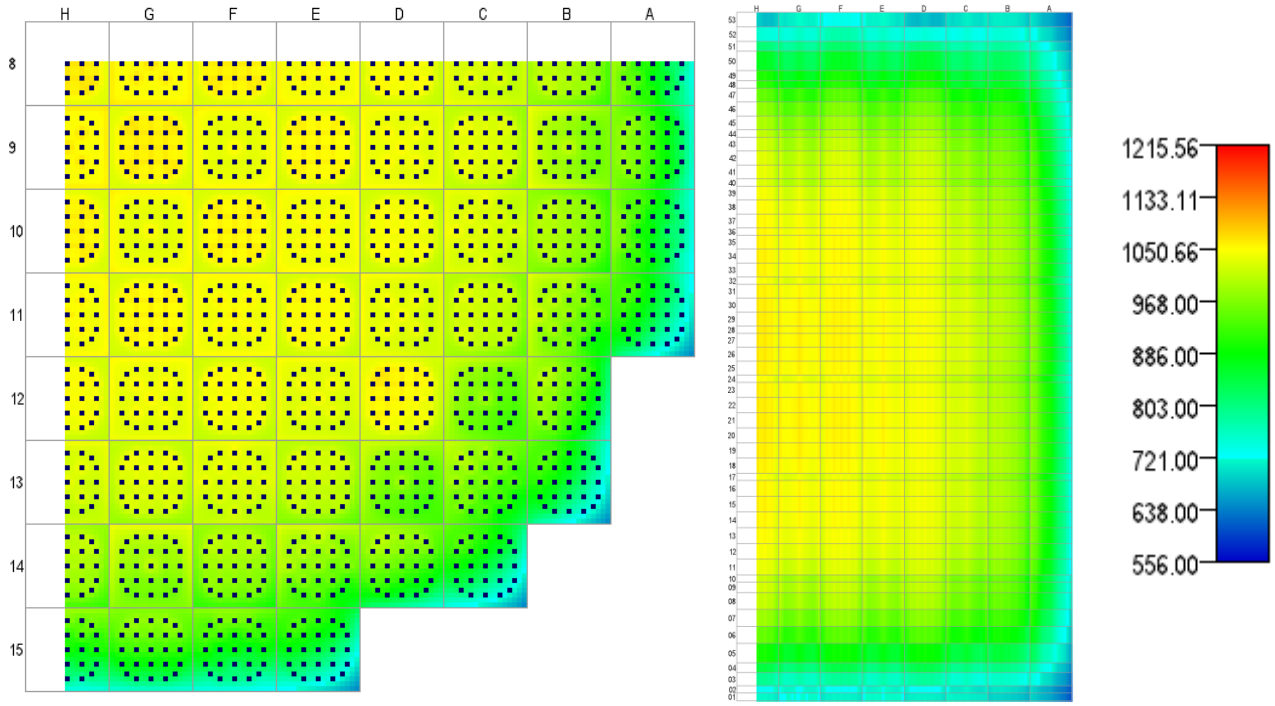

Figure A.1.10. Radially Averaged Fuel Temperature (K), State 10, 5.139 GWd/MT.

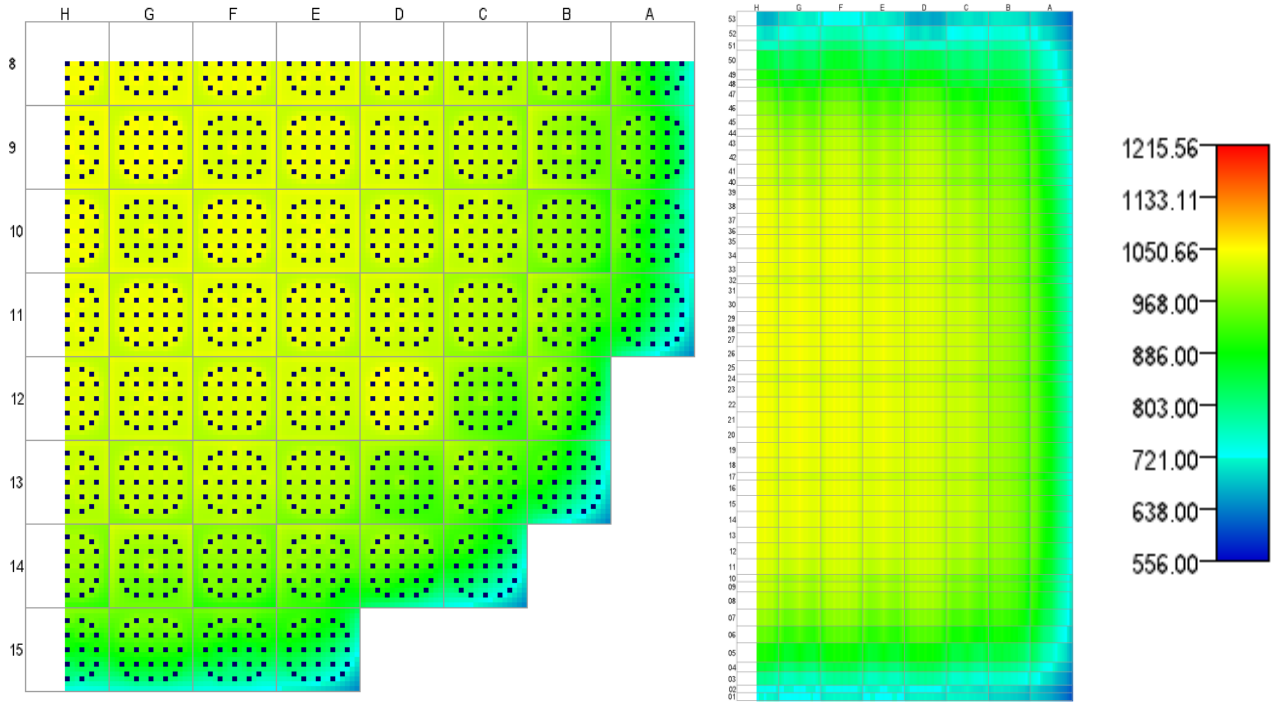

Figure A.1.11. Radially Averaged Fuel Temperature (K), State 11, 5.700 GWd/MT

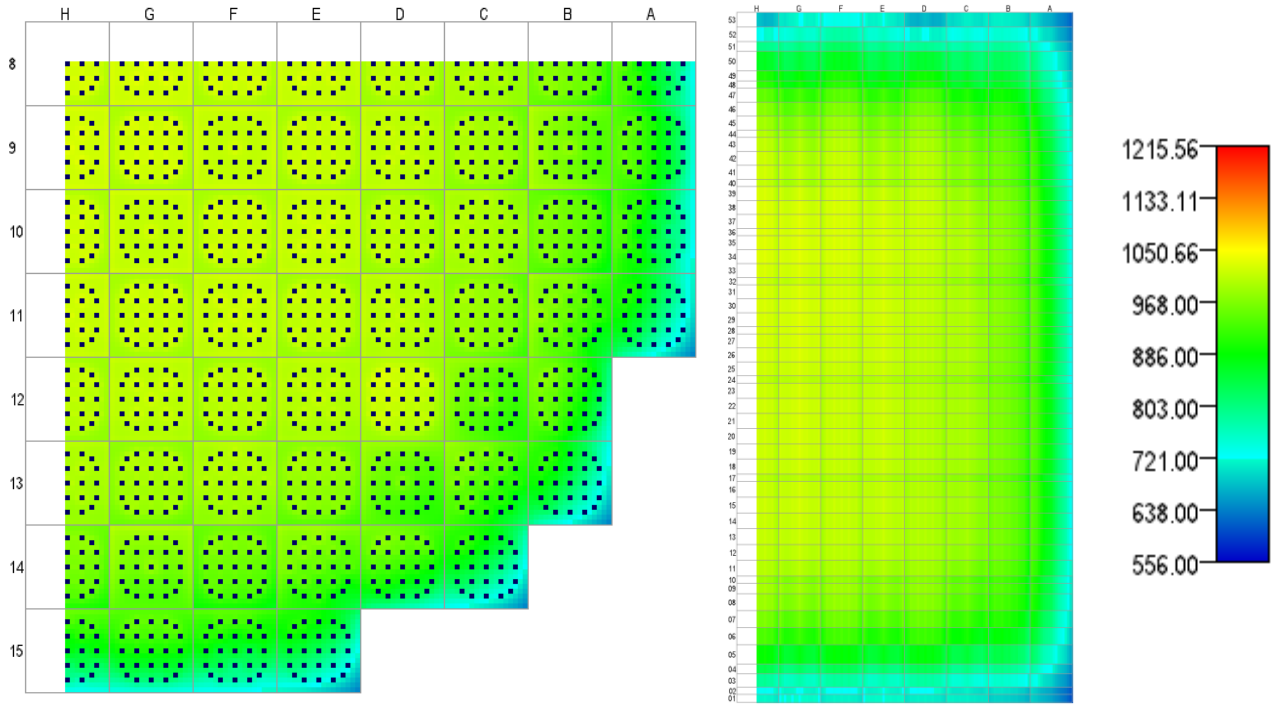

Figure A.1.12. Radially Averaged Fuel Temperature (K), State 12, 6.273 GWd/MT.

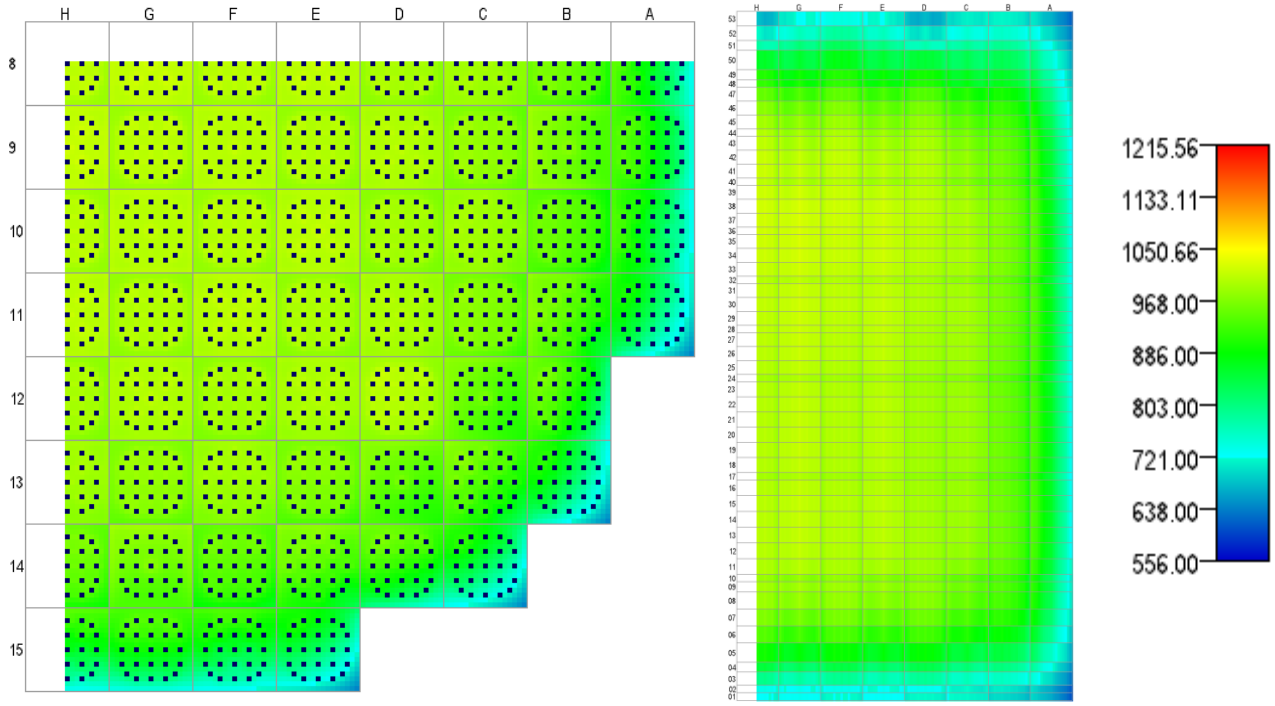

Figure A.1.13. Radially Averaged Fuel Temperature (K), State 13, 7.000 GWd/MT.

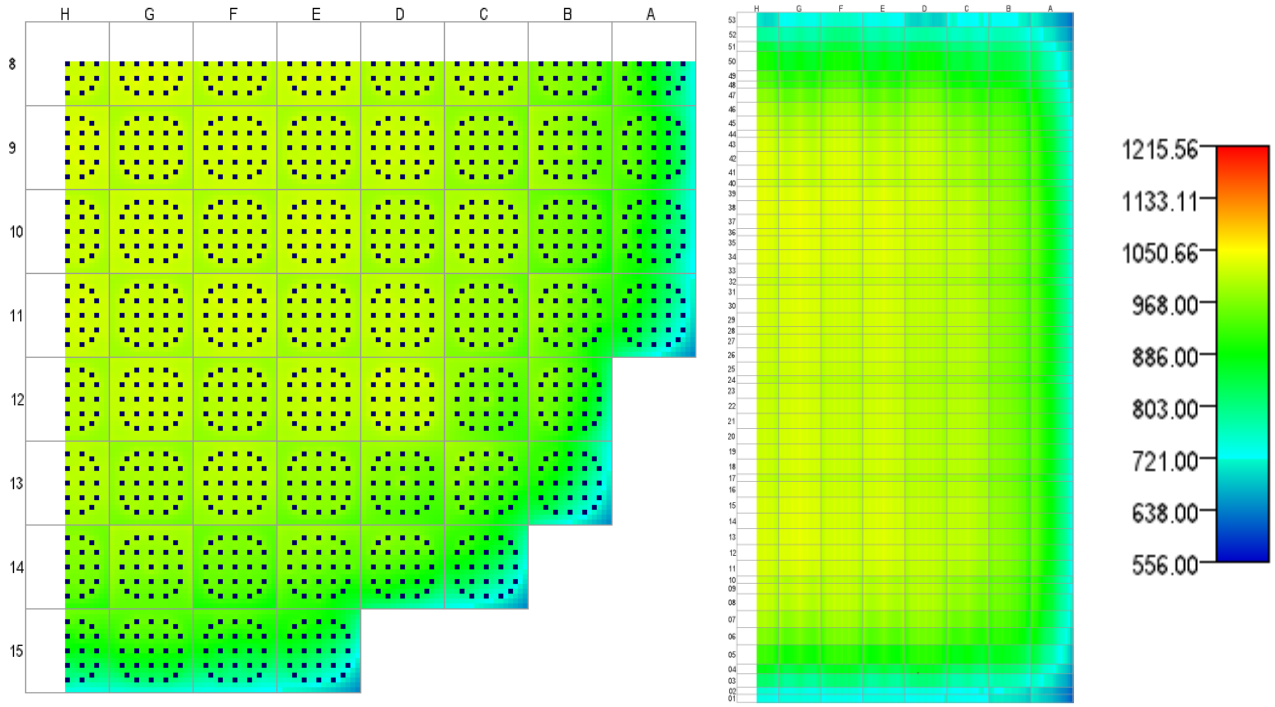

Figure A.1.14. Radially Averaged Fuel Temperature (K), State 14, 7.463 GWd/MT.

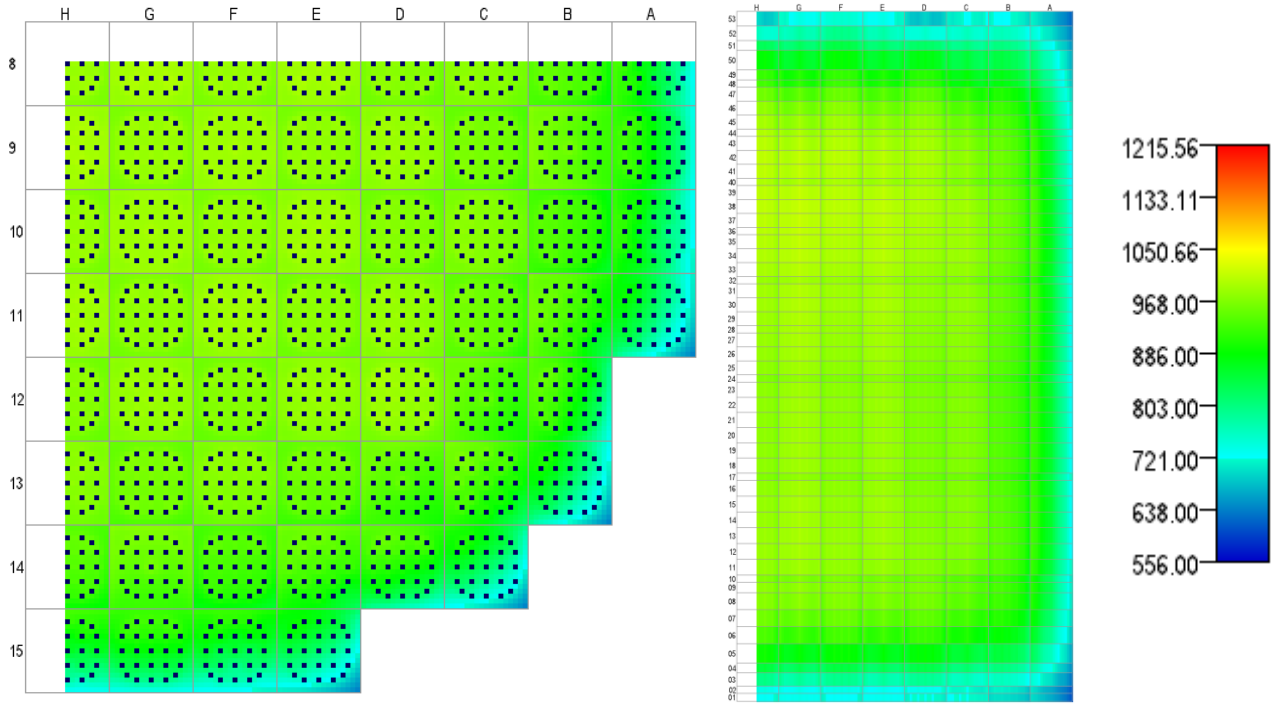

Figure A.1.15. Radially Averaged Fuel Temperature (K), State 15, 7.978 GWd/MT.

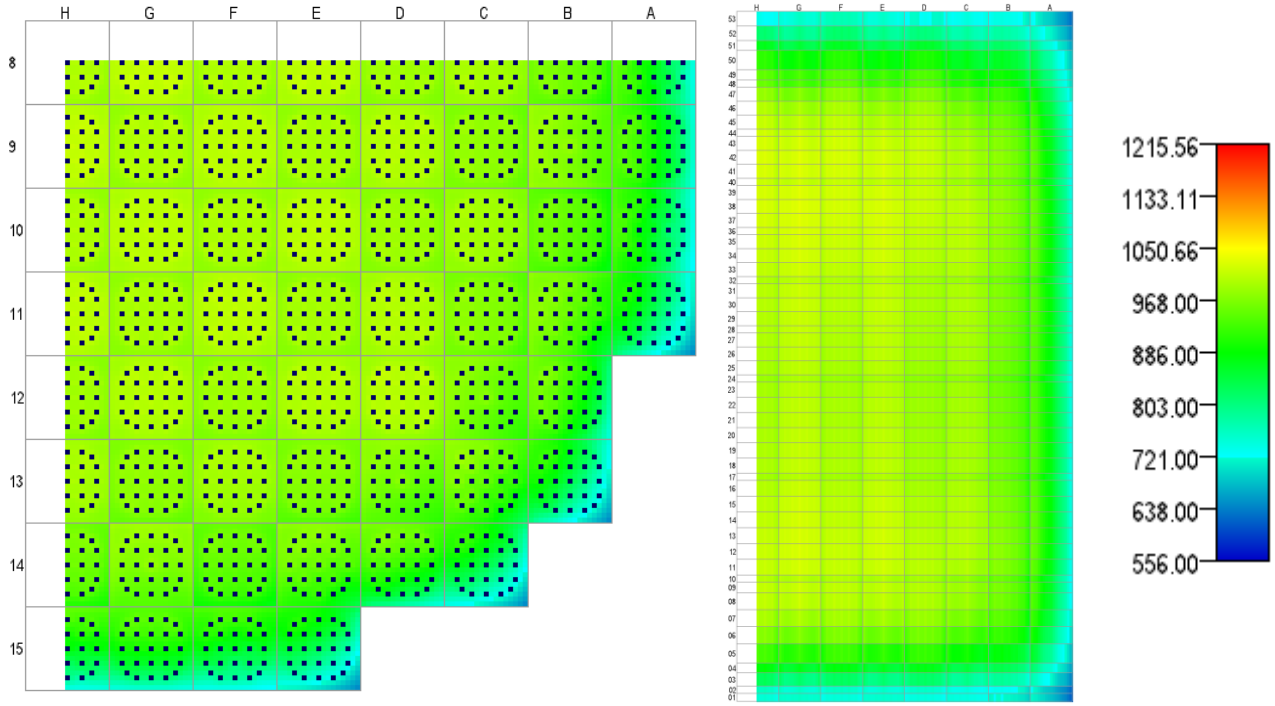

Figure A.1.16. Radially Averaged Fuel Temperature (K), State 16, 8.493 GWd/MT.

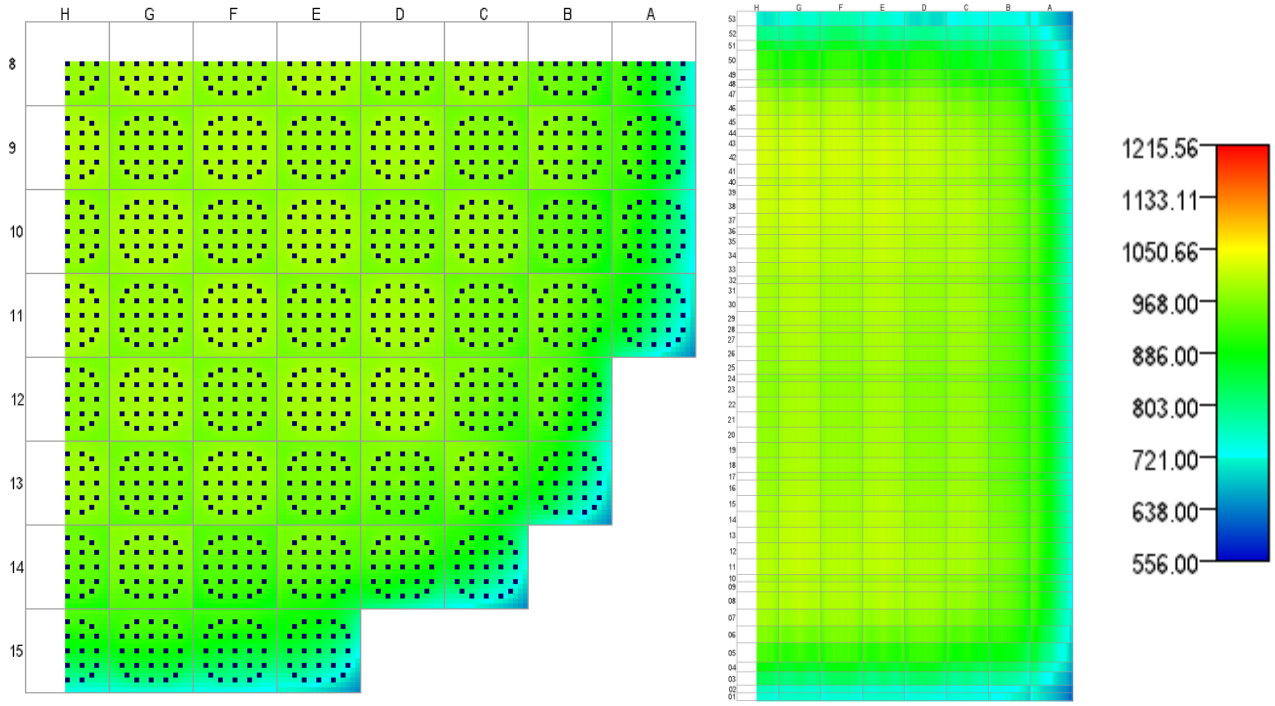

Figure A.1.17. Radially Averaged Fuel Temperature (K), State 17, 9.140 GWd/MT.

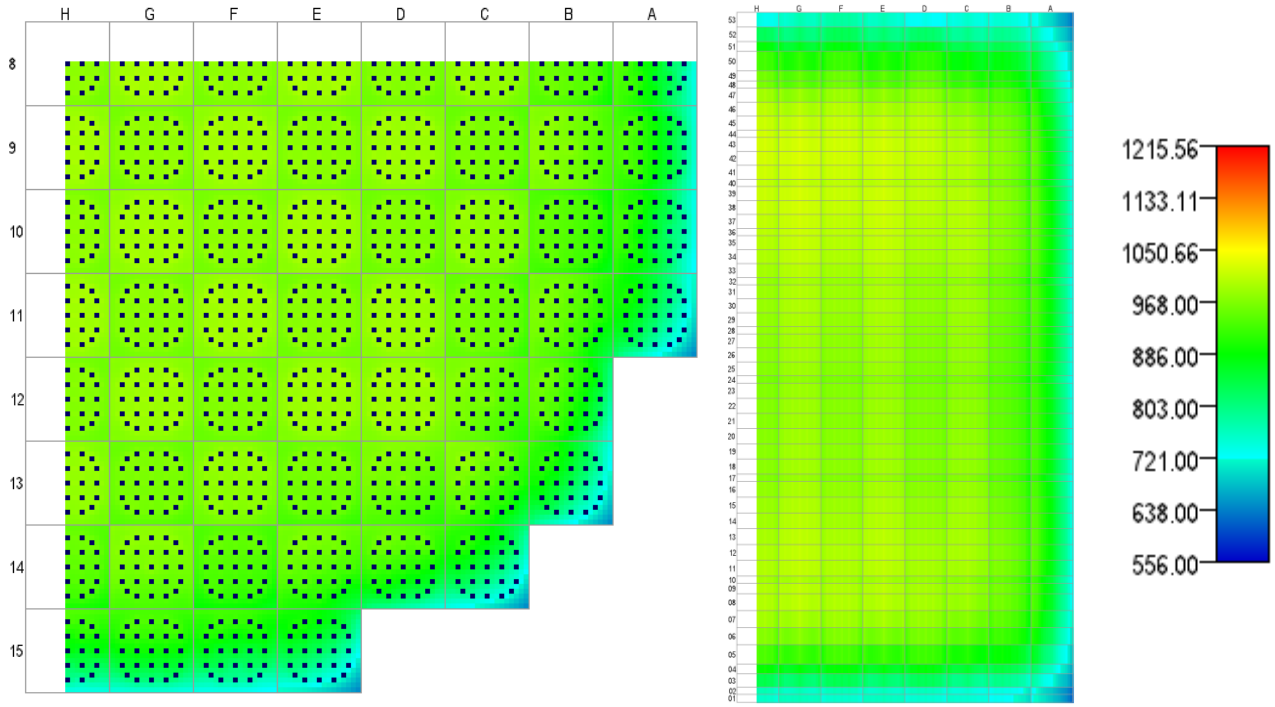

Figure A.1.18. Radially Averaged Fuel Temperature (K), State 18, 9.602 GWd/MT.

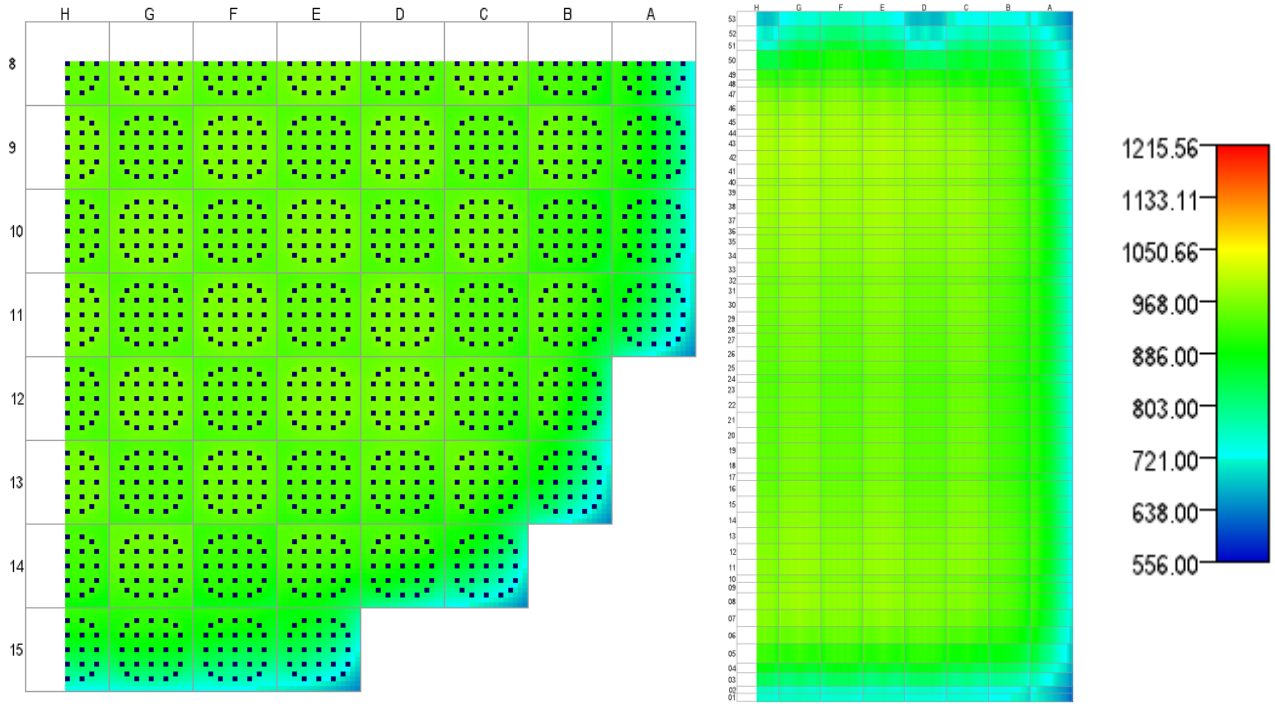

Figure A.1.19. Radially Averaged Fuel Temperature (K), State 19, 10.344 GWd/MT.

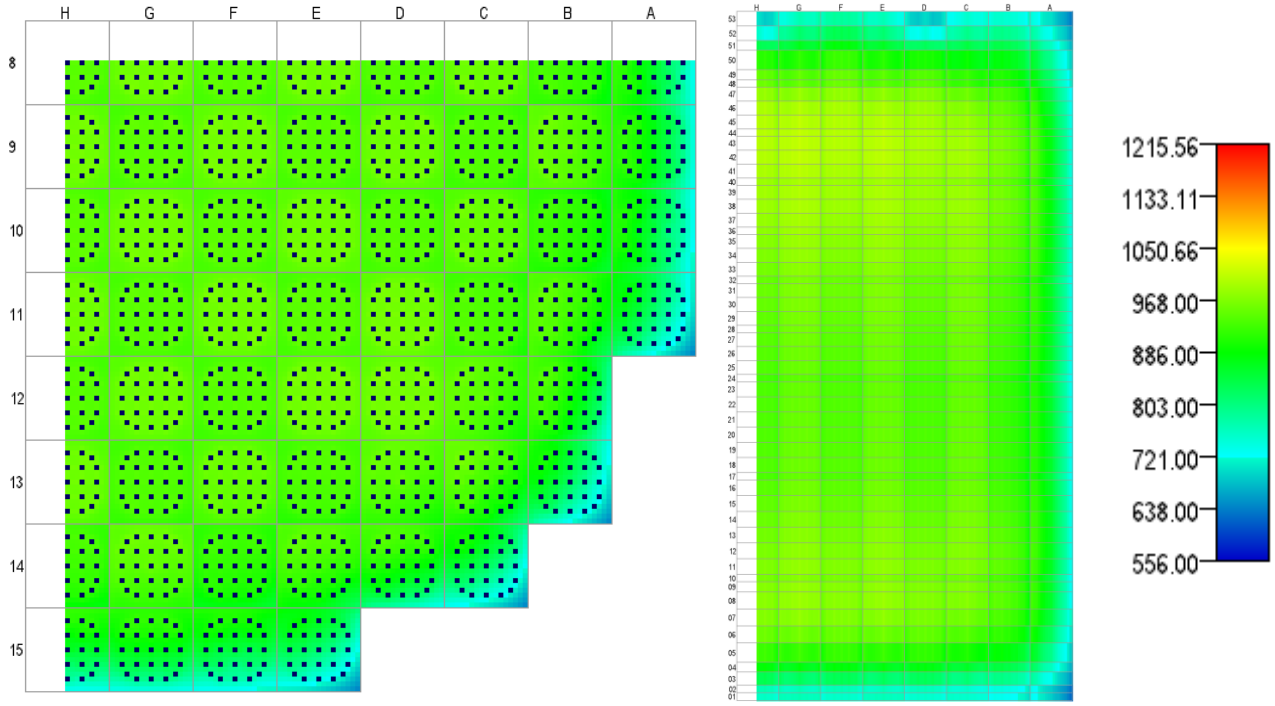

Figure A.1.20. Radially Averaged Fuel Temperature (K), State 20, 10.842 GWd/MT.

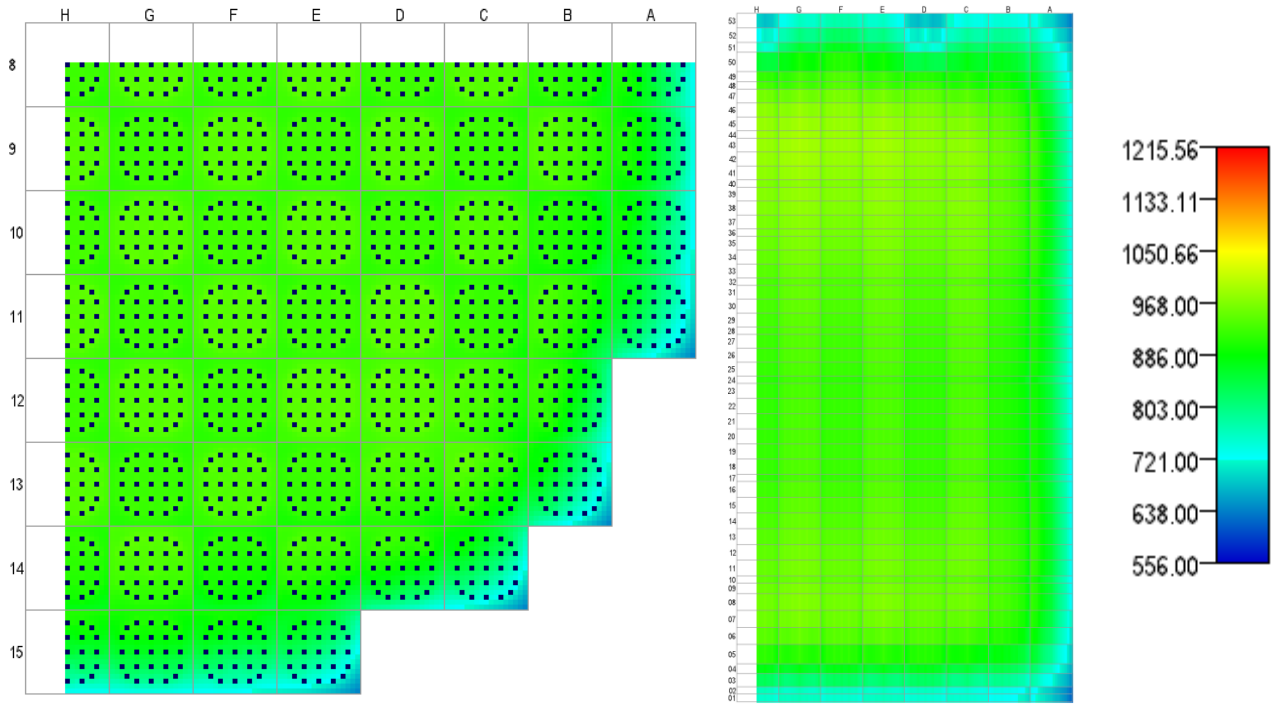

Figure A.1.21. Radially Averaged Fuel Temperature (K), State 21, 11.314 GWd/MT

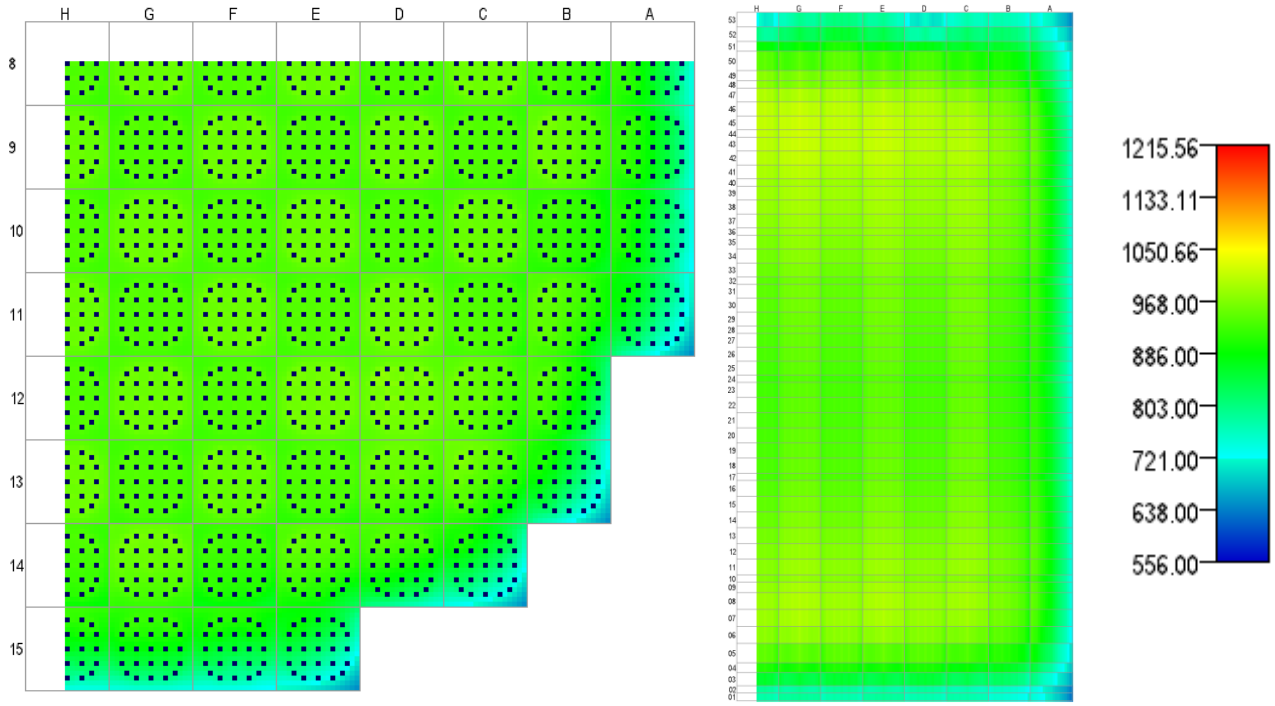

Figure A.1.22. Radially Averaged Fuel Temperature (K), State 22, 11.988 GWd/MT.

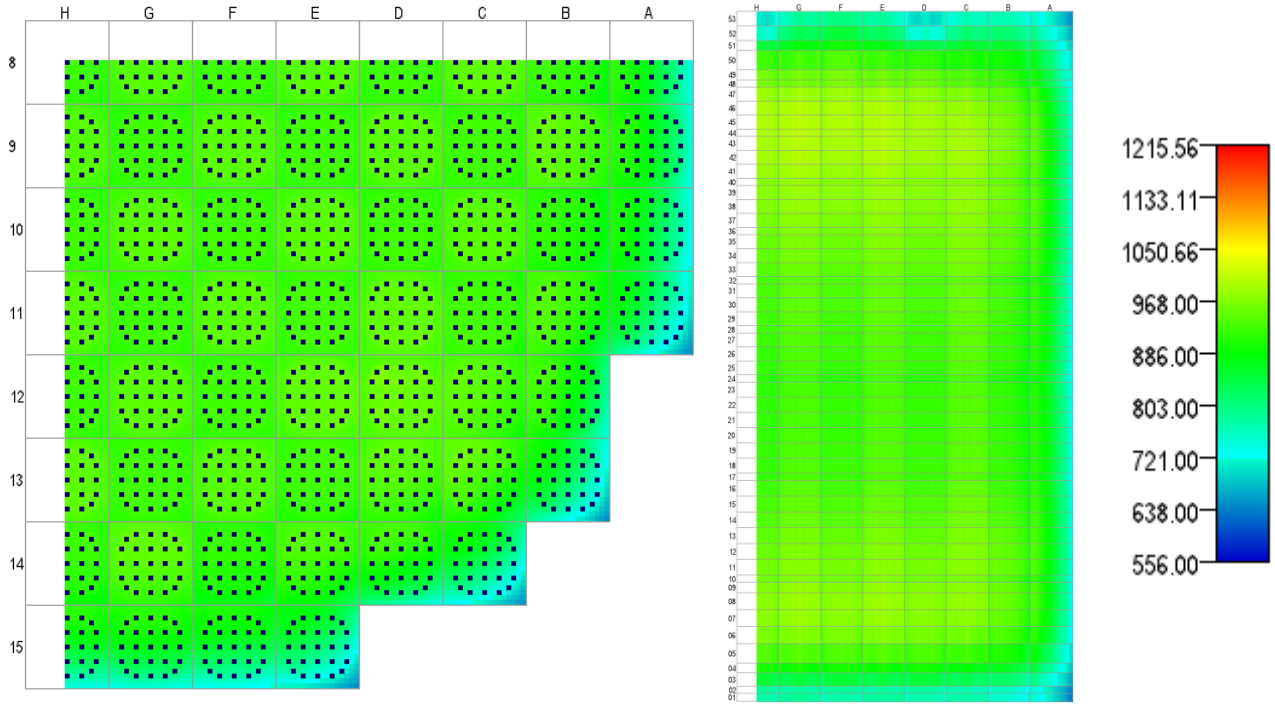

Figure A.1.23. Radially Averaged Fuel Temperature (K), State 23, 12.552 GWd/MT.

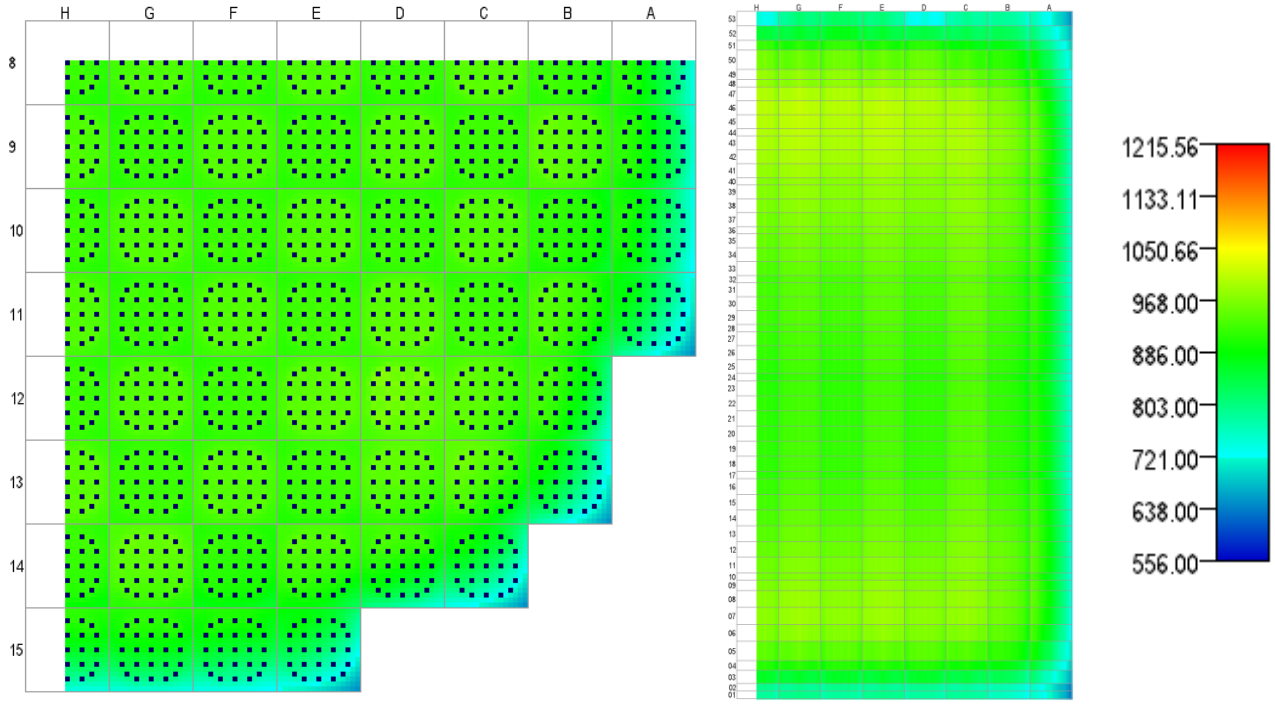

Figure A.1.24. Radially Averaged Fuel Temperature (K), State 24, 13.360 GWd/MT.

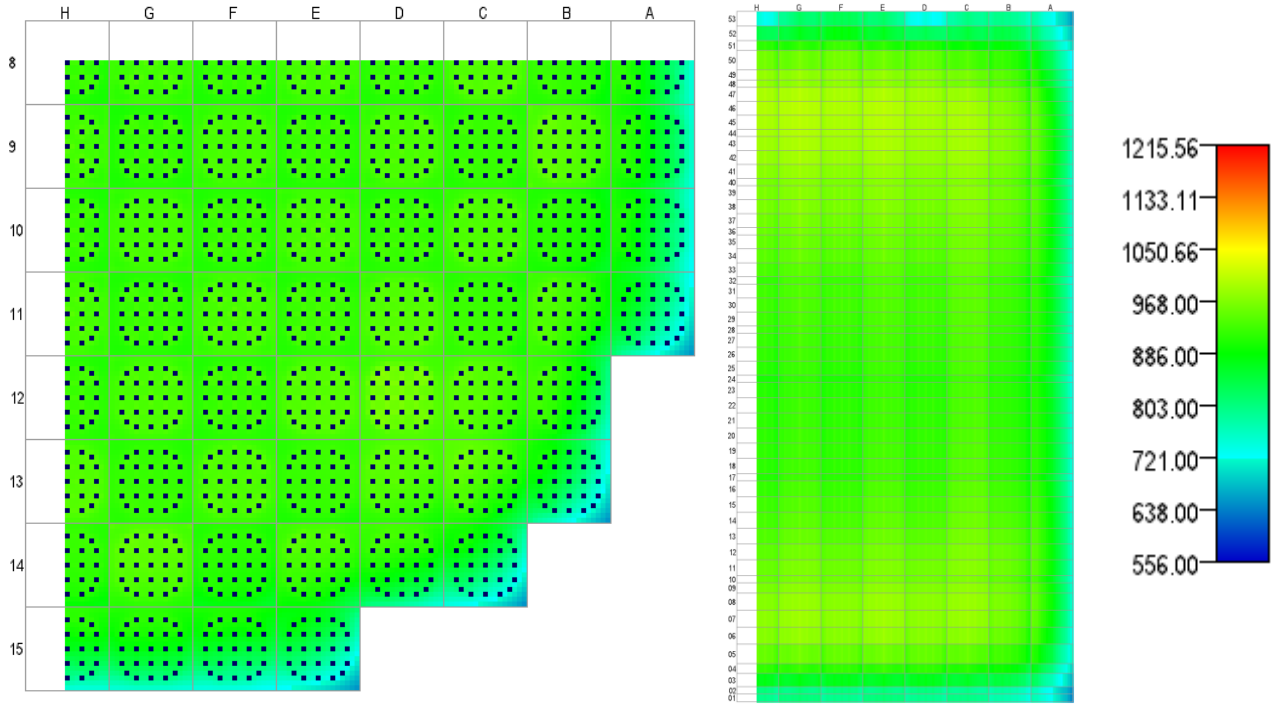

Figure A.1.25. Radially Averaged Fuel Temperature (K), State 25, 14.285 GWd/MT.

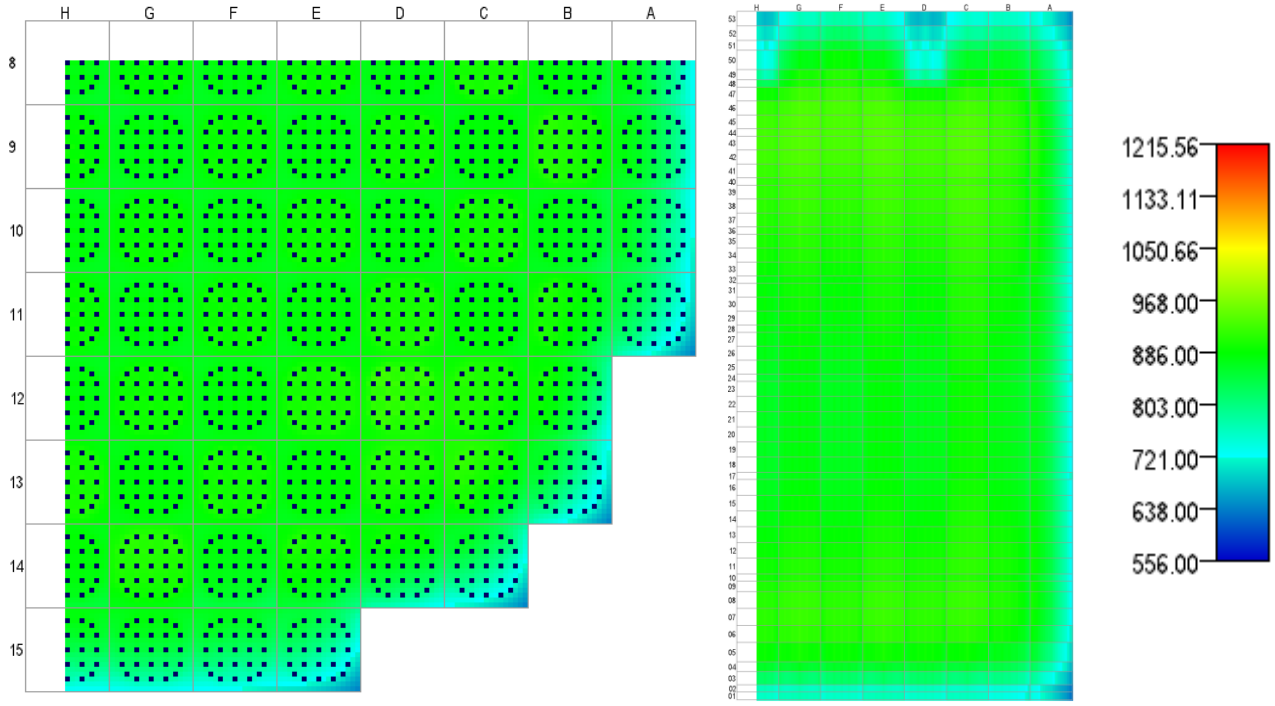

Figure A.1.26. Radially Averaged Fuel Temperature (K), State 26, 14.385 GWd/MT.

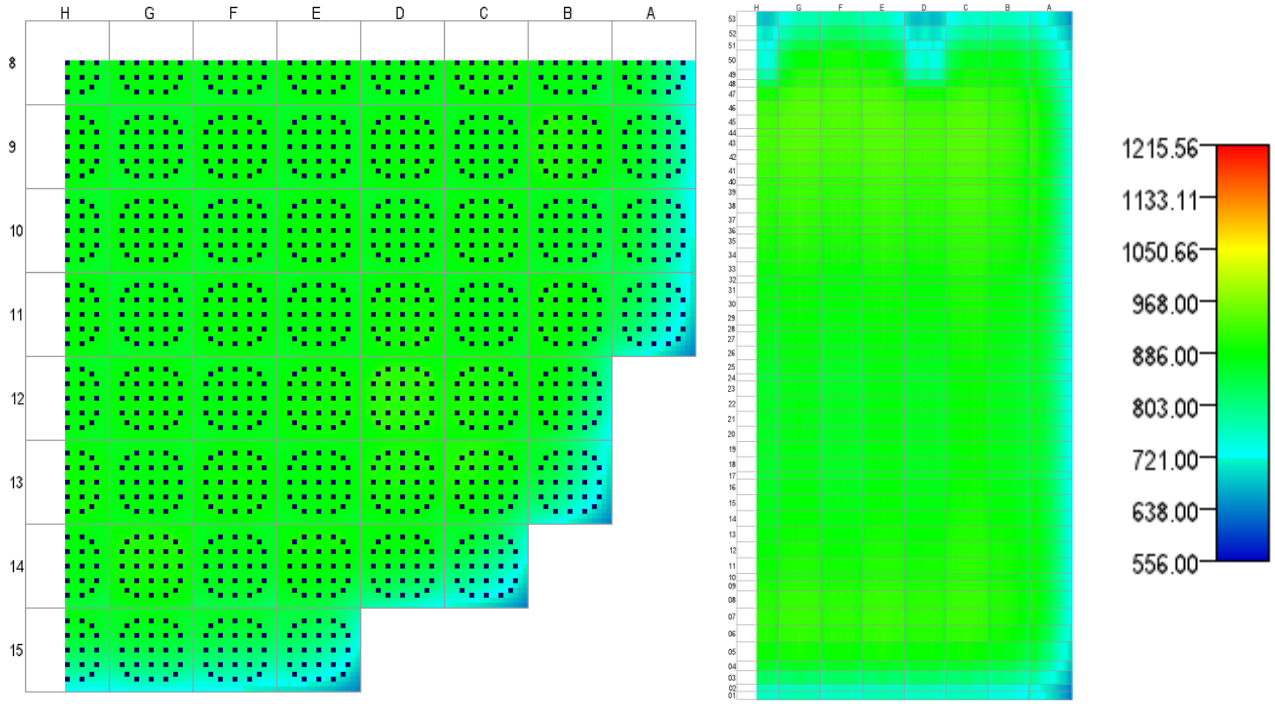

Figure A.1.27. Radially Averaged Fuel Temperature (K), State 27, 15.018 GWd/MT.

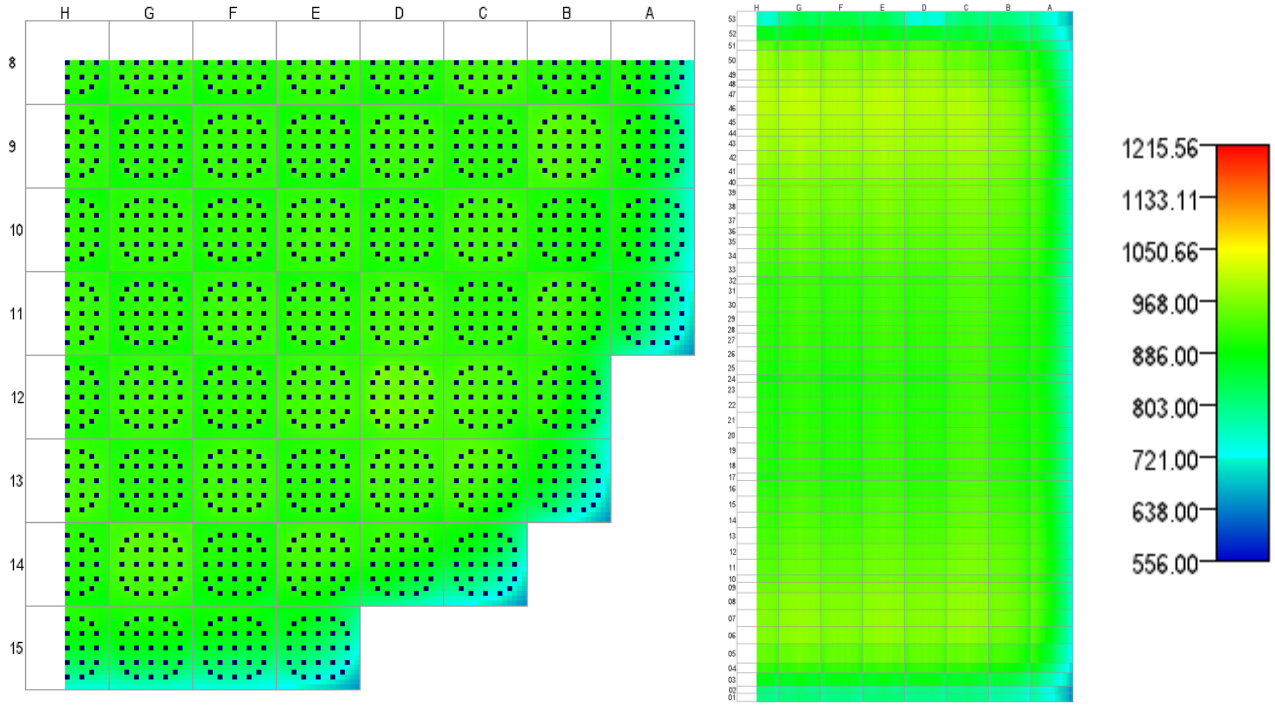

Figure A.1.28. Radially Averaged Fuel Temperature (K), State 28, 15.118 GWd/MT.

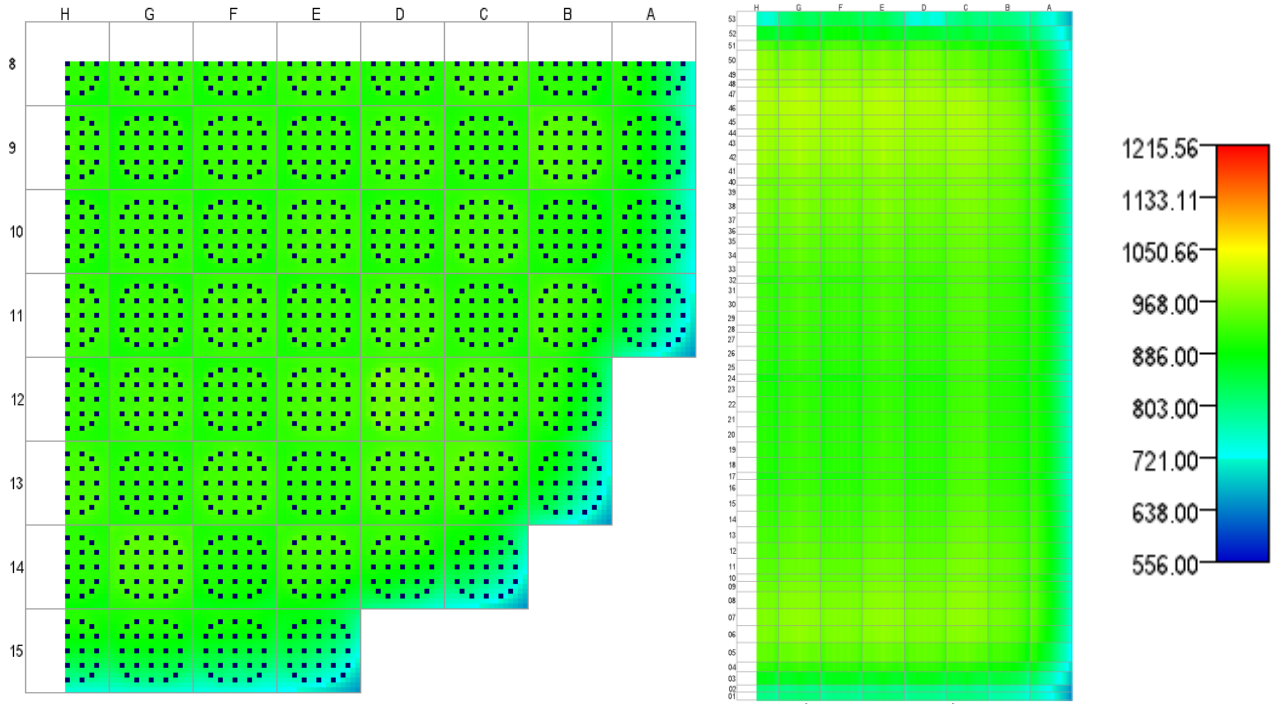

Figure A.1.29. Radially Averaged Fuel Temperature (K), State 29, 15.308 GWd/MT.

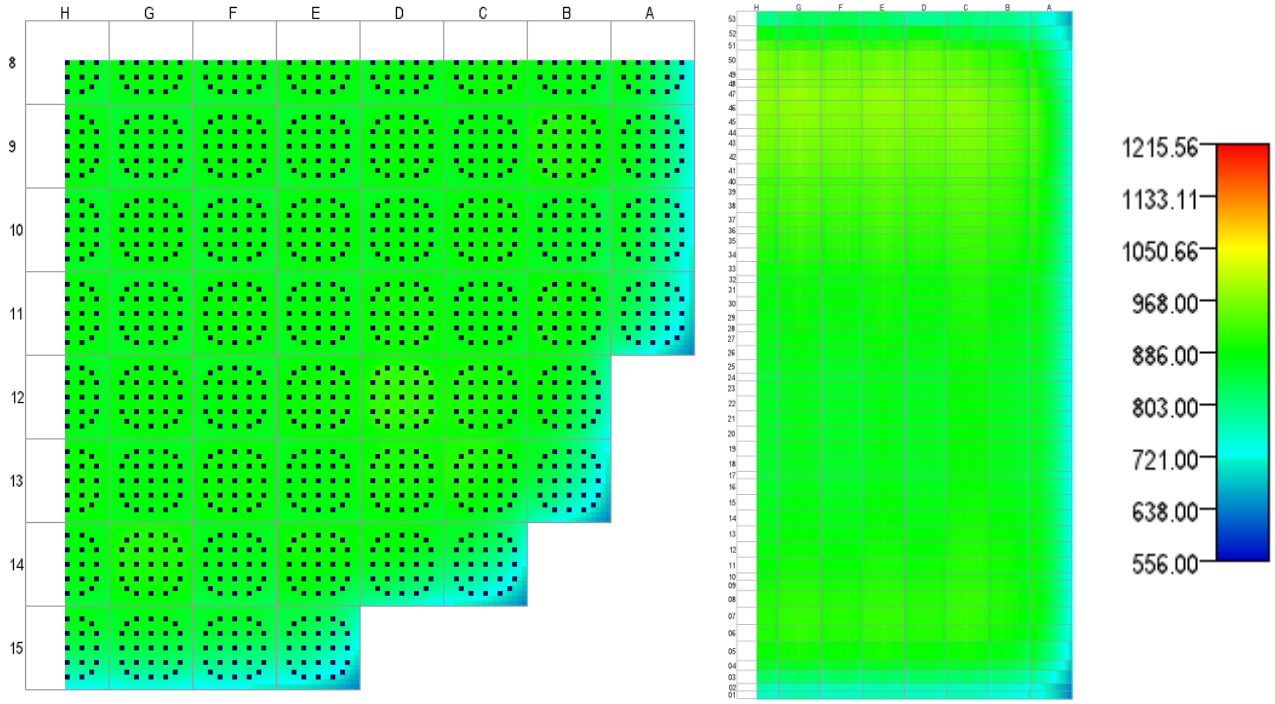

Figure A.1.30. Radially Averaged Fuel Temperature (K), State 30, 15.774 GWd/MT.

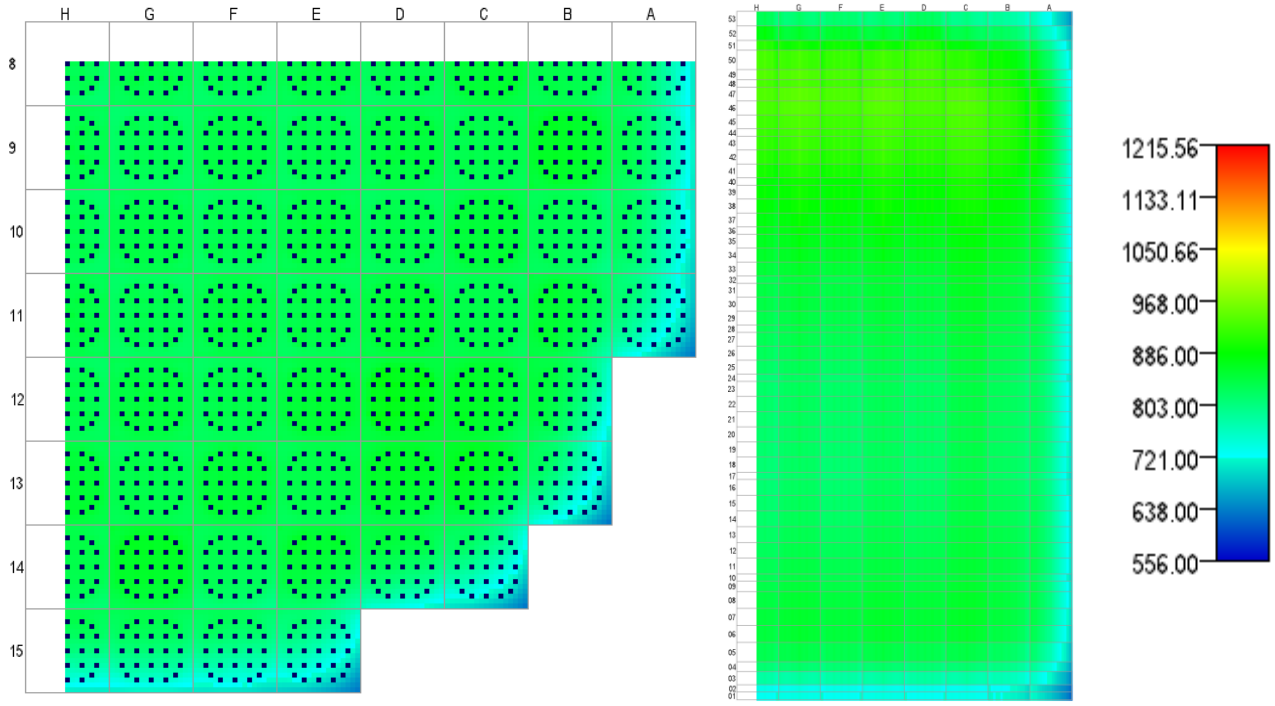

Figure A.1.31. Radially Averaged Fuel Temperature (K), State 31, 16.270 GWd/MT.

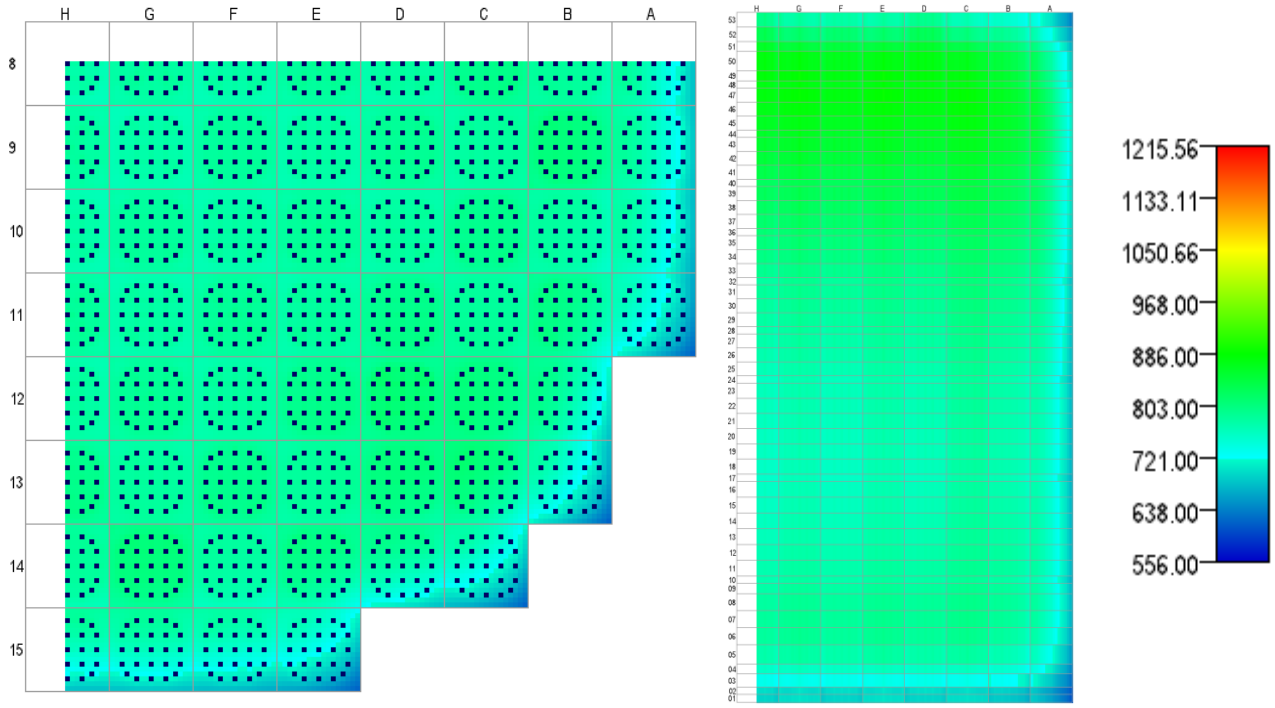

Figure A.1.32. Radially Averaged Fuel Temperature (K), State 32, 16.932 GWd/MT.

A.2. Fuel-Clad Gap Thickness

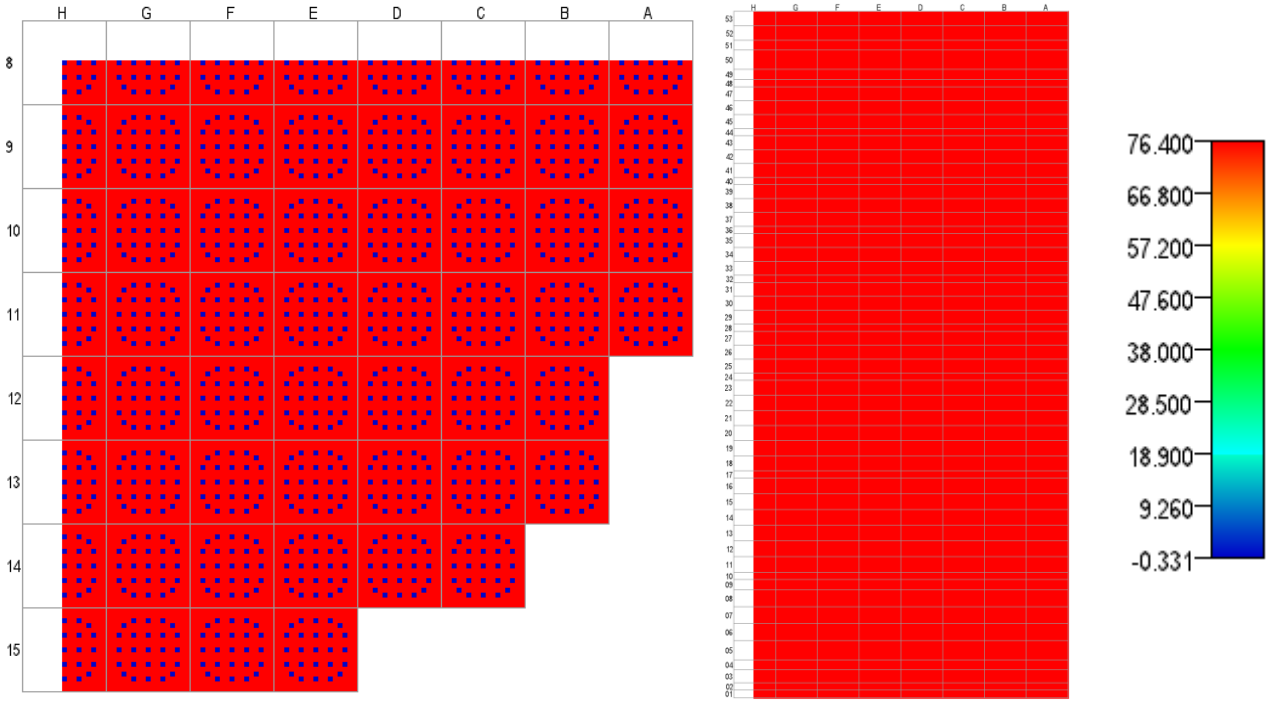

Figure A.2.1. Fuel-Clad Gap Thickness (microns), State 1, 0.000 GWd/MT.

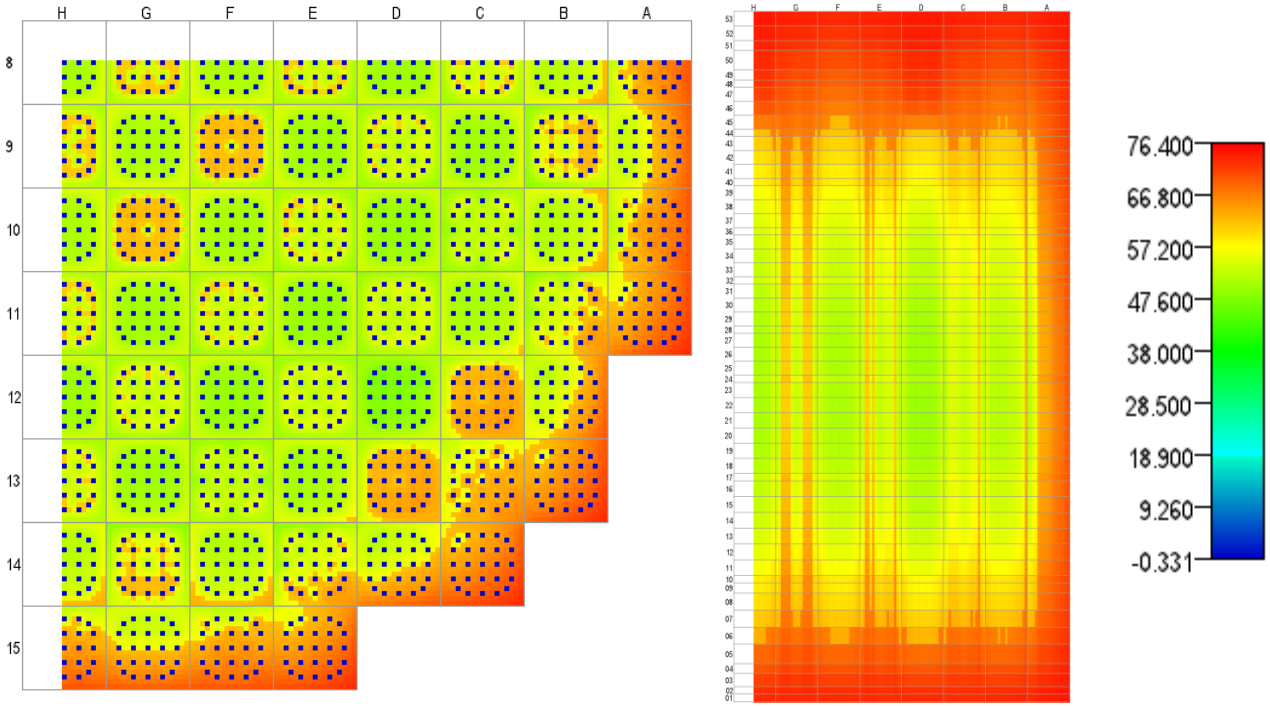

Figure A.2.2. Fuel-Clad Gap Thickness (microns), State 2, 0.346 GWd/MT.

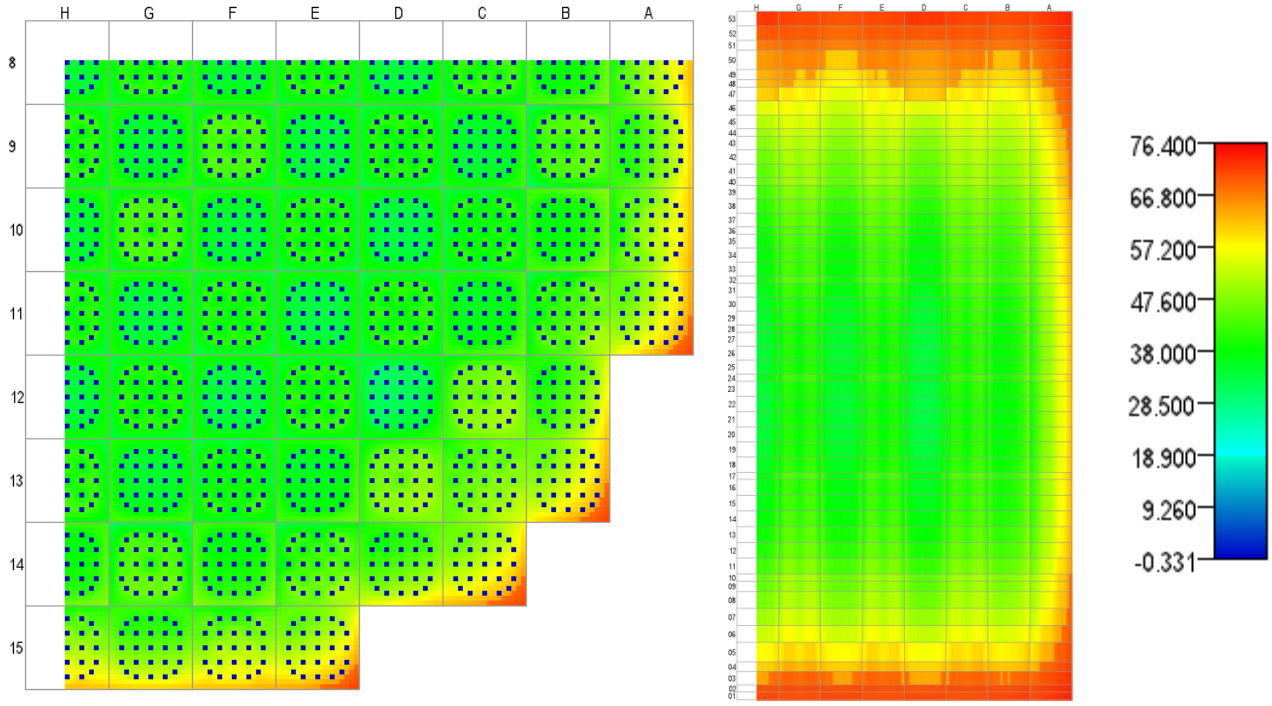

Figure A.2.3. Fuel-Clad Gap Thickness (microns), State 3, 1.230 GWd/MT.

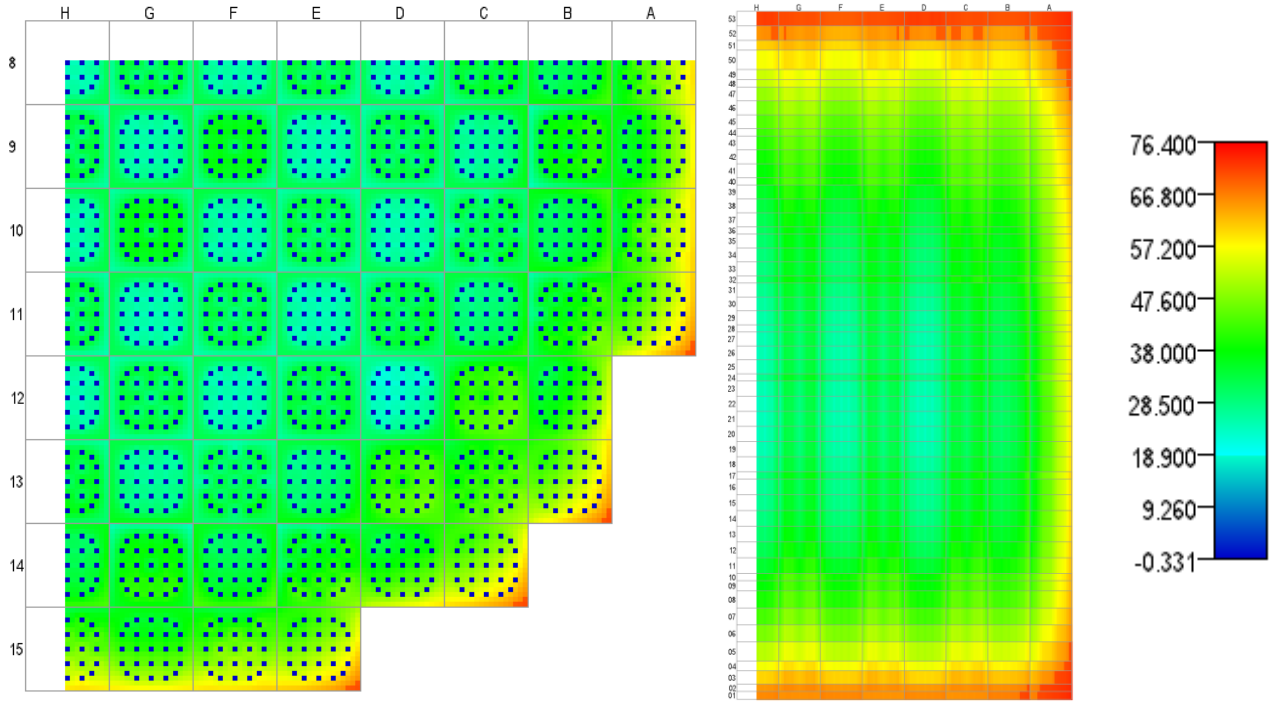

Figure A.2.4. Fuel-Clad Gap Thickness (microns), State 4, 1.919 GWd/MT.

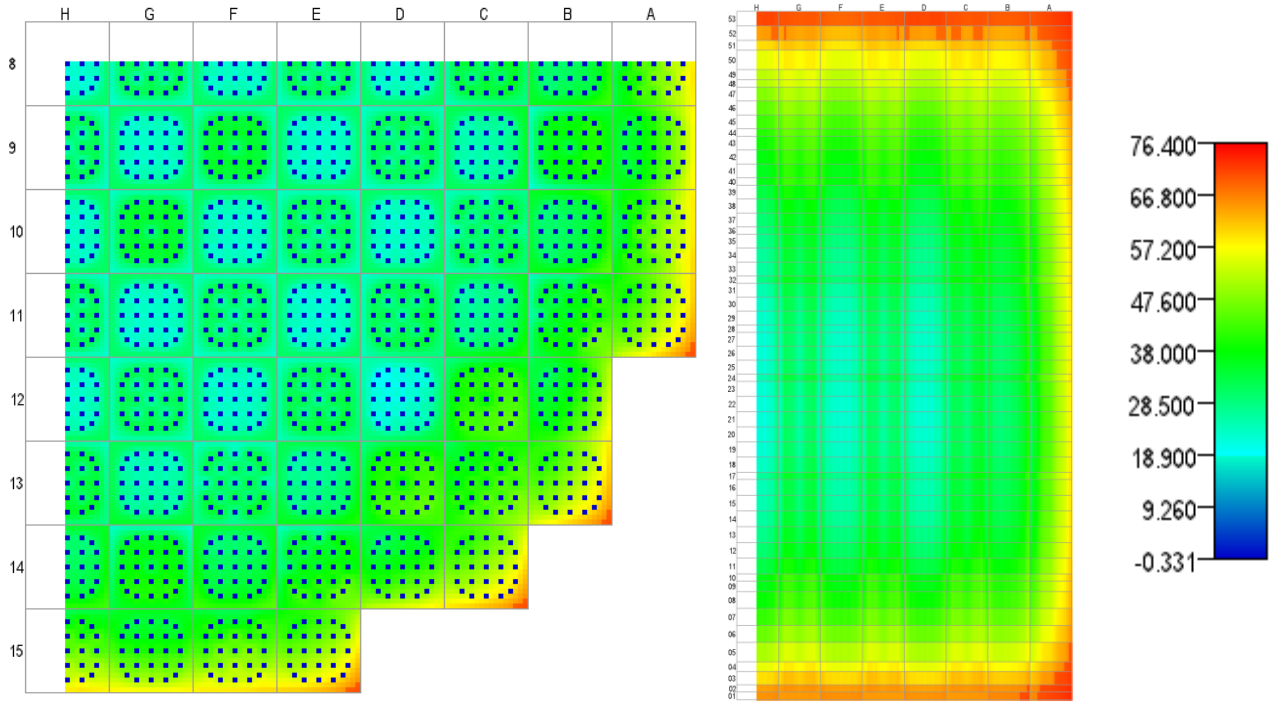

Figure A.2.5. Fuel-Clad Gap Thickness (microns), State 5, 2.457 GWd/MT.

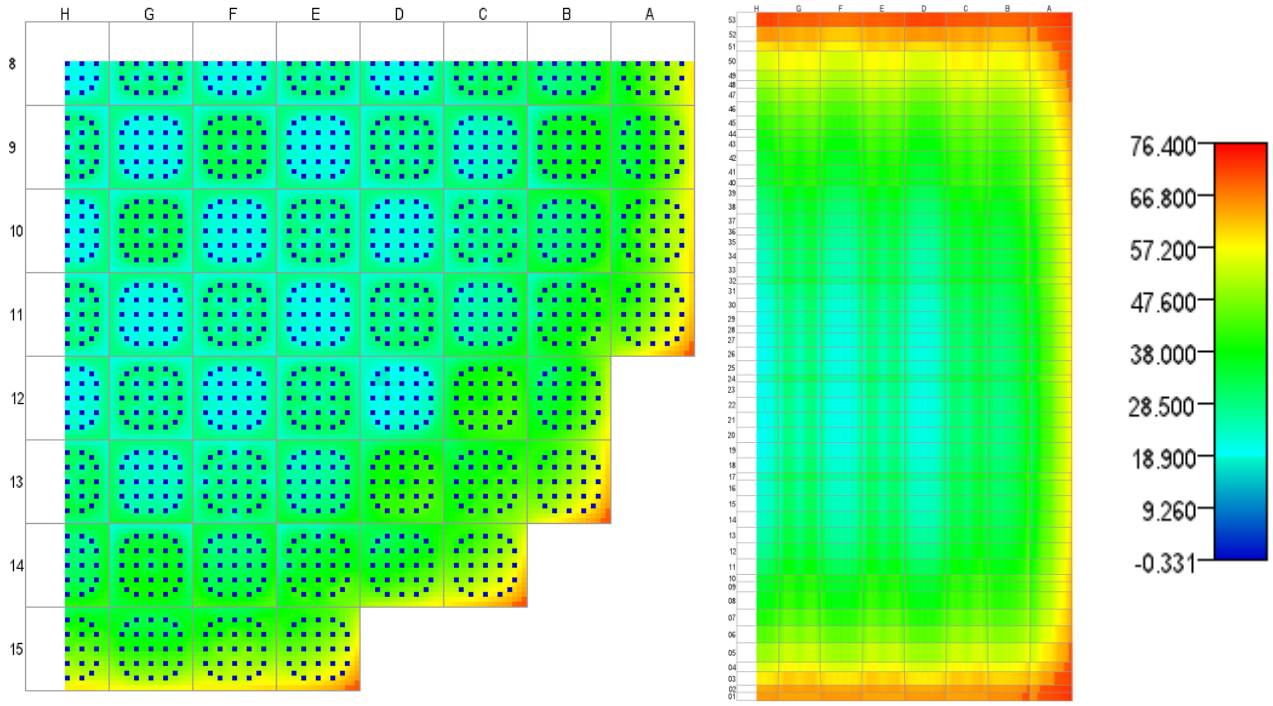

Figure A.2.6. Fuel-Clad Gap Thickness (microns), State 6, 2.994 GWd/MT.

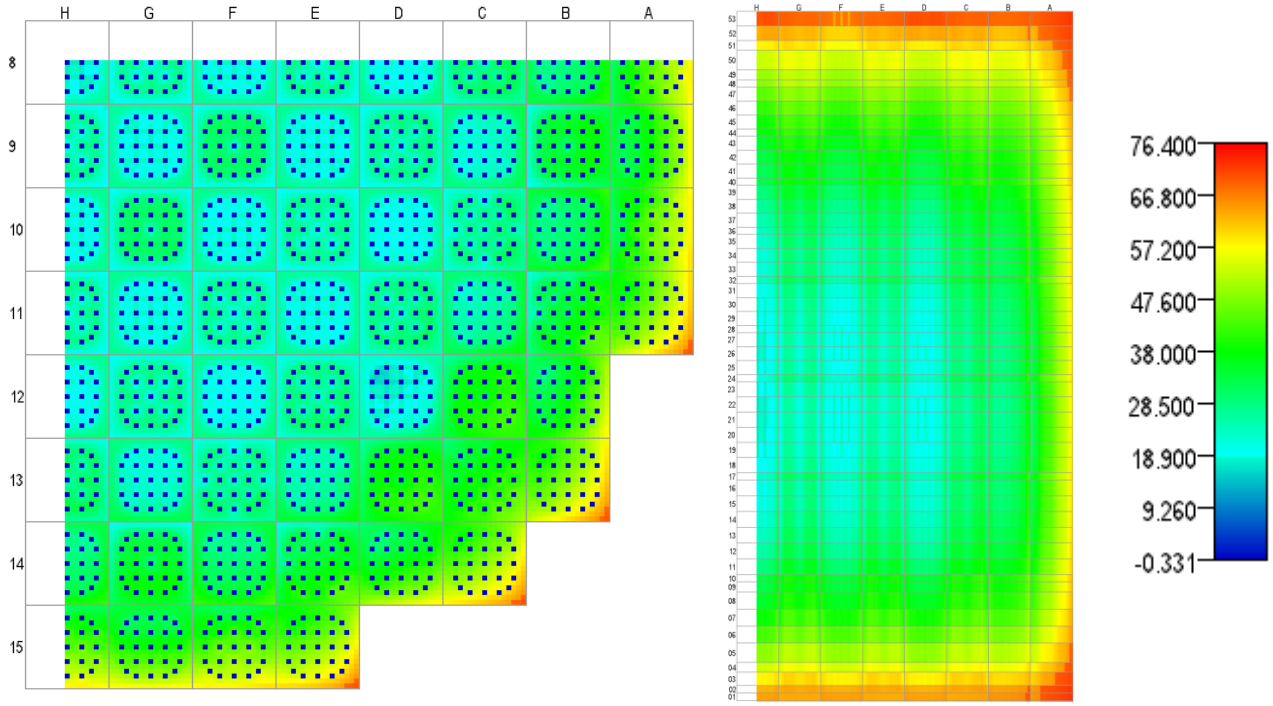

Figure A.2.7. Fuel-Clad Gap Thickness (microns), State 7, 3.562 GWd/MT.

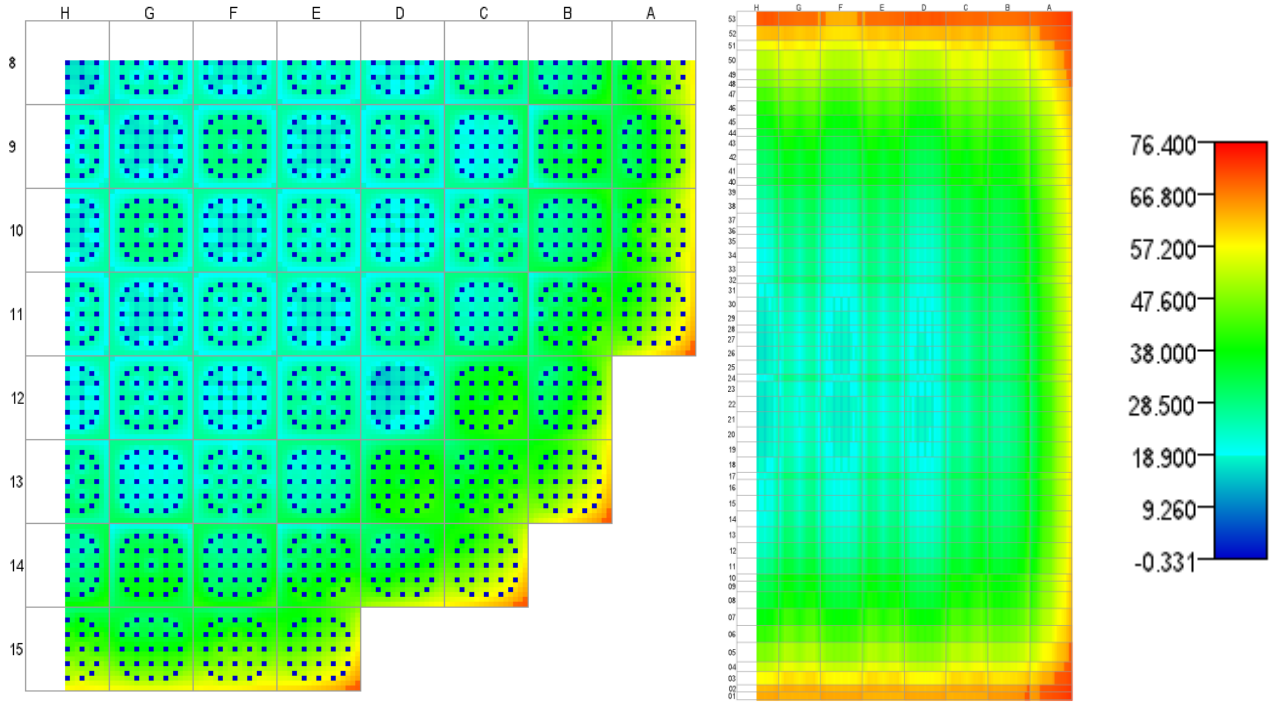

Figure A.2.8. Fuel-Clad Gap Thickness (microns), State 8, 4.065 GWd/MT.

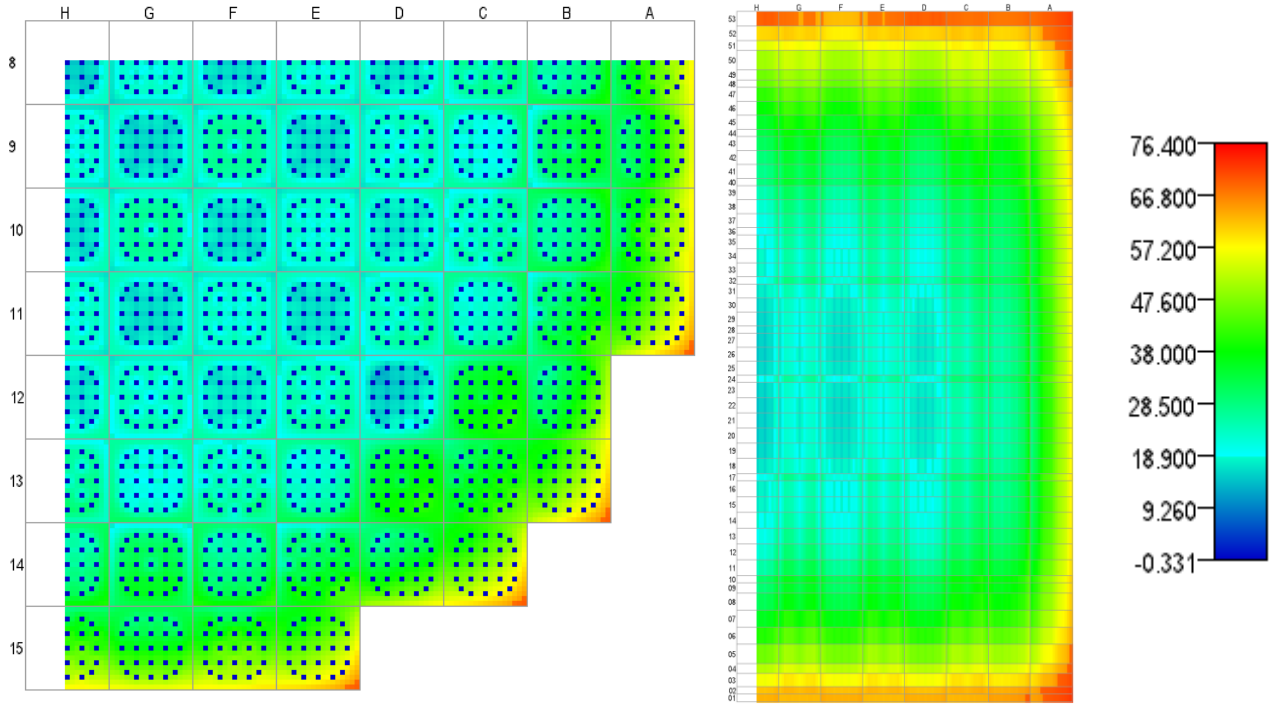

Figure A.2.9. Fuel-Clad Gap Thickness (microns), State 9, 4.642 GWd/MT.

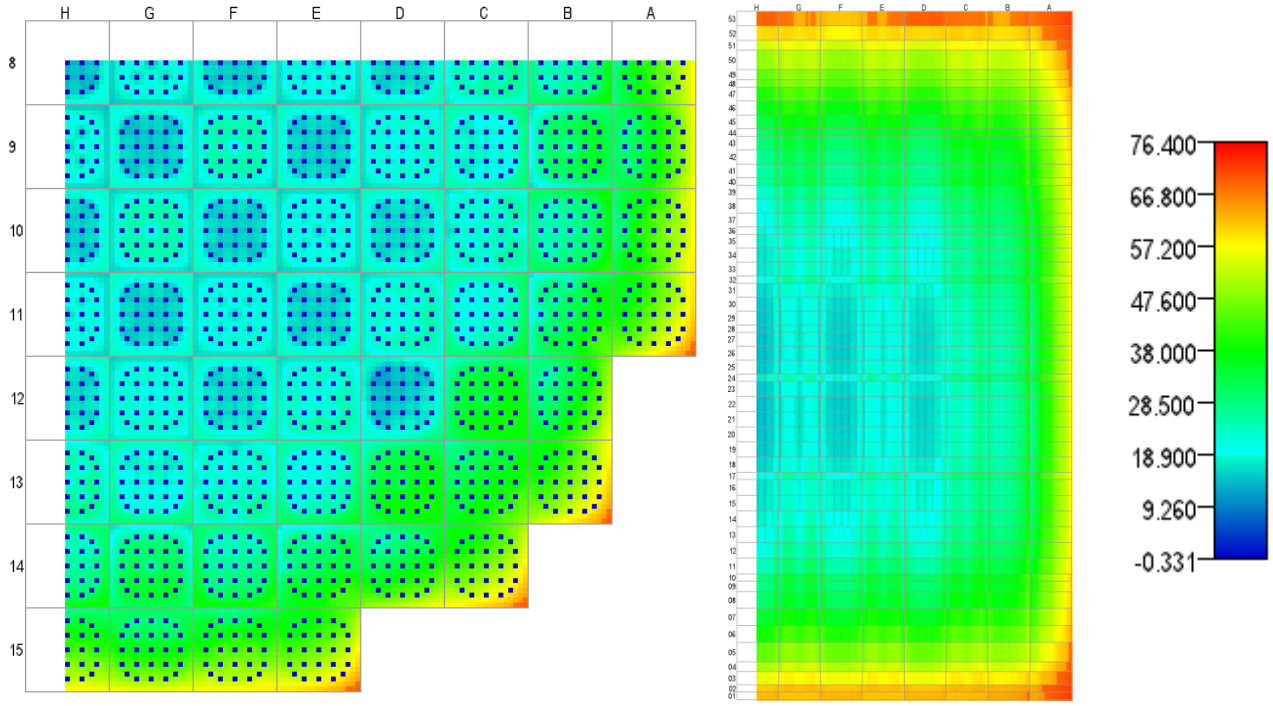

Figure A.2.10. Fuel-Clad Gap Thickness (microns), State 10, 5.139 GWd/MT.

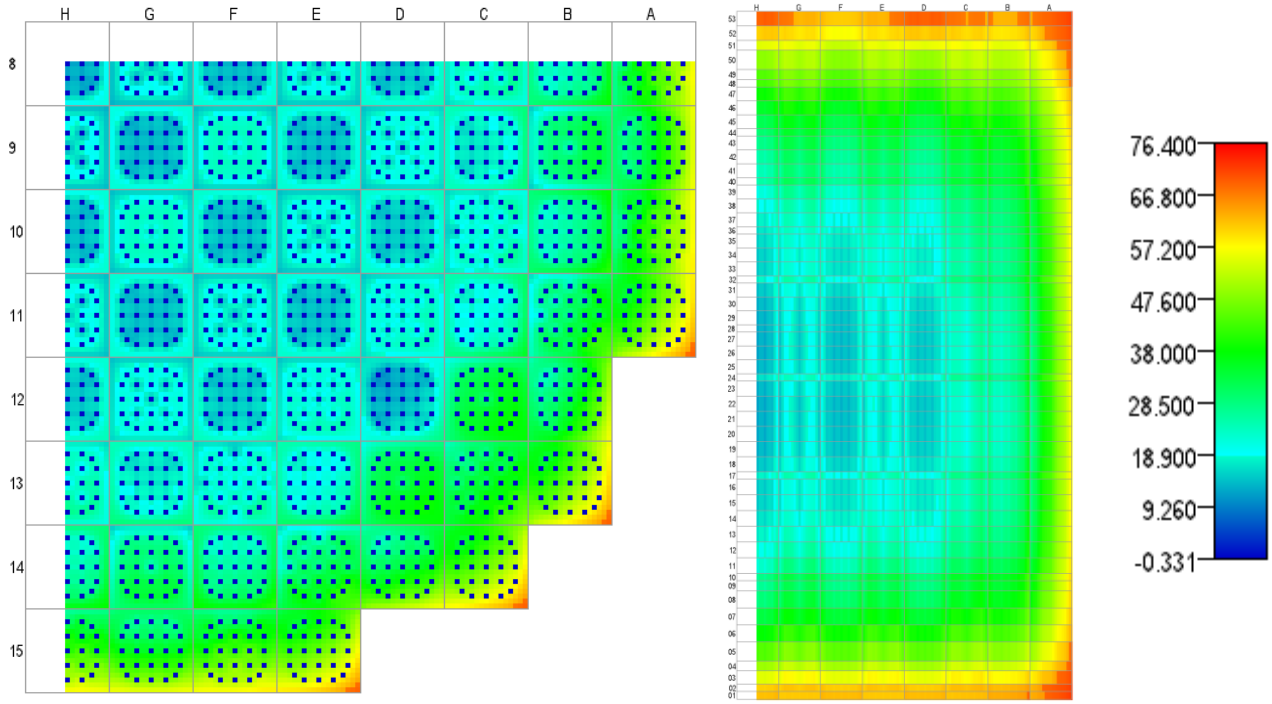

Figure A.2.11. Fuel-Clad Gap Thickness (microns), State 11, 5.700 GWd/MT.

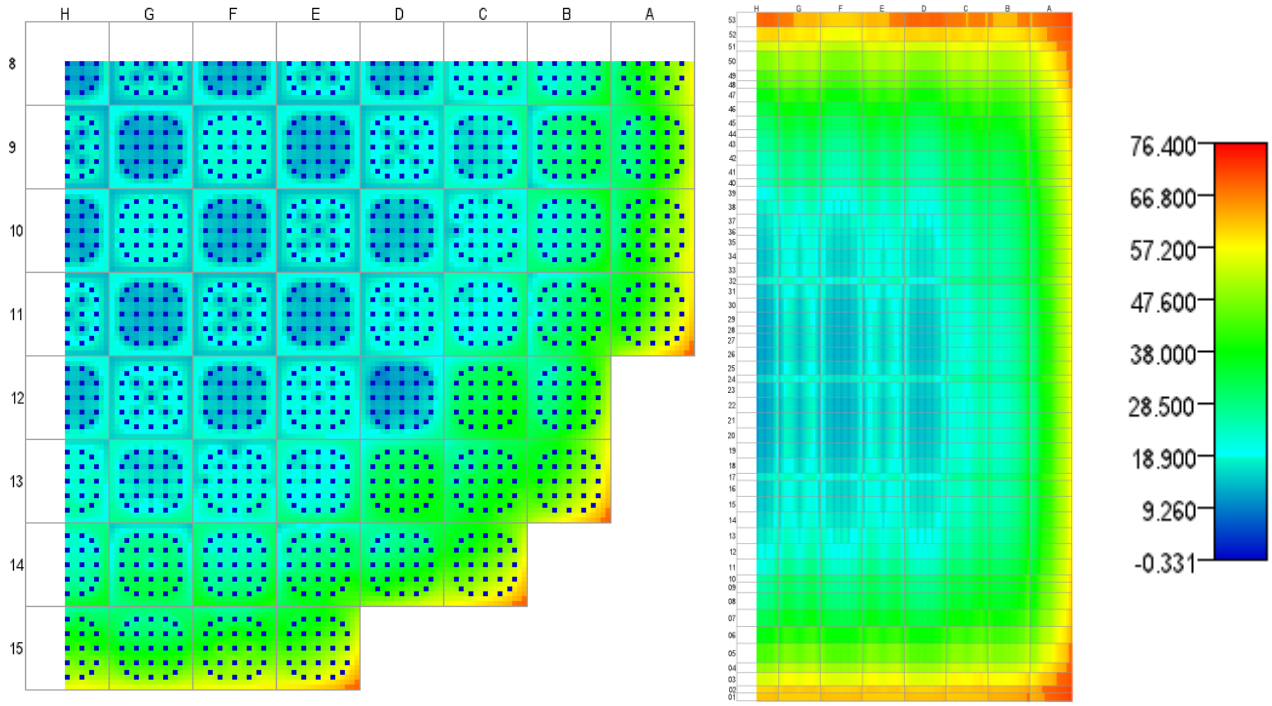

Figure A.2.12. Fuel-Clad Gap Thickness (microns), State 12, 6.273 GWd/MT.

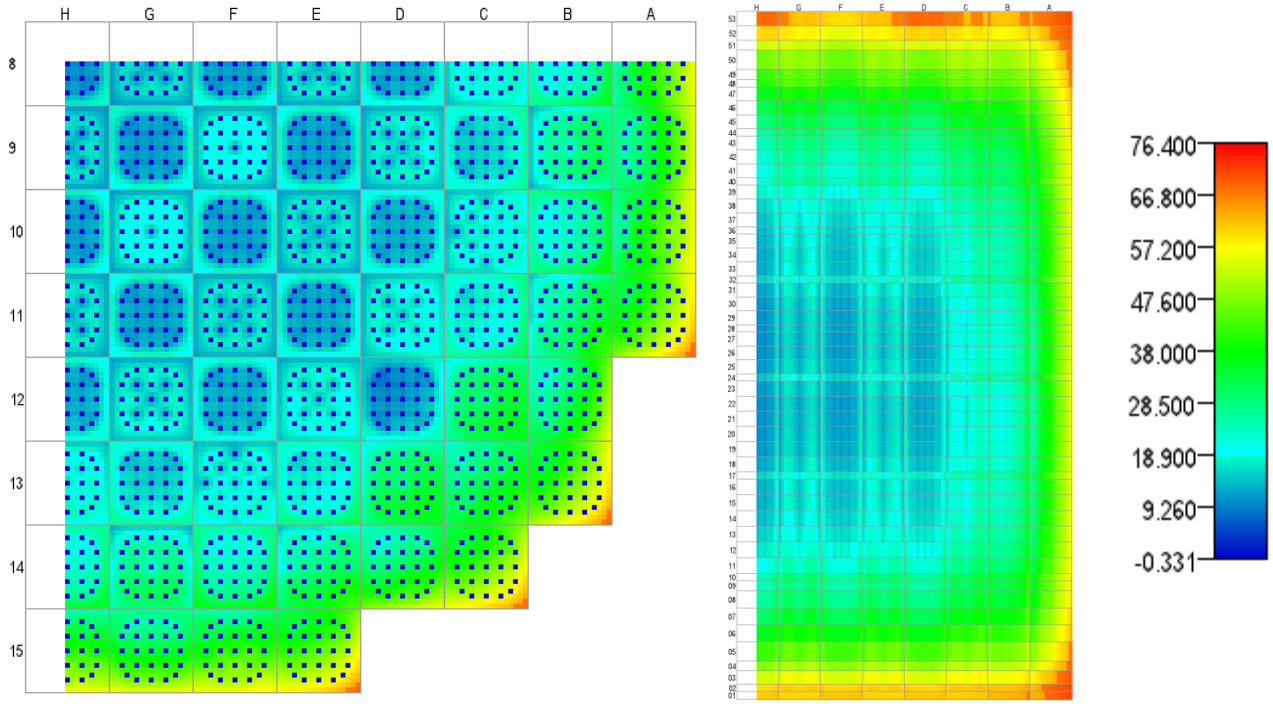

Figure A.2.13. Fuel-Clad Gap Thickness (microns), State 13, 7.000 GWd/MT.

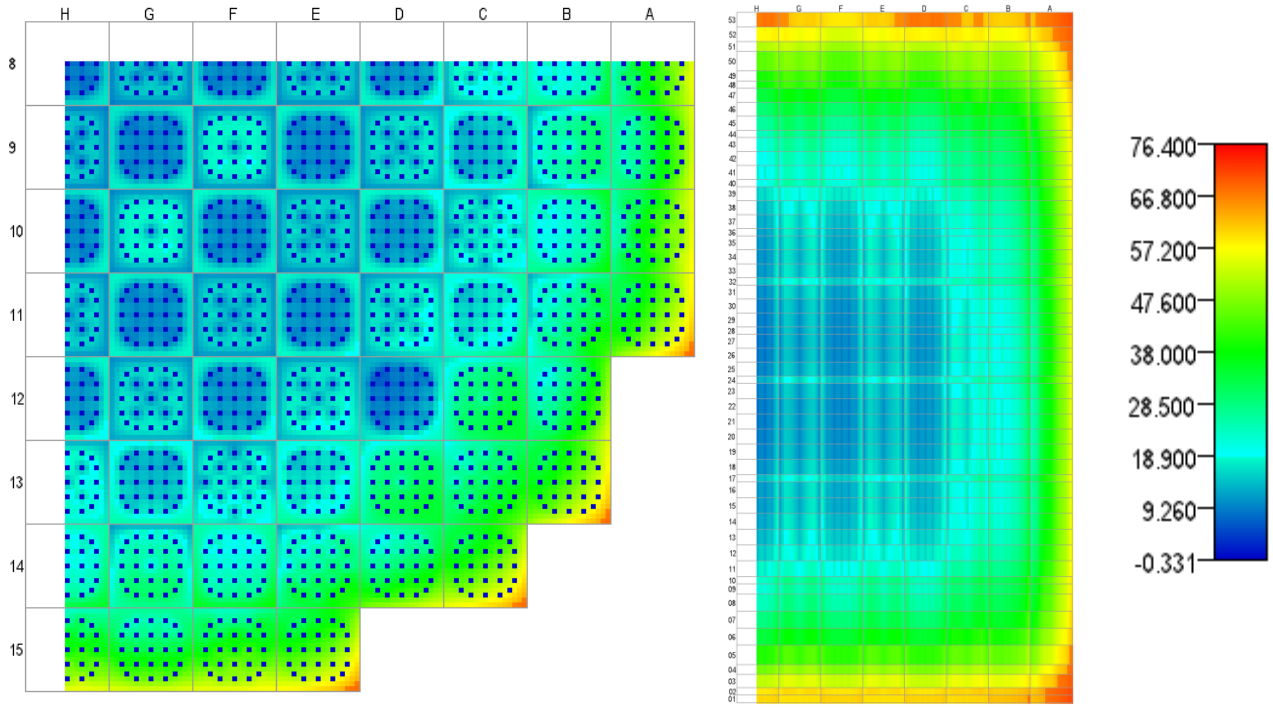

Figure A.2.14. Fuel-Clad Gap Thickness (microns), State 14, 7.463 GWd/MT.

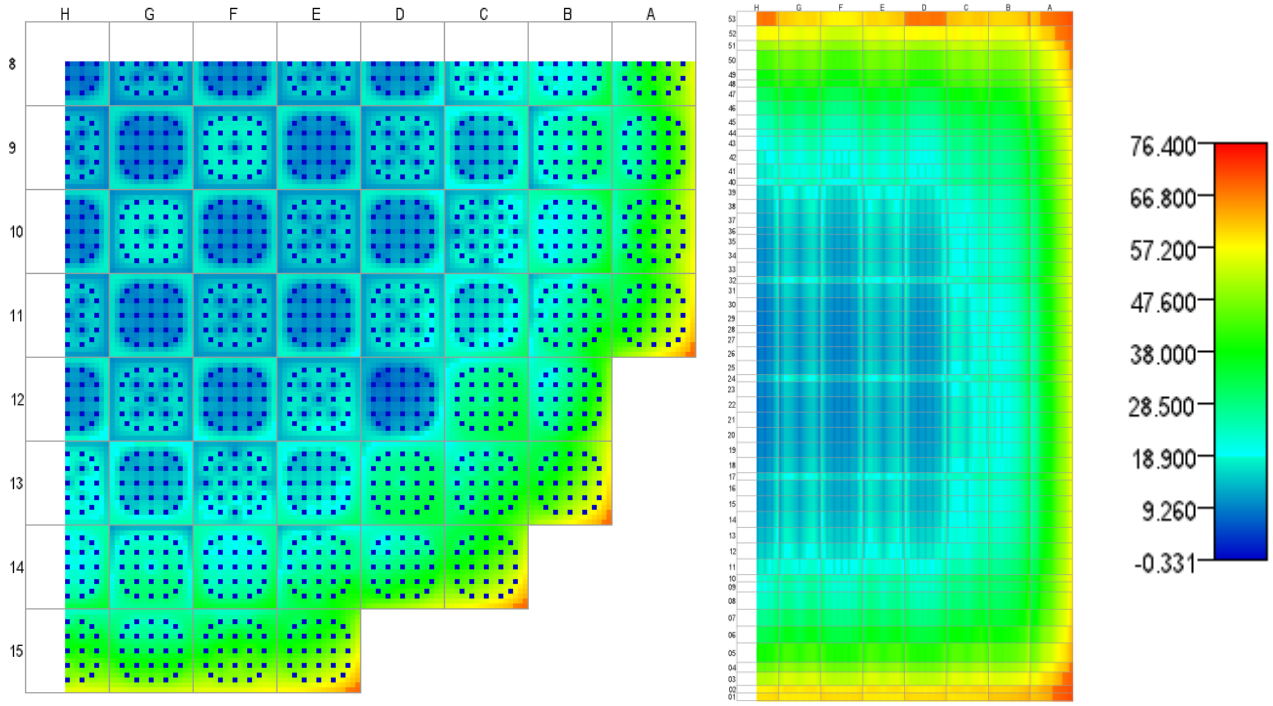

Figure A.2.15. Fuel-Clad Gap Thickness (microns), State 15, 7.978 GWd/MT.

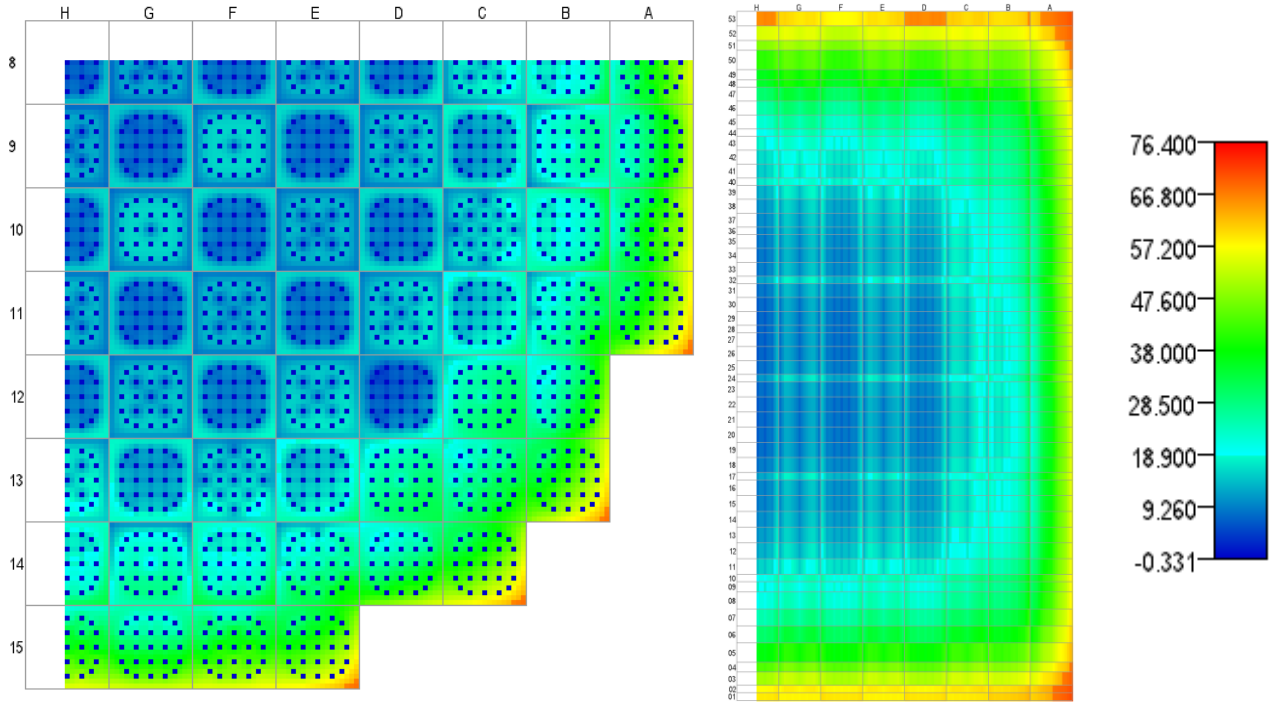

Figure A.2.16. Fuel-Clad Gap Thickness (microns), State 16, 8.493 GWd/MT.

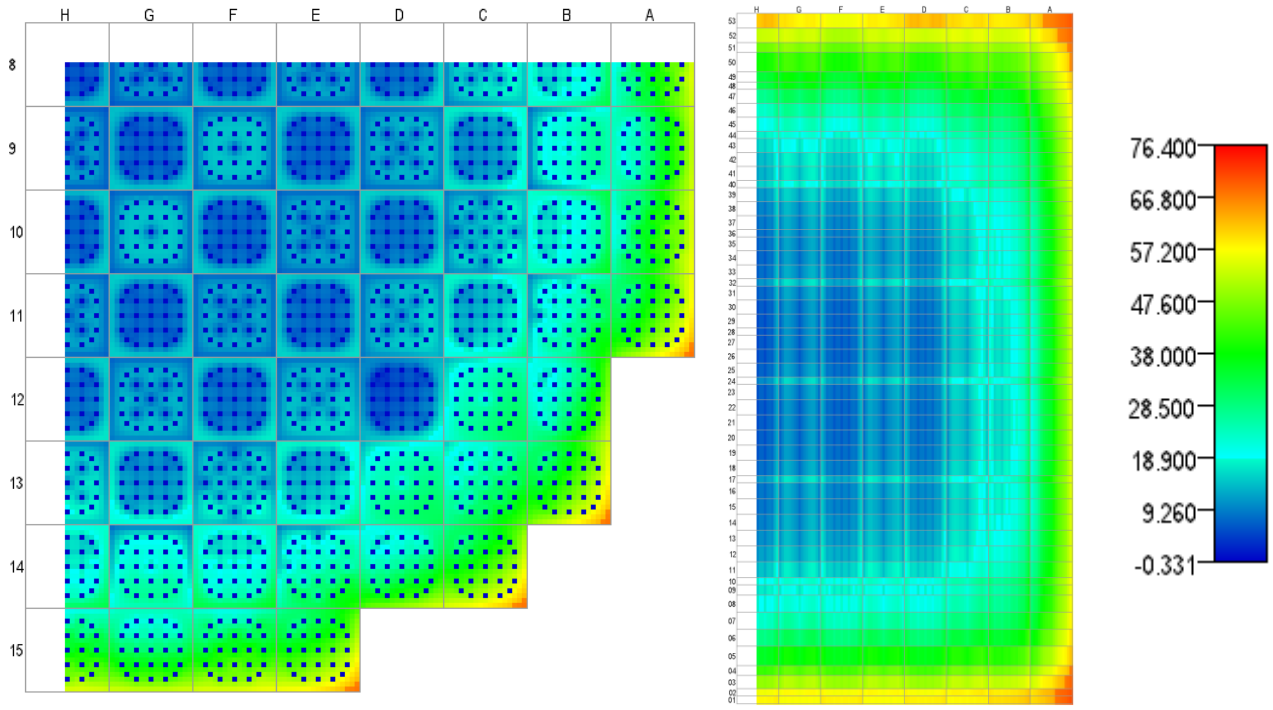

Figure A.2.17. Fuel-Clad Gap Thickness (microns), State 17, 9.140 GWd/MT.

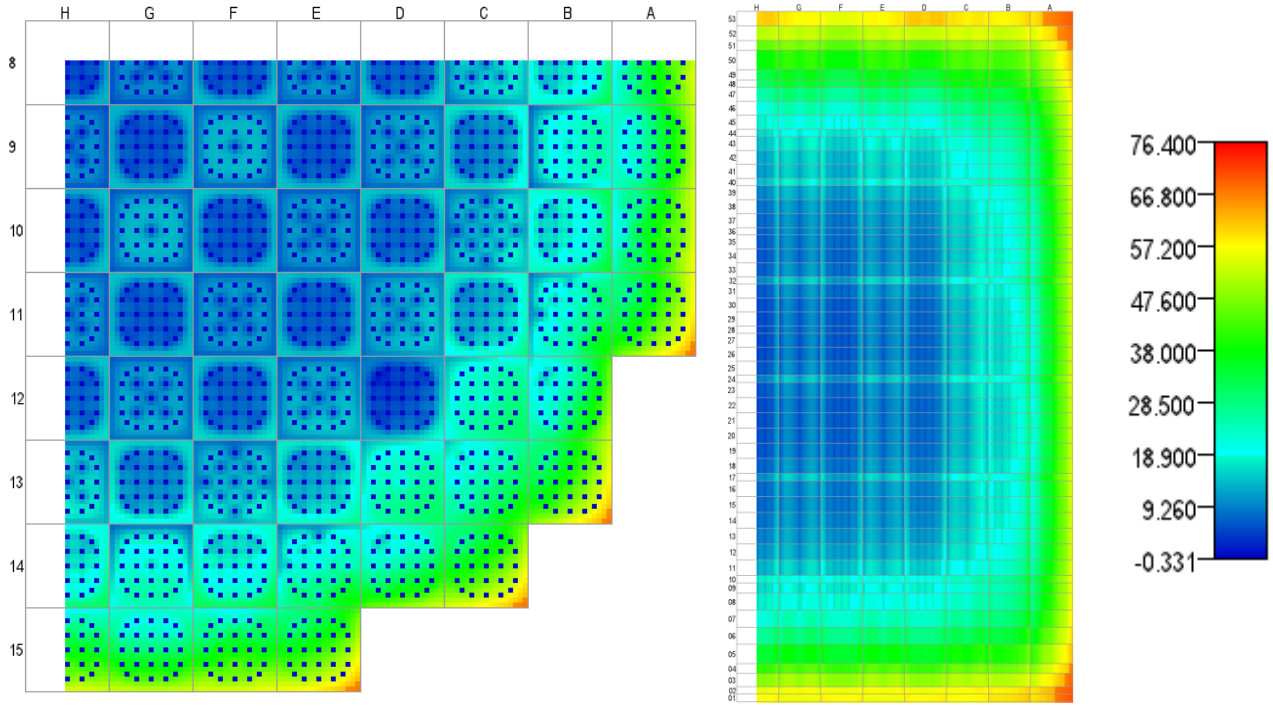

Figure A.2.18. Fuel-Clad Gap Thickness (microns), State 18, 9.602 GWd/MT.

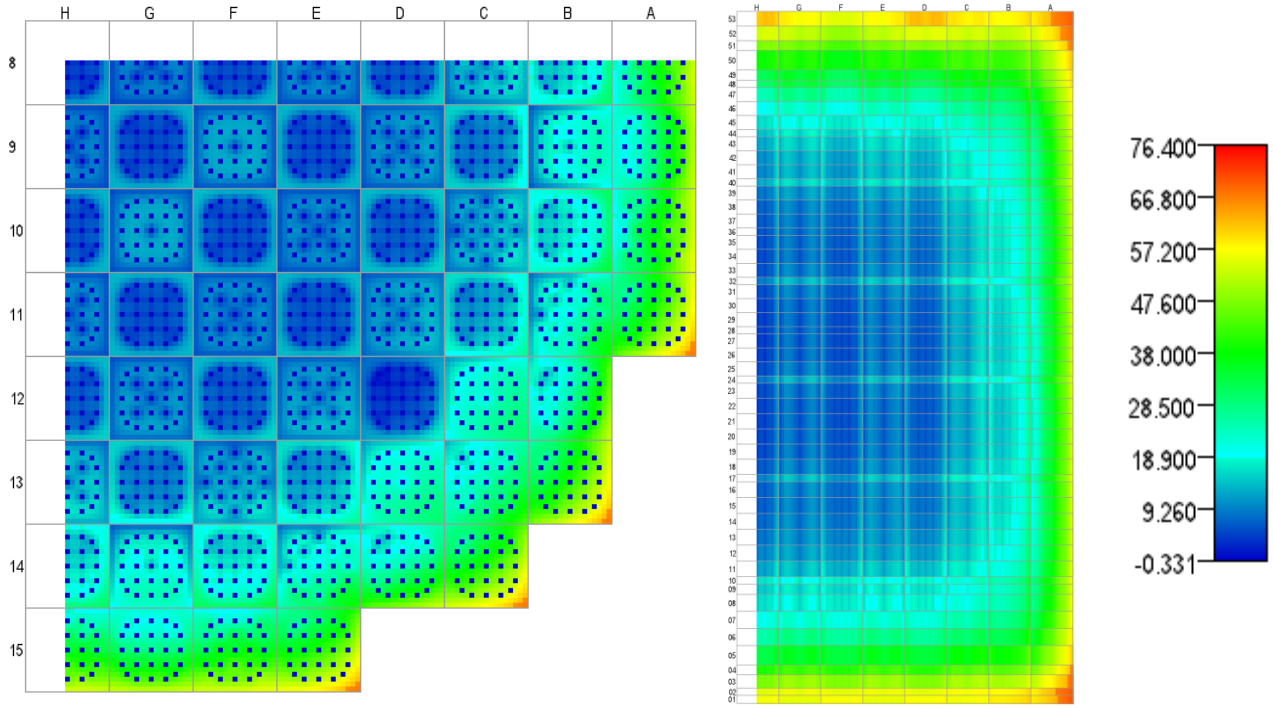

Figure A.2.19. Fuel-Clad Gap Thickness (microns), State 19, 10.344 GWd/MT.

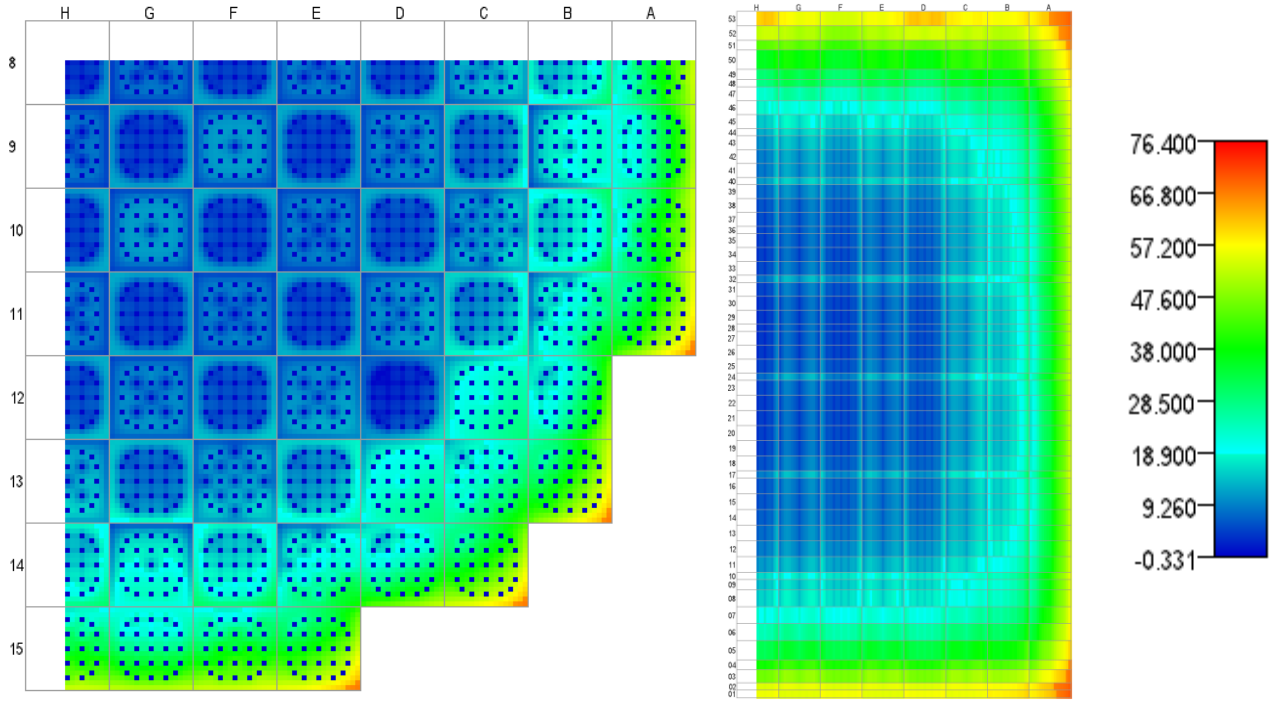

Figure A.2.20. Fuel-Clad Gap Thickness (microns), State 20, 10.842 GWd/MT.

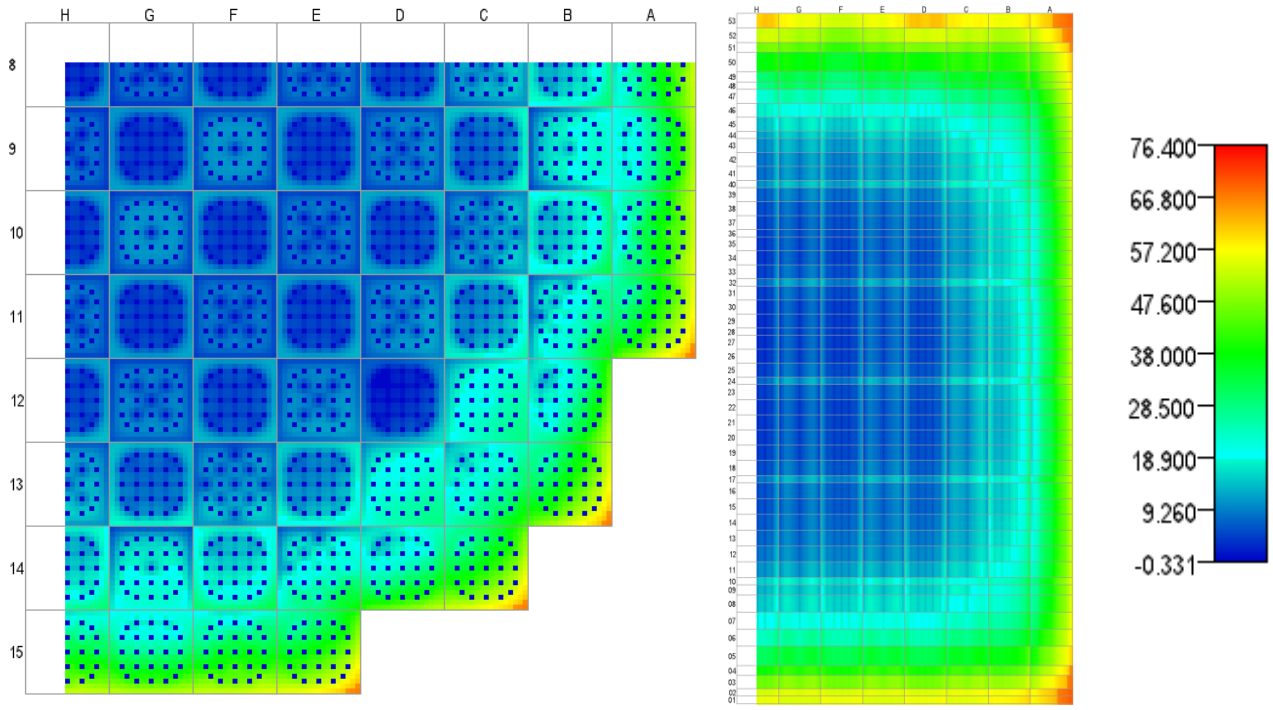

Figure A.2.21. Fuel-Clad Gap Thickness (microns), State 21, 11.314 GWd/MT.

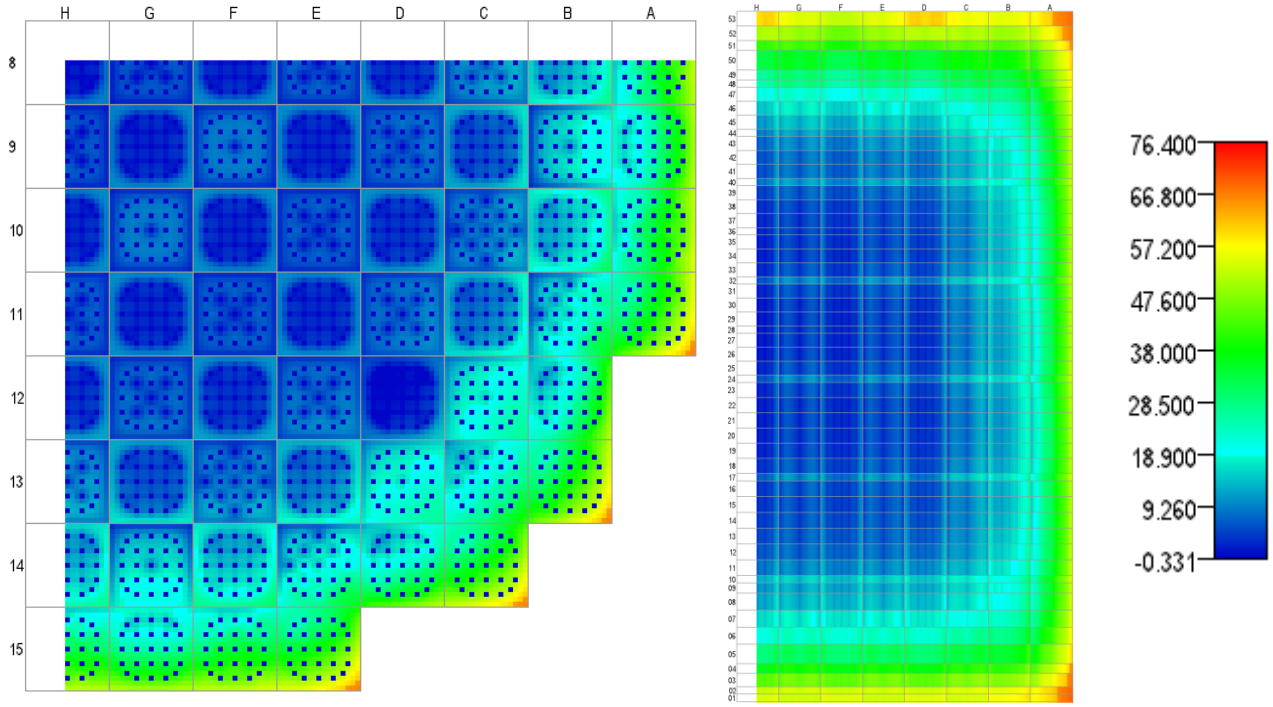

Figure A.2.22. Fuel-Clad Gap Thickness (microns), State 22, 11.988 GWd/MT.

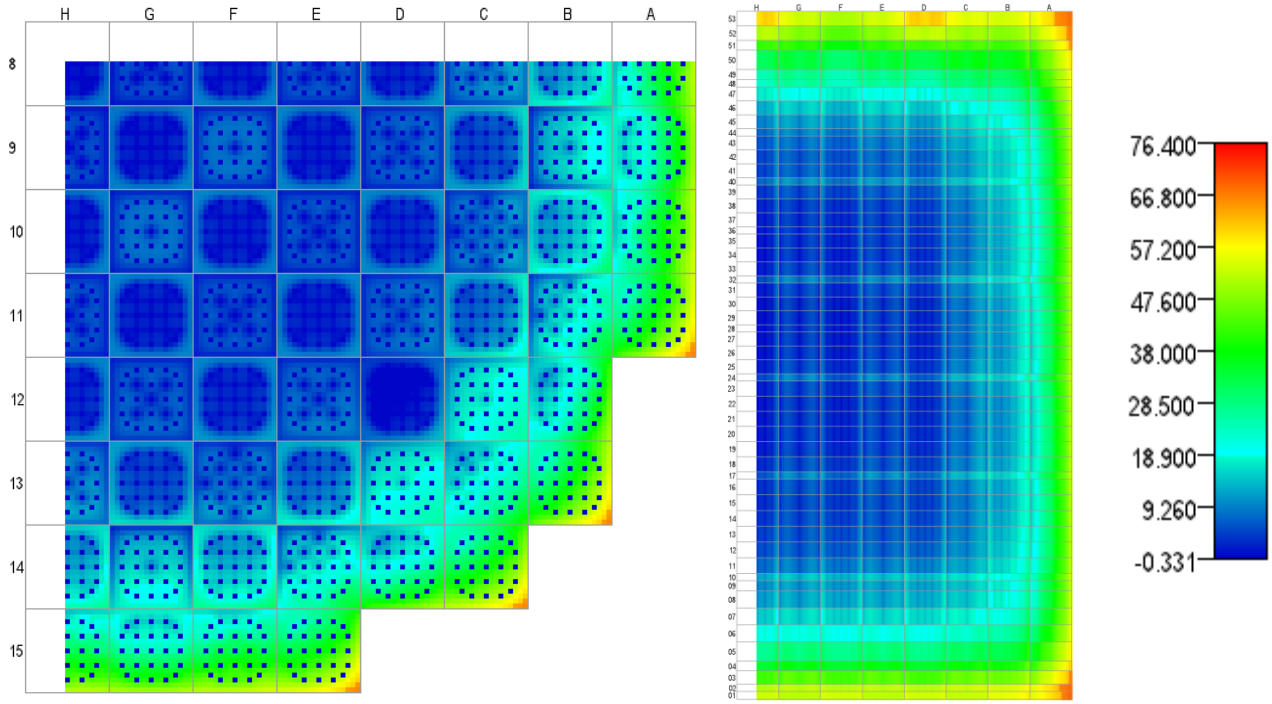

Figure A.2.23. Fuel-Clad Gap Thickness (microns), State 23, 12.552 GWd/MT.

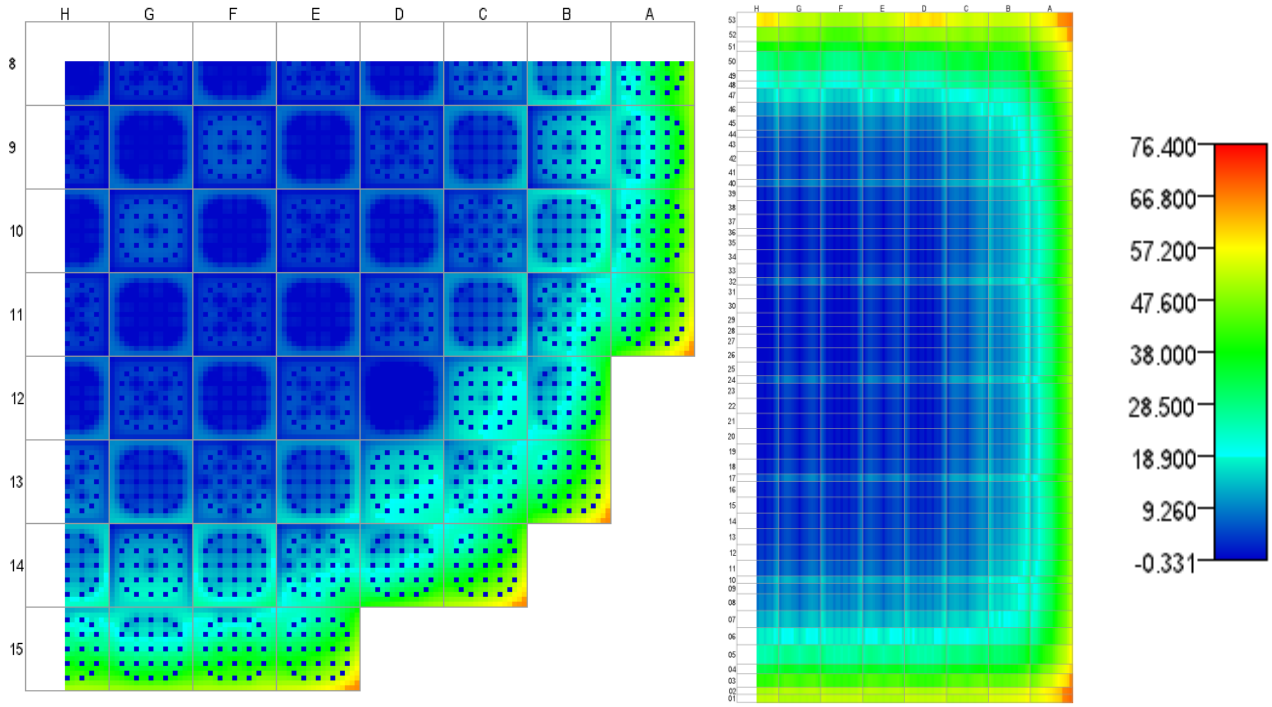

Figure A.2.24. Fuel-Clad Gap Thickness (microns), State 24, 13.360 GWd/MT.

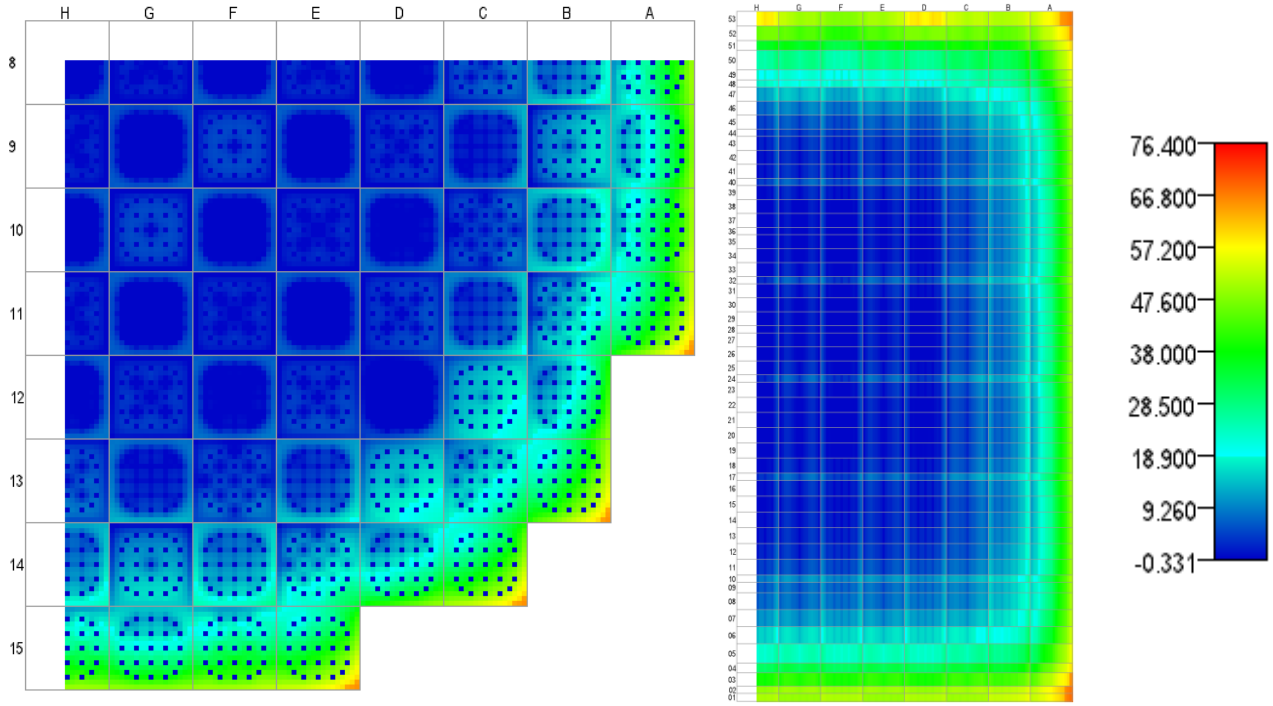

Figure A.2.25. Fuel-Clad Gap Thickness (microns), State 25, 14.285 GWd/MT.

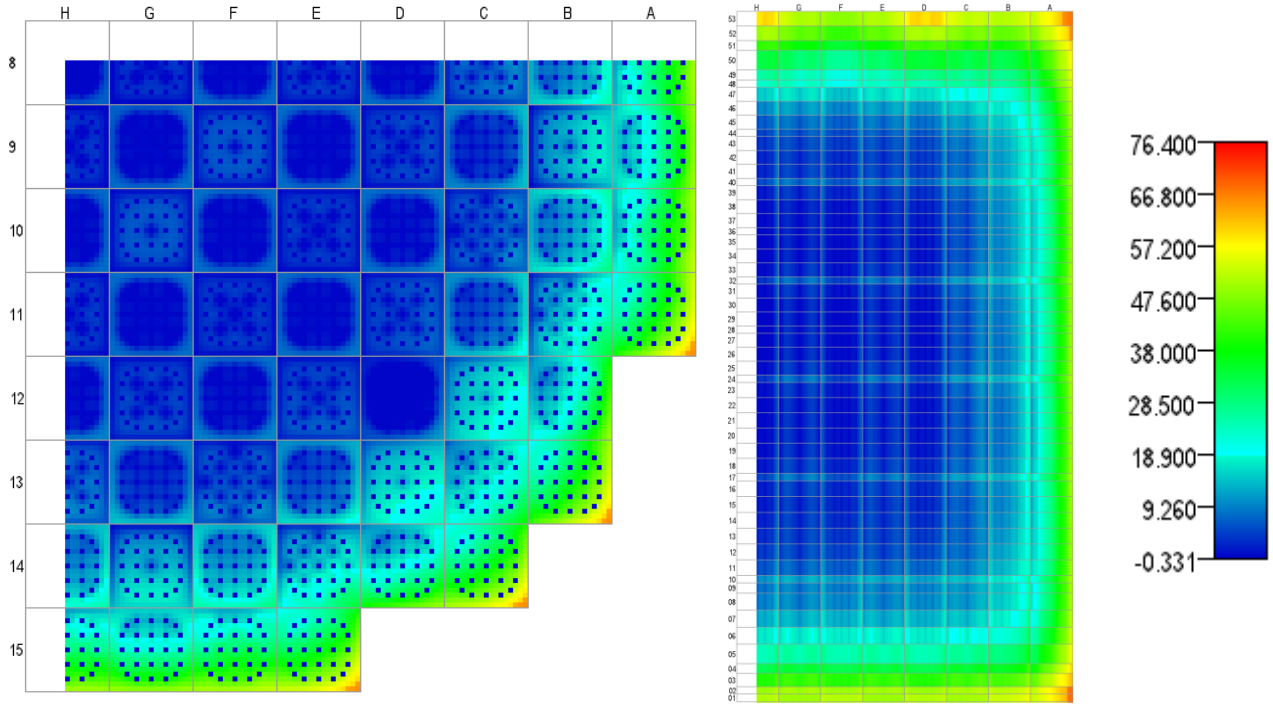

Figure A.2.26. Fuel-Clad Gap Thickness (microns), State 26, 14.385 GWd/MT.

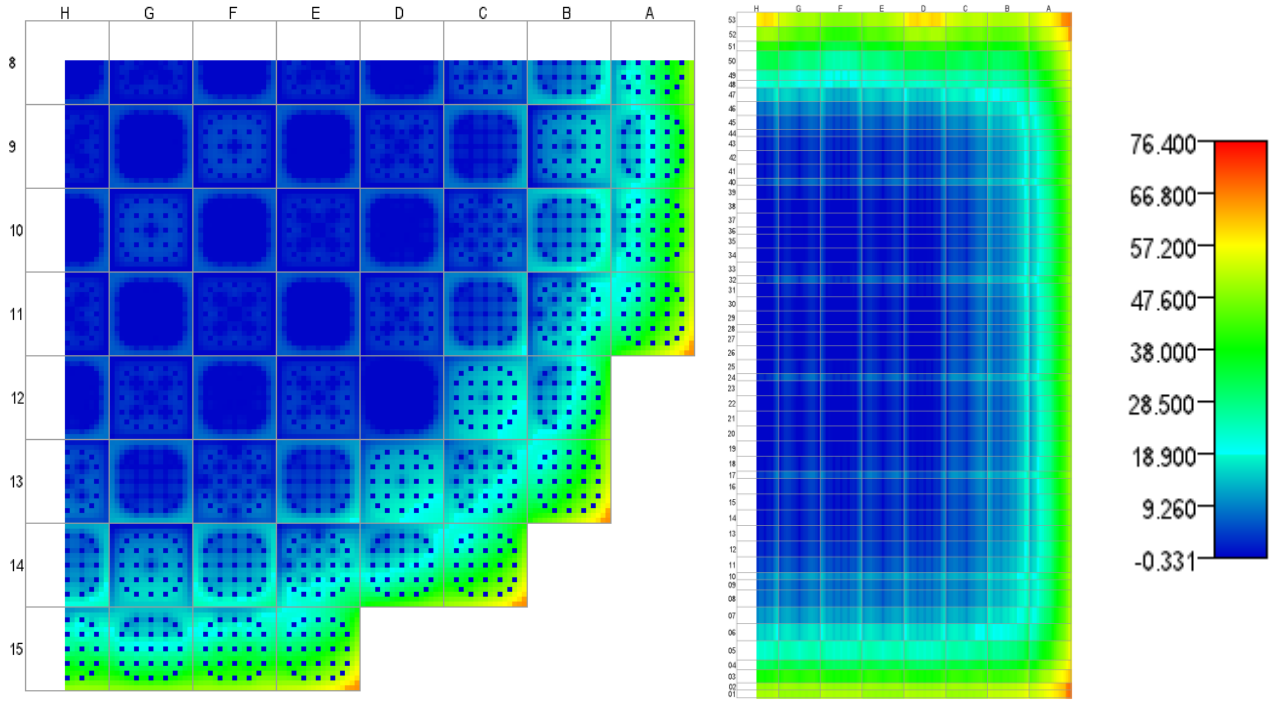

Figure A.2.27. Fuel-Clad Gap Thickness (microns), State 27, 15.018 GWd/MT.

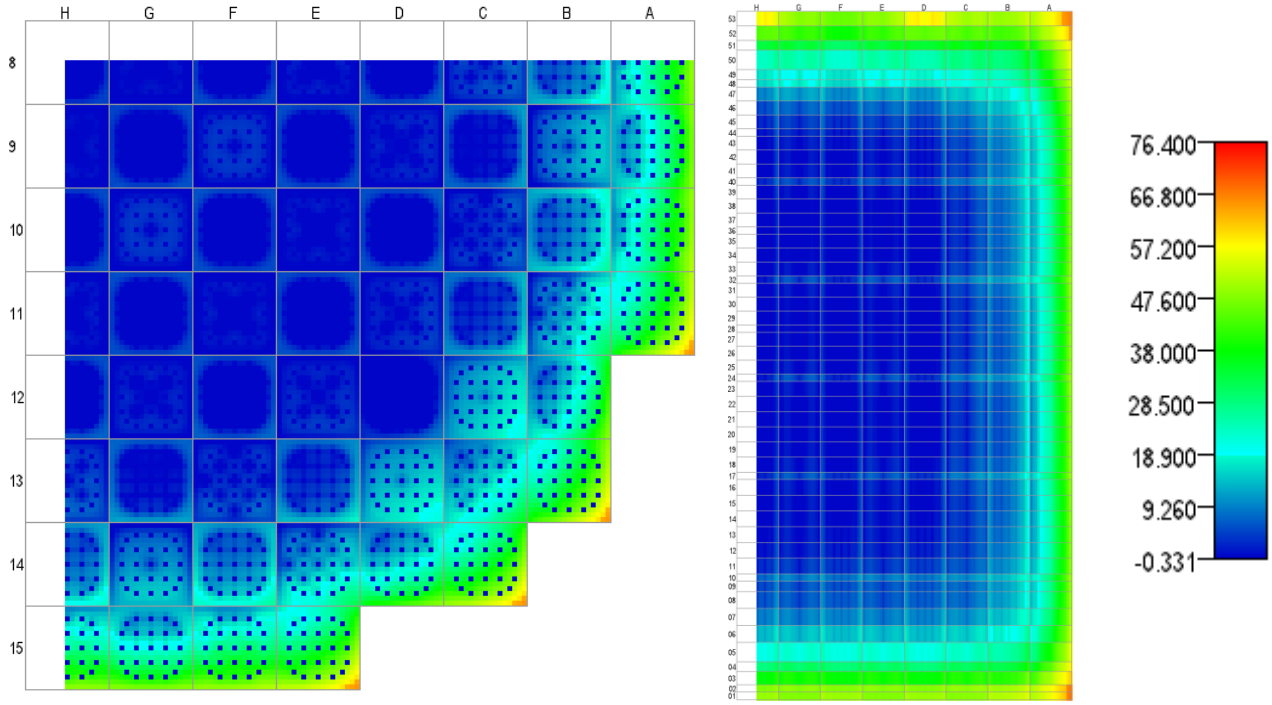

Figure A.2.28. Fuel-Clad Gap Thickness (microns), State 28, 15.118 GWd/MT.

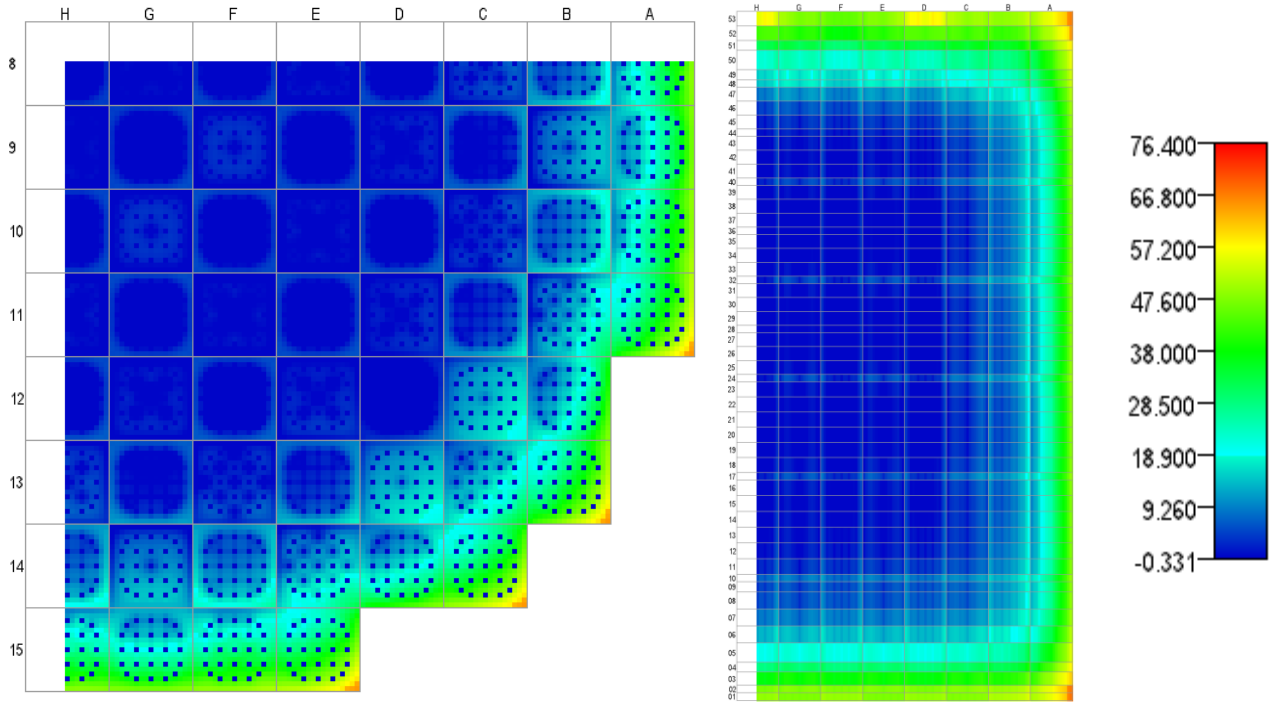

Figure A.2.29. Fuel-Clad Gap Thickness (microns), State 29, 15.308 GWd/MT.

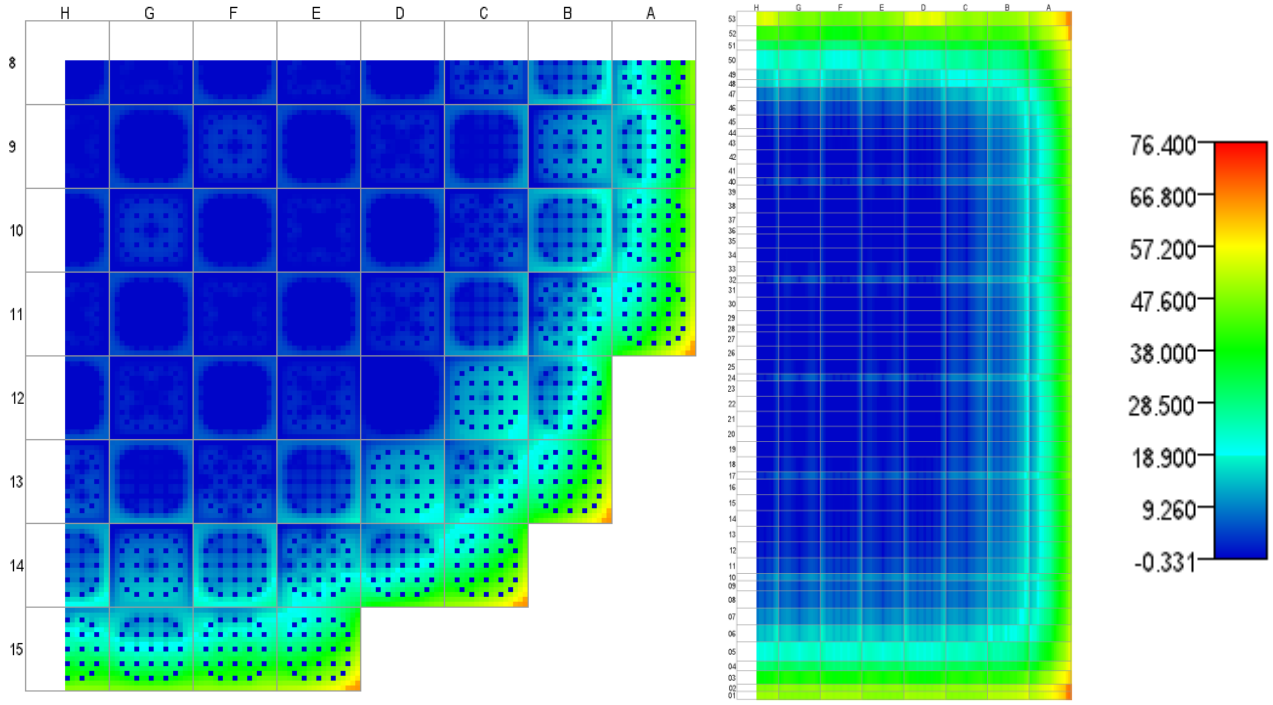

Figure A.2.30. Fuel-Clad Gap Thickness (microns), State 30, 15.774 GWd/MT.

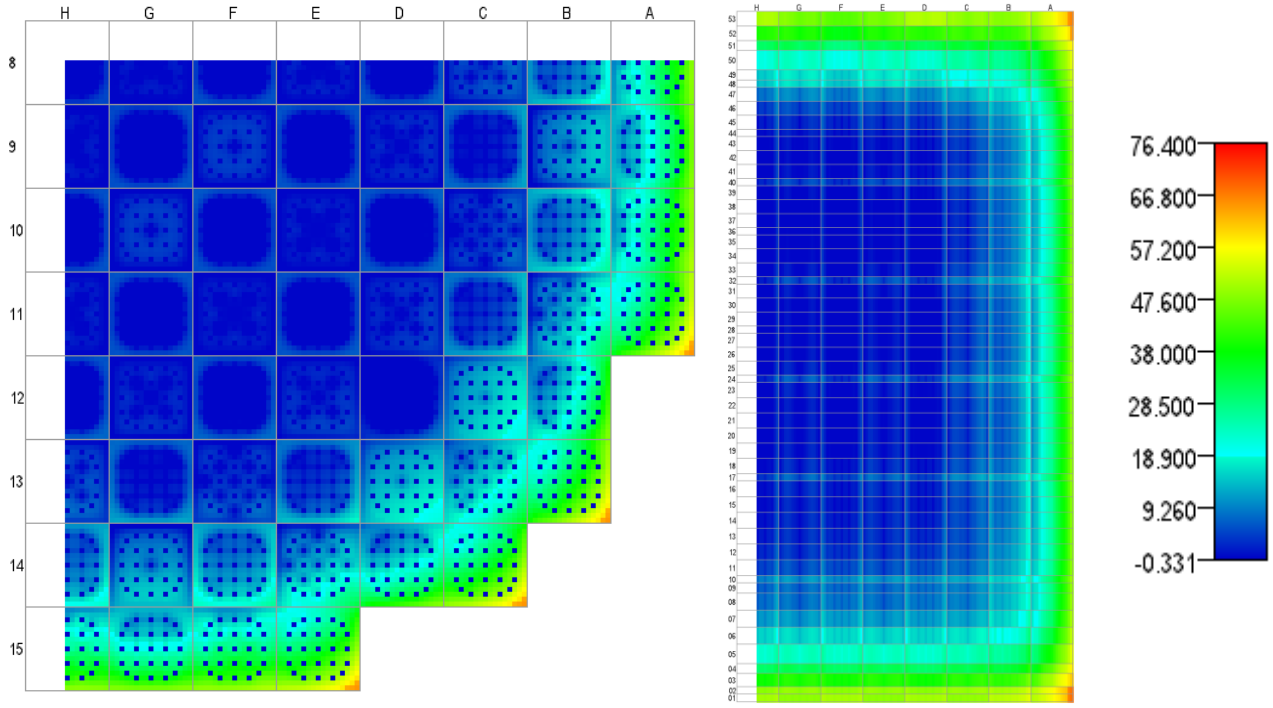

Figure A.2.31. Fuel-Clad Gap Thickness (microns), State 31, 16.270 GWd/MT.

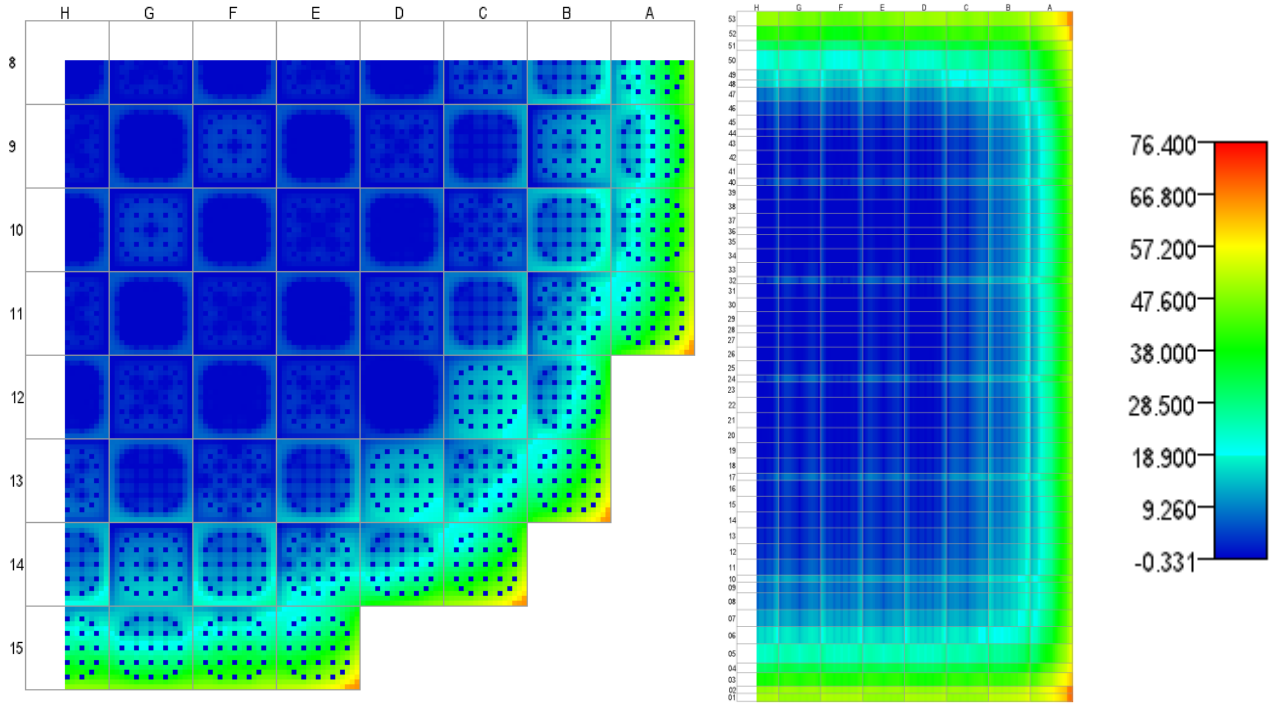

Figure A.2.32. Fuel-Clad Gap Thickness (microns), State 32, 16.932 GWd/MT.

A.3. Clad Hoop Stress

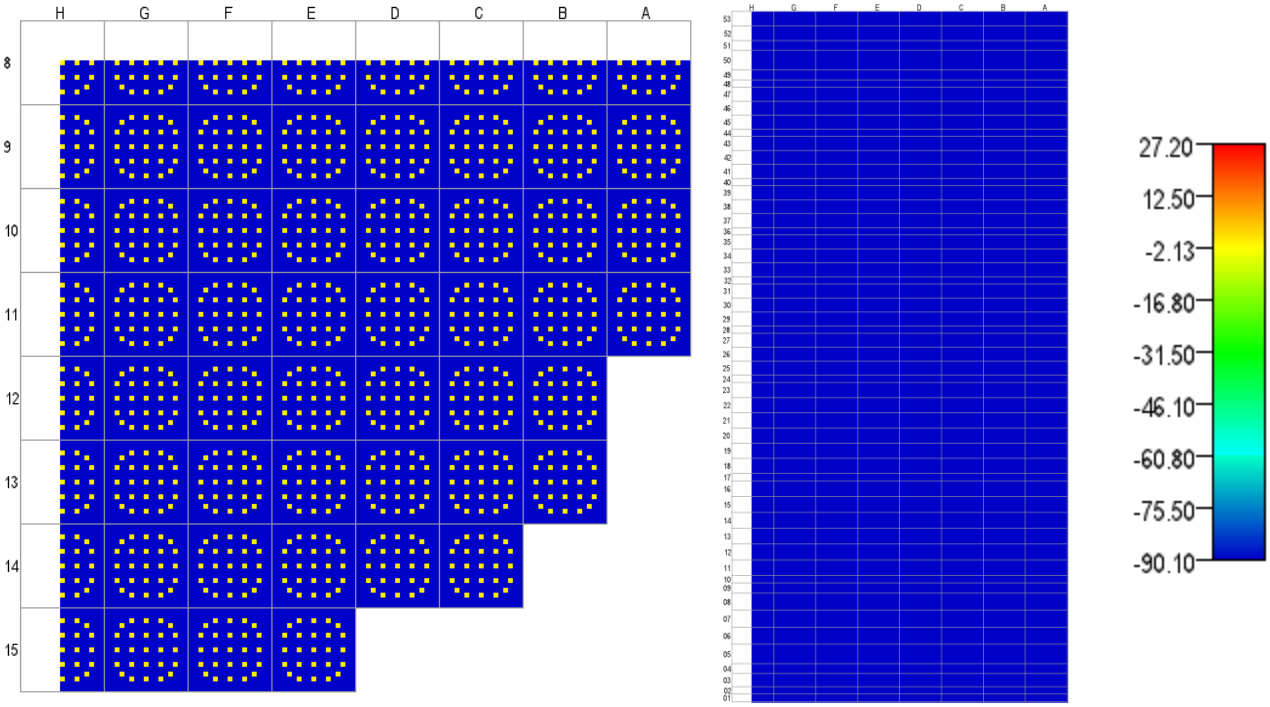

Figure A.3.1. Maximum Clad Hoop Stress (MPa), State 1, 0.000 GWd/MT.

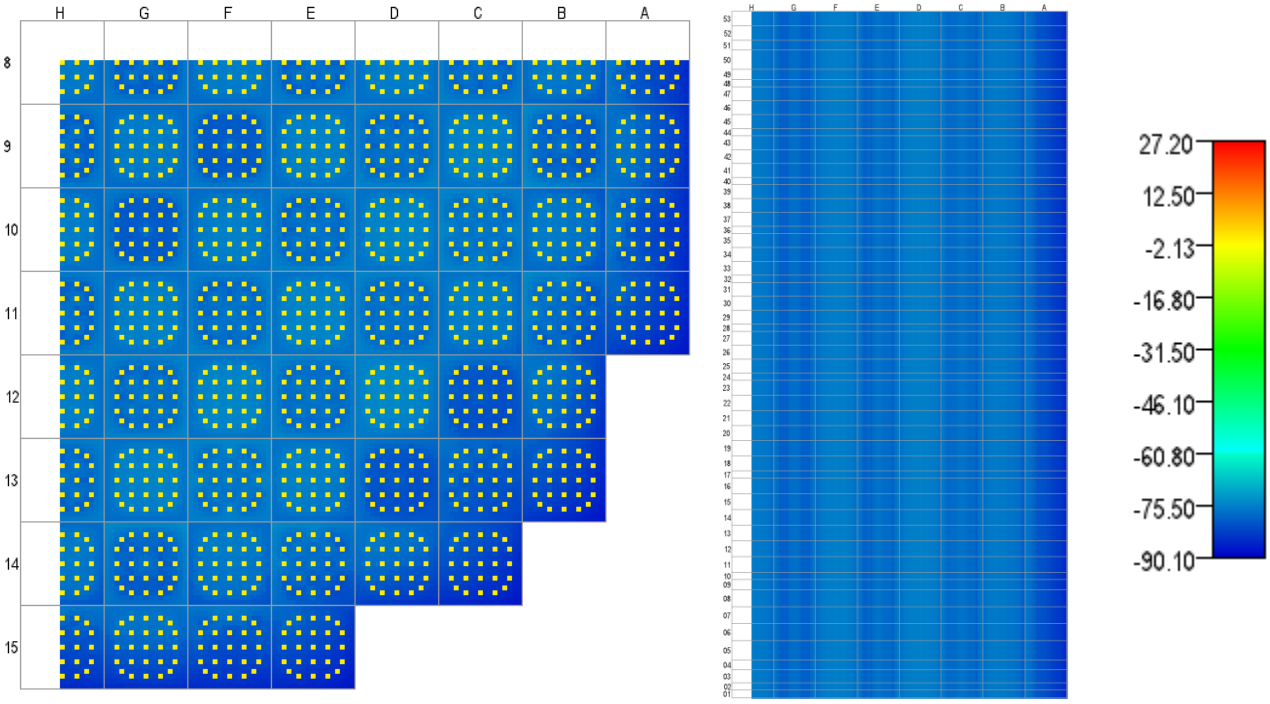

Figure A.3.2. Maximum Clad Hoop Stress (MPa), State 2, 0.346 GWd/MT.

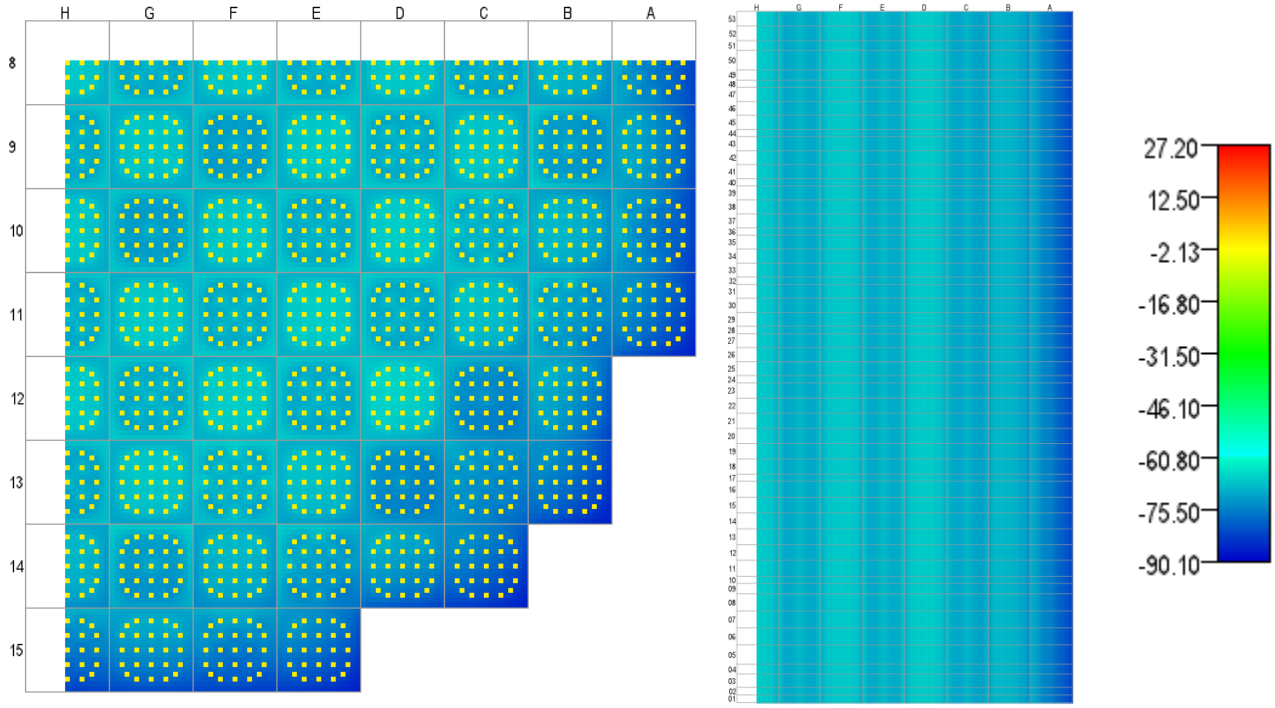

Figure A.3.3. Maximum Clad Hoop Stress (MPa), State 3, 1.230 GWd/MT.

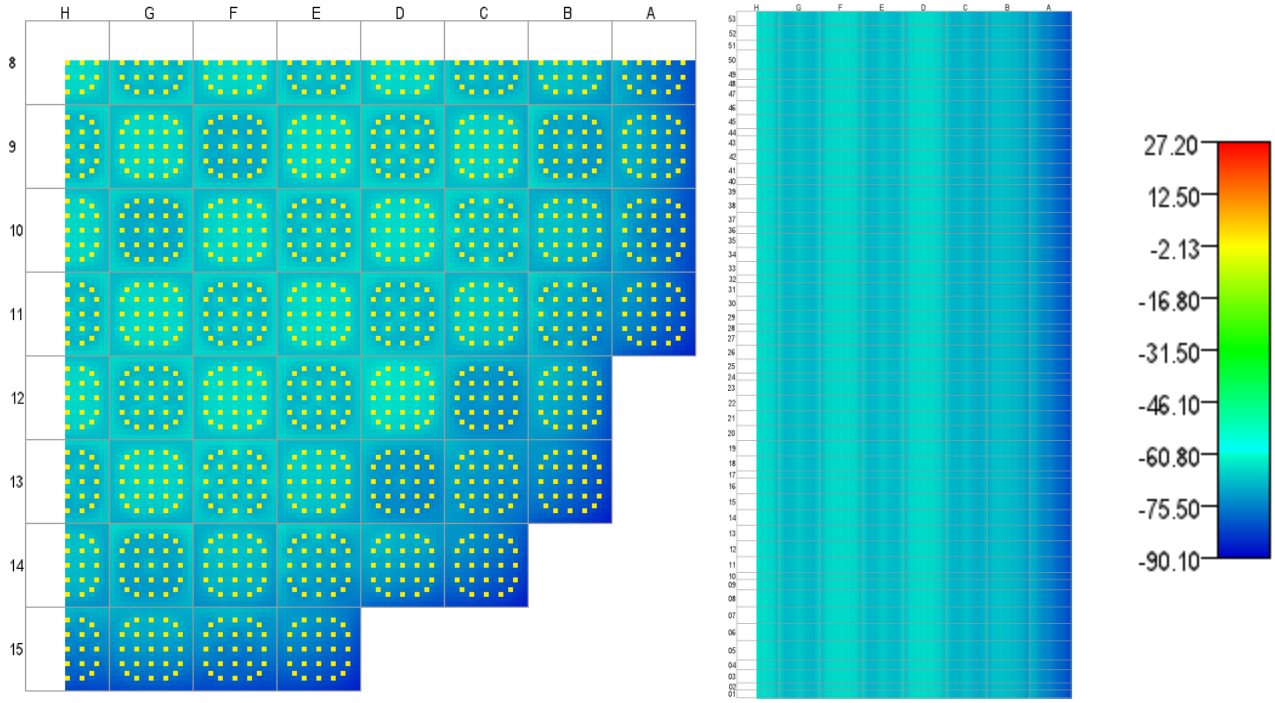

Figure A.3.4. Maximum Clad Hoop Stress (MPa), State 4, 1.919 GWd/MT.

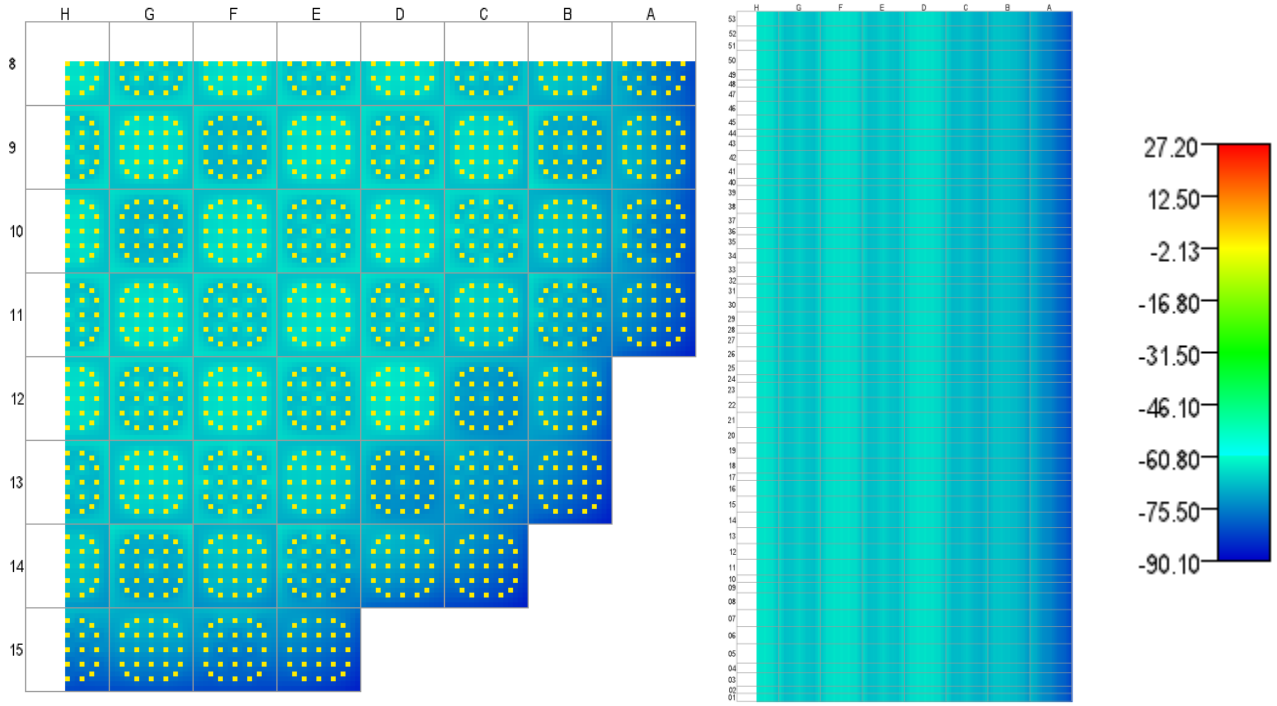

Figure A.3.5. Maximum Clad Hoop Stress (MPa), State 5, 2.457 GWd/MT.

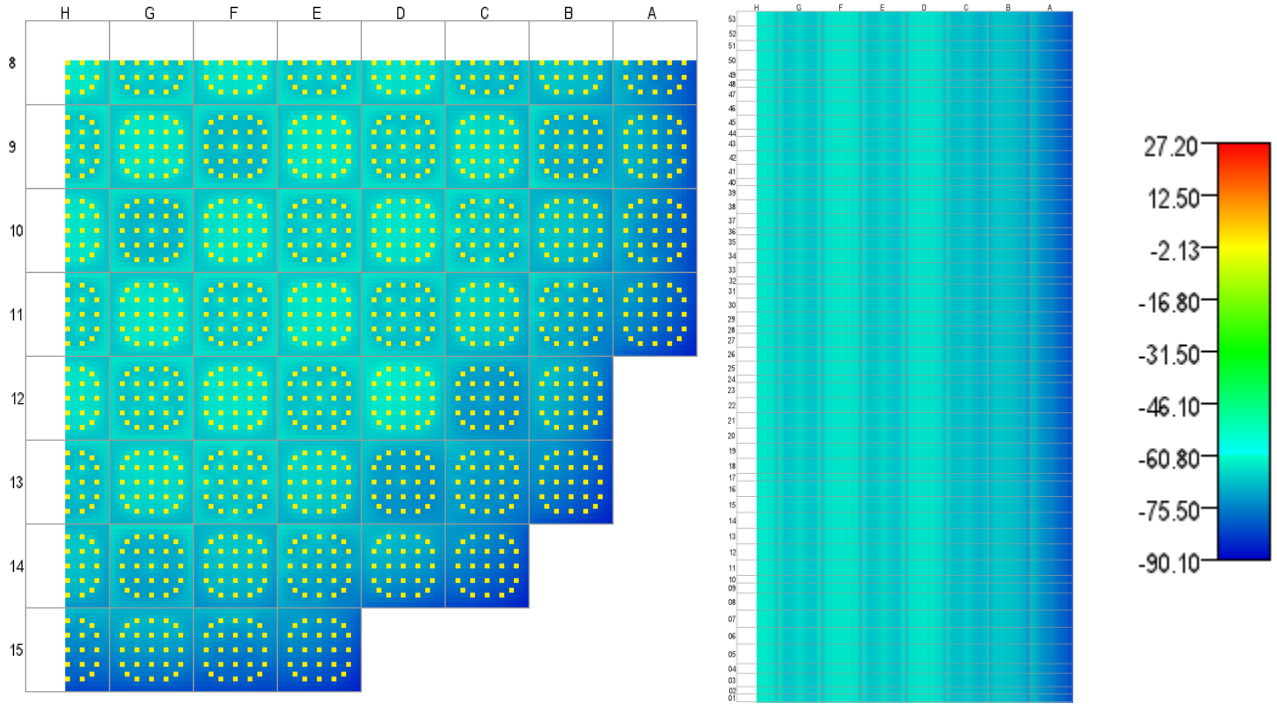

Figure A.3.6. Maximum Clad Hoop Stress (MPa), State 6, 2.994 GWd/MT.

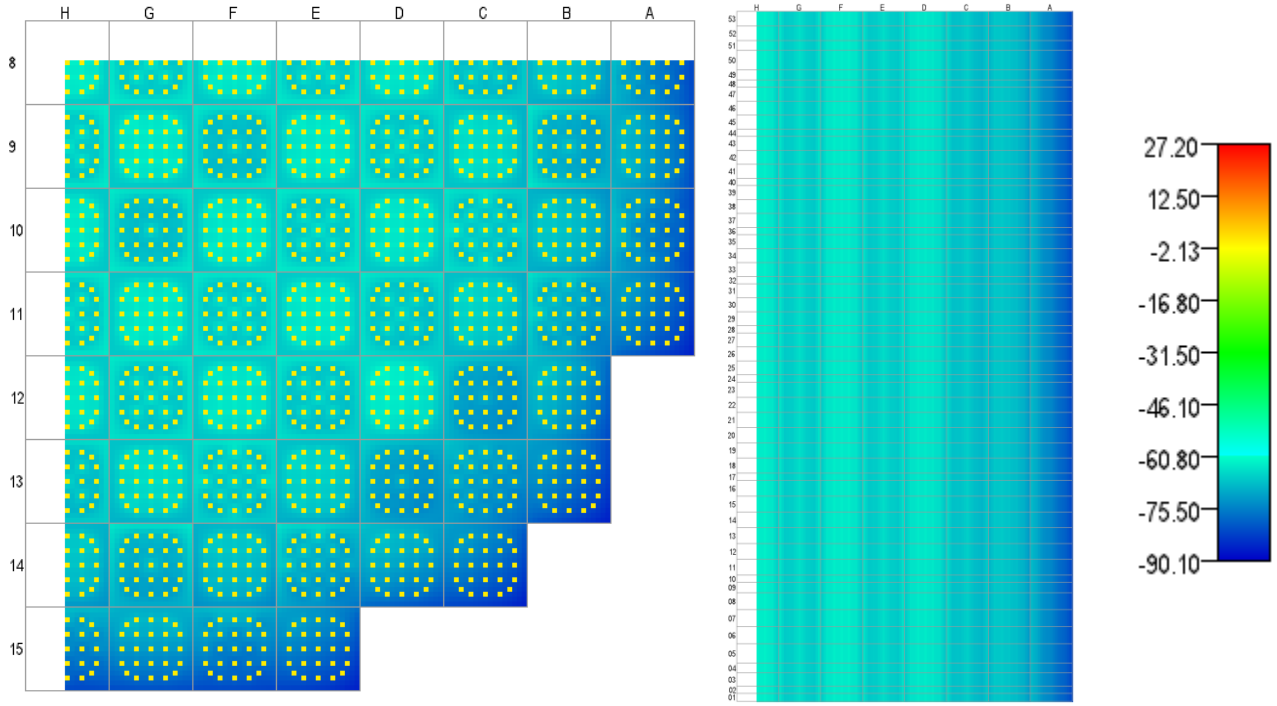

Figure A.3.7. Maximum Clad Hoop Stress (MPa), State 7, 3.562 GWd/MT.

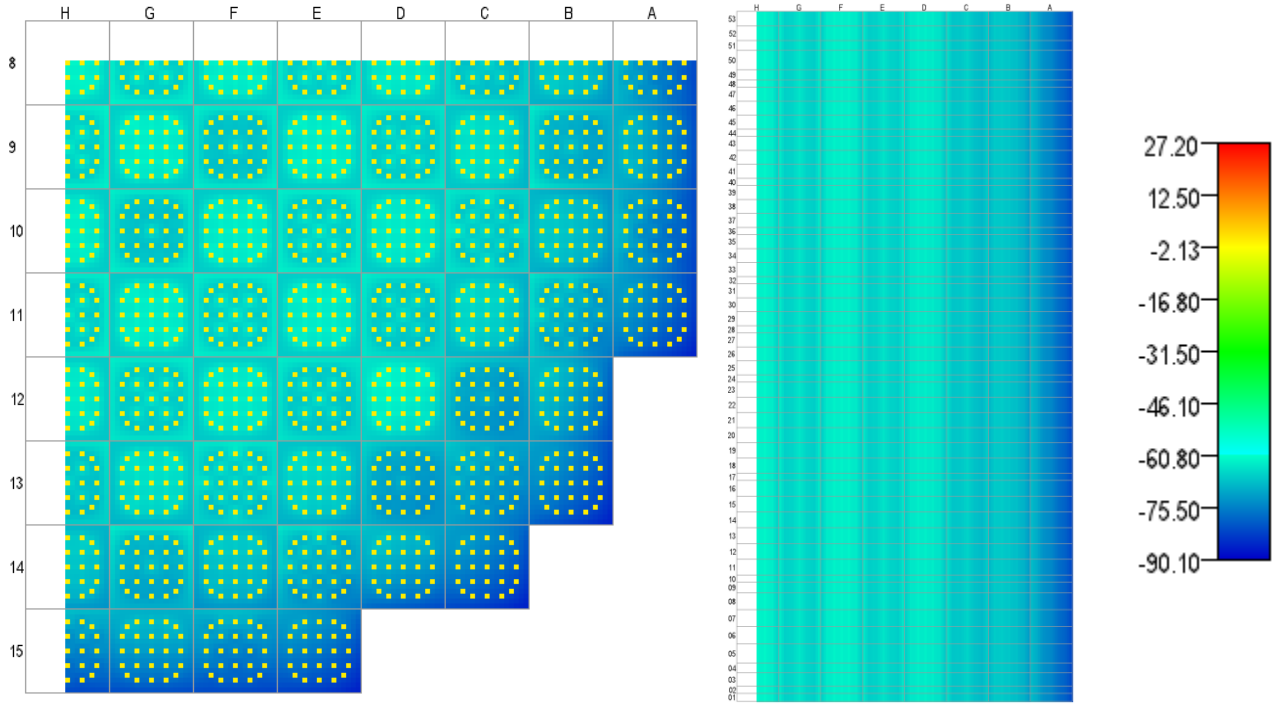

Figure A.3.8. Maximum Clad Hoop Stress (MPa), State 8, 4.065 GWd/MT.

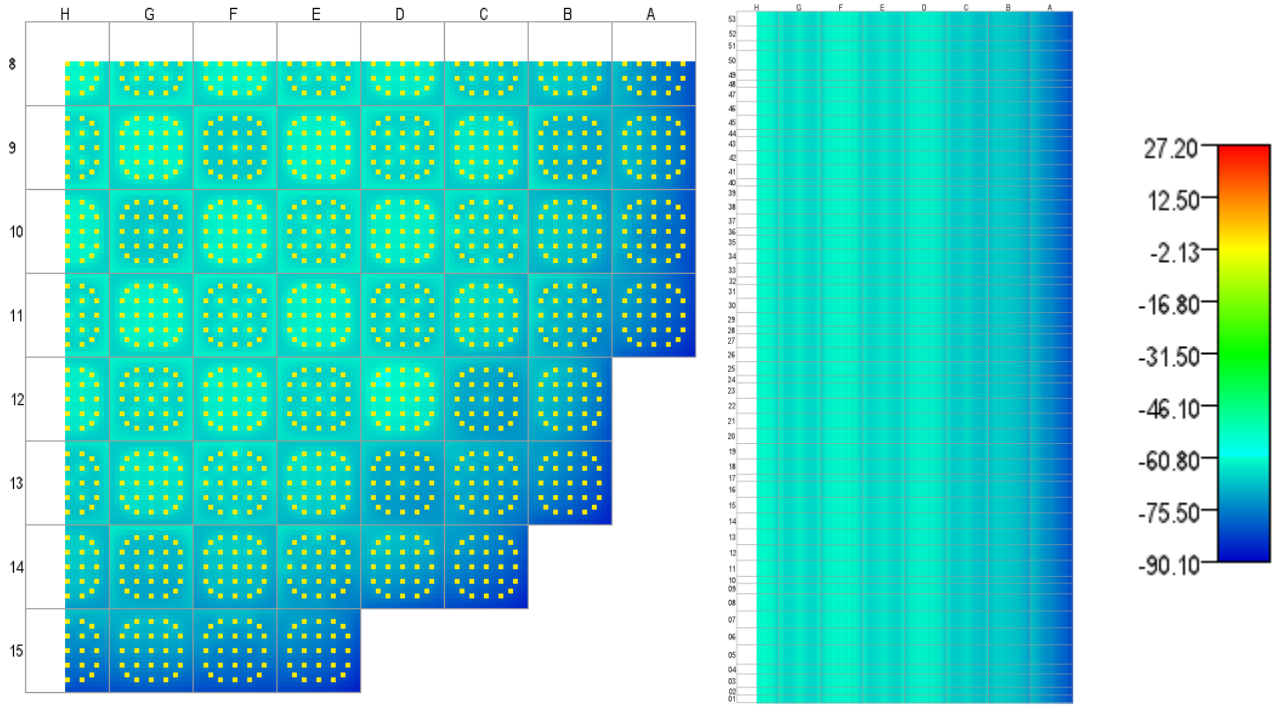

Figure A.3.9. Maximum Clad Hoop Stress (MPa), State 9, 4.642 GWd/MT.

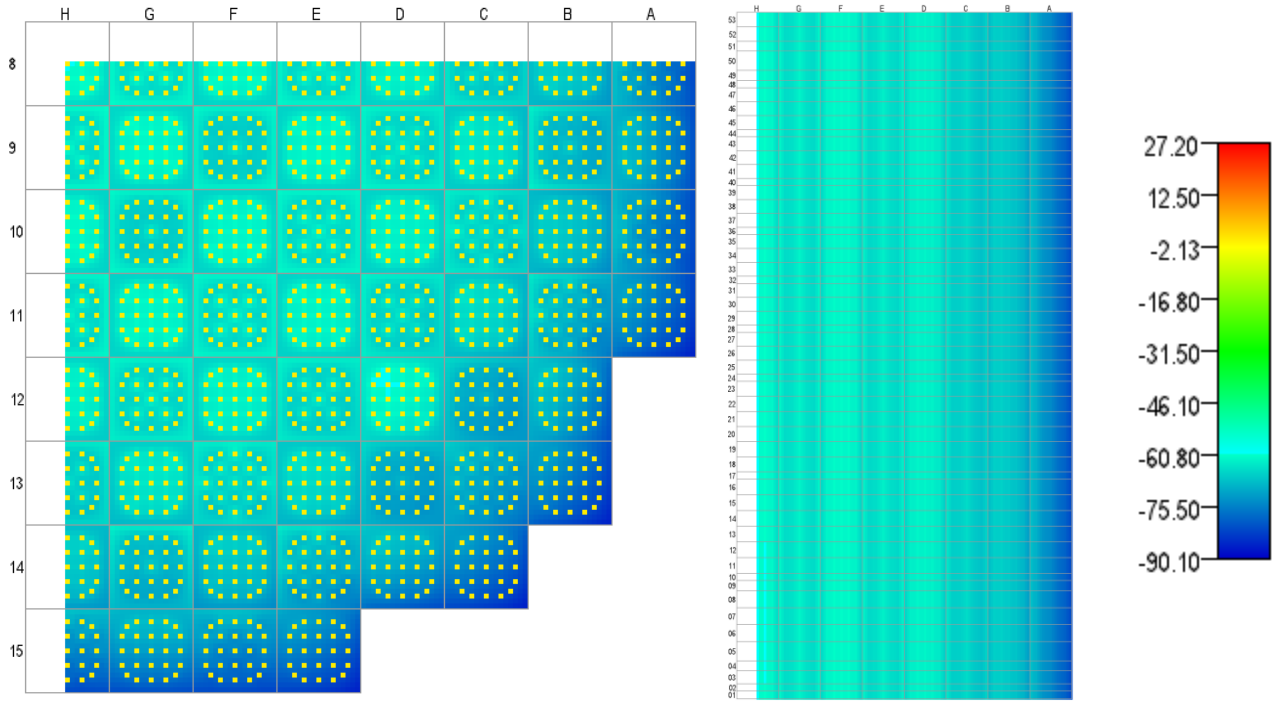

Figure A.3.10. Maximum Clad Hoop Stress (MPa), State 10, 5.139 GWd/MT.

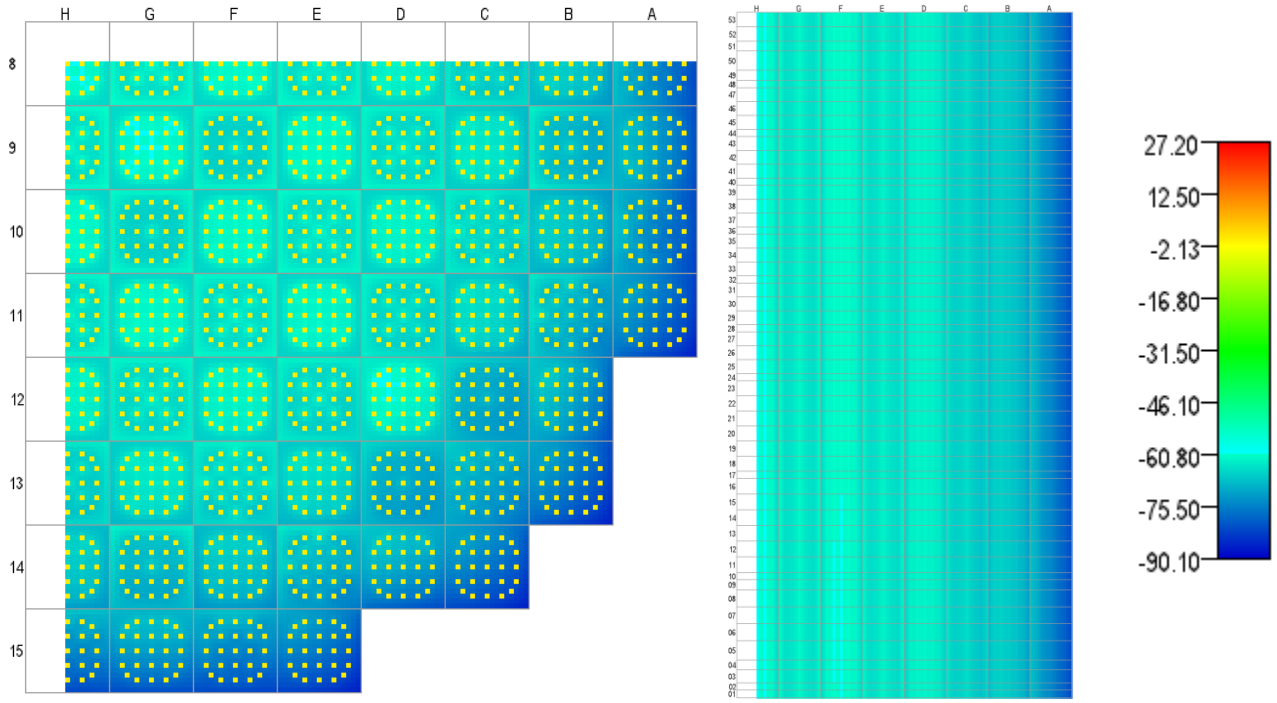

Figure A.3.11. Maximum Clad Hoop Stress (MPa), State 11, 5.700 GWd/MT.

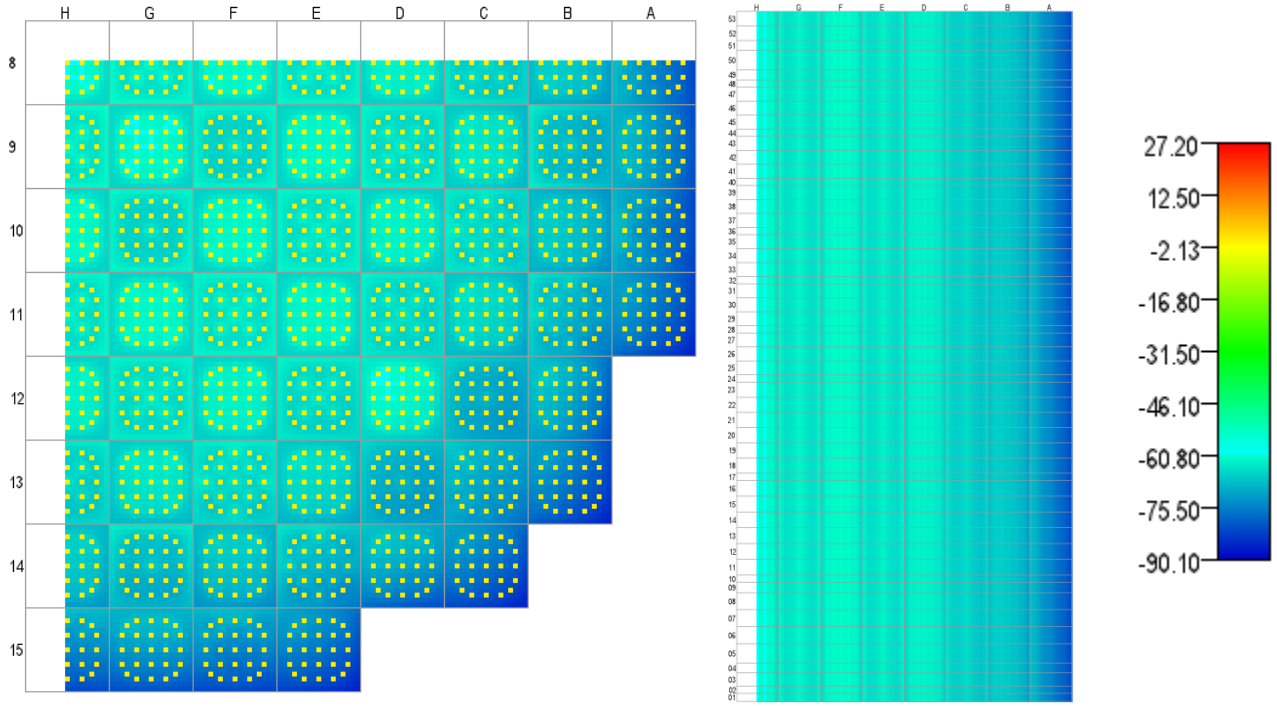

Figure A.3.12. Maximum Clad Hoop Stress (MPa), State 12, 6.273 GWd/MT.

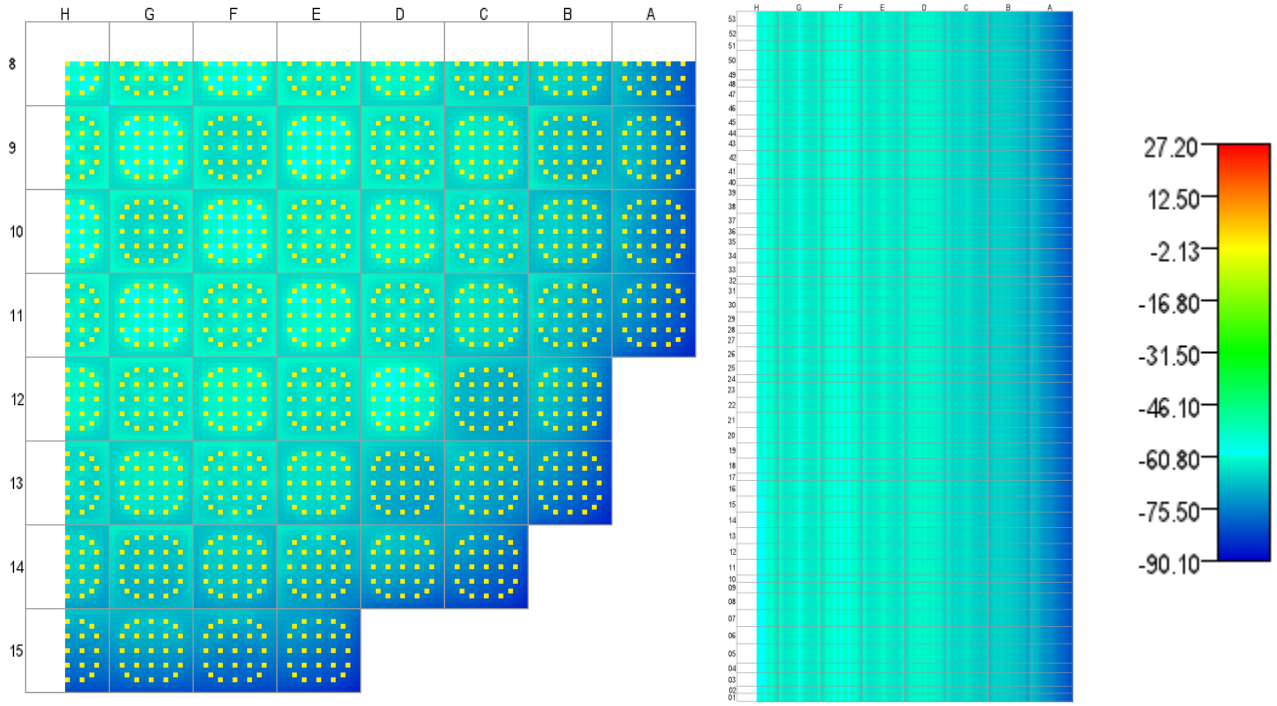

Figure A.3.13. Maximum Clad Hoop Stress (MPa), State 13, 7.000 GWd/MT.

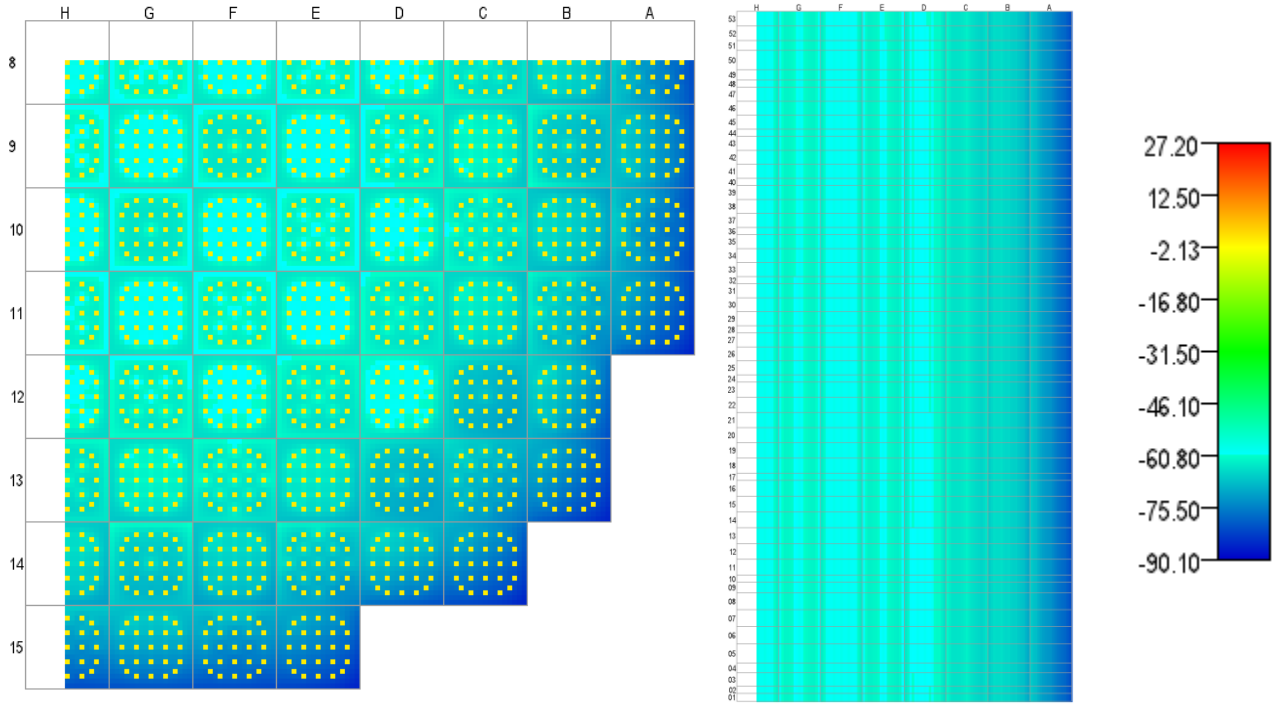

Figure A.3.14. Maximum Clad Hoop Stress (MPa), State 14, 7.463 GWd/MT.

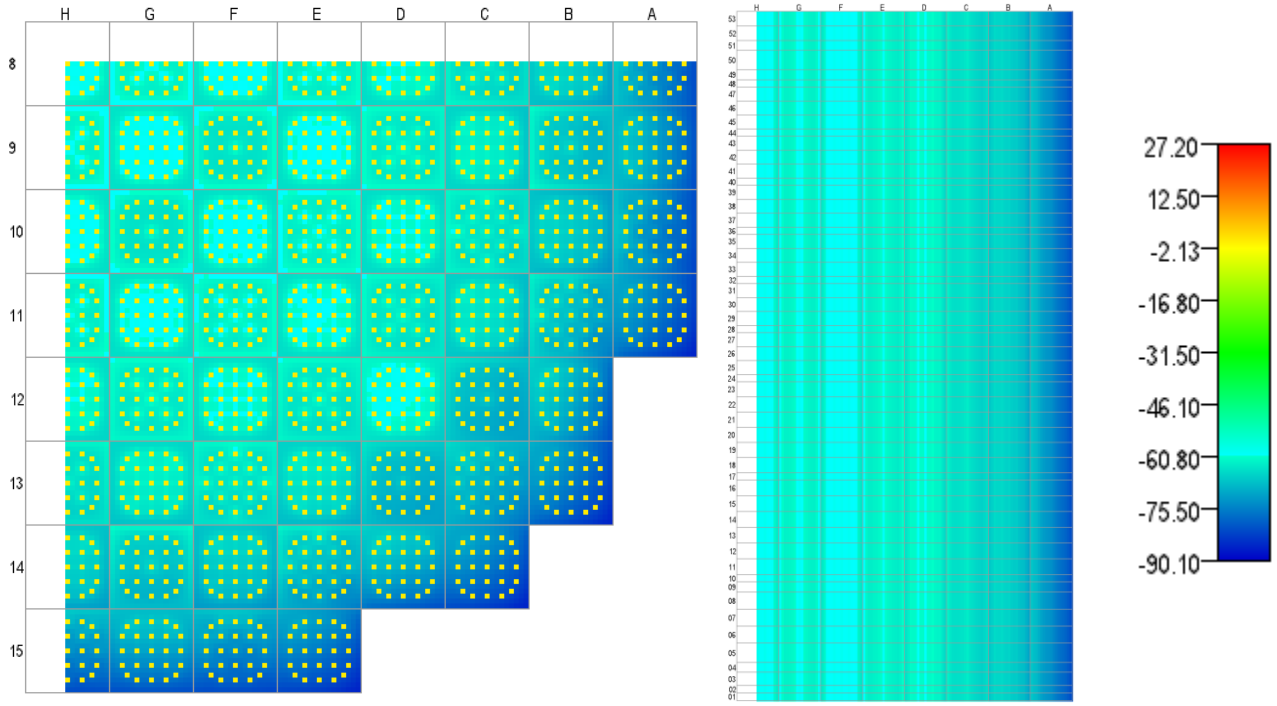

Figure A.3.15. Maximum Clad Hoop Stress (MPa), State 15, 7.978 GWd/MT.

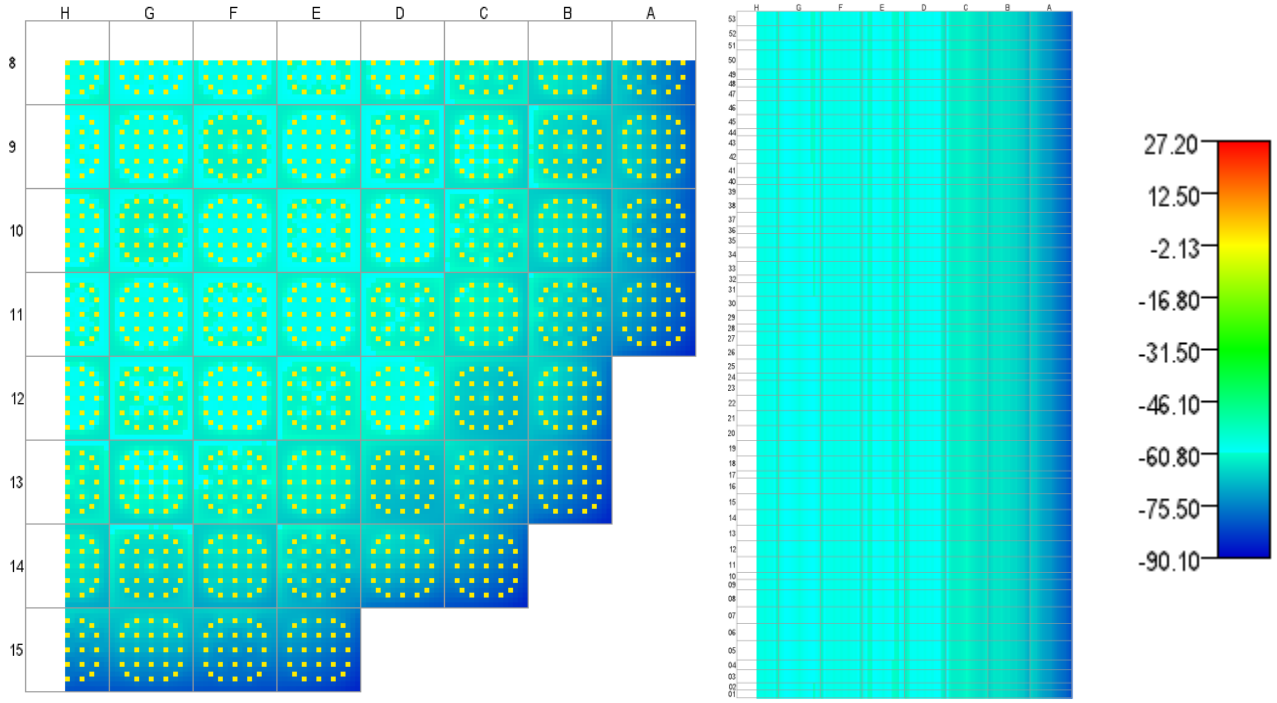

Figure A.3.16. Maximum Clad Hoop Stress (MPa), State 16, 8.493 GWd/MT.

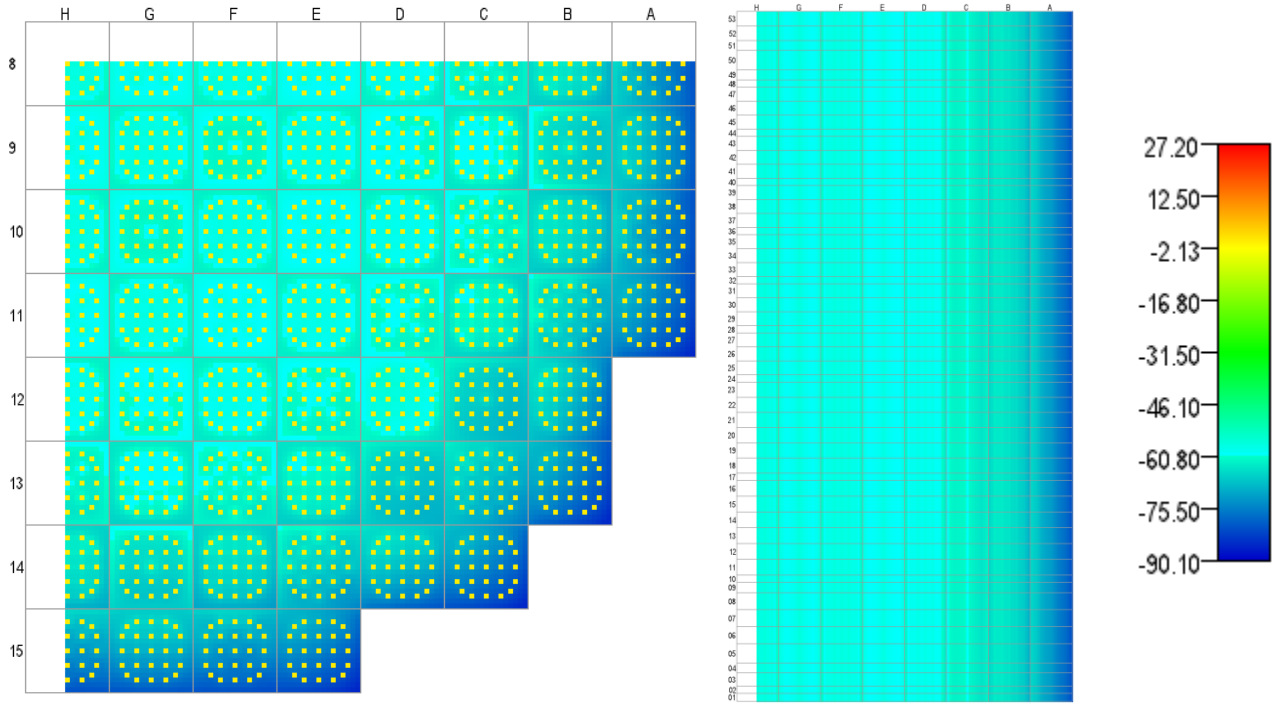

Figure A.3.17. Maximum Clad Hoop Stress (MPa), State 17, 9.140 GWd/MT.

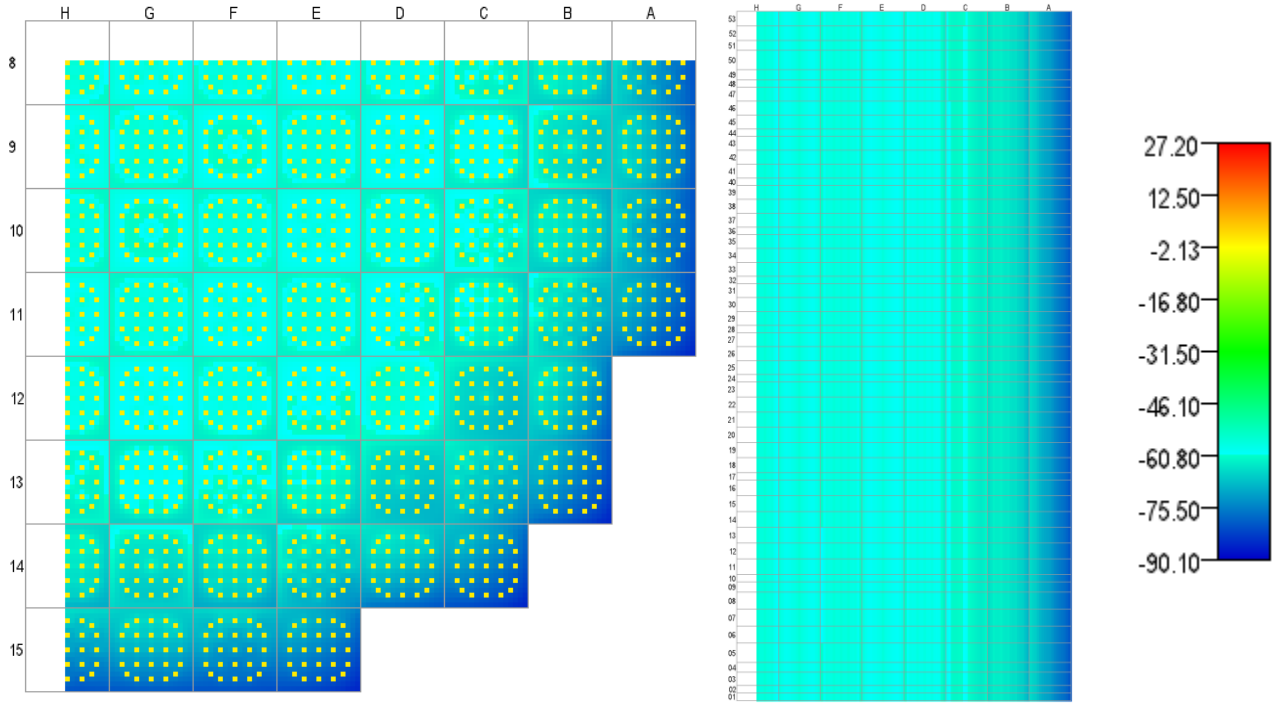

Figure A.3.18. Maximum Clad Hoop Stress (MPa), State 18, 9.602 GWd/MT.

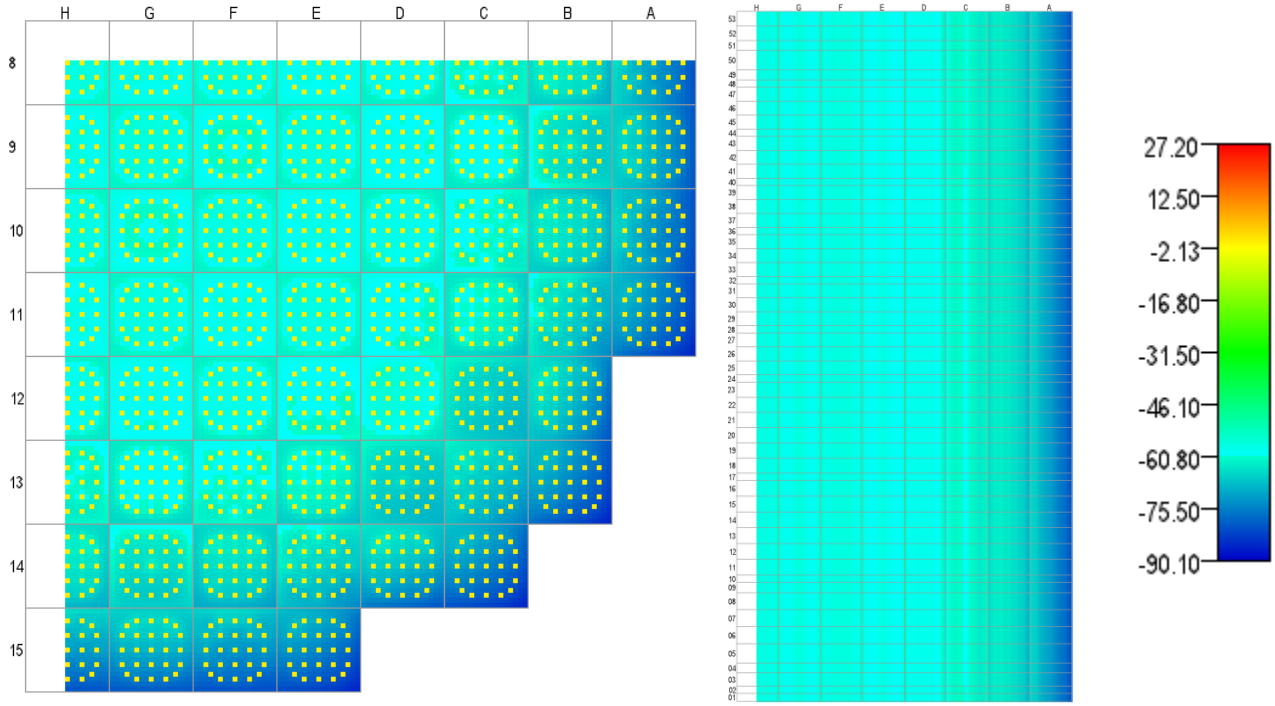

Figure A.3.19. Maximum Clad Hoop Stress (MPa), State 19, 10.344 GWd/MT.

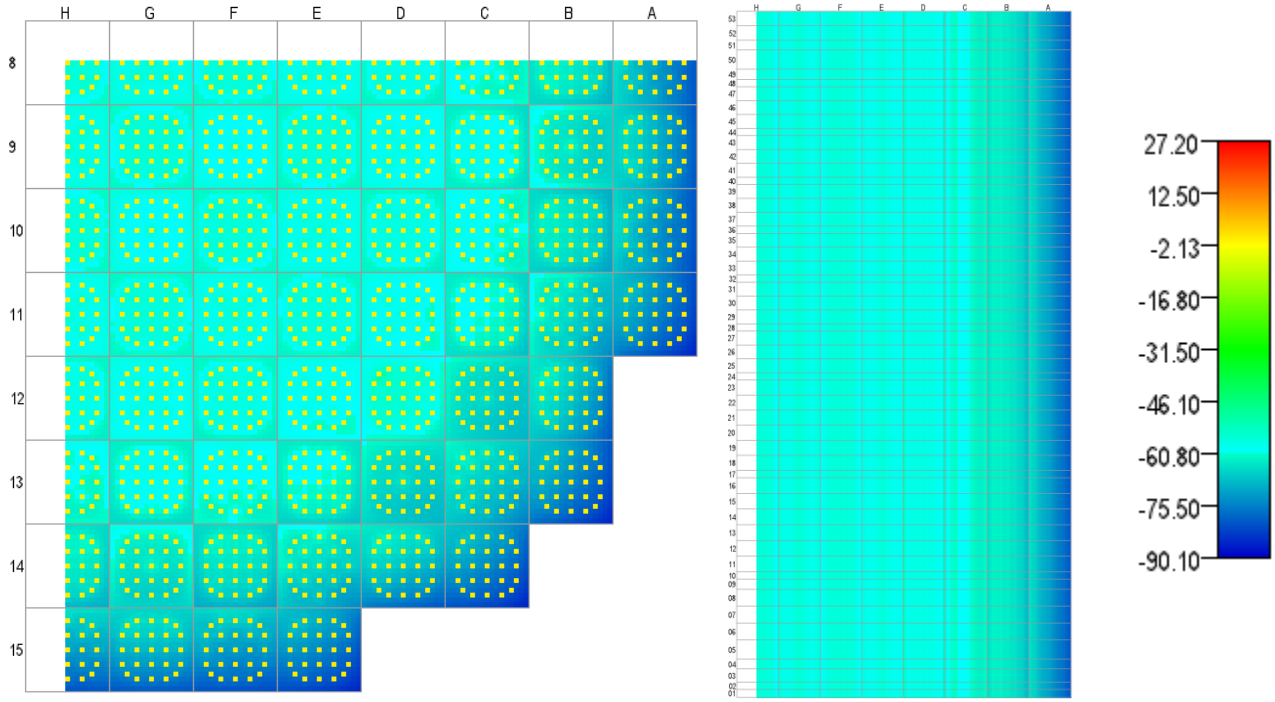

Figure A.3.20. Maximum Clad Hoop Stress (MPa), State 20, 10.842 GWd/MT.

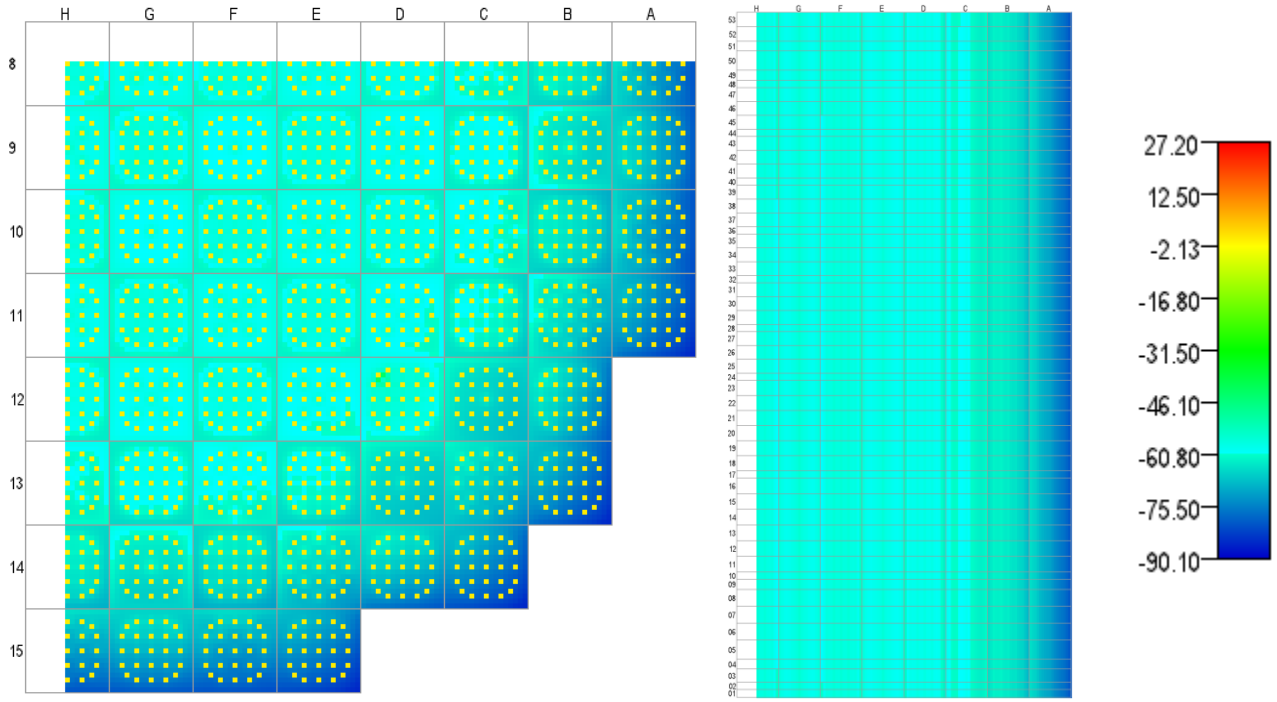

Figure A.3.21. Maximum Clad Hoop Stress (MPa), State 21, 11.314 GWd/MT.

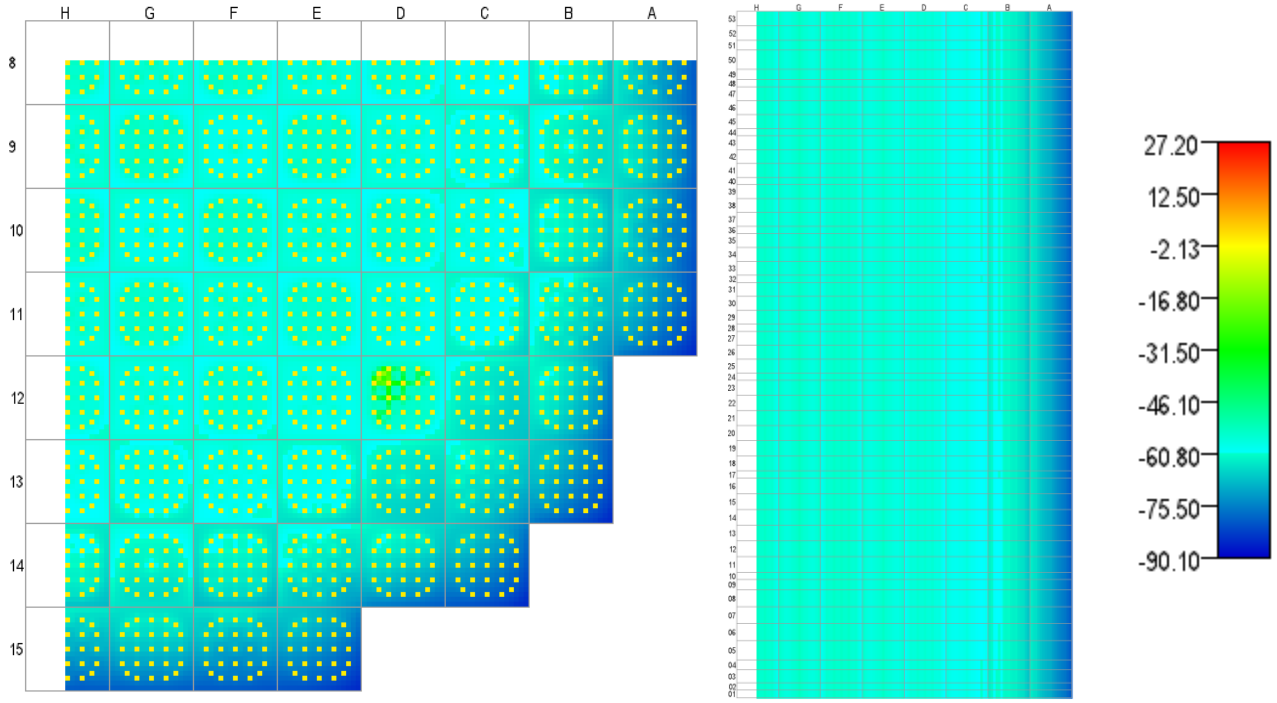

Figure A.3.22. Maximum Clad Hoop Stress (MPa), State 22, 11.988 GWd/MT.

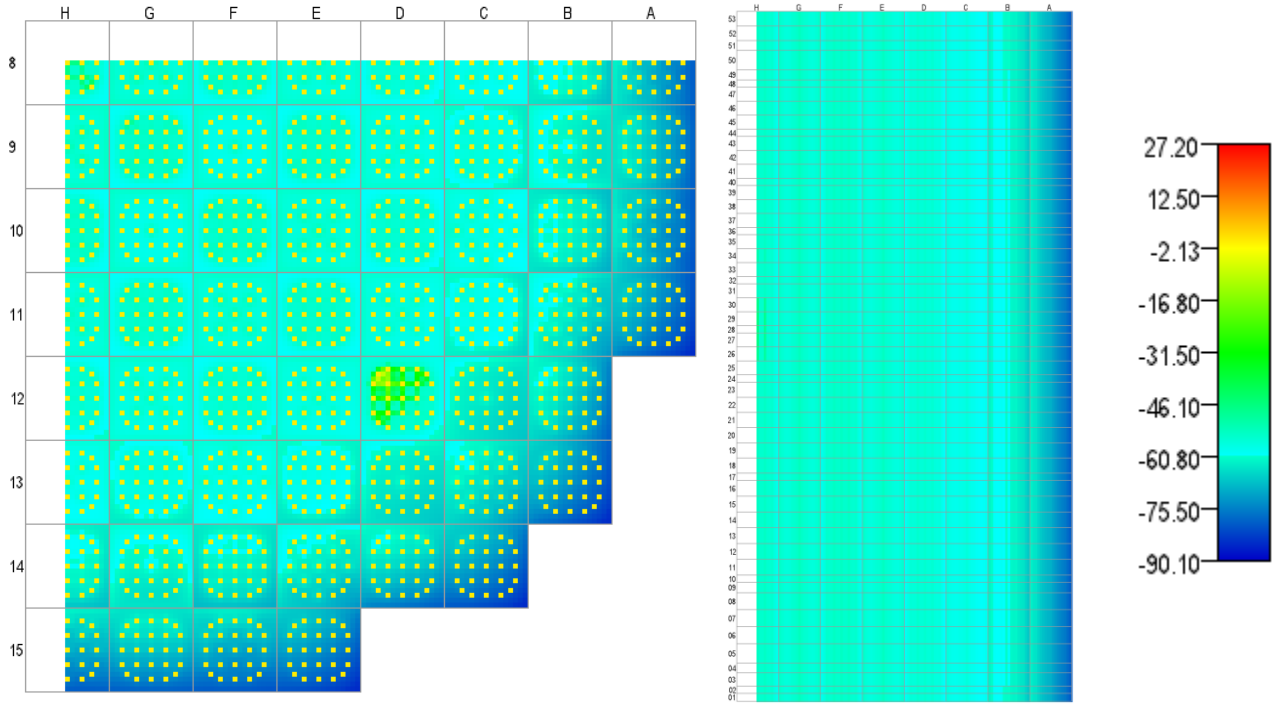

Figure A.3.23. Maximum Clad Hoop Stress (MPa), State 23, 12.552 GWd/MT.

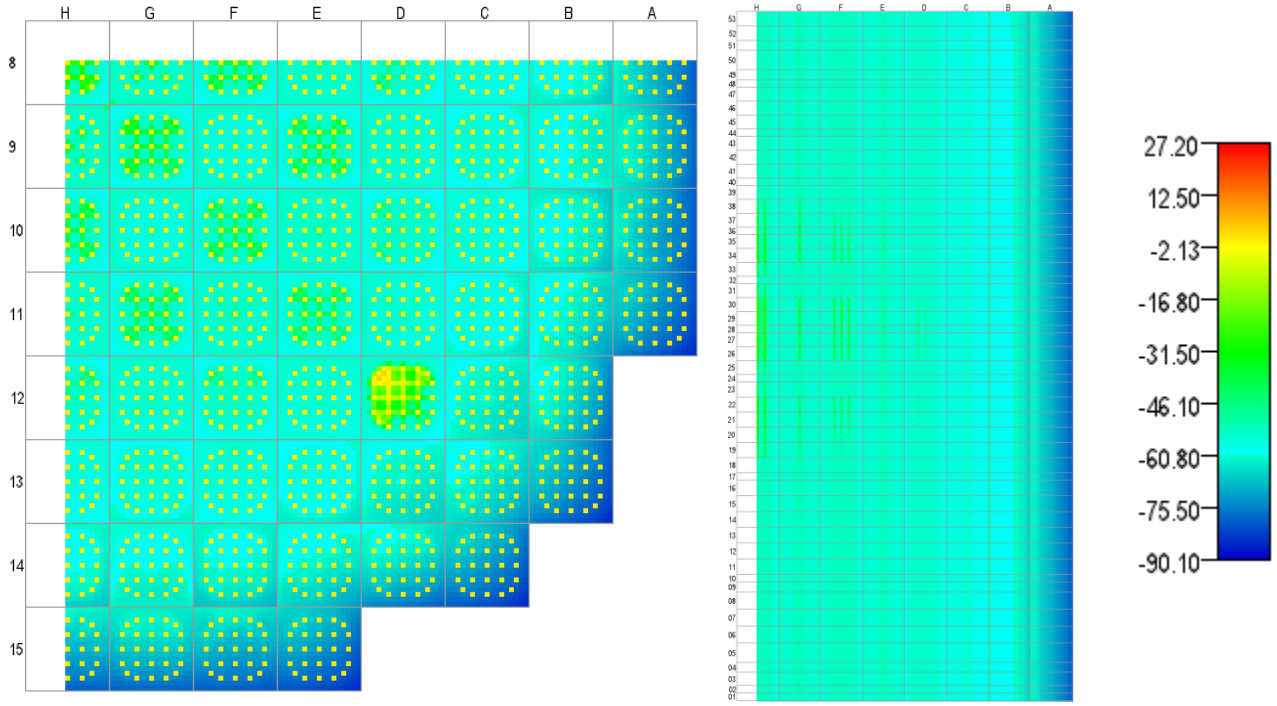

Figure A.3.24. Maximum Clad Hoop Stress (MPa), State 24, 13.360 GWd/MT.

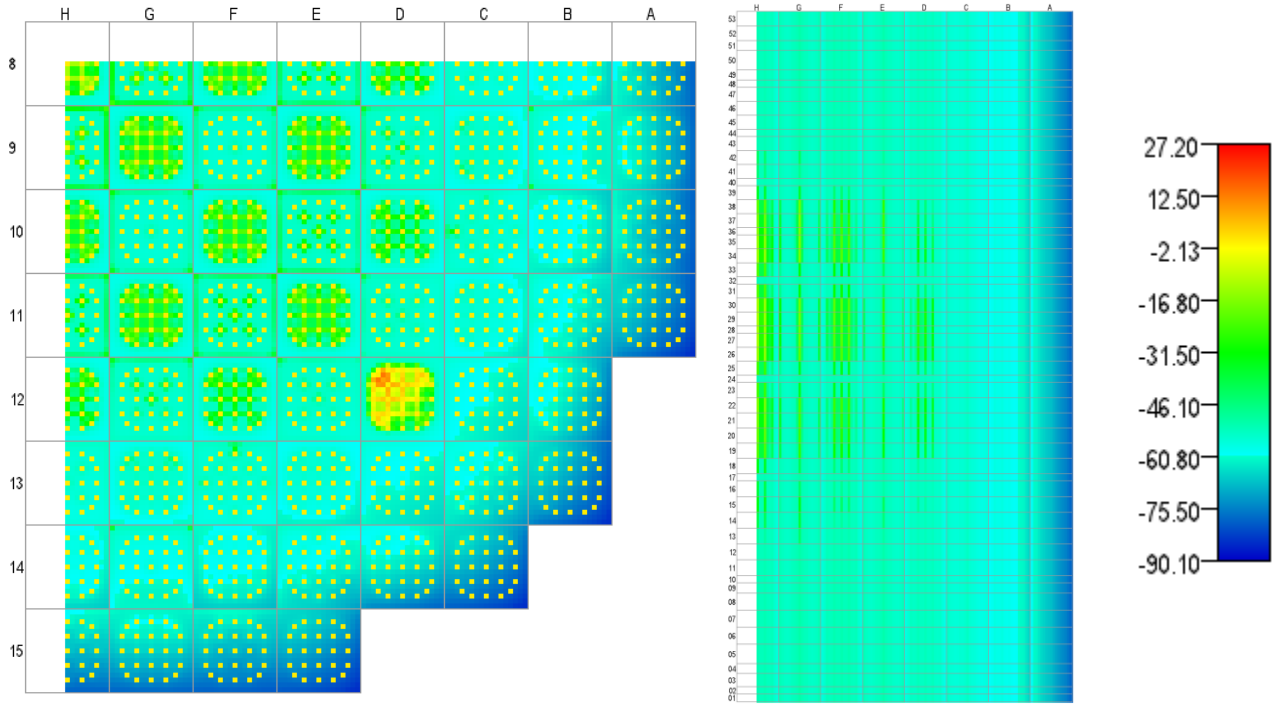

Figure A.3.25. Maximum Clad Hoop Stress (MPa), State 25, 14.285 GWd/MT.

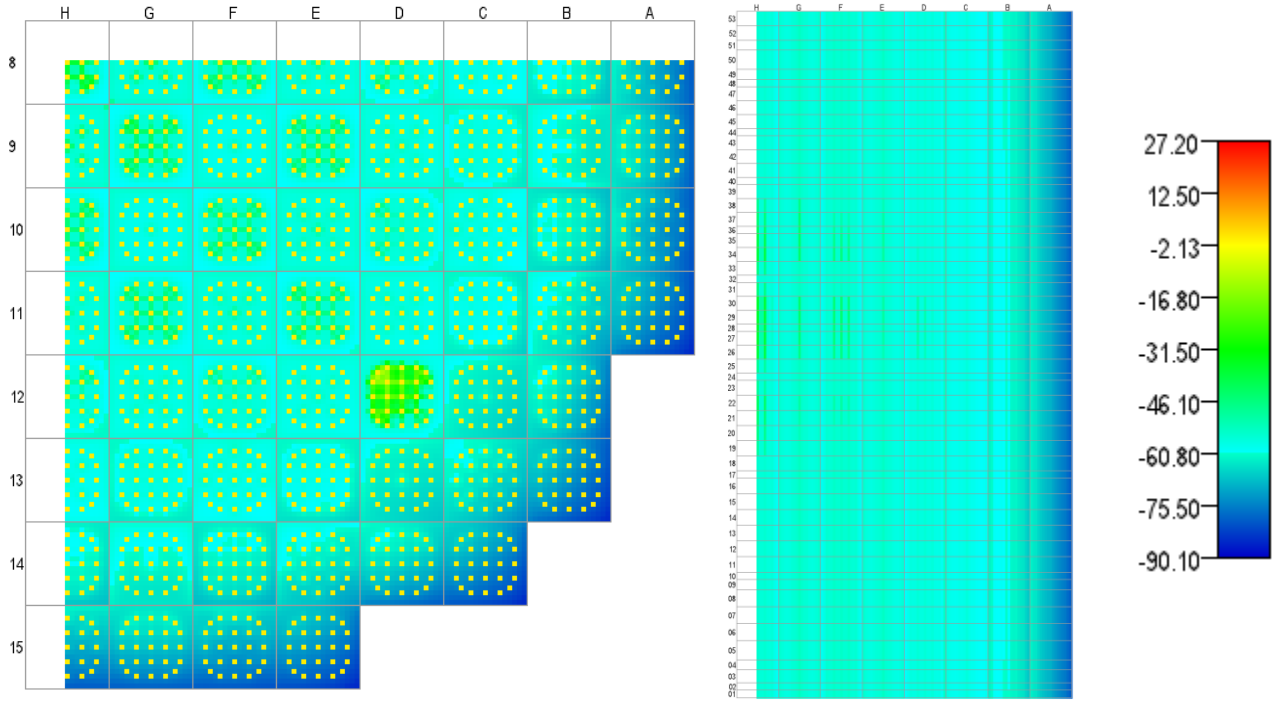

Figure A.3.26. Maximum Clad Hoop Stress (MPa), State 26, 14.385 GWd/MT.

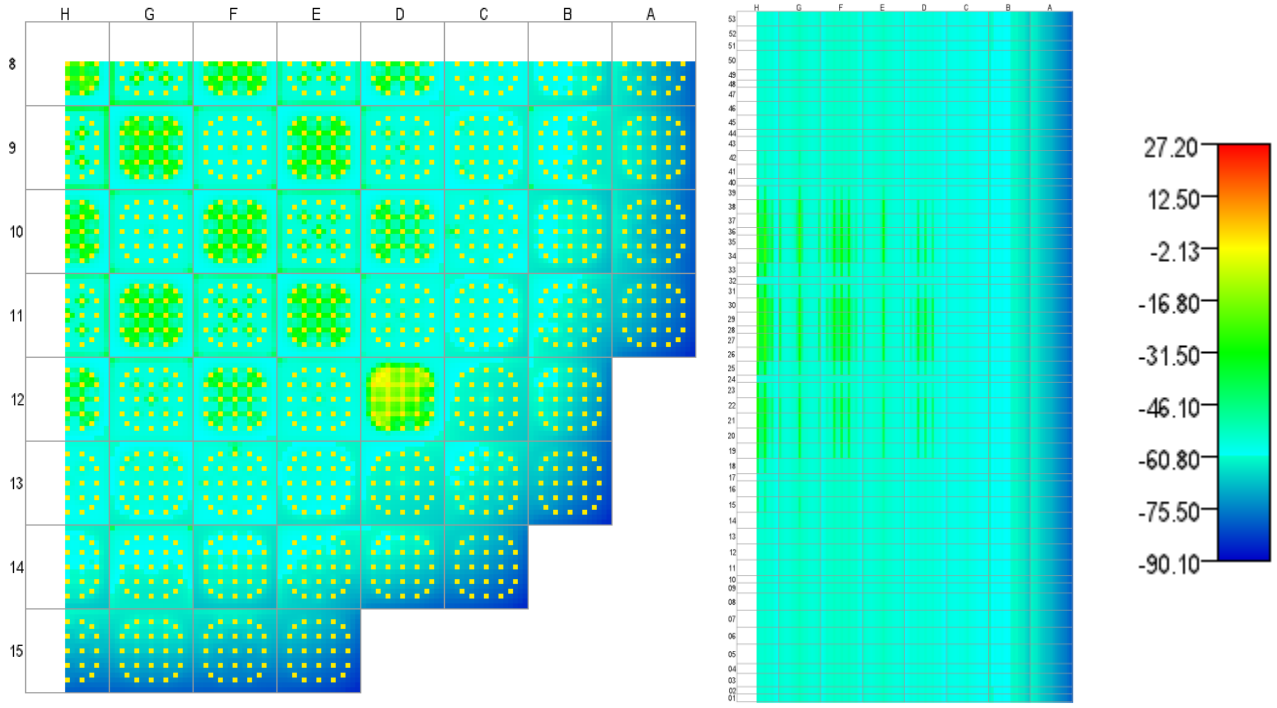

Figure A.3.27. Maximum Clad Hoop Stress (MPa), State 27, 15.018 GWd/MT.

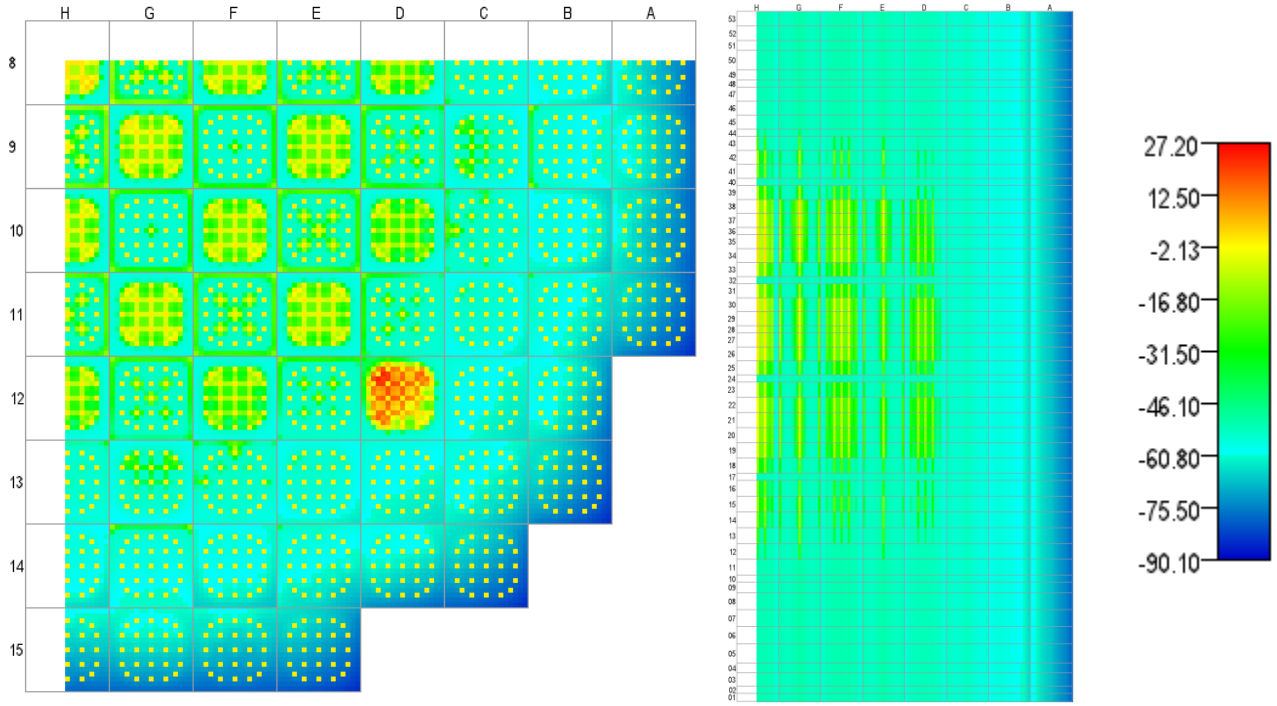

Figure A.3.28. Maximum Clad Hoop Stress (MPa), State 28, 15.118 GWd/MT.

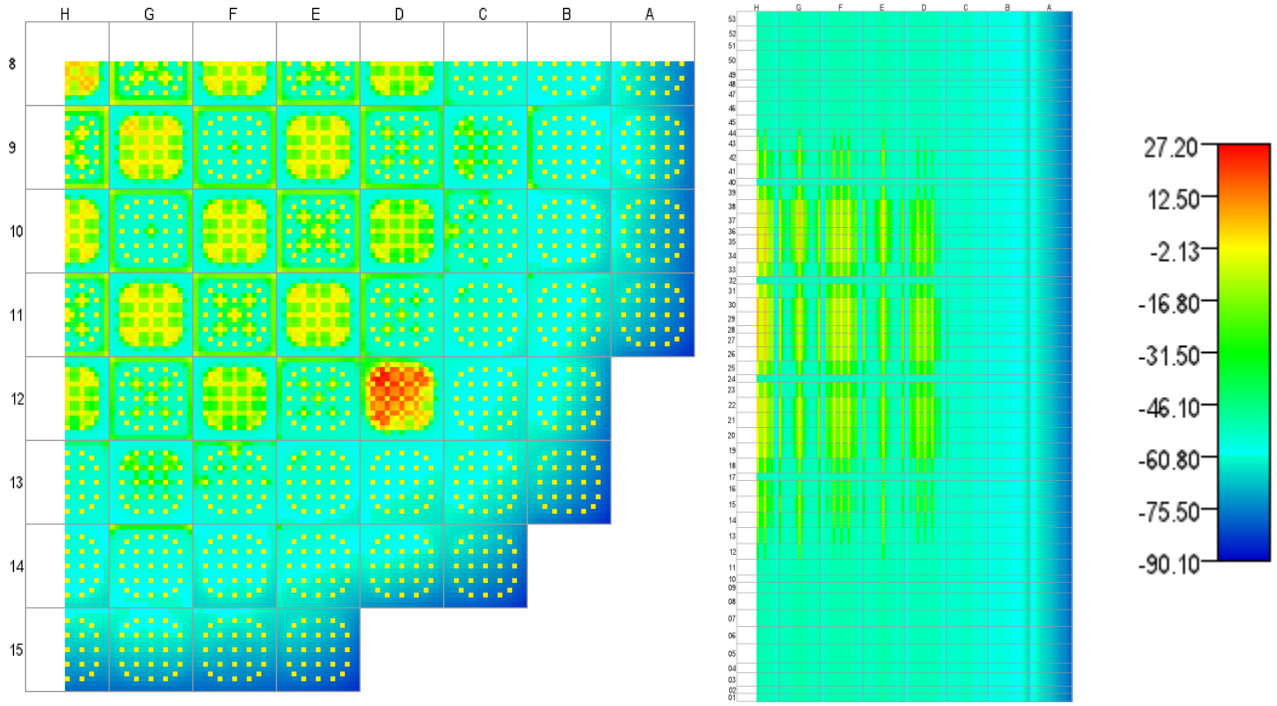

Figure A.3.29. Maximum Clad Hoop Stress (MPa), State 29, 15.308 GWd/MT.

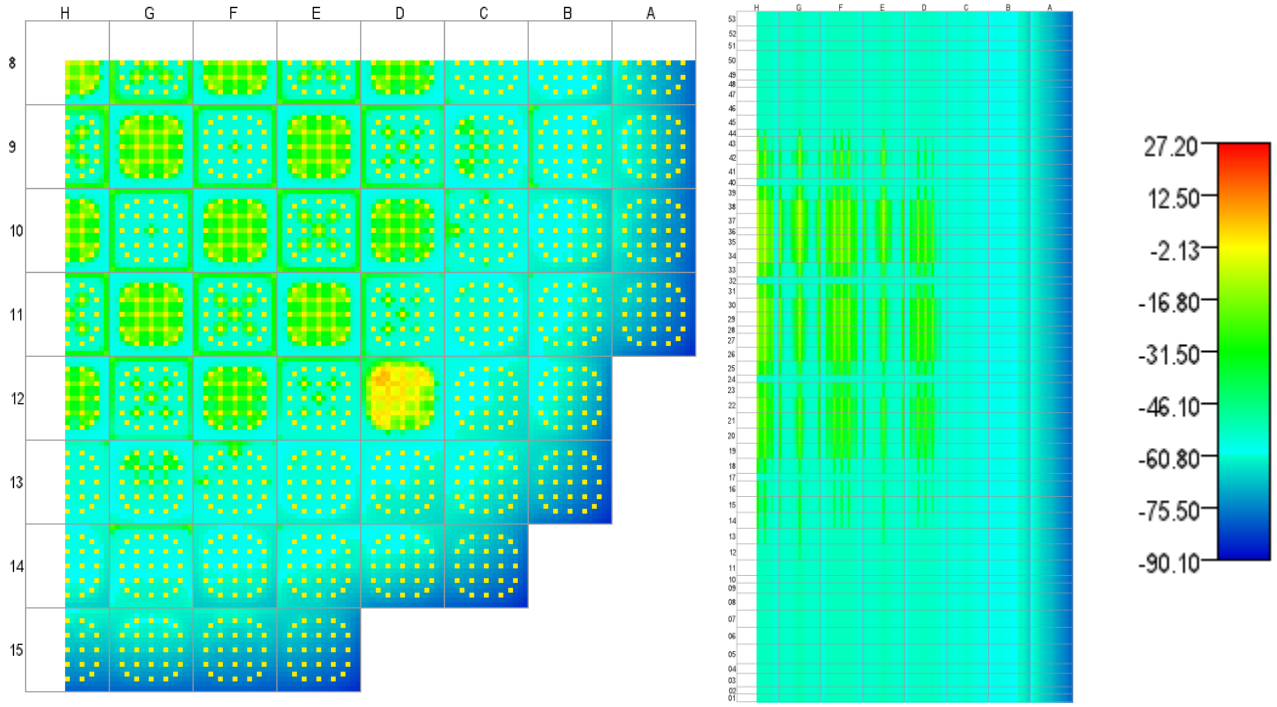

Figure A.3.30. Maximum Clad Hoop Stress (MPa), State 30, 15.774 GWd/MT.

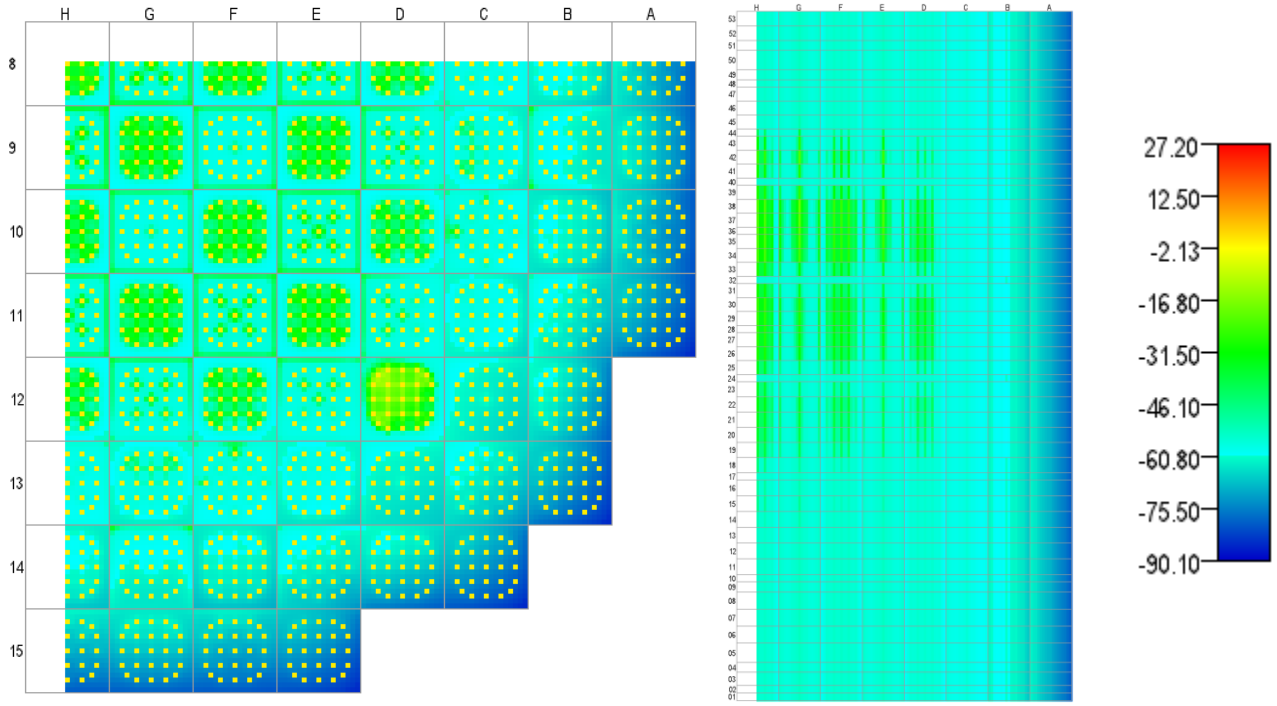

Figure A.3.31. Maximum Clad Hoop Stress (MPa), State 31, 16.270 GWd/MT.

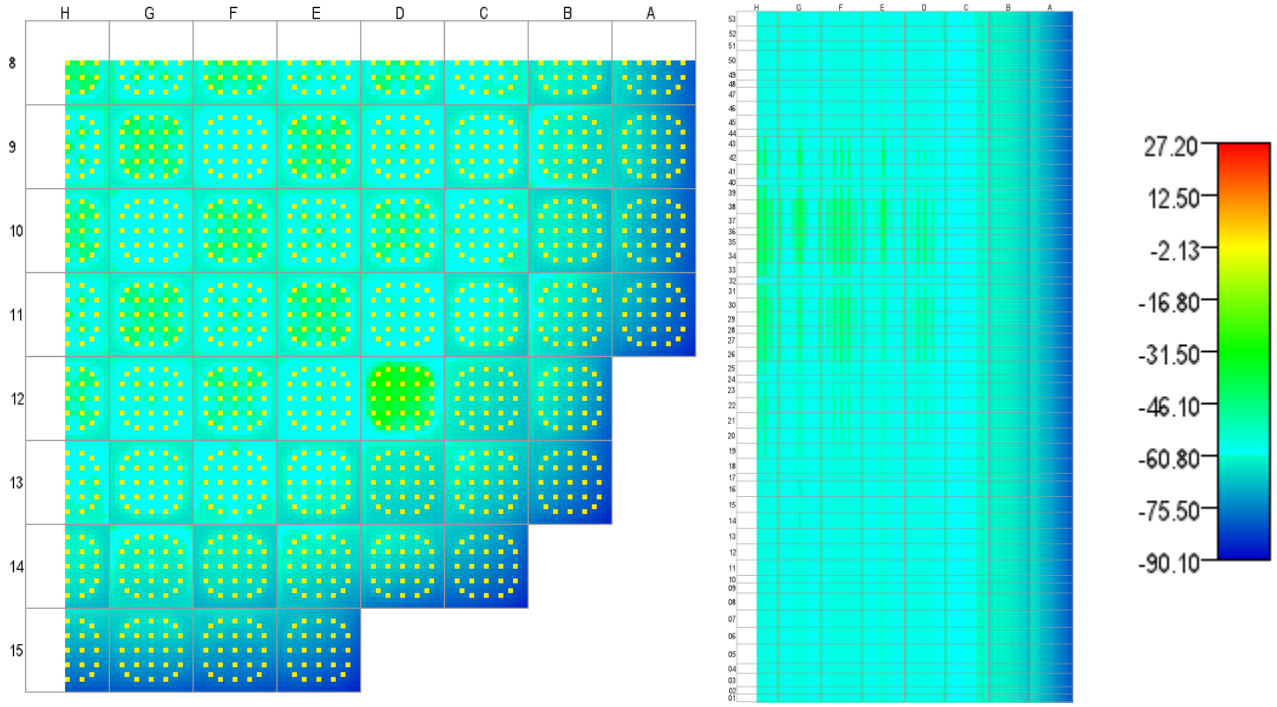

Figure A.3.32. Maximum Clad Hoop Stress (MPa), State 32, 16.932 GWd/MT.

APPENDIX B – INLINE VS. COUPLED EXPANDED RESULTS

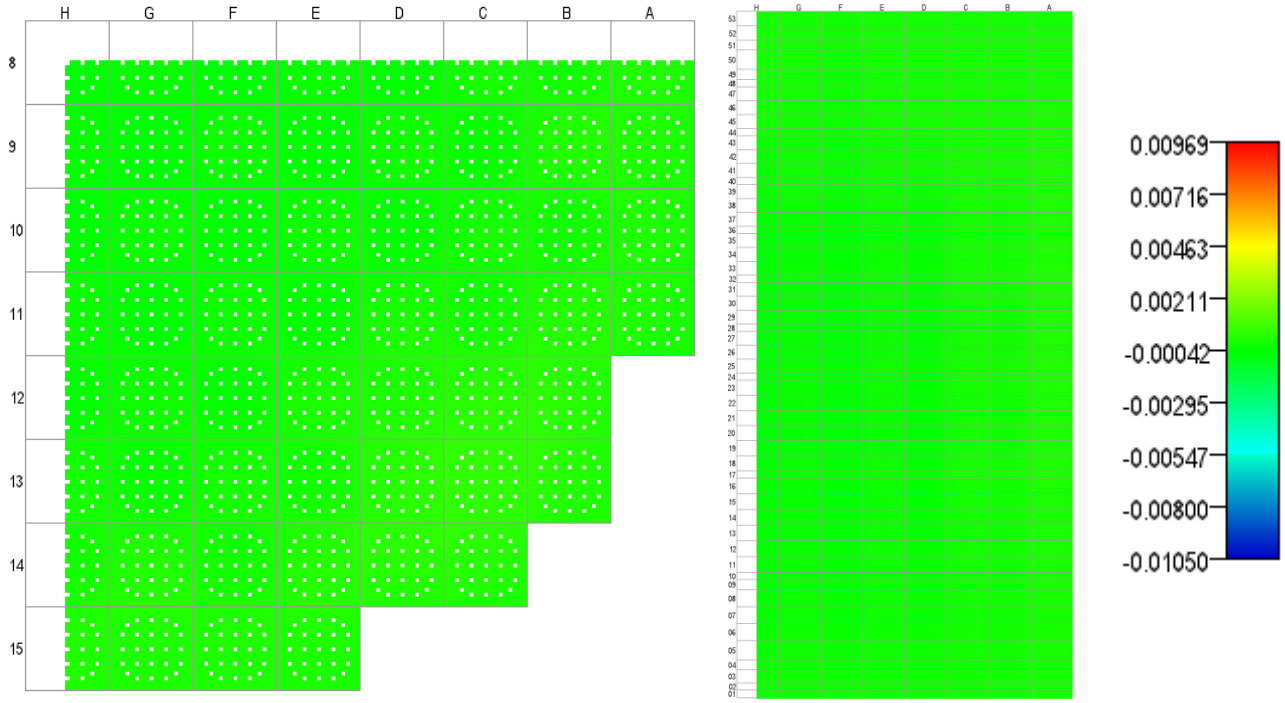

Figure B.1. Normalized Pin Power Difference, State 1, 0.000 GWd/MT.

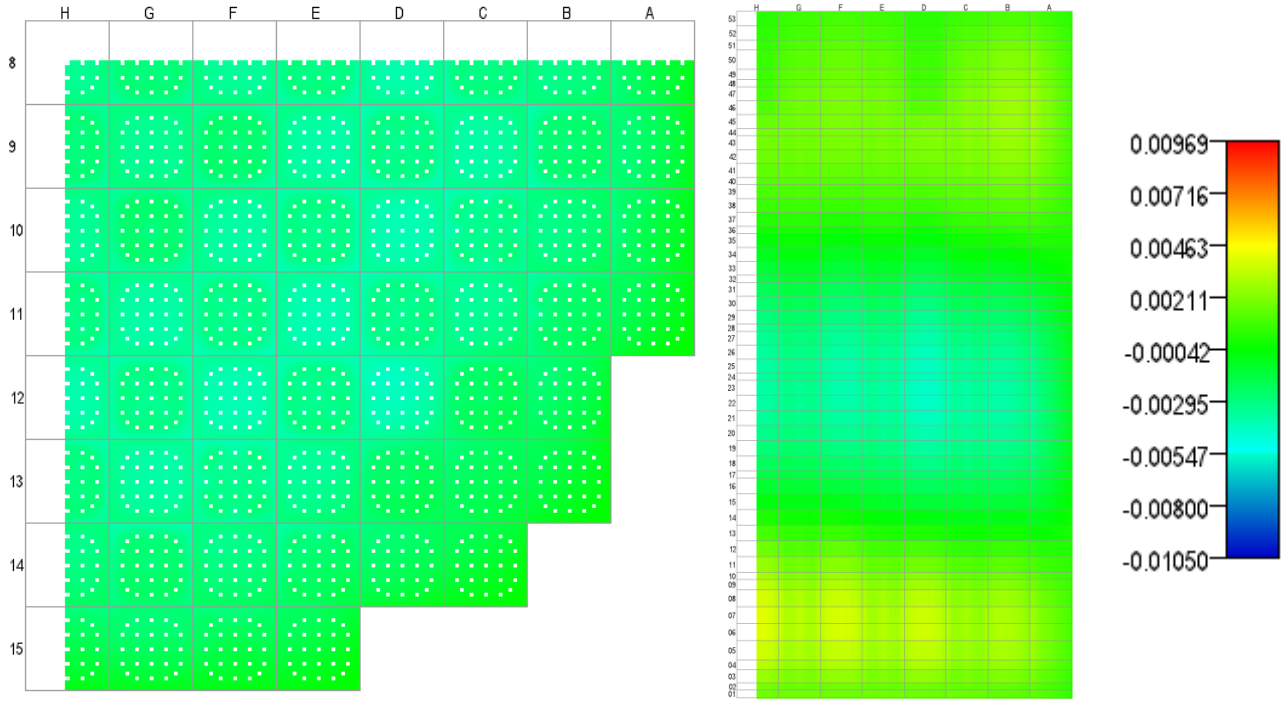

Figure B.2. Normalized Pin Power Difference, State 2, 0.346 GWd/MT.

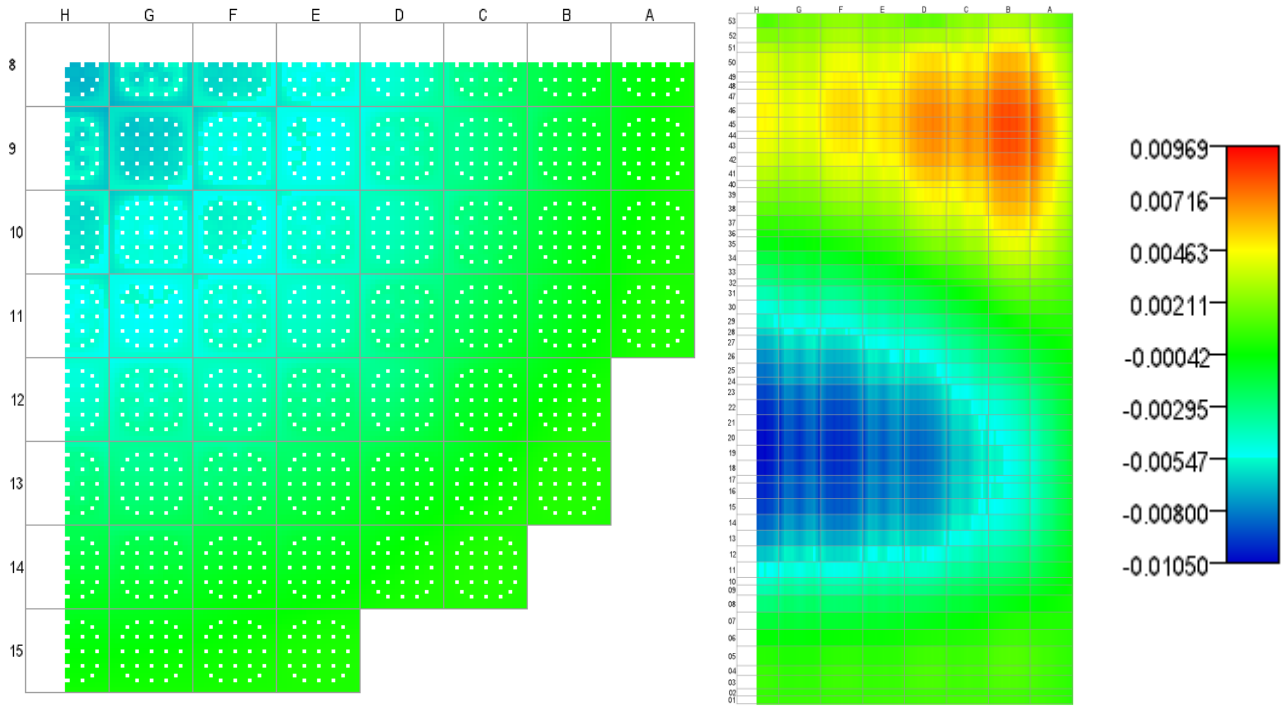

Figure B.3. Normalized Pin Power Difference, State 3, 1.230 GWd/MT.

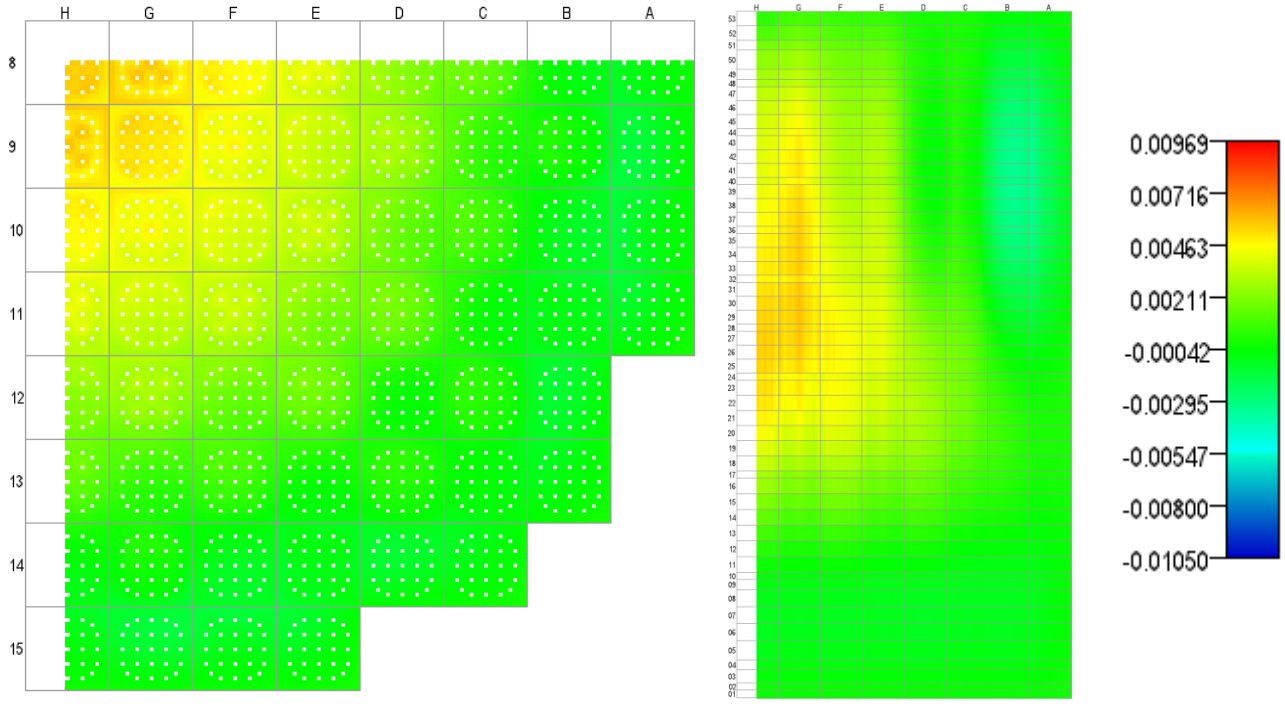

Figure B.4. Normalized Pin Power Difference, State 4, 1.919 GWd/MT.

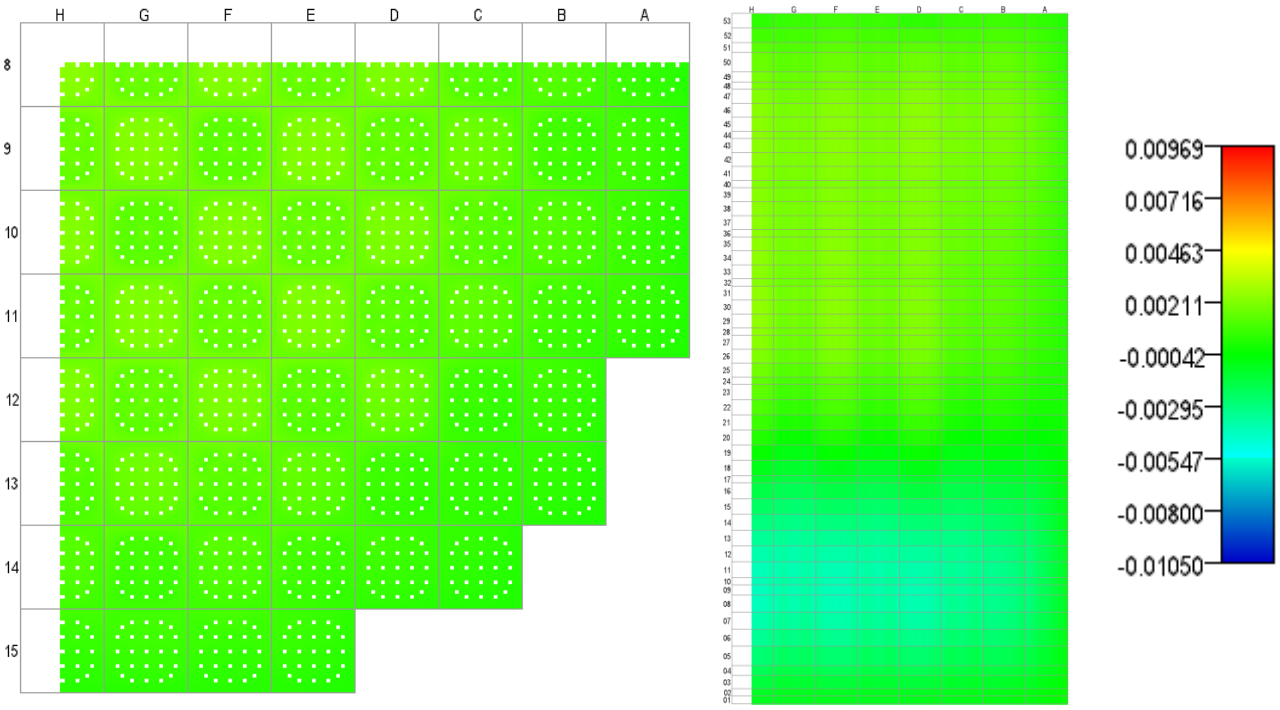

Figure B.5. Normalized Pin Power Difference, State 5, 2.457 GWd/MT.

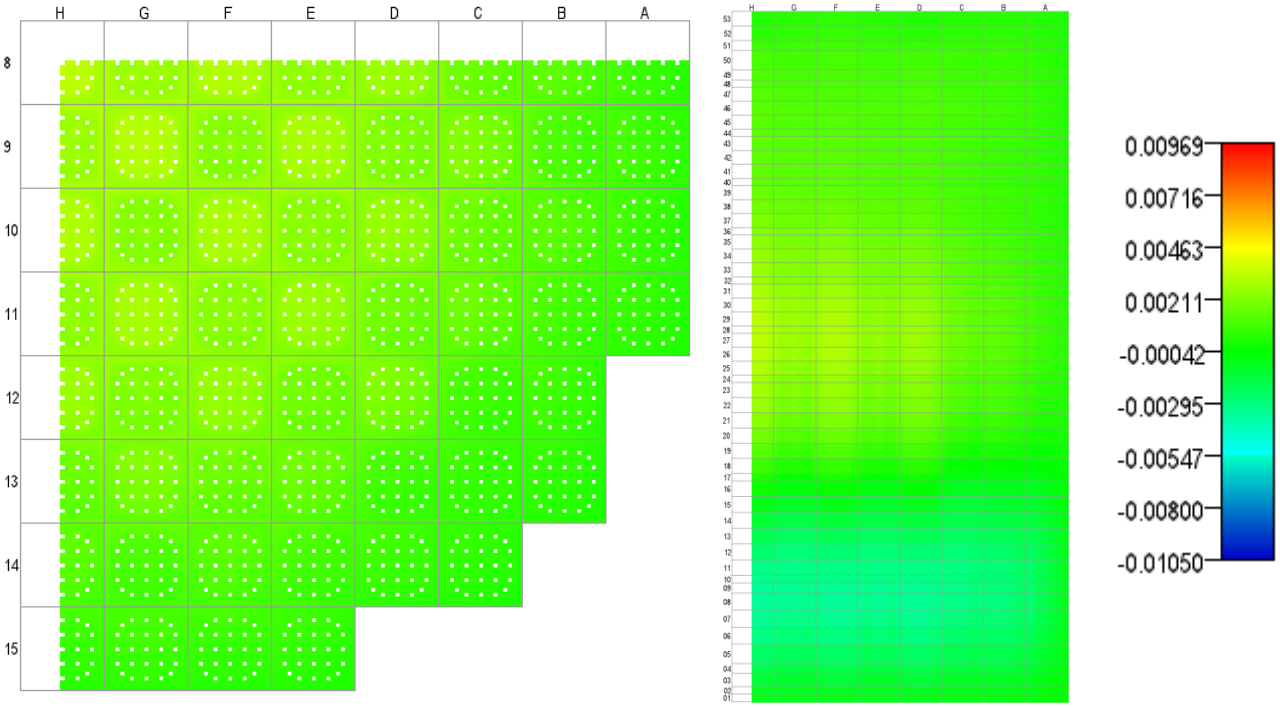

Figure B.6. Normalized Pin Power Difference, State 6, 2.994 GWd/MT.

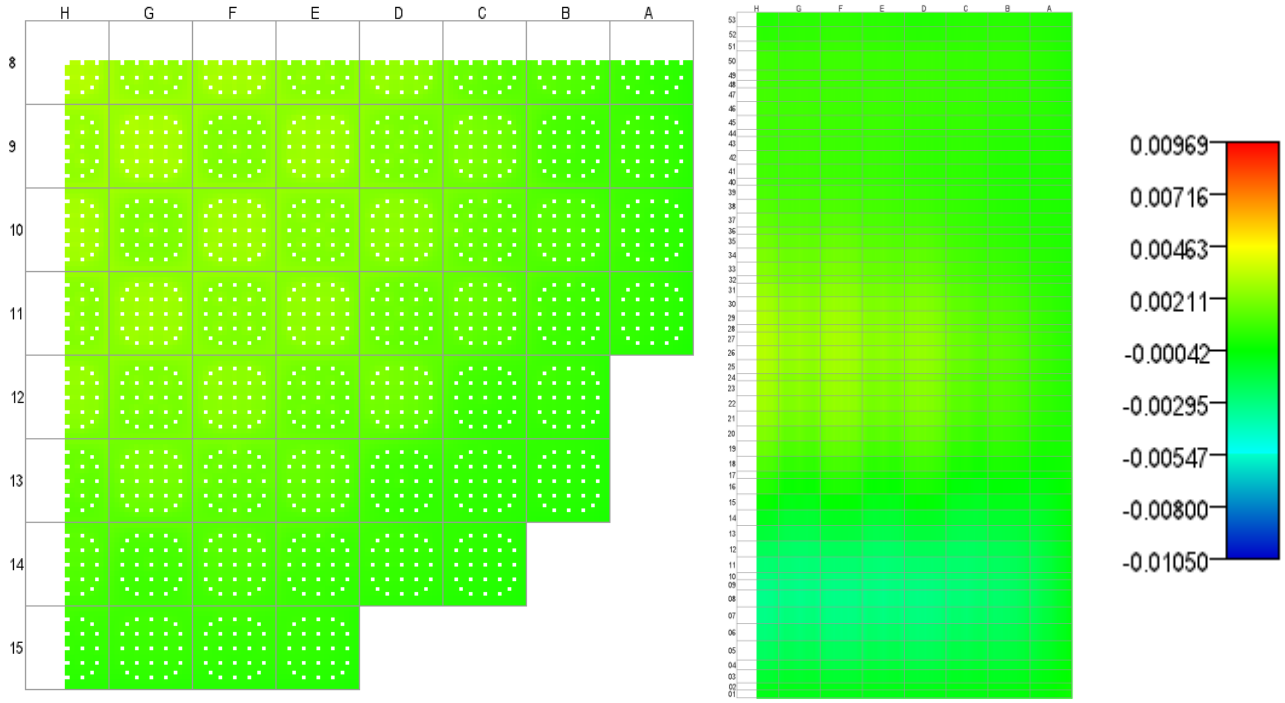

Figure B.7. Normalized Pin Power Difference, State 7, 3.562 GWd/MT.

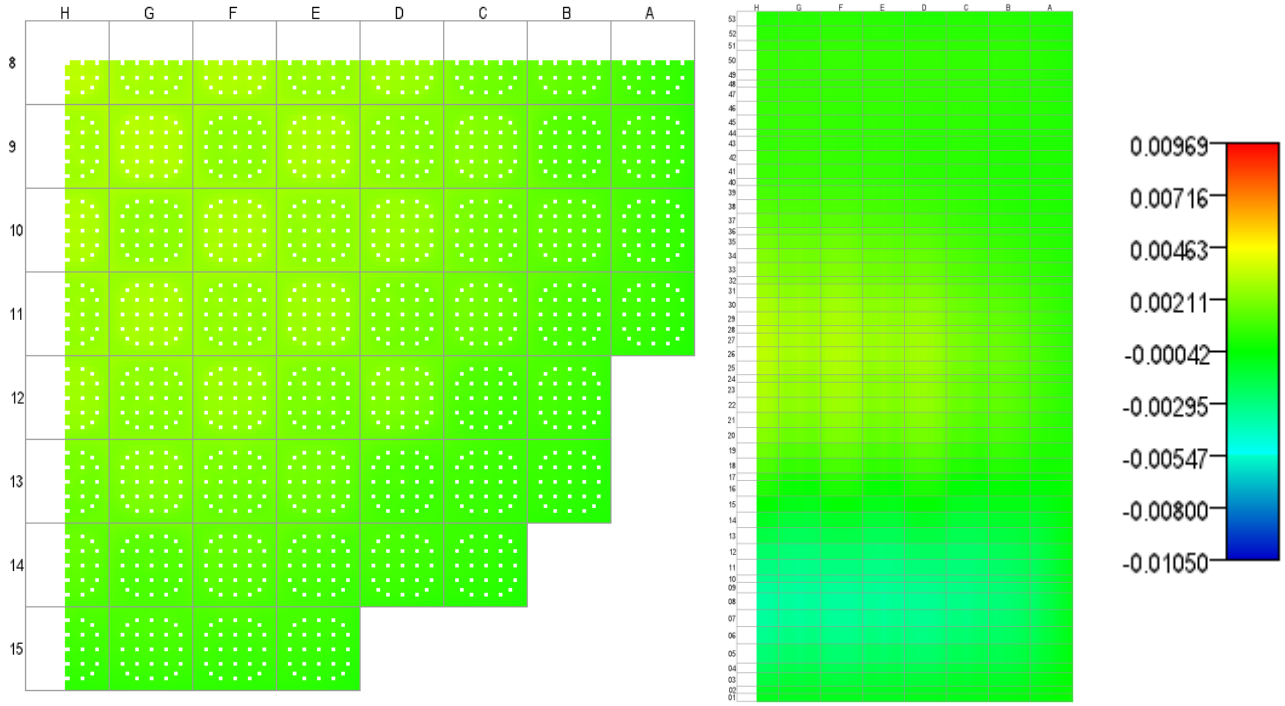

Figure B.8. Normalized Pin Power Difference, State 8, 4.065 GWd/MT.

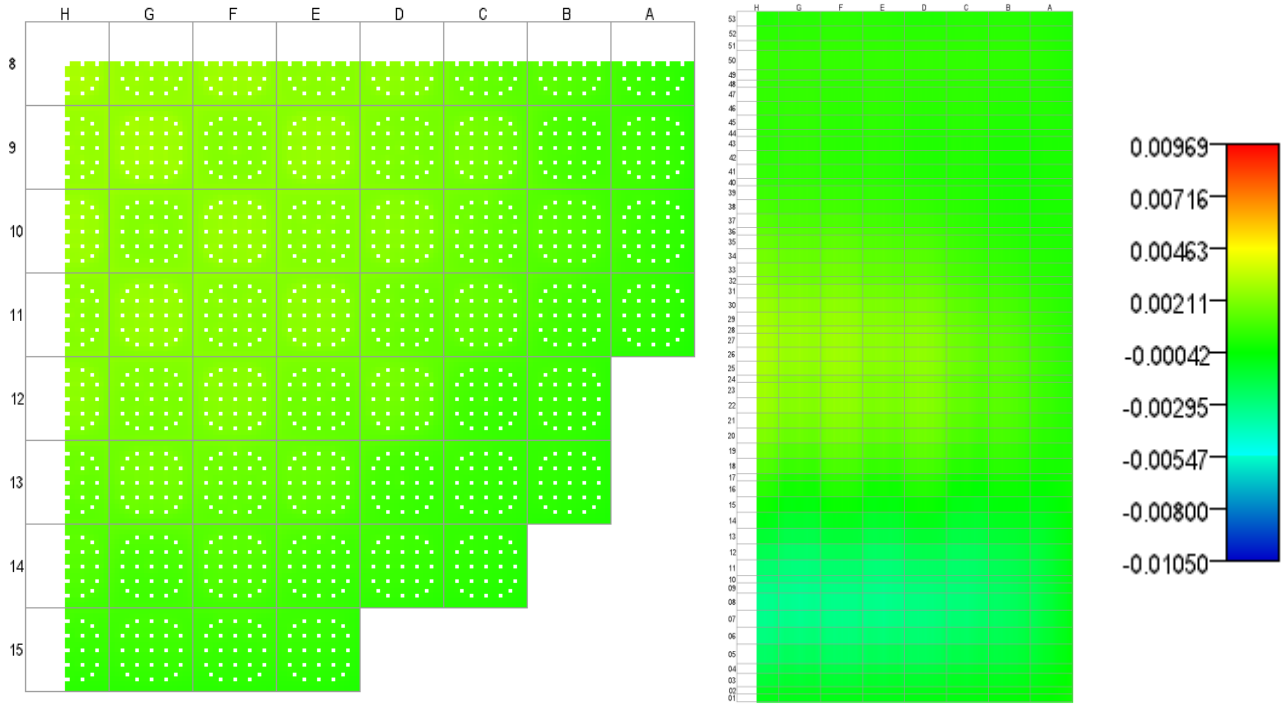

Figure B.9. Normalized Pin Power Difference, State 9, 4.642 GWd/MT.

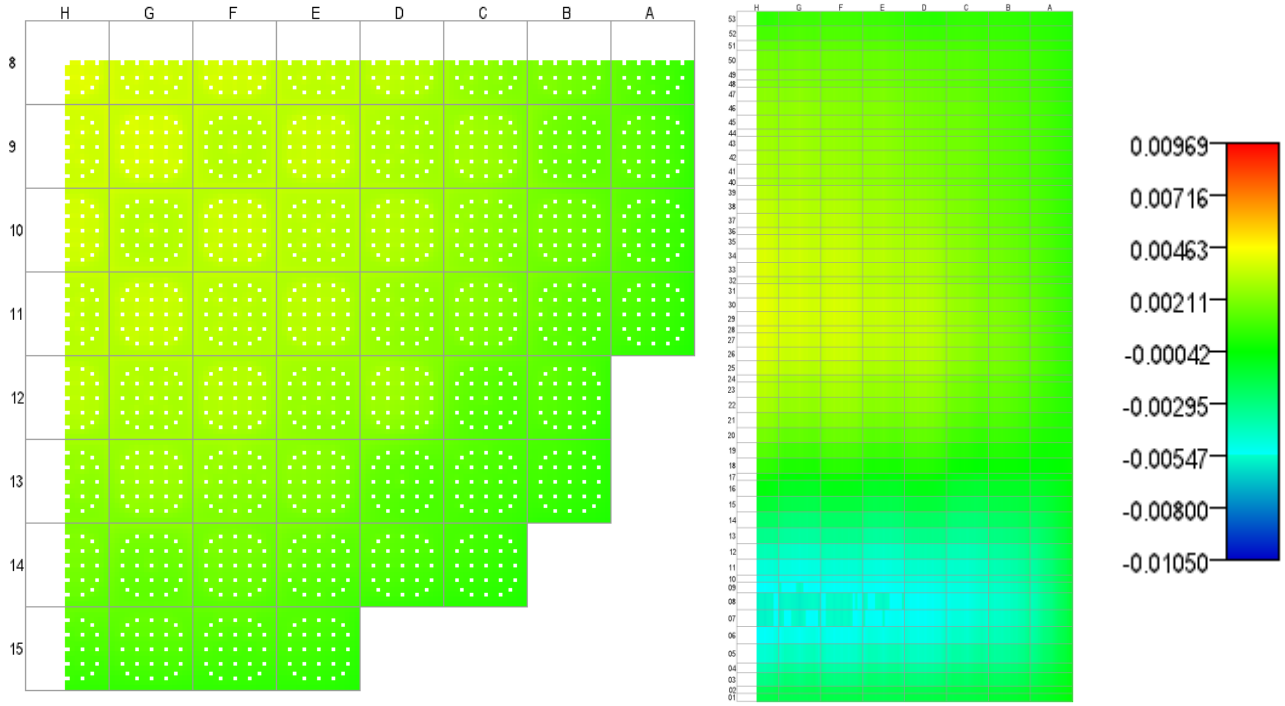

Figure B.10. Normalized Pin Power Difference, State 10, 5.139 GWd/MT.

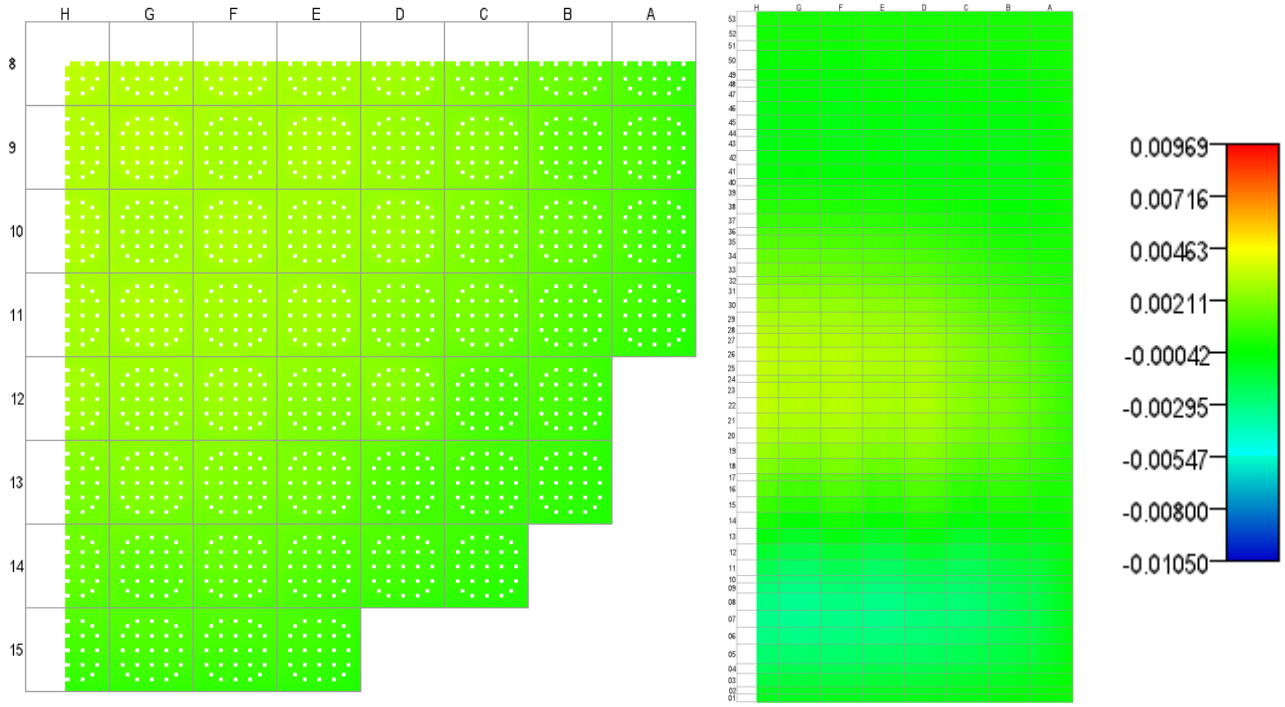

Figure B.11. Normalized Pin Power Difference, State 11, 5.700 GWd/MT.

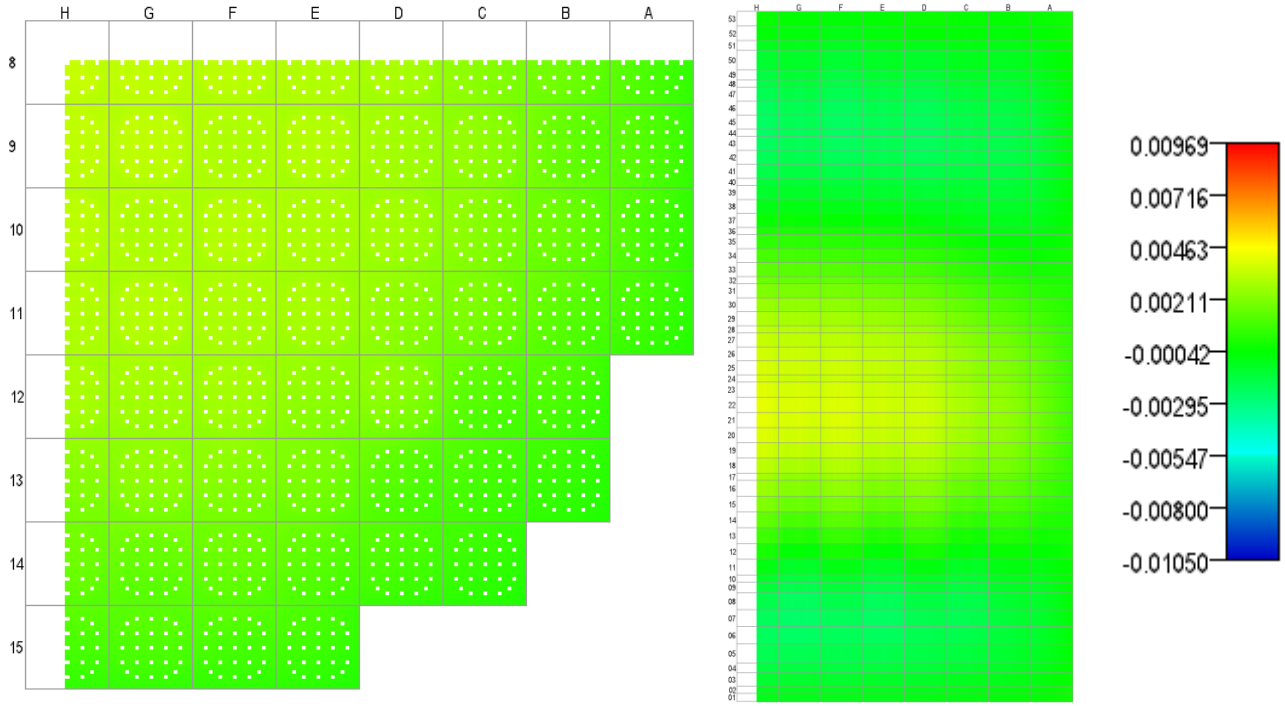

Figure B.12. Normalized Pin Power Difference, State 12, 6.273 GWd/MT.

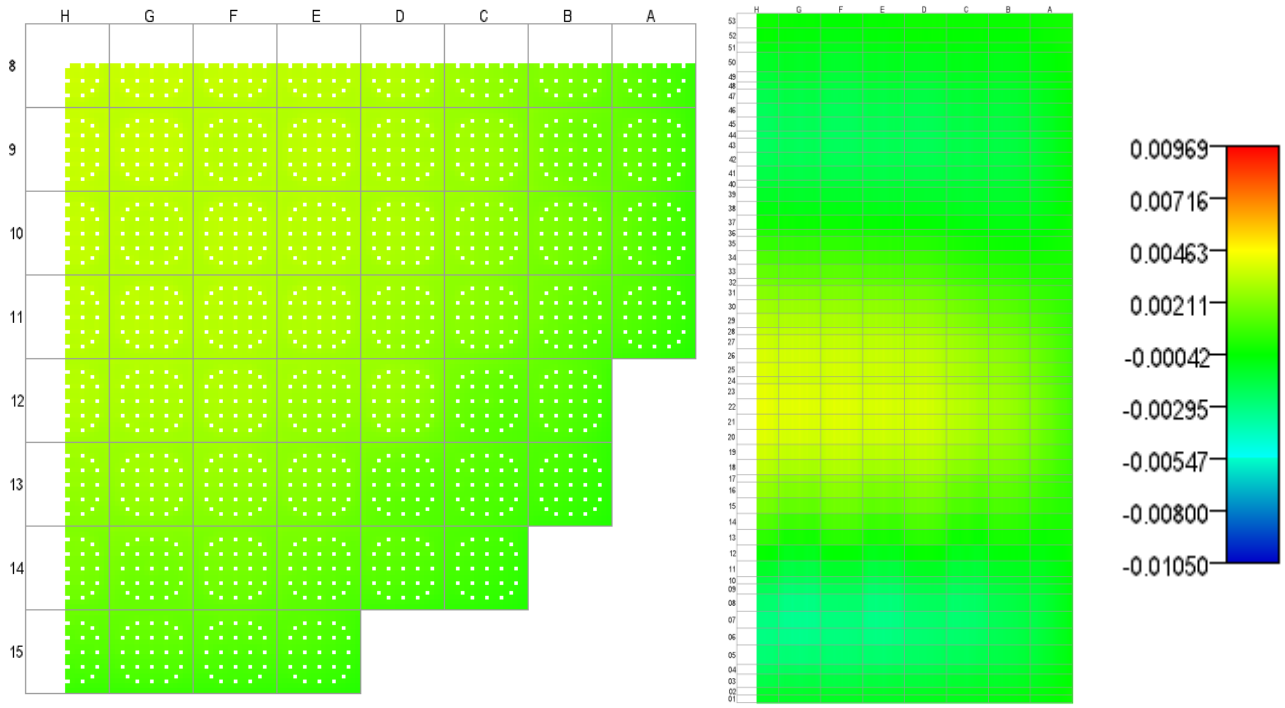

Figure B.13. Normalized Pin Power Difference, State 13, 7.000 GWd/MT.

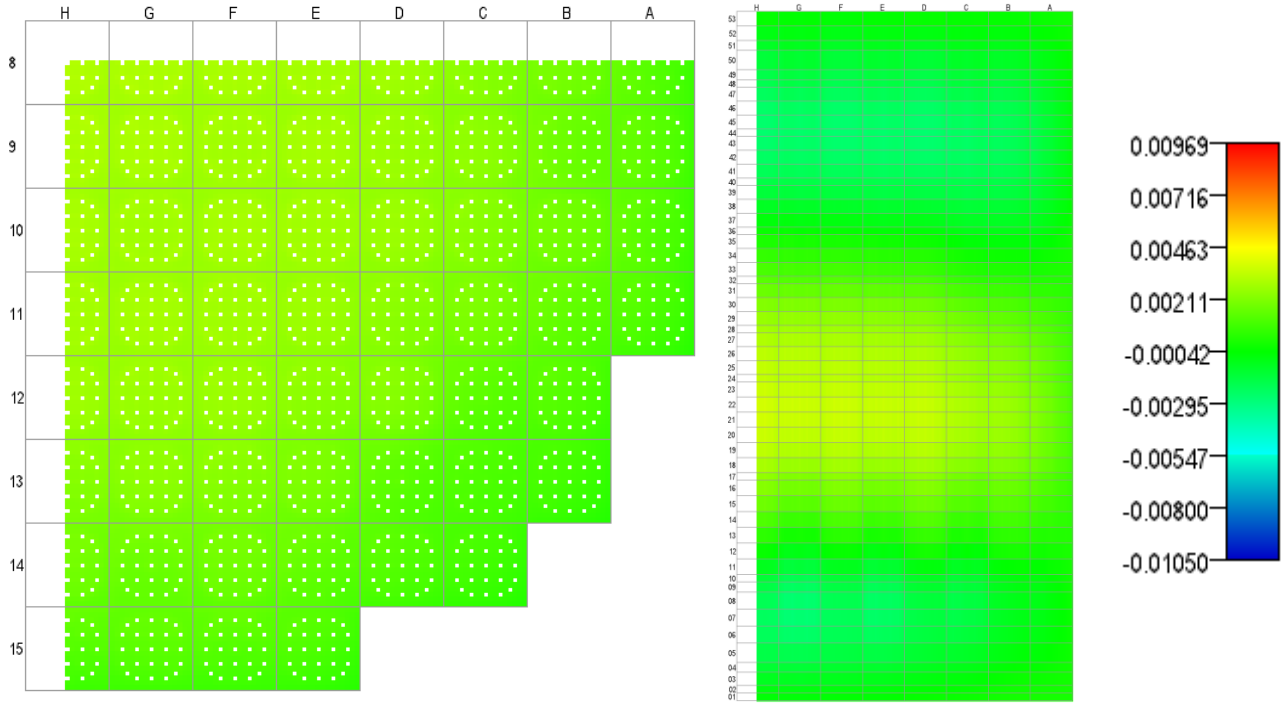

Figure B.14. Normalized Pin Power Difference, State 14, 7.463 GWd/MT.

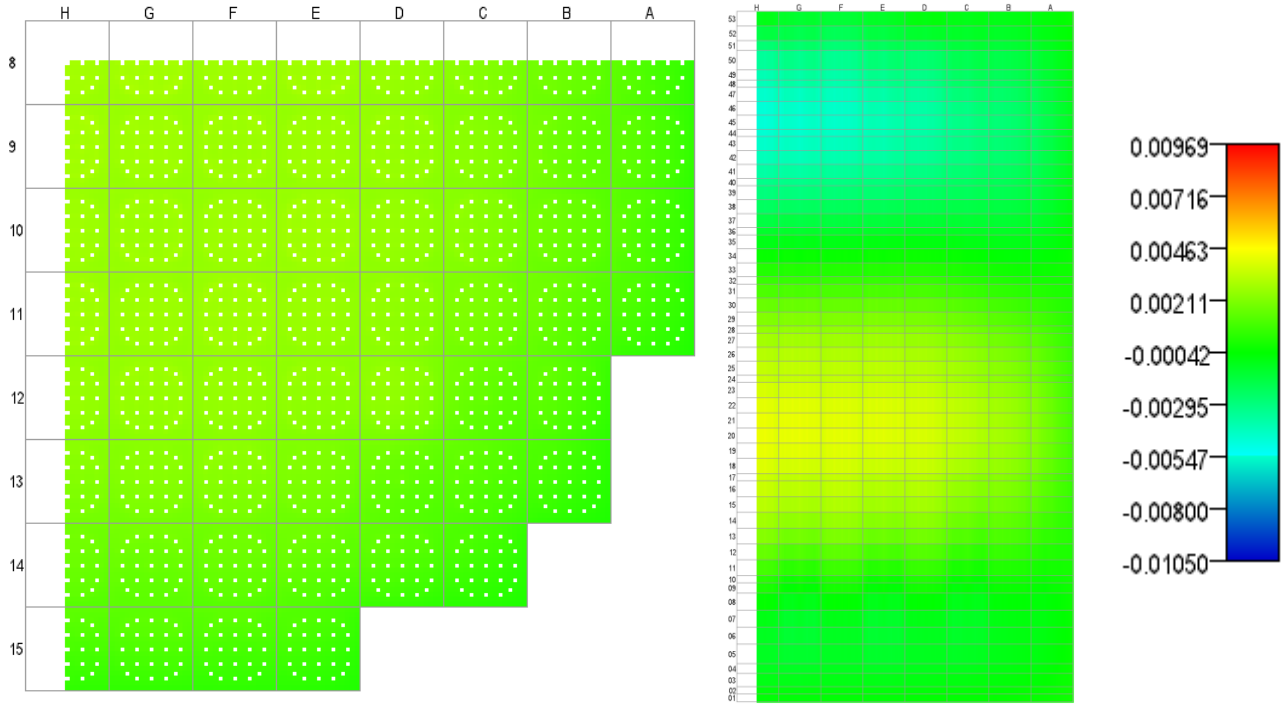

Figure B.15. Normalized Pin Power Difference, State 15, 7.978 GWd/MT.

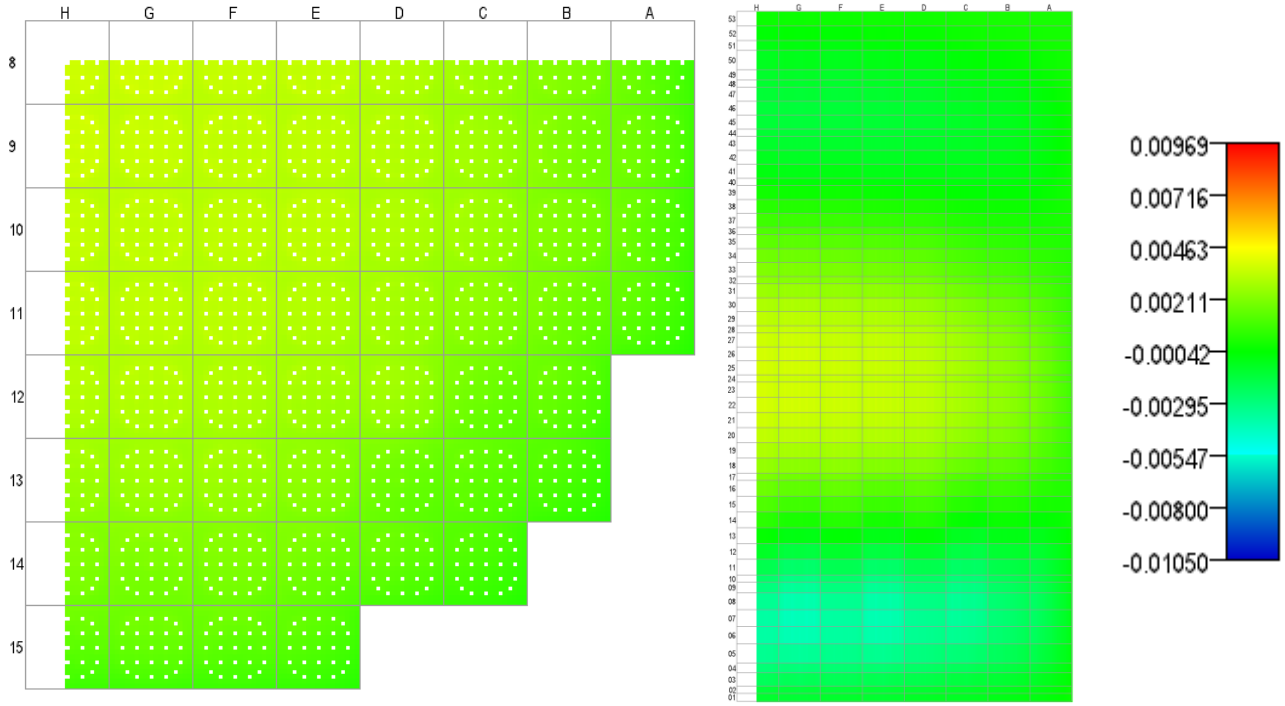

Figure B.16. Normalized Pin Power Difference, State 16, 8.493 GWd/MT.

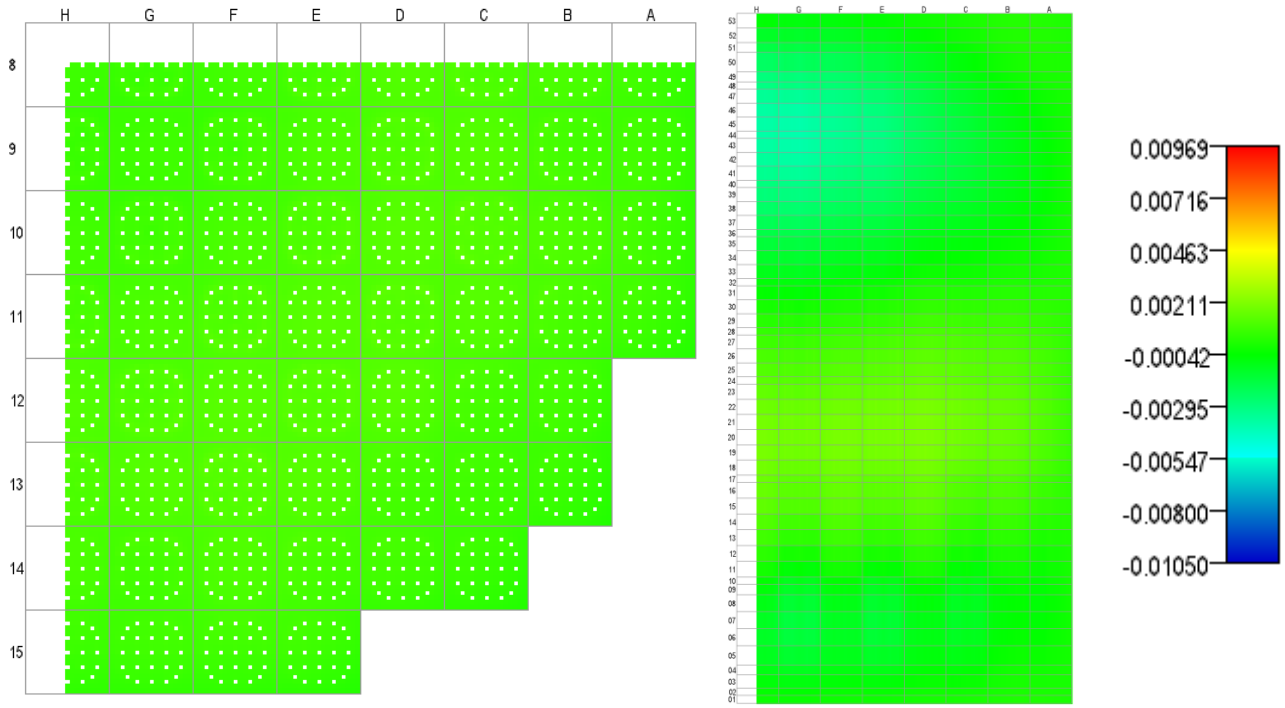

Figure B.17. Normalized Pin Power Difference, State 17, 9.140 GWd/MT.

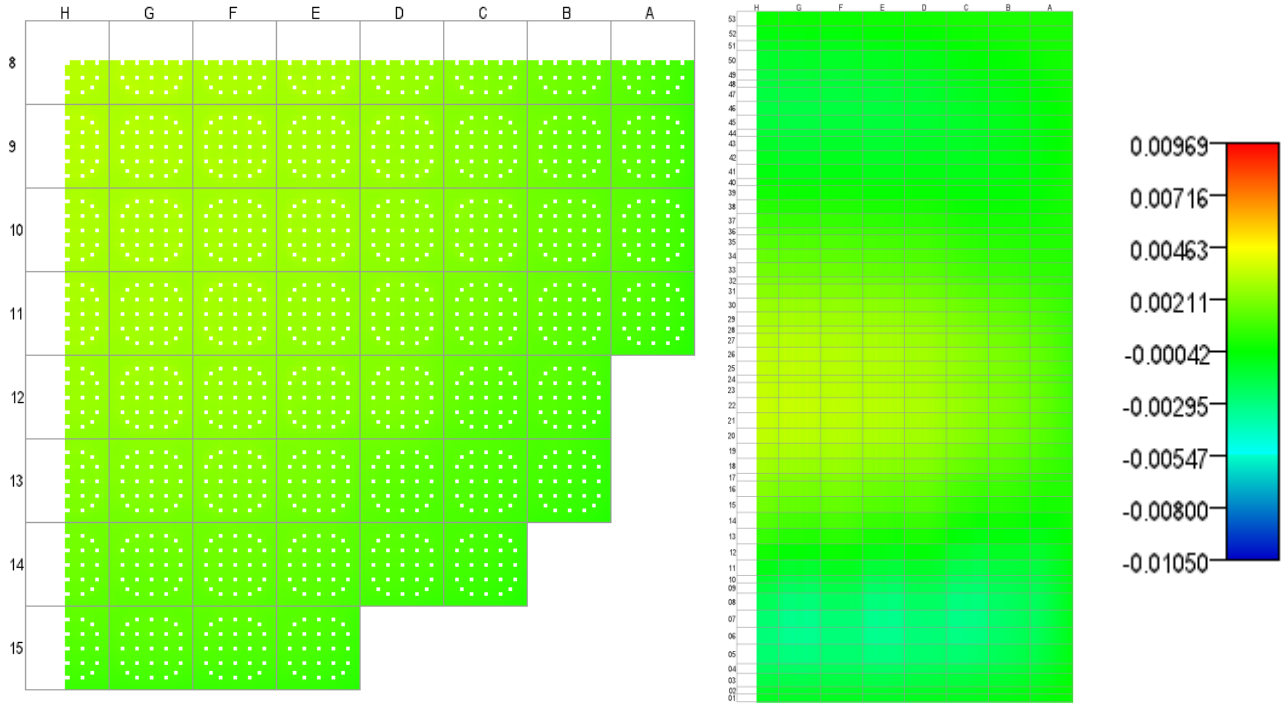

Figure B.18. Normalized Pin Power Difference, State 18, 9.602 GWd/MT.

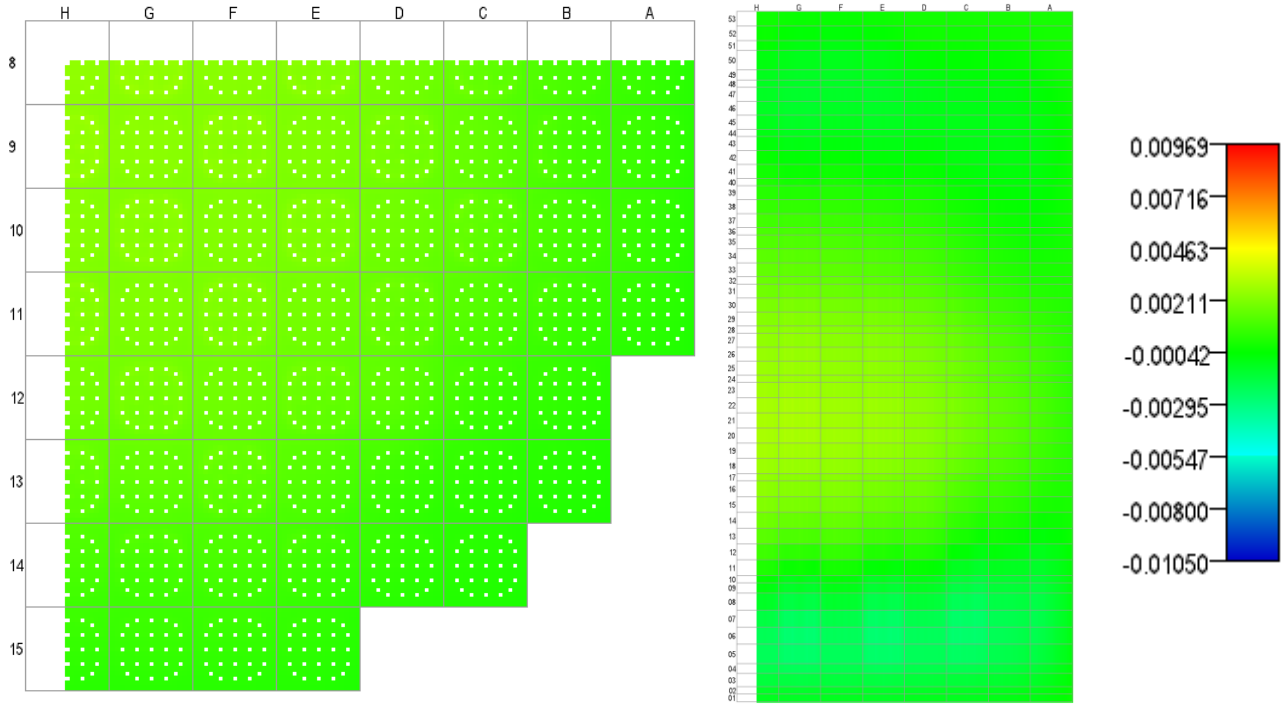

Figure B.19. Normalized Pin Power Difference, State 19, 10.344 GWd/MT.

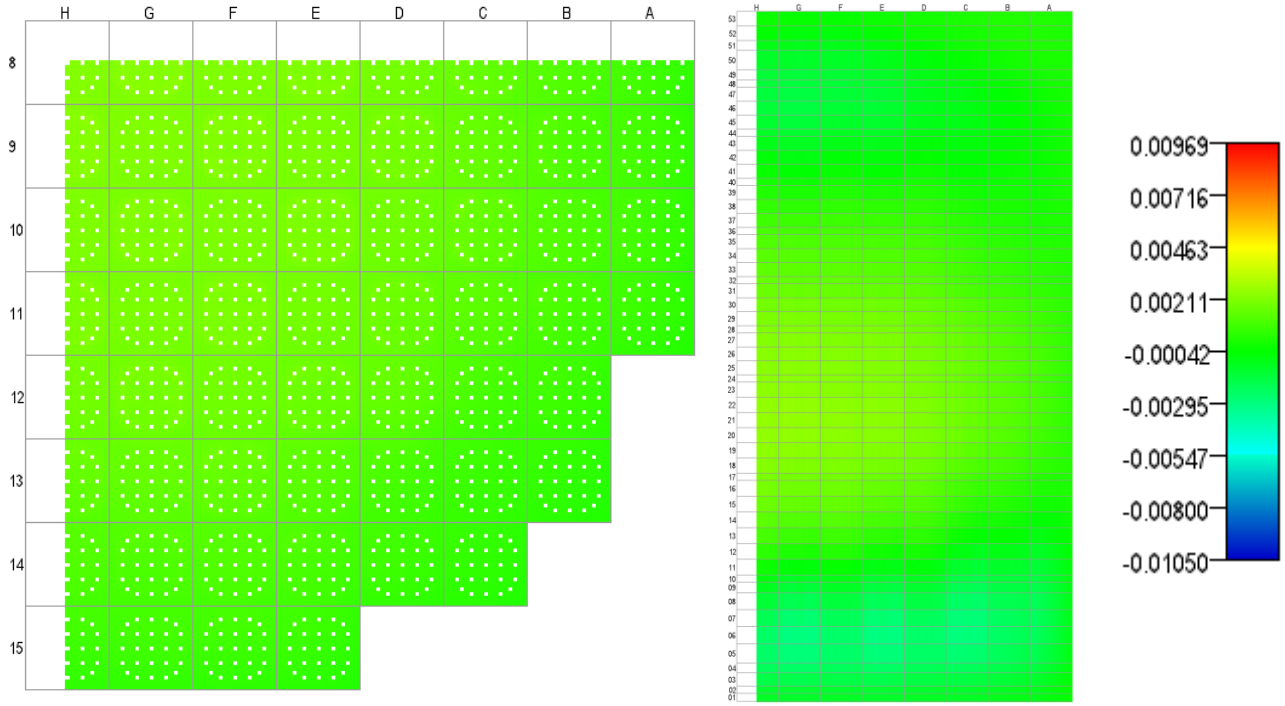

Figure B.20. Normalized Pin Power Difference, State 20, 10.842 GWd/MT.

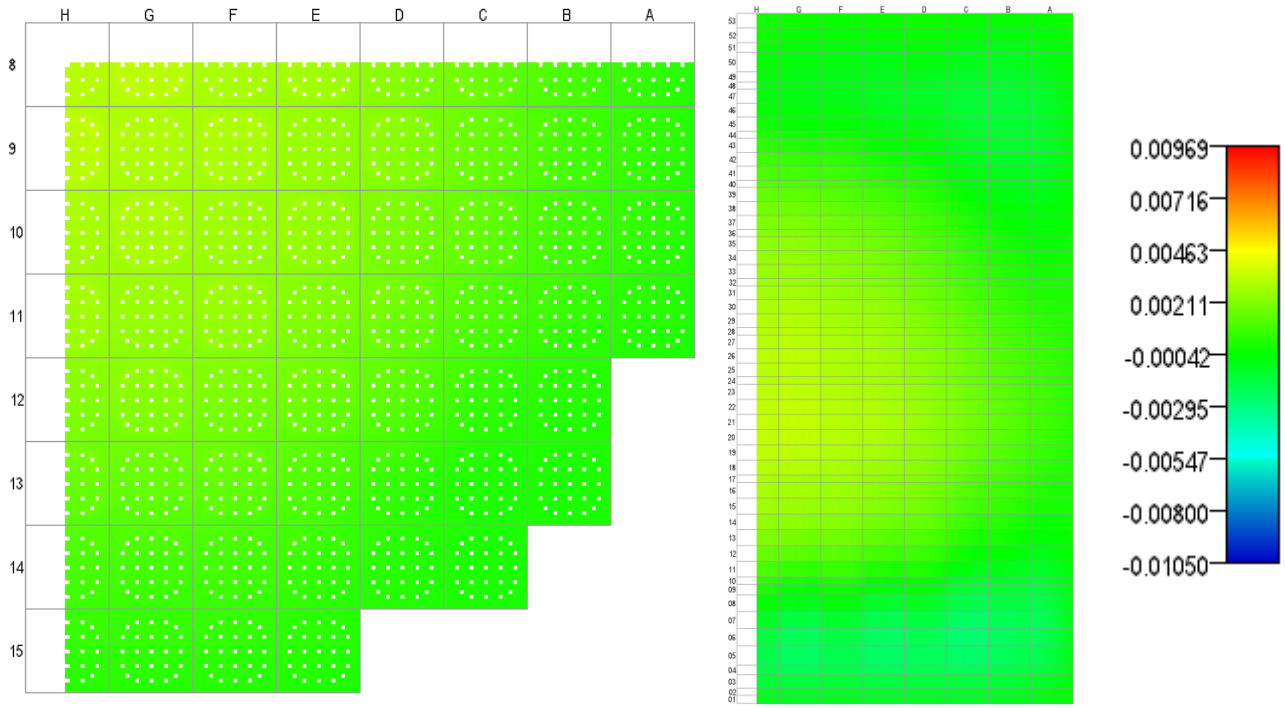

Figure B.21. Normalized Pin Power Difference, State 21, 11.314 GWd/MT.

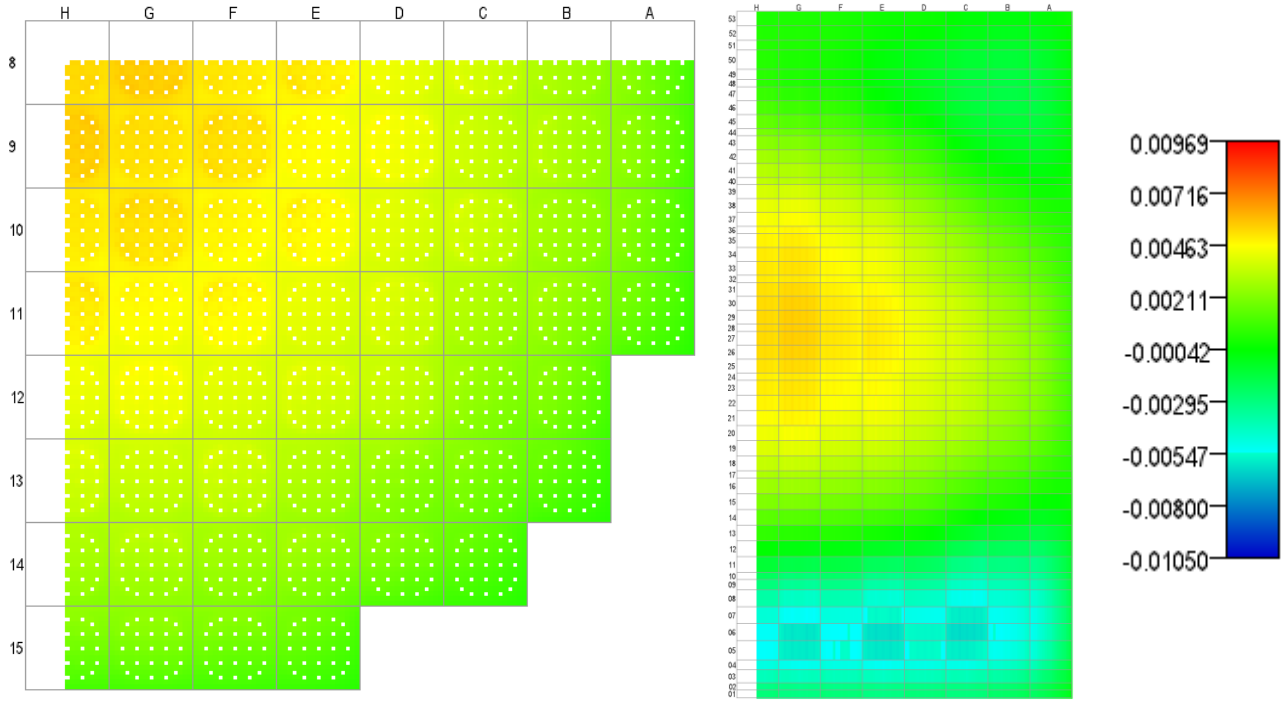

Figure B.22. Normalized Pin Power Difference, State 22, 11.988 GWd/MT.

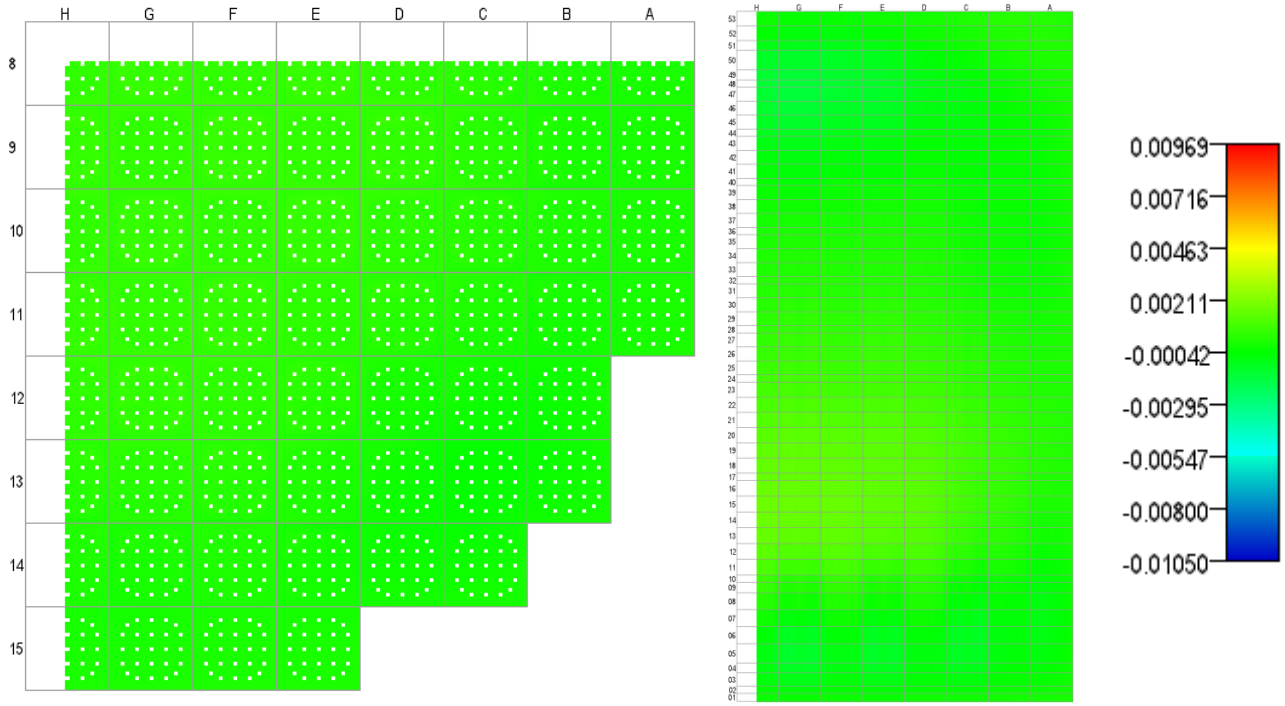

Figure B.23. Normalized Pin Power Difference, State 23, 12.552 GWd/MT.

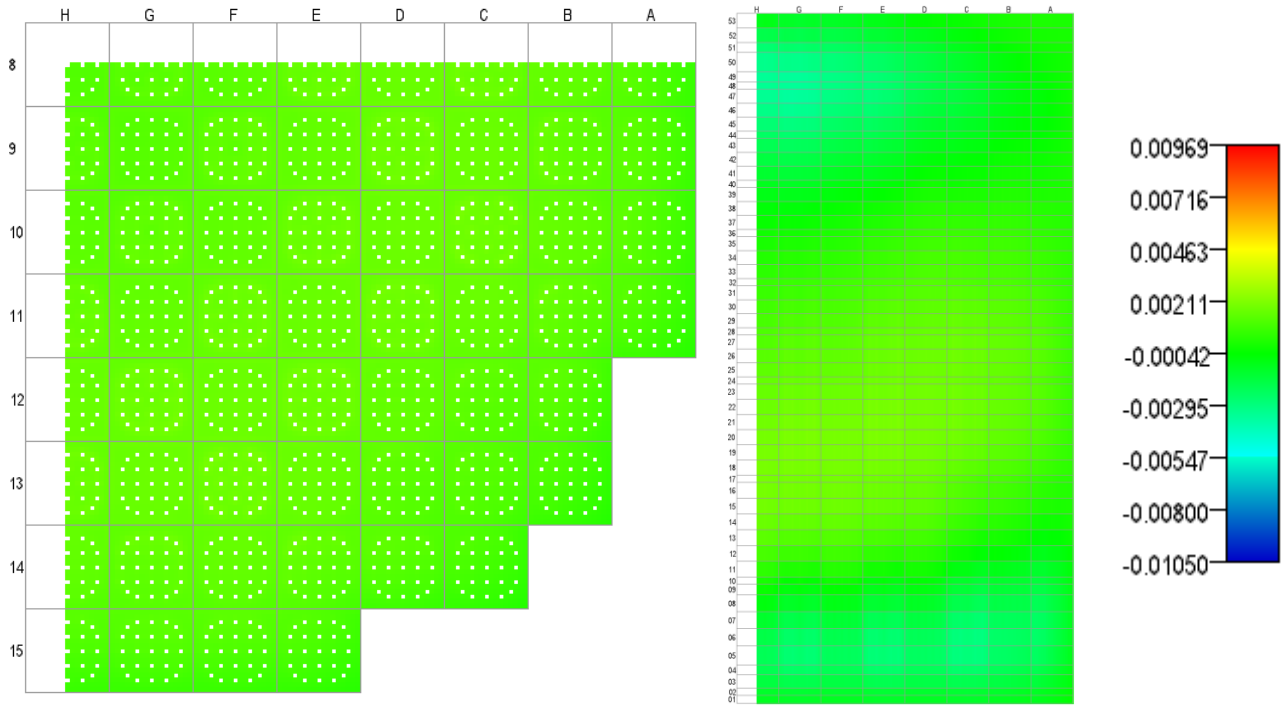

Figure B.24. Normalized Pin Power Difference, State 24, 13.360 GWd/MT.

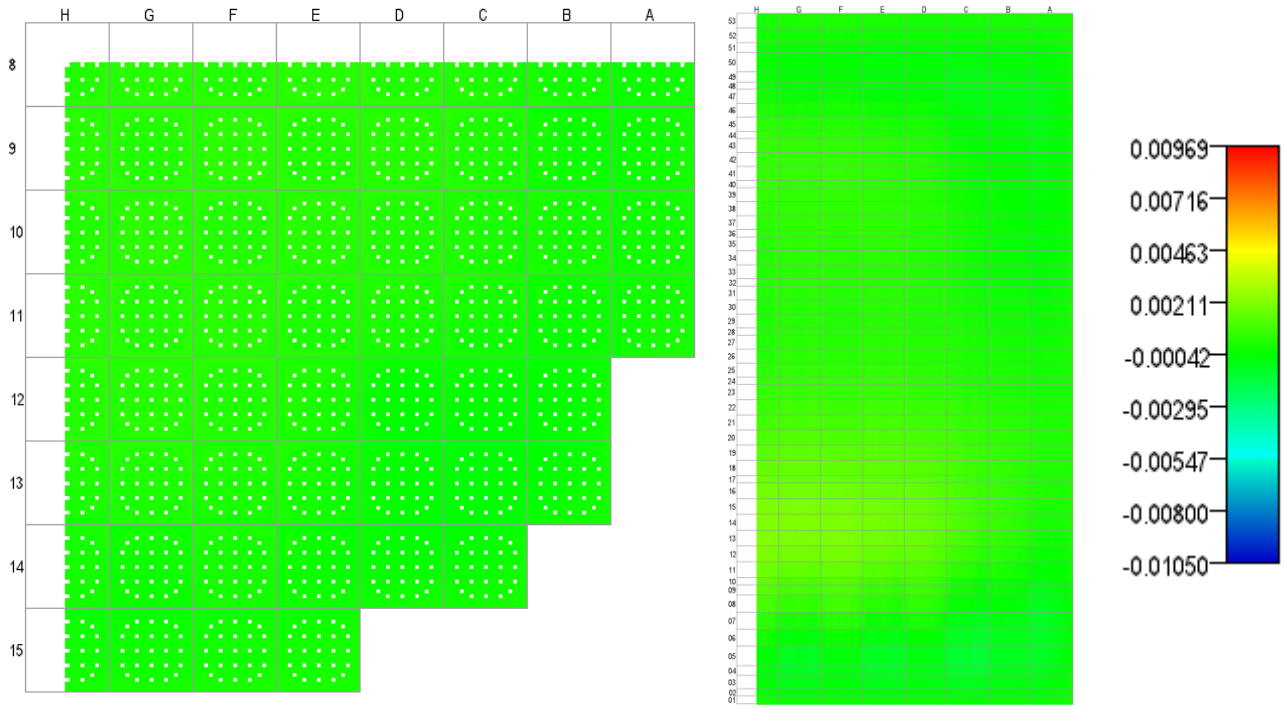

Figure B.25. Normalized Pin Power Difference, State 25, 14.285 GWd/MT.

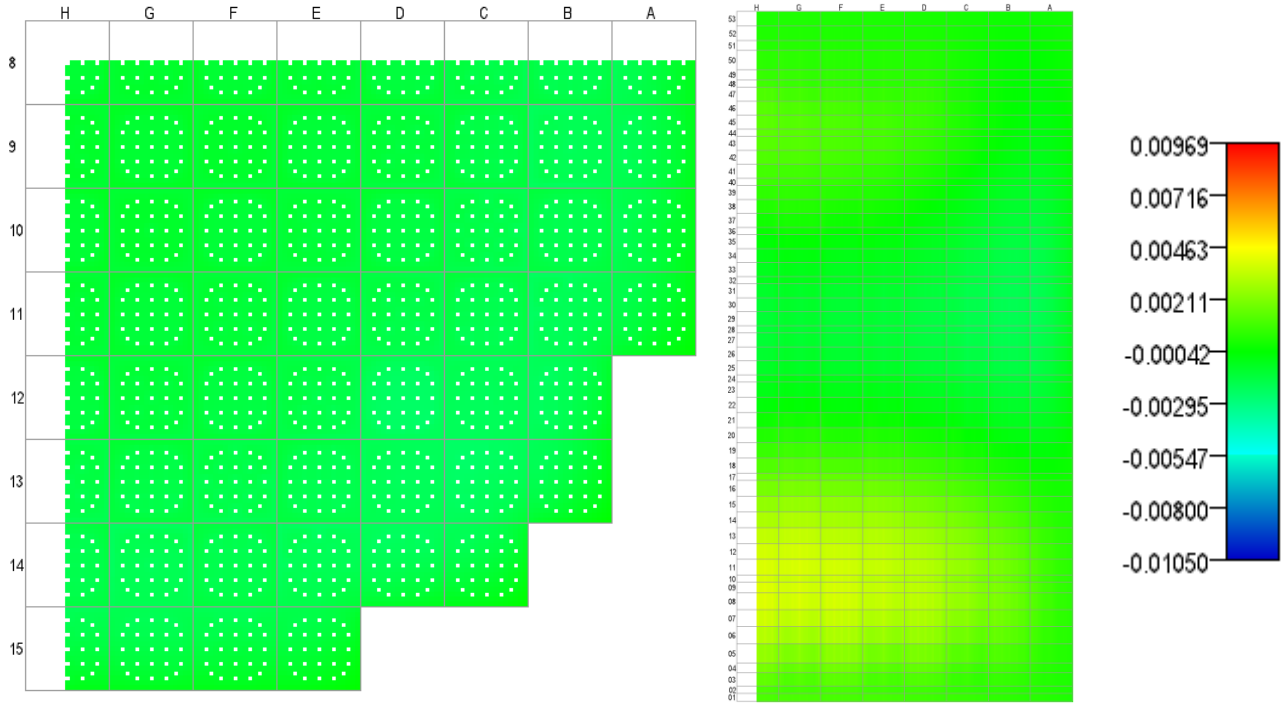

Figure B.26. Normalized Pin Power Difference, State 26, 14.385 GWd/MT.

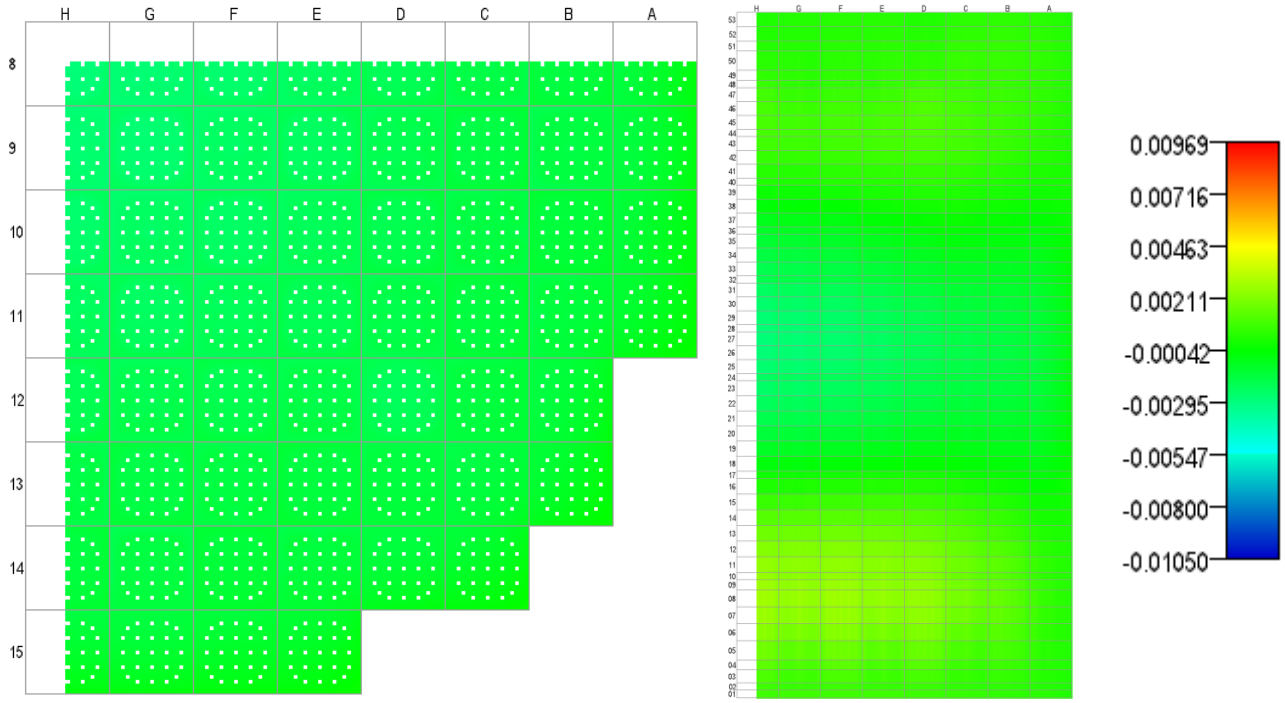

Figure B.27. Normalized Pin Power Difference, State 27, 15.018 GWd/MT.

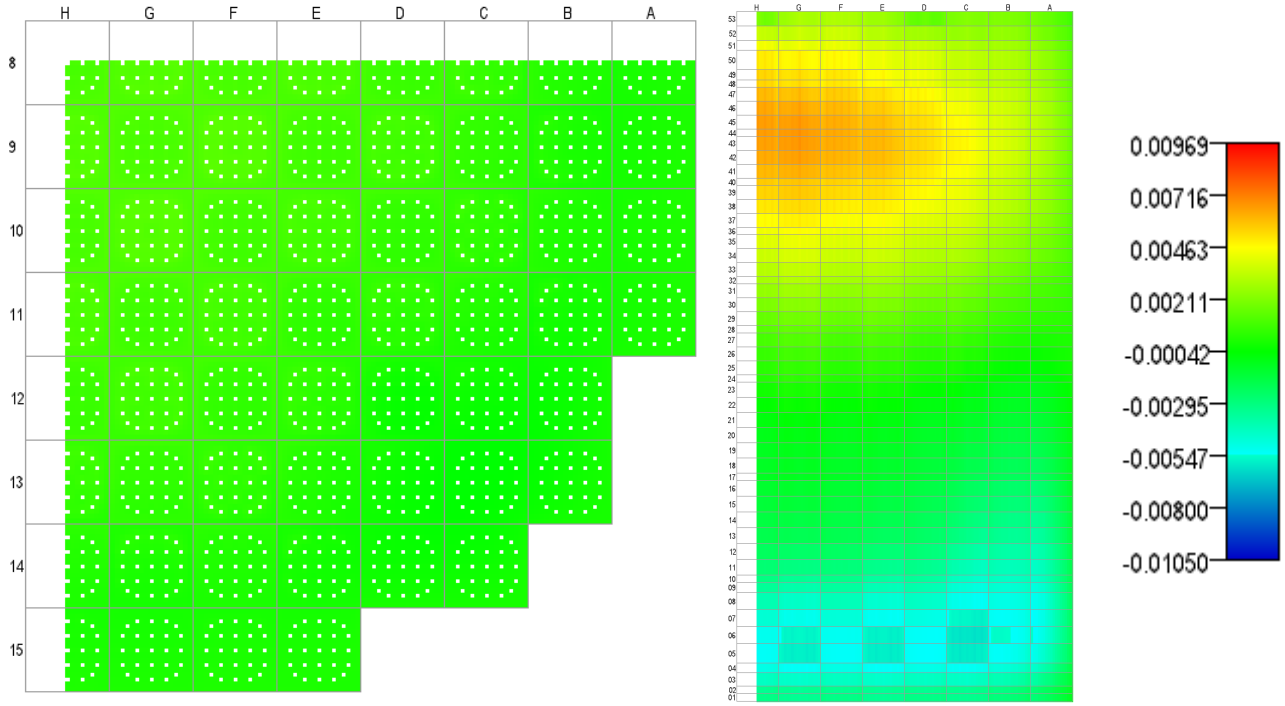

Figure B.28. Normalized Pin Power Difference, State 28, 15.118 GWd/MT.

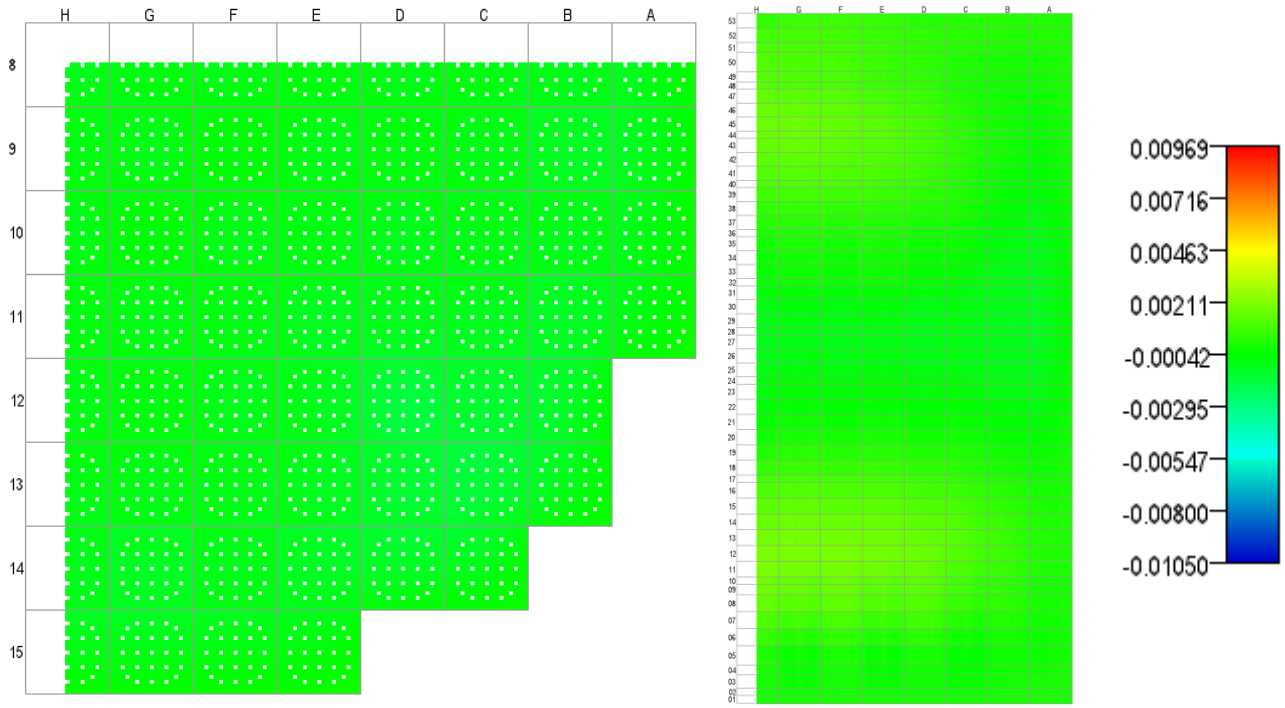

Figure B.29. Normalized Pin Power Difference, State 29, 15.308 GWd/MT.

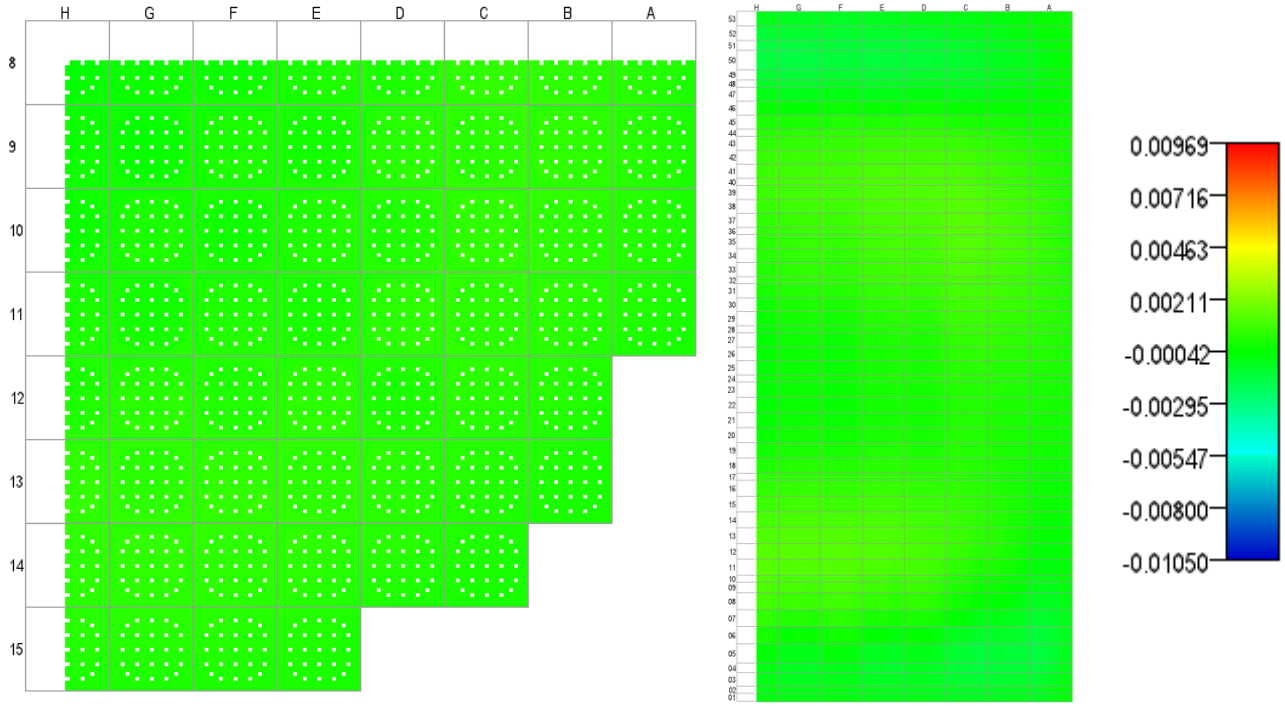

Figure B.30. Normalized Pin Power Difference, State 30, 15.774 GWd/MT.

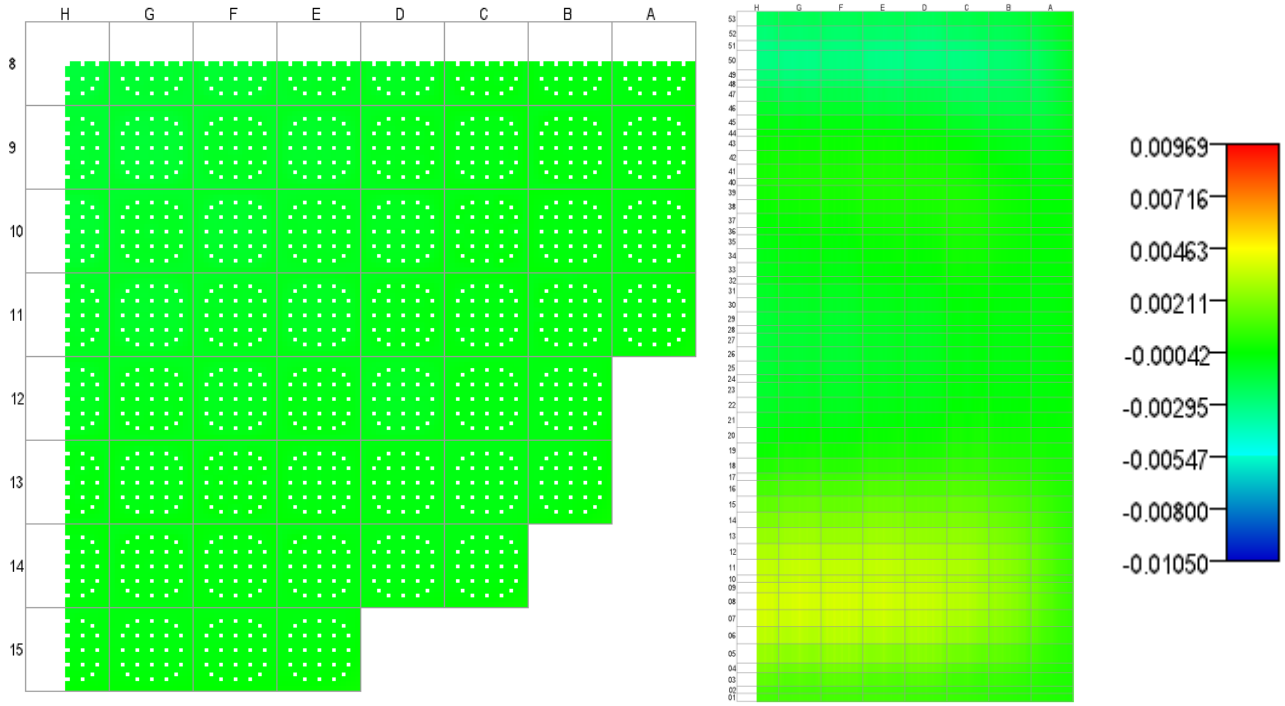

Figure B.31. Normalized Pin Power Difference, State 31, 16.270 GWd/MT.

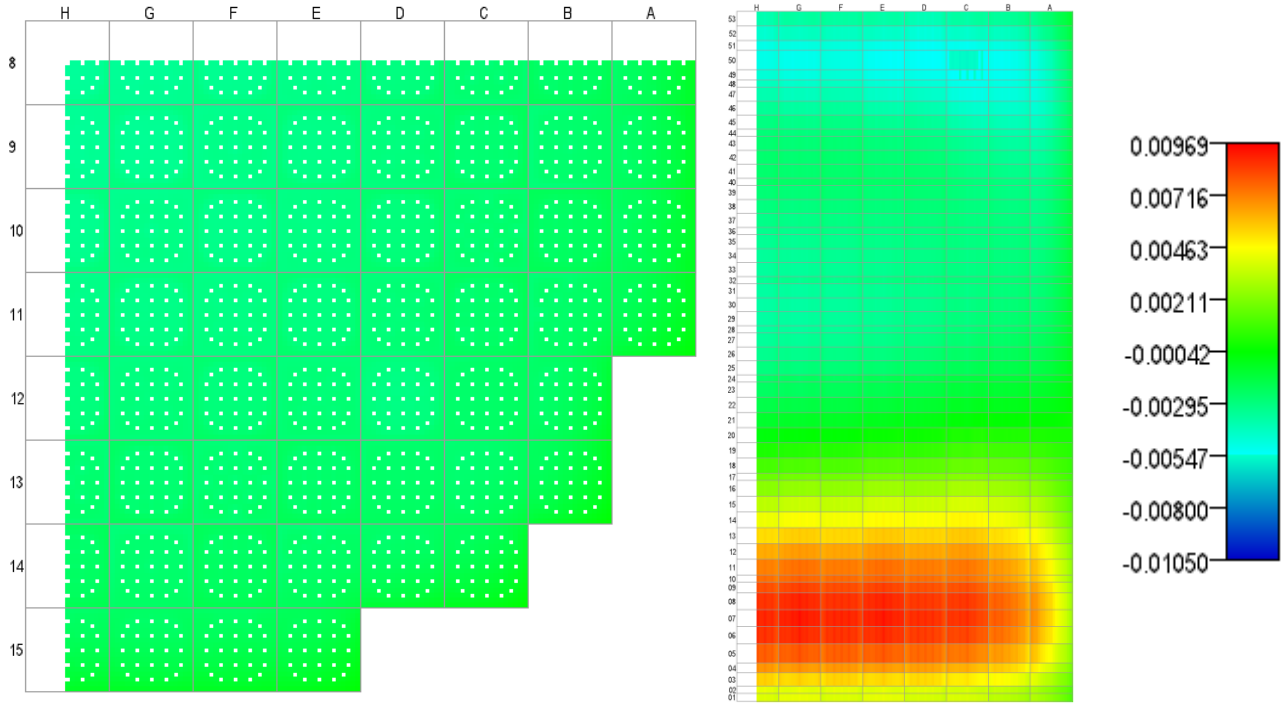

Figure B.32. Normalized Pin Power Difference, State 32, 16.932 GWd/MT.